

**OXIDATION STUDIES
ON
SUPPORTED METAL CATALYSTS**

by

John W. Curley, B.Sc (Hons)

**A Thesis presented to Dublin City University
for the degree of Doctor of Philosophy**

**This work was carried out under the supervision of
Dr. Odilla Finlayson, School of Chemical Sciences,
at Dublin City University, Glasnevin, Dublin 9.**

March 1995

I hereby certify that this material , which I now submit for assessment on the programme of study leading to the award of Ph D is entirely my own work and has not been taken from the work of others save and to the extent that such work has been cited and acknowledged within the text of my work

Signed John Curley Date 25/3/95
JOHN CURLEY

Table of Contents

Abstract	i
Acknowledgements	ii
Introduction	iii

Chapter 1 The Total Oxidation of Alkanes

1	Introduction	2
1.1	Total Oxidation of Methane	6
1.2	The Oxidation of Higher Alkanes	28

Chapter 2 Thermal Stability of "Saffil" Fibre

2	Introduction	48
2.1	Experimental	69
2.1.1	Preparation of Al ₂ O ₃ Samples	69
2.1.2	Surface Area Determination	70
2.1.3	Total Pore Volume Measurements	74
2.1.4	X-Ray Diffraction Measurements	77
2.1.5	Thermogravimetric Measurements	77
2.2	Results/Discussion	78
2.3	Conclusions	96
2.4	References	97

Chapter 3 Preparation and Characterisation of Pt/Al₂O₃ Catalysts

3	Introduction	101
3.1	Experimental	112
3 1 1	Catalyst Preparation	112
3 1 2	Estimation of Nitrate Uptake by the Al ₂ O ₃ Support Material	114
3 1 3	H ₂ Chemisorption Measurement	114
3 1 4	Atomic Absorption Spectroscopy	116
3 1 5	Activity Measurements	118
3 1 6	DSC Activity Measurements	120
3 2	Characterisation of DSC Activity Measurement	122
3 2 1	The Effect of Experimental Conditions on DSC Measurement	127
3.3	Results and Discussion	134
3 4	Conclusions	162
3 5	References	164

Chapter 4 Study of Pt-Sn/Al₂O₃ and Pt/SnO₂ Catalysts

4	Introduction	168
4 1	Pt-Sn/Al ₂ O ₃ System	168
4 1 1	Pt/SnO ₂ System	187
4 2	Experimental	195
4 2 1	Preparation of Catalyst Samples	195
4 2 2	Aging Studies	197
4 2 3	X-Ray Diffraction Measurements	197
4 2 4	X-Ray Photoelectron Spectroscopy	198
4 2 5	H ₂ Chemisorption Measurements	198
4 2 6	BET Surface Area Analysis	199
4 2 7	DSC Activity Measurement	199
4 2 8	Atomic Absorption Spectroscopy	200
4 3	Results and Discussion	201
4.4	Conclusions	236
4 5	References	237
5	Conclusions	242
Appendix I	I	
Appendix II	III	

Abstract

The aim of this work was to examine Pt/Al₂O₃, Pt-Sn/Al₂O₃ and Pt/SnO₂ catalysts for the oxidation of 1-butane. The main conclusion which can be drawn from this study is that, although less active initially compared with the Pt/SnO₂ and Pt/Al₂O₃ samples, the Pt-Sn/Al₂O₃ catalysts were more resistant to thermal aging, maintaining a higher catalytic activity than the former catalysts after aging at 1073K. For example for 5wt% Pt/Al₂O₃, 5wt% Pt/SnO₂ and 5wt% Pt, 3wt% Sn/Al₂O₃ catalysts prior to aging the light off temperatures (LOTs) were 433K, 428K and 468K respectively. After aging the LOTs for the corresponding samples was 478K, 499K and 468K respectively. There was no correlation between Pt particle size and activity. For the majority of catalysts examined there was an increase in catalytic activity at a distinct temperature compared with initial activity, which may have been due to a secondary reaction or to the presence of different catalytic sites on the surface of the catalysts.

The Al₂O₃ support material consisted mostly of η -Al₂O₃ and was stable up to 1070K, but at higher temperatures the surface area and pore volume decreased. Treatment of the Al₂O₃ with HNO₃ or HCl (to increase support acidity) led to an increase in surface area. High temperature exposure of acid treated samples caused a more rapid decrease in surface area initially and the formation of higher amounts of α -Al₂O₃ compared with the untreated Al₂O₃, possibly due to the formation of cation vacancies during acid pretreatment. Addition of the cations La³⁺, Si⁴⁺ and Ce³⁺ to the untreated Al₂O₃ had little effect on surface area loss at 1370K but prevented α -Al₂O₃ formation. After 48h at 1370K the surface area of untreated Al₂O₃ and acid pre-treated Al₂O₃ was similar, and the major cause of surface area loss was not due to α -Al₂O₃ formation, but possibly pore loss.

Preparation variables for Pt/Al₂O₃ catalysts were examined. Pre-treatment of the Al₂O₃ support with HNO₃ led to an increase in Pt uptake, higher Pt dispersion and higher catalytic activity compared with untreated catalysts studied while pre-treatment with HCl or H₂O had the opposite effect. The method of impregnation also affected the catalysts, with spray impregnation being the most effective method. Drying at 310K for 16h after impregnation led to a nonhomogeneous distribution of Pt. The HCl and H₂O pre-treated catalysts exhibited an increase in activity after reduction in H₂, the opposite being the case for the other Pt/Al₂O₃ catalysts examined.

In Pt-Sn/Al₂O₃ catalysts Sn was present in the form of Sn(II) and/or Sn(IV) and also as a Sn-aluminate species. From H₂ chemisorption measurements, Sn loadings ≤ 1 wt% led to higher uptakes of H₂ compared to Pt/Al₂O₃ samples. For Pt/SnO₂ catalysts no detectable amounts of H₂ chemisorption occurred and surface Pt was in the form of a substrate bonded species, Pt-O-Sn.

Acknowledgements

Firstly I would like to thank my supervisor, Dr Odilla Finlayson, for her help and guidance during my postgraduate years. I must also thank the academic and technical staff in the School of Chemical Sciences. I wish to thank Prof N Brown and his staff in the University of Ulster, Coleraine, who were kind enough to carry out the XPS work. I am also indebted to Forbairt and, in particular, Mr Terry Slowey who allowed me to analyse some of my samples using their X-ray diffractometer.

I wish to express my sincere gratitude and thanks to all the postgraduate students in the School of Chemical Sciences, past and present, who certainly made life "interesting" during my time as a postgraduate student. In particular Eamonn and Alan, and the members of the old guard and the "twilight zone", Teri, Conor, Pookie, Fintan, Maureen, Gerry, Barry, Kieran, John and James. I must also mention the members of the "write up self-help group", Mark, Mary, Pat and Dominic.

Finally I wish to express my thanks to my family for their patience, support and encouragement, without which this work would not have been completed. Especially to my mother for her long hours spent in the preparation of this thesis and also to my sister Mary, who was one of my greatest supporters, stood by me through thick and thin and nearly beat me to it in the end.

Introduction

Reactions involving total and partial catalytic oxidation are of industrial and economic importance. Much of the chemical industry is based on the use of catalysts for the selective production of partially oxidised products which are worth more than the hydrocarbons from which they are derived. Catalysts are used to accelerate reactions which without catalysis, although thermodynamically favoured, would normally proceed too slowly or at too high a temperature to be economically viable.

The total oxidation of various substances over heterogeneous catalysts is used for the destruction of waste industrial and automobile exhaust gases and the purification of technological gases and for catalytic combustion (heaters). In this case the advantages of using heterogeneous catalysts are that reaction can be initiated at a lower temperature than would occur without catalysis, it allows better control over a wider range of fuel/air ratios, produces less pollutants compared with normal combustion and in some cases can improve fuel efficiency. The main disadvantages with the use of heterogeneous catalysts are that the catalysts are normally expensive (many using precious metals such as Pt) and have a finite life. They can be poisoned and when catalysts are operated at high temperatures deactivation can occur due to sintering of the active phase. In the case of supported catalysts, thermal degradation of the support material can also cause loss of surface area of the active phase resulting in deactivation. The aim of this work was to overcome some of these problems. The major focus of this thesis is the development of efficient oxidation catalysts for the combustion of *i*-butane.

The structure of the thesis is composed of four chapters. The first chapter is a literature review on the total oxidation of alkanes. Chapter 2 details the investigation of the thermal stability of the Al_2O_3 support material used in the study. The effect of acid pretreatments on the surface area and thermal stability of the support material was determined, as acid washing was used to increase the acidity of the support during the preparation of supported Pt catalysts. Finally results of an investigation into the effect of addition of various cations to the Al_2O_3 support on the thermal stability of the Al_2O_3 are given.

Chapter 3 details the effects of preparation variables (including support pretreatment, pH of impregnating solution, impregnation method, and drying temperature) on the physical characteristics of Pt/ Al_2O_3 catalysts and on their activity for *i*-butane oxidation.

Pt-Sn/ Al_2O_3 and Pt/ SnO_2 catalysts are described in chapter 4 involving characterisation and *i*-butane activity measurement, before and after aging at high temperature in air. The performance of both systems was compared with that of Pt/ Al_2O_3 catalysts.

CHAPTER 1

The Total Oxidation of Alkanes

1 Introduction

The aim of this chapter is to review the literature on the oxidation of hydrocarbons. Catalytic oxidation, both total and partial, are industrially important processes. The majority of oxidation catalysts have been developed for reactions involving partial oxidation, e.g. in the reaction of butane to give maleic anhydride and acrylonitrile (1). The total oxidation of hydrocarbons to CO_2 and H_2O is important both in combustion of fuels to liberate energy and for pollution control, in automotive exhaust catalysts, for fume abatement devices and for odour control (1, 2, 3). In catalytic combustion, mixtures of fuel and air are passed over a catalyst maintained at a high enough temperature to favour total oxidation (2).

For total oxidation a highly active, nonselective catalyst is required (1). In general two types of catalyst are used for oxidation reactions: metal oxides and noble metals (supported and unsupported) (1, 4). According to Spivey (1), up to 1989 the literature on catalytic oxidation over metal oxides was more extensive than was that on noble metals. In their review of high temperature combustion Zwinkels et al. (5) stated that catalytic combustion over noble metal catalysts has been the subject of many investigations over several decades and compared to base metal oxides, noble metals exhibited higher specific activity, and their application as oxidation catalysts has been always favoured. Practical limitations such as high volatility, ease of oxidation and limited supply restrict the use of noble metals, with Pt and Pd the most commonly used for catalytic applications (5). The main advantage of metal oxide catalysts over noble metals is the lower cost of the raw material and also the higher thermal stability at selected compositions(5).

Metal oxide catalysts have been classified on the basis of stability by Golodets (6). The most stable oxides are the alkali and alkali earth metals, such as, Sc, Ti, V, Cr, Mn, the rare earth metals and the actinides, Ge, Sn, In, Zn, Al (heat of formation of the oxide, $\Delta H_{298} > 65$ kcal/g-mole oxygen). Oxides with intermediate stability include those of the metals Fe, Co, Ni, Cd, Sb, Pb ($\Delta H_{298} = 40\text{-}65$ kcal/g-mole oxygen). Finally oxides which are unstable ($\Delta H_{298} < 40$ kcal/g-mole oxygen) include the noble metals, Ru, Rh, Pd, Pt, Ir, Au and Ag. It has been suggested that this classification is useful because at moderate temperatures, metals which do not form stable bulk oxides remain reduced during oxidation processes (6). However this assumes that the mechanism of oxidation involves only molecular oxygen (O_2). Lattice oxygen in stable metal oxides and in those of intermediate stability is known to be involved in the oxidation reactions of hydrocarbons and other reactants in an O_2 containing atmosphere (1). The above classification of metal oxides on the basis of stability also leads to the conclusion that there is some level of oxygen - metal interaction which is optimum for metal

oxide catalysis. This is due to the fact that the catalytic activity of the catalyst is inversely proportional to the strength of chemisorption of the reactants provided that the adsorption is sufficiently strong for the reactants to achieve high surface coverage (7). This explains the qualitative behaviour shown in Fig.1.0, commonly known as the "volcano" plot.

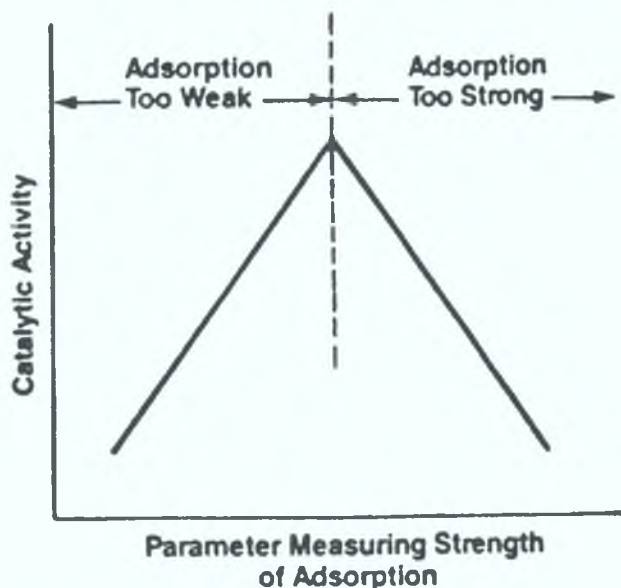


Fig.1.0 : Volcano Plot, chemisorption of reactants versus catalytic activity (7).

If reactant chemisorption is insufficiently strong then only a small amount of the surface is covered and the catalytic activity will be low. On the other hand if the reactant is chemisorbed strongly, the catalyst will rapidly deactivate as active sites are irreversibly covered (7).

Metal oxide catalysts can also be classified on the basis of electrical conductivity as follows: p-type semiconductors, n-type semiconductors, and insulators (1, 6). Lattice conductivity arises due to an excess of quasi-free electrons in n-type semiconductors. Apart from vanadium pentoxide (V_2O_5), n-type oxides are generally not active oxidation catalysts. In contrast, p-type semiconductor oxides are usually active oxidation catalysts and the basis of electrical conductivity is by means of positive holes, as the lattice is electron deficient. P-type oxides gain oxygen when heated in air whilst n-type oxides lose oxygen under the same treatment. Therefore for p-type oxides, oxygen adsorption occurs more easily as electrons can readily be removed from the metal cations to form active species such as O^- . On n-type oxides oxygen adsorption can only occur on pre-reduced surfaces, by replacing oxide ions removed in the reducing pretreatment. Finally insulators are generally not active catalysts (1, 6).

Sokolovskii (8) has recently reviewed the literature regarding oxidative catalysis on solid oxides. He concluded that there were two requirements for efficient oxidation catalysts. Firstly, efficient catalysts of complete oxidation had to provide a high rate of primary oxygen activation. Therefore they had to have a large number of sites that could co-ordinate the molecule of oxygen and also be able to donate and accept electrons. He stated that these properties were exhibited by oxides of 3d elements with unfilled d shells. The second requirement for efficient total oxidation was that the catalysts had to provide a slow transformation of active oxygen into lattice oxygen. For this to occur the reaction temperature and reactant composition had to provide a sufficiently low concentration of oxygen vacancies in the catalyst in order to decrease the rate of the active - to - lattice oxygen transition. Sokolovskii (8) concluded that at low temperatures the rate determining step of total oxidation reactions was the decomposition of oxidised surface species and that the reaction rate would be higher with faster oxygen binding. At high temperatures the reaction rate was determined by the step involving the interaction between the oxidised reactant and the catalyst and an inverse correlation between the reaction rate and the initial heat of oxygen binding on the catalyst surface was observed (8).

The noble metals mainly used for oxidation catalysis are Pt, Pd, Au, and Ag, either on their own or in combination with Ru, Rh, Os and Ir as bimetallics or alloys (1, 6). Metal catalysts are used either supported on various carriers (for example Al_2O_3 , SiO_2 , pumice, coal etc), or in compact form, such as wire, gauze, plate powder, film or single crystal (6). Noble metals normally form unstable oxides (1), but at high temperatures oxidation does occur. For example Pt and Pd undergo oxidation when used in the oxidation of NH_3 at 1273K (6) and at temperatures above 773K prolonged exposure of supported Pd to O_2 has been observed to cause structural changes in the Pd metal resulting in loss of catalytic activity for CH_4 oxidation (9). Noble metal catalyst are generally more active than metal oxides but are less resistant to certain poisons especially halogens, As, Pb and P (1).

Hydrocarbons vary widely in their ease of oxidation. In his review Dywer (4) gave a set of guide-lines for the ease of oxidation of hydrocarbons but the rules can only be treated in a qualitative sense, as they do not account for differences in oxidation mechanisms over different catalysts.

They are in order of ease of oxidation given below (4)

- Branched chain > straight chain,
- Ethynes > olefins > saturated,
- $C_n > C_3 > C_2 > C_1$,
- Aliphatic > alicyclic > aromatic

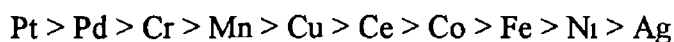
From a study carried out on the oxidation of hydrocarbons over CuO catalysts (10) the conclusions given below were reached

- CH_4 is the most difficult hydrocarbon to oxidise, while acetylene is the least difficult,
- The ease of oxidation increases with carbon number,
- For a given carbon number, the ease of oxidation increases with decreasing degree of saturation

Trim (2) has reviewed the literature on kinetic studies of total oxidation involving catalysis up to 1983. In the following sections the literature on the total oxidation of methane and higher alkanes will be examined

1.1 Total Oxidation of Methane

The oxidation of CH_4 is one of the most studied alkane oxidation reactions and is the most difficult alkane to oxidise (2, 10) Anderson et al (11) examined the catalytic oxidation of CH_4 over a number of catalysts using a microcatalytic reactor as part of a study to develop devices to monitor CH_4 concentrations in coal mine atmospheres They tested thirty catalyst samples, fourteen of which were prepared by impregnating porous supports with aqueous solutions of metal nitrates or chlorides and then calcining them in air at 523K Decomposition catalysts were prepared by evaporating aqueous solutions of mixed metal nitrates and heating to a temperature $> 1123\text{K}$, while precipitation catalysts were made by adding an alkali to aqueous metal nitrate solutions In the microcatalytic method a continuous stream of O_2 was passed at $40\text{cm}^3\text{min}^{-1}$ @ STP through 5cm^3 of catalyst sample in a heated quartz reactor The effluent gas from the reactor was passed through a dryer, then into a GC column connected to a TCD At appropriate time intervals, 0.66cm^3 CH_4 was introduced into the O_2 stream (i.e. the reaction was carried out in excess O_2) and the products were monitored using the TCD Catalysts were tested at different temperatures using a constant ratio of feed rate of CH_4 to bulk volume of catalyst sample Using the Arrhenius equation, activation energies were obtained for reaction on the different catalytic surfaces The apparent activation energies for the most active catalysts ranged between 15 kcal mol^{-1} and 25 kcal mol^{-1} and with the active impregnation catalysts between 21 and 25 kcal mol^{-1} The activity of metals and metal oxides supported on Al_2O_3 per gram of active metal decreased in the order



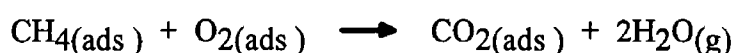
Co_3O_4 was found to be the most active single component catalyst for the oxidation of CH_4 , in agreement with a previous study by Yant and Hawk (12) However activity was decreased by impregnation on Al_2O_3 due to the formation of CoAl_2O_4 Finally the study indicated that the kinetics of the oxidation reaction over the catalysts was reasonably approximated by an empirical first order rate equation with respect to the CH_4 concentration (11)

In contrast to results of the above study Kainz and Horwatitsh (13) found that the activity of Pt and Pd was close to that of the most active metal oxides, Co_3O_4 and MnO_2 In that study the temperature required to attain 99.8% conversion was used as a measure of catalytic activity However in both the studies mentioned above (11, 13) no account was taken of the fact that there was a difference in surface area between the samples examined, so an unambiguous

judgement on relationships between the specific activity of metals and metal oxides cannot be made from their results

Mezaki and Watson (14) examined the total oxidation of CH₄ over 0.5 wt% Pd/Al₂O₃ catalyst using a flow-type integral reactor. The kinetics of the oxidation reaction was investigated by consideration of various possible Langmuir-Hinshelwood type models. The calculations were based on the amount of CH₄ converted during reaction at temperatures between 593K and 653K. Eighty four models were linearised and fitted to the experimental rate data. A reaction mechanism was proposed in which the surface reaction between gaseous CH₄ and adsorbed oxygen was proposed to be the controlling step (14)

Similarly Ahuja and Mathur (15) used the initial rate data for the oxidation of CH₄ over Pd to study the reaction mechanism. By the means of a regression analysis of the rate data, they eliminated possible reaction schemes and deduced that the most probable mechanism for reaction was (15)



Although the above mechanism differs from that proposed by Mezaki and Watson (14), it did agree in that the existence of intermediate oxidation products was improbable (15)

The reaction over Al₂O₃ supported Pt, Pd, Rh and Ir was studied by Firth and Holland (16) using a microcalorimetric method. At a partial pressure of 0.02 atm CH₄ and 0.215 atm O₂, the activation energies for CH₄ reaction on Pt, Rh, and Ir were determined to be 48, 27 and 17 kcal mol⁻¹, respectively. For Pd, above 563K, the activation energy was determined to be 33 kcal mol⁻¹, while below this temperature it was found to be 12 kcal mol⁻¹. For all the metals examined the kinetics of the reaction was found to be first order with respect to CH₄. When the O₂ partial pressure was varied between 0.05 and 0.9 atm, the order with respect to O₂ was 0 for all metals. The rate equation for the reaction was (16)

$$r = k p_{\text{CH}_4}^1 p_{\text{O}_2}^0 \quad (I)$$

where p_{CH_4} and p_{O_2} represent the partial pressures of CH₄ and O₂ respectively, r is the reaction rate and k the rate constant. It was found that at the temperatures stated above, the reaction over Ir and Pt was inhibited by O₂ partial pressures below 0.7 and 0.3 atm respectively. The kinetic results indicated that on Pd, Pt and Ir at certain temperatures CH₄ was adsorbed on two types of site, one that could also adsorb oxygen and one which could not

Kemball (17) examined the catalytic activity of Pd-Au alloys for CH₄ oxidation. The study was carried out at temperatures between 743K and 983K, with the partial pressures for O₂ and CH₄ varied between 40-660 torr and 3.8-7.6 torr respectively. Over catalyst samples containing Au concentrations below 60 atm % the kinetics of the oxidation reaction were described by equation (I) but at higher Au contents the order with respect to O₂ was found to be 0.25.

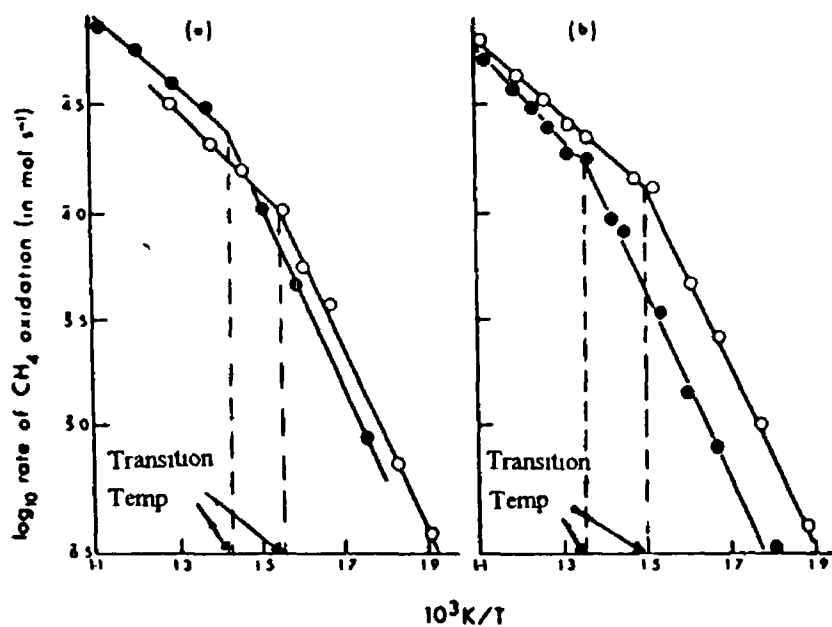
The oxidation of CH₄ over Pt/Al₂O₃ under excess O₂ was studied by Salmikov et al (18). The results of the study indicated that the reaction was first order with respect to CH₄ and that the kinetics could be described by equation (II)

$$r = k e^{(-E/RT)} C \quad (II)$$

where r represents the rate of oxidation, k is the rate constant, e is the exponential function, E is the activation energy (kJmol⁻¹), R is the universal gas constant, T is the temperature (K) and C is the CH₄ concentration.

Using a pulse flow technique, Cullis and Willat (9) examined CH₄ oxidation over supported Pt and Pd in order to determine the mechanism of reaction and elucidate the role of the support in these reactions. In particular, they studied the adsorption of O₂ on the precious metal catalysts and the role of adsorbed O₂ in the oxidation reaction. The effect of the particle size of the precious metal and of interaction between the metal and the support material were also assessed. The supports examined were ThO₂, TiO₂, γ -Al₂O₃, α -Al₂O₃, SiO₂ and SnO₂. Precious metal catalysts supported on these powdered refractory metal oxides, were prepared with metal loadings ranging from 1 to 40%. The catalysts were characterised using N₂ physisorption, H₂ chemisorption, transmission electron microscopy, scanning electron microscopy and x-ray photoelectron spectroscopy. The reaction was investigated at temperatures in the range 500-873K using reactant mixtures with CH₄ / O₂ ratios varying from 1 / 10 to 10 / 1. They found that in this temperature range the catalytic effect of the support materials, with the exception of SnO₂, was negligible. In the case of SnO₂, at 873K, 25% conversion occurred in a CH₄ atmosphere and 100% conversion occurred in a CH₄ / O₂ atmosphere (4.0 x 10⁻⁵ mol CH₄, 1.8 x 10⁻⁵ mol O₂). For supported Pt and Pd catalysts, both the support and the precious metal played a role in the catalytic activity. In both CH₄ and O₂ rich atmospheres, on a given support, increasing the Pd loading caused an increase in the rate of conversion of CH₄. However the activity per unit mass and per unit area of Pd

metal decreased with increasing loading. Similar results were obtained for Pt in CH_4 rich mixtures. For example the rate of CH_4 conversion using a CH_4/O_2 ratio of 0.5, at 623K, over 2.7 wt% Pd/ TiO_2 was $0.89 \times 10^{-2} \text{ mol s}^{-1} \text{ g}^{-1}$ precious metal compared with the corresponding value of $0.34 \times 10^{-2} \text{ mol s}^{-1} \text{ g}^{-1}$ precious metal over 40 wt% Pd/ TiO_2 . In general lower rates of conversion were obtained over Pt than over Pd. Orders of reaction with respect to both CH_4 and O_2 were found to be the same as those mentioned in previous studies (11, 16, 18) i.e. 1 and 0 respectively. Activation energies were calculated for a number of Pt and Pd catalysts (9). In general an increase in metal loading, had little effect on activation energies. Rates of CH_4 oxidation were measured as a function of temperature. Plots of the logarithm of reaction rate versus reciprocal temperature exhibited a sudden change in slope at a point which was called the transition temperature, illustrated for Pd catalysts in Fig 1.1



(a) (○), 2.7 wt% Pd on TiO_2 , (●), 2.7 wt% Pd on $\gamma\text{-Al}_2\text{O}_3$

(b) (○), 20 wt% Pd on ThO_2 , (●), 2.7 wt% Pd on $\alpha\text{-Al}_2\text{O}_3$

Fig 1.1 Plots of the logarithm of reaction rate versus reciprocal temperature for the oxidation of CH_4 over Pd catalysts (9)

The value of the transition temperature depended on the catalyst, the support and the composition of the reaction mixture. At this transition temperature Pt catalysts underwent a sudden increase in activity. For example over a 3 wt% Pt/ThO₂ catalyst CH₄ conversion doubled between 642K and 647K, while over a 2.7 wt% Pt/γ-Al₂O₃ catalyst conversion increased by a factor of eight between 610K and 673K. Pd catalysts were found to undergo a much more gradual increase. Below the transition temperature, the activation energies for Pt catalysts were higher than those for the Pd catalysts while above the transition temperature the reverse was found to be the case. The activation energies over a 2.7 wt% Pt/TiO₂ in the low and high temperature region were 116 ± 4 kJ mol⁻¹ and 19 ± 2 kJ mol⁻¹ respectively whereas for the corresponding Pd catalyst values for the low and high temperature region of 83 ± 5 kJ mol⁻¹ and 35 ± 3 kJ mol⁻¹ respectively were determined.

The adsorption of oxygen by the supported precious metal catalysts was also studied. Again it was observed that the amount of oxygen adsorbed depended on the precious metal, its loading and the support material used. For example it was found that based on metal loading, weight for weight a Pd/γ-Al₂O₃ adsorbed approximately 100 times more oxygen than the Pt/Al₂O₃. Pd samples were found to take up more oxygen when supported on γ-Al₂O₃ than when supported on TiO₂, ThO₂ or when unsupported, despite the fact that γ-Al₂O₃ was not found to adsorb oxygen on its own. A direct correlation could be made between the amount of oxygen adsorbed at various temperatures and the extent of CH₄ conversion for supported Pd samples see Fig 1.2

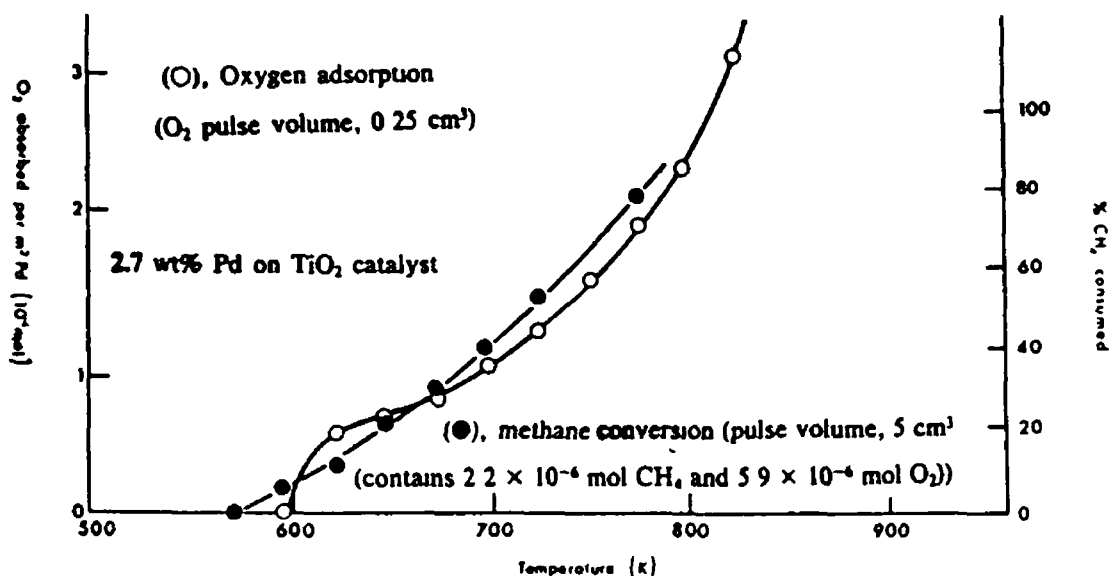


Fig.1.2 . Correlation between the amount of O₂ adsorbed at various temperatures and the extent of CH₄ conversion for supported Pd catalysts (9)

The differences in catalytic activity between Pt and Pd were attributed to differences in the ability of the metals to adsorb oxygen prior to reaction (9) The oxidation activity for CH₄ of Pt(IV) oxide and Pd(II) oxide was also investigated The former oxide was found to be more active, requiring a much lower temperature for the oxidation reaction to occur Using a 0.5 cm³ pulse containing 1.04 x 10⁻⁶ mol CH₄, a 2.7 wt% PtO₂/ThO₂ catalyst converted 3 x 10⁻⁷ mol CH₄ at 550K while this level of conversion was achieved over a 2.7 wt% PdO/ThO₂ at a temperature of above ca. 650K The order of reaction over these samples with respect to CH₄ was determined to be 0.6 and 0.8 respectively for Pt(IV) and Pd(II) oxide Prolonged exposure of the precious metals to O₂ at high temperature caused structural changes in the Pd samples which did not occur in the Pt samples Fresh Pd(II) oxide samples consisted of particles of approximately 250µm in diameter, but when exposed to O₂ at 775K particles agglomerated to form loosely bound clumps of ca. 2mm in diameter However the rate of CH₄ oxidation was found to be independent of the metal particle size under CH₄ rich conditions Although the average diameter of metal particles in a 2.7 wt% Pd/Al₂O₃ increased from 14 to 80 nm after heat treatment between 723-823K, the catalytic activity toward CH₄ oxidation changed little after heat treatment (9)

Anderson and Tsai (19) investigated the oxidation of CH₄ over a number of catalyst samples using a microreactor flow system at a total pressure of 1 atm The products of the reaction were analysed by GC Eight different samples were examined, namely Cr₂O₃ supported on pumice, unsupported MgO, MgO/BaO, acidified ferric sulphate, H-ZSM5 and Pd supported on either γ-Al₂O₃, SiO₂ (with or without added CH₂Cl₂), or charcoal Depending on the sample, reaction temperatures ranged from 495K to 791K and CH₄/O₂ molar ratios were used varying from 99 to 0.28 The %CH₄ conversion varied from 19.1%, over Pd/charcoal at a CH₄/O₂ ratio of 1.68, to 1.2% over H-ZSM5 at a CH₄/O₂ ratio of 8.35 Again no account was taken of the active phase surface area of the catalysts and different reaction conditions were used for different catalysts so no comparison of catalytic activity can be made No attempt was made to study the kinetics of the reaction over these samples (19)

Martí et al (20) investigated Pd/Zr catalysts prepared from Pd₁Zr₃ alloy for CH₄ oxidation under both O₂ lean and rich conditions The catalyst samples were prepared from both amorphous and crystalline alloy samples As a reference material 5 wt% Pd on ZrO₂ was prepared by impregnation of ZrO₂ with (NH₄)₄PdCl₄, followed by calcination in air for 2h at 773K and then reduction in H₂ for 2h at 573K Another reference was prepared by the calcination of water insoluble hydroxides containing 25.6 wt% Pd on ZrO₂ followed by reduction in the same manner as for the first reference sample Kinetic studies were carried out in a

continuous fixed-bed microreactor and the reaction was monitored using an on-line quadrupole mass spectrometer. For reaction under CH₄ lean conditions a gas mixture of composition 1 % CH₄, 4 % O₂ and 95 % He, at a flow rate of 300 cm³min⁻¹, was used and the temperature was increased from 400 to 800K. For experiments under CH₄ rich conditions a gas mixture of 16.64 % CH₄, 2.08 % O₂ and the balance He, was used. In the latter case a total flow rate of 150 cm³min⁻¹ was utilised and the temperature was increased from 673 to 973K. Under CH₄ lean conditions fresh reduced 5 wt% Pd/ZrO₂ exhibited an increase in reaction rate after pretreatment in the reaction mixture for 2h at 723K compared with freshly reduced catalysts. Similar results were obtained for the reference sample prepared by coprecipitation. It was suggested that this was due to a redispersion of Pd under reaction conditions. It was determined that the overall activity of the catalysts prepared from Pd₁Zr₃ was dependent on the activation conditions used, with turnover frequencies ranging from 2 x 10⁻³ to 3.3 x 10⁻³s⁻¹. Activation was either carried out in situ, by heating the catalyst in the reaction mixture at a temperature in the range of 573K to 723K for 2h, or by heating in air for 2h at these temperatures. A sample prepared by in situ activation at 698K of an amorphous alloy precursor was found to be most active exhibiting a turnover frequency of 3.3 x 10⁻³ s⁻¹ and a reaction rate of 1.41 mol(Kg h)⁻¹ compared with values 0.8 x 10⁻³ s⁻¹ and 0.17 mol(Kg h)⁻¹ for 5 wt% Pd/ZrO₂. It was suggested that the higher activity of the alloy catalysts under these conditions was derived from the extremely large interfacial area between the Pd and PdO phases and ZrO₂ (20)

Under CH₄ rich conditions only three catalyst samples were examined, namely the two reference samples (5 wt% Pd/ZrO₂ and 25.6 wt% Pd/ZrO₂) and an alloy sample which was activated in situ at 623K. There were high product selectivities for CO and H₂ over all the catalysts examined (23.3 - 24 % CO and 23.6 - 24.2 % H₂). The alloy sample was less selective for CO than the two reference samples, 23.3 % compared with 24.2 % and 24.0 % respectively over 25.6 % Pd/ZrO₂ and 5 % Pd/ZrO₂. Above 870K the reaction was influenced by the formation of carbonaceous deposits but the effect of the carbonaceous deposits was not reported (20)

The catalytic reactivity of a series of La based perovskite-type oxides for CH₄ oxidation have been investigated and compared with that of a 1 wt% Pt/Al₂O₃ catalyst (21). The Pt sample was prepared by an impregnation method followed by drying and reduction in H₂ at 773K or 1473K. Perovskite samples were prepared by decomposition of metal acetates and/or nitrates, followed by drying and calcination at either 1123K or 1473K. Reactivity was measured in a quartz reactor using a gaseous mixture of CH₄ and air at a space velocity of

between 45000 and 50000 hr⁻¹. The oxidation activity was defined as the temperature at which 50 % conversion was attained. The order of increasing catalytic activity was as follows (21)



The activities for cation substituted perovskite-type oxides was also examined and it was found that their activity was strongly affected by the nature of foreign cation as well as by its amount. Although LaMnO₃ was less active than the Pt sample, the catalytic activity increased as La ions were substituted by Sr ions. Among the perovskite-type oxides, Sr²⁺ substituted lanthanum manganate, La_{0.6}Sr_{0.4}MnO₃, was the most active for the oxidation reaction. However at high temperatures, i.e. above 873K, the Pt sample was much more active than any of the perovskite type catalysts. The reaction kinetics were studied and the results obtained could be expressed in the form of equation (I) given previously. However the reaction order with respect to O₂ tended to decrease as the reaction temperature increased. It was found that on Pt/Al₂O₃ samples reaction occurred by a Langmuir-Hinshelwood mechanism (21) in which the surface reaction between adsorbed oxygen and adsorbed CH₄ was the rate determining step. In contrast reaction over the perovskite catalysts could be described by an Rideal-Eley mechanism (21) where adsorbed oxygen was assumed to react with gaseous CH₄. At low temperatures, the reaction involved adsorbed oxygen while the activity of lattice oxygen was negligibly low. With a rise in temperature, the lattice oxygen became reactive and the coverage of adsorbed oxygen decreased. Thus at elevated temperatures the lattice O₂ became the active species and reacted predominantly with hydrocarbon molecules. Although the activity of the adsorbed oxygen increased exponentially as the temperature rose, the surface coverage decreased due to the exothermic nature of the adsorption process. Thus the kinetics of the reaction of CH₄ oxidation over perovskite type oxides could be explained by parallel reactions of adsorbed O₂ and lattice O₂ (21)

Doshi et al (22) examined the CO and CH₄ oxidation properties of p-type and n-type conducting La - based perovskites, K₂NiF₄ structures and solid electrolyte compositions in the perovskite family. For CH₄ oxidation, reaction was studied by passing a mixture of 2 % CH₄ and 98 % air at 100cm³min⁻¹ through a reactor. The temperature was raised from room temperature in steps of 20K at a rate of 2Kmin⁻¹ and reaction was monitored by gas chromatography. For CH₄ oxidation it was determined high conductivity, such as that exhibited by K₂NiF₄ superconducting oxides and some perovskite oxides did not lead to high catalytic activity. Higher activity was exhibited by p-type or n-type conductors which

possessed good oxide ion conduction coupled with poor electronic conductivity. Examples were $\text{LaFe}_{0.8}\text{Nb}_{0.2}\text{O}_{3-\delta}$ and $\text{La}_{0.8}\text{Sr}_{0.2}\text{YO}_{2.9}$. However both 0.5 wt% Pt and 0.5 wt% Pd supported by Al_2O_3 were more active, giving complete CH_4 conversion below 800K whereas complete conversion could not be achieved over the other catalyst samples examined at comparable or higher temperatures (22).

Zhang et al (23) examined the CH_4 oxidation activity of supported $\text{La}_{0.8}\text{Sr}_{0.2}\text{MnO}_3$ with loadings between 0 and 50 wt%. The influences of Mn_2O_3 pretreatment and calcination temperature on catalytic activity were determined. The support material used was either untreated $\text{La}_2\text{O}_3 \cdot 19\text{Al}_2\text{O}_3$ or the same material supporting 10 or 20wt% Mn_2O_3 . The catalysts were prepared by the citrate process, in which the support was suspended in an aqueous solution of citric acid to which an aqueous solution containing the nitrates of the required component metals were added. After evaporation to dryness the samples were calcined at 773K for 1h, followed by a further calcination for 2h in air at temperatures ranging from 873K to 1473K. For comparison the activity of a 1.1 wt% Pt/ Al_2O_3 commercial catalyst was also examined. CH_4 activity measurements were carried out in a flow reactor using a reactant mixture containing 2.5 vol% CH_4 , 20 vol% O_2 and 77.5 vol% N_2 , at a flow rate of $60 \text{ cm}^3 \text{ min}^{-1}$. The activity of the supported perovskite catalyst was enhanced by support pretreatment with Mn_2O_3 , to a level which could not be reached by supported $\text{La}_2\text{O}_3 \cdot 19\text{Al}_2\text{O}_3$ or Mn_2O_3 . The % conversion of CH_4 at 673K over 20 wt% $\text{La}_{0.8}\text{Sr}_{0.2}\text{MnO}_3/\text{La}_2\text{O}_3 \cdot 19\text{Al}_2\text{O}_3$ was ca. 30% compared with ca. 60% over the same catalyst pretreated with 10 wt% Mn_2O_3 . The high catalytic activity was believed to be contributed to both by the supported perovskite and the supported Mn_2O_3 . In general for all catalysts examined calcination at temperatures of 1073K and above resulted in a decrease in activity although pretreatment with Mn_2O_3 increased thermal stability compared with identical unpretreated samples. Finally it was found that $\text{La}_{0.8}\text{Sr}_{0.2}\text{MnO}_3$ was more active than the 1.1 wt% Pt/ Al_2O_3 catalyst. The temperature at which 30% CH_4 conversion occurred over the commercial Pt/ Al_2O_3 , calcined at 873K, was ca. 380K compared with a value of 350K for the supported perovskite sample, calcined at the same temperature (23).

Hexa-aluminates, $\text{M}'\text{O} \cdot 6\text{Al}_2\text{O}_3$, and substituted hexa-aluminates, $\text{M}'(\text{M}'')_x\text{-Al}_{11-x}\text{O}_{19-\alpha}$ ($\text{M}' = \text{Ba, Sr, Ca}$, $\text{M}'' = \text{Cr, Mn, Fe, Co, Ni}$) are other catalytic systems which have been investigated for the complete oxidation of CH_4 . Machida et al (24) investigated a series of cation substituted Ba hexa-aluminates, $\text{BaMAl}_{11}\text{O}_{19-\alpha}$ ($\text{M} = \text{Cr, Mn, Fe, Co and Ni}$), for the high temperature combustion of CH_4 . The samples were prepared by the hydrolysis of the appropriate metal alkoxides. All the samples were calcined at 1573K. Catalytic

activity was measured using a continuous flow system with a reaction mixture of 1 vol% CH₄ and 99 vol% air, at a flow rate of 48000 cm³ h⁻¹. Activity was expressed as the temperatures at which 10% and 90% CH₄ conversion were attained, (T_{10%} and T_{90%} respectively). The results determined for surface areas and CH₄ combustion activities for the catalysts in the study are given in Table 1.0. The catalyst containing Mn was most active, followed by Fe and Co. The rapid increase in activity of the samples was thought to be due to their larger surface area as the combustion was believed to proceed via homogeneous gas-phase reaction initiated by radical formation at the catalyst surface. The large surface area appeared to significantly promote the radical formation. The activity of the cation substituted hexa-aluminates appeared to be related to the reduction/oxidation behaviour of the transition elements within the crystal lattice. The high catalytic activity of the Mn substituted catalyst was believed to be due to the reversible oxidation/reduction cycle of Mn between the di- and tri-valent states (24).

Table 1.0 Surface areas and CH₄ combustion activities of BaMAl₁₁O_{19-α} (24)

Cation Substituted M	Surface Area ^a (m ² g ⁻¹)	T _{10%} * (K)	T _{90%} * (K)
Al	15.3	983	1003
Cr	15.7	973	1043
Mn	13.7	813	1013
Fe	11.1	833	1053
Co	15.2	963	993
Ni	11.1	983	1043

Note ^a = After calcination at 1573K

* = Temperatures at which conversion levels were 10% and 90%

Hicks et al (25) undertook a study to characterise the effect of catalyst structure on the intrinsic activity of Pt and Pd for CH₄ oxidation. They compared turnover frequencies over Pt and Pd supported on α-AlOOH, γ-Al₂O₃, ZrO₂ and 12% Y₂O₃/ZrO₂. The metals were deposited on the supports by ion exchange or incipient wetness impregnation. The catalyst samples were dried at 373K overnight and then calcined in air at 773K or 973K for 2h. The metal dispersion of each sample was determined by volumetric chemisorption. Rates of CH₄ oxidation were measured using a fixed bed micro-reactor. CO₂ was the only reaction

product observed. Reaction temperatures ranged from 623K to 643K for Pt and 533K to 623K for Pd. Infrared spectra of adsorbed CO were also recorded. Activity was measured as turnover frequencies calculated as the number of moles of CO₂ formed per second per mole of surface Pt or Pd atoms present initially, at 608K. For Pt catalyst samples there appeared to be no correlation between dispersion and turnover frequency. For example 0.84 % Pt/Al₂O₃ and 0.3 % Pt/ZrO₂ both had high dispersion, 90 % and 100 % initially, however the latter sample had a turnover frequency of 0.05 s⁻¹ while the former sample had a turnover frequency of 0.005 s⁻¹ at the same temperature. However the oxidation reaction was found to be structure sensitive over Pt catalysts. Two types of Pt were found to be present in the samples examined: firstly a dispersed phase, which was characterised by a narrow IR band at 2068 cm⁻¹ for adsorbed CO and was converted to PtO₂ under reaction conditions. The other phase was a crystalline phase, characterised by an IR band for adsorbed CO at 2080 cm⁻¹, which under reaction conditions was covered by a layer of adsorbed oxygen. The dispersed phase was 10 to 100 times less active than the crystalline phase. For Pt samples containing the dispersed phase turnover frequencies ranged from 0.001 s⁻¹ to 0.01 s⁻¹ while over the crystalline phase turnover frequencies of between 0.05 s⁻¹ to 0.10 s⁻¹ were determined.

For the CH₄ oxidation reaction over the dispersed phase the average apparent activation energy was found to be between 33 kcal mol⁻¹ and 39 kcal mol⁻¹ while a value of 28 kcal mol⁻¹ was measured for the crystalline phase. Whether or not the dispersed or crystalline phase was formed depended more on the support material and the manner of preparation than on the degree of dispersion of the Pt on the support. For example three of the catalysts were prepared by the ion exchange of chloroplatinic acid H₂PtCl₆·6H₂O on an Al₂O₃ support. Two calcined in air at 773K contained the dispersed phase while one calcined at 973K contained large crystallites with low dispersion. A sample prepared by depositing a Pt amine complex, Pt(NH₃)₄Cl₂, onto α-AlOOH (precalcined at 1323K for 2h in air) contained the crystalline phase (25).

For Pd catalysts, turnover frequencies were found to depend on the size of the metal crystallites and possibly on the distribution of sites on the metal surface (25). Samples which consisted of low concentrations of small Pd particles, highly dispersed on γ-Al₂O₃ had low CH₄ oxidation activity. By contrast three samples which consisted of large Pd crystallites exhibited high activity. Under reaction conditions, the small crystallites on Al₂O₃ were converted into dispersed PdO, while larger crystallites are converted to smaller ones covered with adsorbed oxygen. The results indicated that CH₄ oxidation activity over dispersed PdO was 10 to 100 times lower than over small Pd crystallites, with an average turnover

frequency 0.08 s^{-1} over the PdO phase compared with 1.3 s^{-1} over the crystallite phase. The size of the Pd crystallites which could be stabilised on the supports, depended on the support composition and the method of preparation. For example small crystallites of Pd were produced by the ion exchange of a small amount of Pd (H_2PdCl_4), less than 0.5 wt%, onto high surface area $\gamma\text{-Al}_2\text{O}_3$. On the other hand large crystallites were produced by depositing a large amount of Pd, 2.3 wt%, on $\gamma\text{-Al}_2\text{O}_3$ or by depositing Pd onto low surface area $\alpha\text{-AlOOH}$ or ZrO_2 support material (25).

Briot et al (26) studied the effect of particle size on the oxidation of CH_4 over $\text{Pt/Al}_2\text{O}_3$ catalysts and also found that the reaction was structure sensitive. The catalysts were prepared by wet impregnation of the support material, which was a mixture of γ - and δ - Al_2O_3 , with aqueous solutions of H_2PtCl_6 a concentration which resulted in a final Pt loading of 1.95 wt%. Subsequently the catalysts were dried at 370K, calcined in N_2 at 770K and reduced in H_2 at the same temperature overnight. The activity measurements were carried out in a continuous flow reactor using a reactant mixture of CH_4 , O_2 , N_2 in the ratio 1:4:95 vol/vol/vol, at a flow rate of $6.3\text{ dm}^3\text{ h}^{-1}$. They found that when samples were exposed to the reactant mixture for 14h, then purged in N_2 at the same temperature and finally cooled to room temperature, they were more active at temperatures between 570K and 720K than catalysts which did not undergo this treatment. In the above temperature range the apparent activation energy for CH_4 oxidation over the untreated catalysts was 24 kcal mol^{-1} compared with 17 kcal mol^{-1} over the treated catalysts. For the catalysts which underwent this pre-treatment the mean Pt particle size increased from 2 to 12 nm. It was thus concluded that large Pt particles were more active for CH_4 oxidation than small ones. Microcalorimetric measurements of the heat of oxygen chemisorption, Q_{ads} , indicated that there was a small decrease in Q_{ads} as the Pt particle size increased from 2 to 12 nm. Hence one reason why large Pt particles were more active was because the Pt - O bond strength was lower on these particles compared with that on the smaller ones. It was also pointed out that an increase in Pt particle size with faceting of crystallites could have led to the existence of preferentially exposed crystal planes which could have been responsible for the increase in activity (26).

In a subsequent study Briot and Primet (27) found that $\text{Pd/Al}_2\text{O}_3$ also exhibited this behaviour for CH_4 oxidation. Apart from the fact that the catalysts contained 1.95 wt% Pd, the conditions used for preparation, activation and activity measurement were the same as those used in the previous investigation (26). Again pre-treatment of catalyst samples in the reactant mixture at 873K resulted in an increase in activity compared with untreated catalysts and the mean Pd particle diameter increased from 7nm to 16nm. Temperature programmed oxidation

studies indicated that the Pd was in the form of bulky PdO for temperatures of reaction higher than 673K. The formation of PdO was found to be favoured on the 16nm Pd particles compared with the 7nm particles. For activation it was determined that aging in both reactants at 873K was required. The main conclusion of the study was that the catalytic oxidation of CH₄ over supported Pd occurred on a PdO phase in an O₂ rich reactant mixture, even if the catalyst was initially in a reduced form (27)

In contrast Baldwin and Burch (28) found an absence of particle size effects for the oxidation of CH₄ over Pd/Al₂O₃ catalysts. They prepared catalysts containing either 1 or 5wt% Pd by wet impregnation of either δ -Al₂O₃ or γ -Al₂O₃ using solutions of PdCl₂ acidified with HCl. After drying at 383K overnight the catalysts were calcined at different temperatures and various lengths of time, ranging from 873K to 1123K and from 1h to 24h respectively. Activity analysis was carried out under continuous conditions using a 1% CH₄ / 99% air gas mixture. They found that their catalysts activated under reaction conditions, i.e. at 673K with the reaction gas mixture, but not when equivalent heat treatments in air alone were carried out, in agreement with Briot and Primet (27). They also determined that there was no correlation between Pd particle size and activity and that Pd supported on δ -Al₂O₃ was considerably more active than Pd supported on γ -Al₂O₃. The latter fact was thought to be due to differences in the morphology of the Pd catalysts on the different supports rather than a direct support effect (i.e. where the support is directly in the reaction scheme compared with an indirect support effect where the support modifies the active phase) (28)

In a further investigation Baldwin and Burch (29) examined the effects of using different Pd precursor salts and different support materials in the preparation of Pd catalysts for CH₄ combustion. Catalysts were prepared with a nominal Pd loading of 5wt%. Two Pd precursor salts were used, namely PdCl₂ and Pd(NO₃)₂. The supports examined were SiO₂ and γ -Al₂O₃. Catalyst samples were calcined at different temperatures, between 673K and 873K, for 16h. Activity measurements were carried out in the same manner as in the previous study (28). Both the precursor salt and the support affected catalytic activity. An Al₂O₃ supported sample prepared using the nitrate precursor salt activated after 40h in the reaction mixture at 623K, from an initial CH₄ conversion of 18.8% increasing to 80%. In contrast a similar sample, prepared using the chloride precursor, was still activating after 65h at 623K, from an initial conversion of 4.6% up to 86% after 65h. Under reaction conditions activation was found to occur over long periods of time (5 to 8 days) for Al₂O₃ supported catalysts while for SiO₂ supported samples activation was much quicker (within minutes or hours). For the Al₂O₃ supported samples the area specific rate constants increased by a

factor of 90 after activation in the reaction mixture at 678K for 60h. The removal of chlorinated species under reaction conditions was found to be unimportant in causing activation. It was suggested that reconstruction of the catalyst under reaction conditions accounted for this phenomenon, with SiO_2 supported samples being reconstructed more easily than the Al_2O_3 supported catalysts, resulting in activation occurring over shorter periods of time. Speculative mechanisms for this reconstruction included chemisorption of an atom or molecule which would cause localised restructuring of surface atoms around the adsorption site (driven by the energy evolved upon oxidation), or carbon deposition on the catalyst surface causing a re-ordering of the surface of the PdO (29).

In a previous study Yao (30) also considered the effect of catalyst structure on the complete oxidation of a number of hydrocarbons including CH_4 . Precious metal wires (Pt, Pd and Rh), wound into spirals, were used as unsupported catalysts. Supported Pt, Pd and Rh catalysts were prepared by the deposition of the metals on either Al_2O_3 or Al_2O_3 which had added CeO_2 . The supported catalysts were calcined in air at increasing temperature steps of 873K, 973K, 1073K and 1173K, each step lasting 4h in duration. Reaction was studied using a quartz flow reactor. Helium was used as the carrier gas, containing the reactant gases which were passed through the catalyst at atmospheric pressure. The dispersion of the precious metal on the catalyst was determined by CO chemisorption at 298K after pre-reduction in hydrogen at 773K. Kinetic parameters for the study were obtained using O_2 /hydrocarbon ratios of 0.7 to 5 times the stoichiometric ratio for each alkane. Turnover numbers were calculated on the basis of moles of CO_2 produced per second minus the total number of moles of precious metal in the catalyst or on the catalyst surface. For precious metal wires the turnover numbers obtained were 5.4 s^{-1} (measured at 673 K), 0.52 s^{-1} and 0.13 s^{-1} (both measured at 773K) for Pd, Rh and Pt respectively. Values for the activation energies determined at the same temperatures were 17, 24, and 21 kcal mol^{-1} for Pd, Rh, and Pt wires respectively. The total reaction order for CH_4 over all the precious metal wires was determined to be positive and less than or equal to one. For the supported catalyst samples the kinetic data was found to be similar to that over the wires. For example the activation energies for supported 0.038 wt% Pd/ Al_2O_3 , 0.03 wt% Rh/ Al_2O_3 and 0.22 wt% Pt/ Al_2O_3 were determined to be 17, 23, and 24 kcal mol^{-1} respectively. However the rate per surface precious metal atom over each supported catalyst was less than for the corresponding wire samples. For example over Pt/ Al_2O_3 the turnover numbers were lower by just less than a factor of eight than those over Pt wire samples, while those over Pd/ Al_2O_3 were at least two orders of magnitude lower than Pd wire samples. Over Pt and Pd catalysts the ratio of turnover numbers for

supported catalysts compared with turnover numbers over the corresponding wire samples increased with decreasing dispersion. The turnover numbers for Rh were also lower when the sample was supported compared with unsupported samples.

Under reaction conditions $\text{CeO}_2/\text{Al}_2\text{O}_3$ supported Pt and Pd were less active than the corresponding samples supported on Al_2O_3 alone, while in contrast the Rh samples were slightly more active with CeO_2 . For Pd and Pt the kinetics of the reaction were different on the $\text{CeO}_2/\text{Al}_2\text{O}_3$ supported samples than with wires or supported on Al_2O_3 alone. For example the order with respect to O_2 and CH_4 during reaction at 1073K over 0.154 wt% Pd, 20 wt% $\text{CeO}_2/\text{Al}_2\text{O}_3$ was 0 and 0.5 respectively, compared with the corresponding values of 0.1 and 0.8 respectively for reaction at between 623K and 773K over Pd wire. However this difference could be removed by reduction of the catalyst in CO for a few minutes at 573K. Thus it was thought that Pt and Pd were in an oxidised state after interaction with CeO_2 and that the oxidised state was less active than that of the metal or the Al_2O_3 supported metal particles (30).

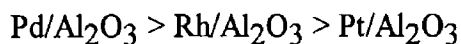
For all the samples examined (30) the differences in activity were explained in terms of oxygen coverage, since the slow step of the alkane oxidation was the dissociative chemisorption of the alkane on the bare metal surface with the breakage of the weakest C - H bond followed by its interaction with adsorbed oxygen on an adjacent site. If the precious metal surface atoms were sites for both O_2 and hydrocarbon chemisorption, then they would compete with each other and their surface coverage would have been interdependent. Compared to Pd and Rh, it was stated that Pt had a higher ionisation potential and its oxide was less stable. Hence the oxygen coverage would have been expected to be less than that for Pd or Rh and more dependent on the O_2 /hydrocarbon ratio and the ease of chemisorption of hydrocarbon (30).

Ribeiro et al (31) claimed that the variation in catalytic activity for CH_4 oxidation reported in the literature was due to different levels of approach to high activity steady state measurements. They studied the oxidation of CH_4 over Pd/ZrO_2 and $\text{Pd}/\text{SiO}_2\text{-Al}_2\text{O}_3$ catalyst samples. All catalysts were prepared by incipient wetness using aqueous solutions of $\text{Pd}(\text{NH}_3)_2(\text{NO}_2)_2$ or PdCl_2 and were calcined at temperatures ranging from 773K to 1123K. Activity measurements were carried out at atmospheric pressure, using a down flow, tubular, stainless steel, fixed bed reactor. They found that there was only a small change in the turnover frequencies when the support, the Pd precursor and the particle size were taken into account. Turnover frequencies ranged from 2×10^{-2} to $8 \times 10^{-2} \text{s}^{-1}$ for CH_4 oxidation under the experimental conditions used, i.e. 2% CH_4 in air at 550K. It was therefore concluded that the oxidation reaction over Pd was structure insensitive under steady state conditions. The large variations for turnover

frequencies reported in the literature were attributed to the use of incompletely activated samples. The oxidation reaction was found to be strongly inhibited over PdO by both CO₂ and H₂O. Treatment of the samples in air at atmospheric pressure and temperatures below 1000K led to the formation of a stable PdO phase which spread as a monolayer on the support surface and had low activity (31).

Oh et al (32) carried out a study on CH₄ oxidation with a single-component noble metal catalysts over wide ranges of temperature and feedstream stoichiometries. Pt, Pd and Rh catalysts were prepared using the technique of incipient wetness on γ -Al₂O₃ spheres or Ce modified γ -Al₂O₃ spheres. Activities were measured using an integral flow reactor system, using 15cm³ of catalyst and a total flow rate of 13 dm³min⁻¹, giving a space velocity of 52000 h⁻¹. The composition of the feed stream was 0.2 vol% CH₄, 0.1 vol% CO (if present) and variable amounts of O₂ in a He carrier stream. Two types of experiment were used to characterise the catalyst activity, one where the feed stream composition was kept constant while the temperature was varied and the other where the feed stream composition was varied at a fixed temperature.

When a feed stream containing 0.2 vol% CH₄, 0.1 vol% CO and 1.0 vol% O₂ was passed over the Al₂O₃ supported noble metal catalysts, temperatures >773K were required for 50% CH₄ conversion. In this excess O₂ atmosphere the catalysts did not light off. The activity of the samples supported on Al₂O₃ was in order of decreasing activity

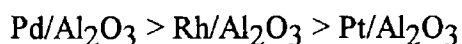


Above 573K, CO₂ was the only product detected in the effluent stream indicating that complete oxidation was occurring (32).

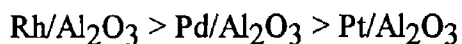
In a reducing atmosphere composed of 0.20 vol% CH₄, 0.10 vol% CO and 0.33 vol% O₂ the temperature required for the onset of CH₄ oxidation over each Al₂O₃ supported sample was similar to that under the oxidising conditions (32). However once reaction occurred, CH₄ conversion increased more sharply with temperature, levelling off between 80 and 90% conversion at temperatures greater than 823K. At temperatures above 773K conversion over each noble metal catalyst was greater than in the oxidising atmosphere. This indicated that CH₄ conversion was sensitive to the stoichiometry of the reaction mixture. In order to explore this phenomenon further, experiments were carried out in which the temperature was kept constant while the O₂ concentration of the reaction mixture was varied. It was determined that over each noble metal CH₄ conversion went through a maximum at an O₂ concentration of somewhat less than the stoichiometric value of 0.45 vol%, i.e. a net reducing atmosphere. Addition of

more O₂ led to a decrease in CH₄ conversion. For example for Pt/Al₂O₃ and Rh/Al₂O₃ maximum conversion of CH₄ occurred with a reaction mixture composition of between 0.40 vol% and 0.42 vol% O₂, while over Pd/Al₂O₃ optimum O₂ composition was lower at 0.35 vol% (32)

Experiments were also carried out with reaction mixtures devoid of CO as part of the same study. Over each noble metal CH₄ oxidation occurred at a temperature comparable to that required for reaction under the CO containing reaction mixture. For the noble metals the activity pattern at 823K was in the order



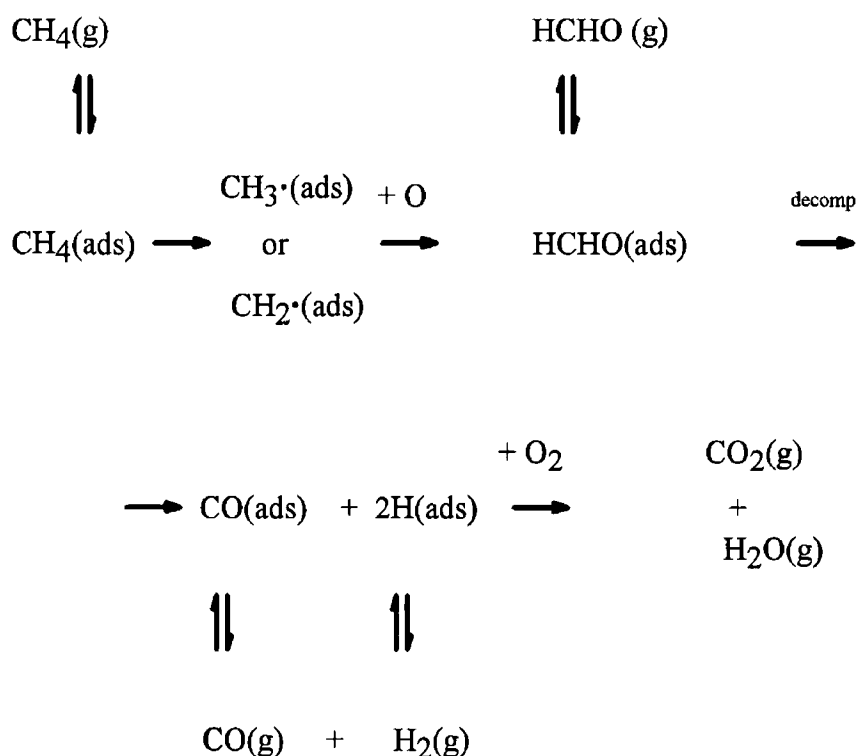
CO₂ was found to be the only reaction product indicating that total oxidation was occurring under oxidising conditions and similar asymptotic CH₄ conversion levels of ~ 90 % for temperatures above 823K were observed, compared with reaction where CO was present. However there was a sharper drop in CH₄ conversion at the lower O₂ concentration in the absence of CO than in the presence of CO. Under reducing conditions indications that partial oxidation was occurring were observed. CO and H₂ were the principal partial oxidation products and the tendency to form partial oxidation products decreased in the order (32)



Ce promoted catalysts were also investigated (32). The addition of Ce led to the retardation of the oxidation of CH₄ over Pt/Al₂O₃ and Pd/Al₂O₃ under oxidising conditions, whereas little effect was observed for Rh/Al₂O₃ samples. The most dramatic effect was observed over Pd/Al₂O₃ samples, where there was a 200K increase in the temperature required to reach 50% conversion of CH₄, compared with reaction over samples without Ce addition. The activity pattern changed from Pd > Rh > Pt, for samples without Ce additions to Rh > Pd = Pt for samples with Ce. For each noble metal catalyst the temperature required for the onset of the CH₄ reaction in the reducing feedstream was little affected by the presence of Ce, but at high temperature CH₄ conversion levels over Pt/Ce/Al₂O₃ and Pd/Ce/Al₂O₃ (~ 65%) were substantially lower than the Ce free catalysts (85 - 90%). It was proposed that this loss in activity for Pd was due to the tendency of Ce to promote the formation of a Pd bulk oxide, which was much less active for CH₄ oxidation than surface oxygen adsorbed on Pd crystallites. A similar argument was made for the deactivation of Pt samples on the addition of Ce (32). Although Ce may have interacted with Rh in a similar manner to Pt and Pd, since

the oxidation state of the Rh/Al₂O₃ surface changed readily in response to the composition of the reaction gas mixture above 473K, the extent and the stability of Rh oxide formation under the reaction conditions was likely to be dominated by the stoichiometry of the reactant gas mixture rather than by the presence of Ce (32)

A reaction mechanism was proposed for the oxidation of CH₄ over the noble metals (32) Under oxidising conditions the noble metal surface was covered in O₂ and the critical step in the oxidation was the dissociative adsorption of CH₄ onto the oxygen covered surface As the concentration in the feed was decreased below the stoichiometric ratio, however, CH₄ could compete successfully with O₂ for active sites, despite its weaker adsorption strength The adsorption rates for both reactants became comparable giving high reaction rates A further decrease in the inlet O₂ concentration led to an insufficient amount of O₂ surface adsorption and hence low CH₄ conversions Although it was acknowledged that a detailed mechanism was not understood a mechanism was proposed involving the interaction of adsorbed methyl or methylene radicals with adsorbed oxygen on the noble metal surface The proposed mechanism is shown below (32)



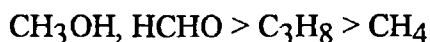
The mechanism was consistent with observed results for CH₄ oxidation under reducing conditions Under the reaction conditions studied it was thought that an adsorbed formaldehyde intermediate, once formed, would rapidly decompose to form adsorbed CO and adsorbed H rather than desorb into the gas phase as formaldehyde (HCHO) molecules It was also suggested that for

Rh/Al₂O₃ samples, but not over Pt or Pd, that the product distribution for CH₄ oxidation was altered by the water - gas shift reaction, i.e.



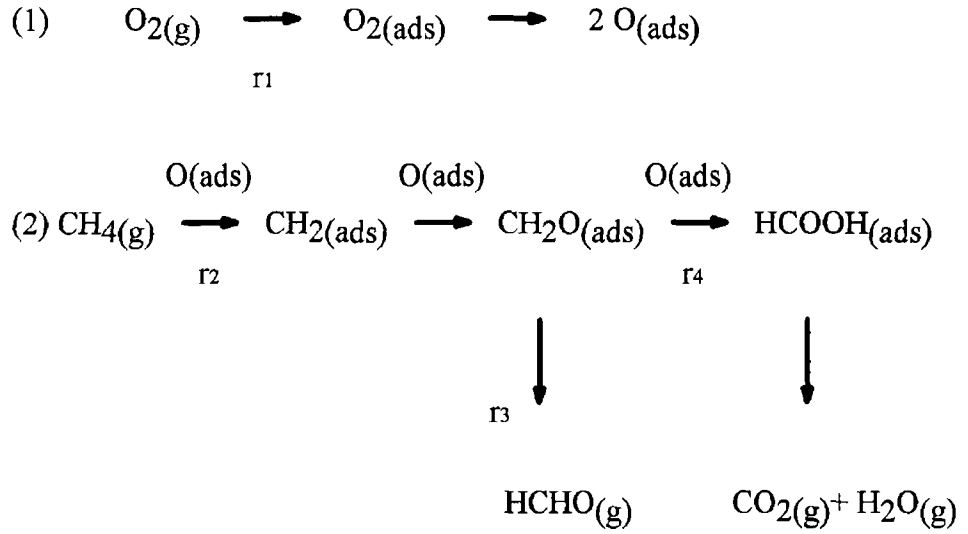
Evidence to substantiate this suggestion came when it was observed that increasing levels of CO₂ in the reaction mixture tended to enhance CO production and suppress H₂ production during CH₄ oxidation, but had no effect on the product selectivity during oxidation over samples of Pt/Al₂O₃ or Pd/Al₂O₃ (32)

An earlier study investigated the CH₄ oxidation reaction under conditions of excess O₂ over Pd catalysts, using a pulse technique (33) It was found that when the ratio of O₂ to CH₄ in the reaction mixture exceeded unity then the catalyst sample suffered bulk oxidation to form PdO At reaction temperatures between 553K and 753K and O₂ to CH₄ ratios of between 3.0 to 0.25 the yield of HCHO as a reaction product was low, less than 0.005 vol% in agreement with the results of Oh et al (32) The oxidation of CH₄ in the presence of propane (C₃H₈), methanol (CH₃OH) or HCHO was also examined In the case of the addition of 7.82 mol% C₃H₈, during reaction at 683K over a Pd sample, the CH₄ conversion dropped from 11.46 %, without C₃H₈ in the reaction mixture, to 7.14 % in the presence of C₃H₈, the latter compound exhibited ca. 10.7 % conversion under the same reaction conditions During reaction at 672K over a sample containing 0.77 % Pd, CH₄ conversion dropped from 6.2 % to 3.75% upon the addition of 4.34 mol% HCHO to the reaction mixture In this case HCHO underwent 100 % conversion under reaction conditions and similar results were obtained when CH₃OH was added to the reaction mixture This indicated that the oxidation activity over the Pd samples for the compounds examined in the study was in the order



In agreement with Oh et al (32) the authors (33) believed that the reaction mechanism for CH₄ oxidation involved a parallel - consecutive reaction process However they proposed that the interaction of gas phase CH₄ with adsorbed oxygen was responsible for the formation of the surface intermediate (CH₂O) whereas Oh et al (32) claimed that the latter formed by the interaction of adsorbed CH₄ with adsorbed oxygen This could be explained by the fact that in the latter study (32) the mechanism was for high amounts of CH₄ conversion, while Cullis et al (33) were dealing with low levels of CH₄ conversion

Golodets (6) proposed the reaction scheme shown below for low conversions when a parallel scheme is valid



The methylene radicals were formed due to the interaction of CH₄ with adsorbed oxygen and were then transformed into CH₂O_(ads) species which could either desorb to form HCHO or be further oxidised to CO₂ and H₂O. The equations shown below describe the above reaction mechanism with respect to the rate of CH₄ conversion (equation (III)), to the oxygen coverage of the catalyst surface (equation (IV)), to the rate of HCHO formation (equation (V)) and the rate of CO₂ production (equation (VI))

$$r = k_2 p_{\text{CH}_4} \quad (\text{III})$$

where r is the rate of CH₄ oxidation, k_2 is the rate constant for reaction r_2 shown above and p_{CH_4} is the partial pressure of CH₄

$$\theta = ((k_1 p_{\text{O}_2} / k_2 p_{\text{CH}_4}) / (v + (k_1 p_{\text{O}_2} / k_2 p_{\text{CH}_4}))) \quad (\text{IV})$$

where θ represents the coverage of O₂ on the surface of the catalyst, k_1 is the rate constant for reaction (1), p_{O_2} is the partial pressure of O₂, v represents the number of moles of O₂ reacting per mole of CH₄ and k_2 and p_{O_2} have been explained previously

$$r_{\text{HCHO}} = rk_3 / k_4((k_3/k_4) + \theta) \quad (\text{V})$$

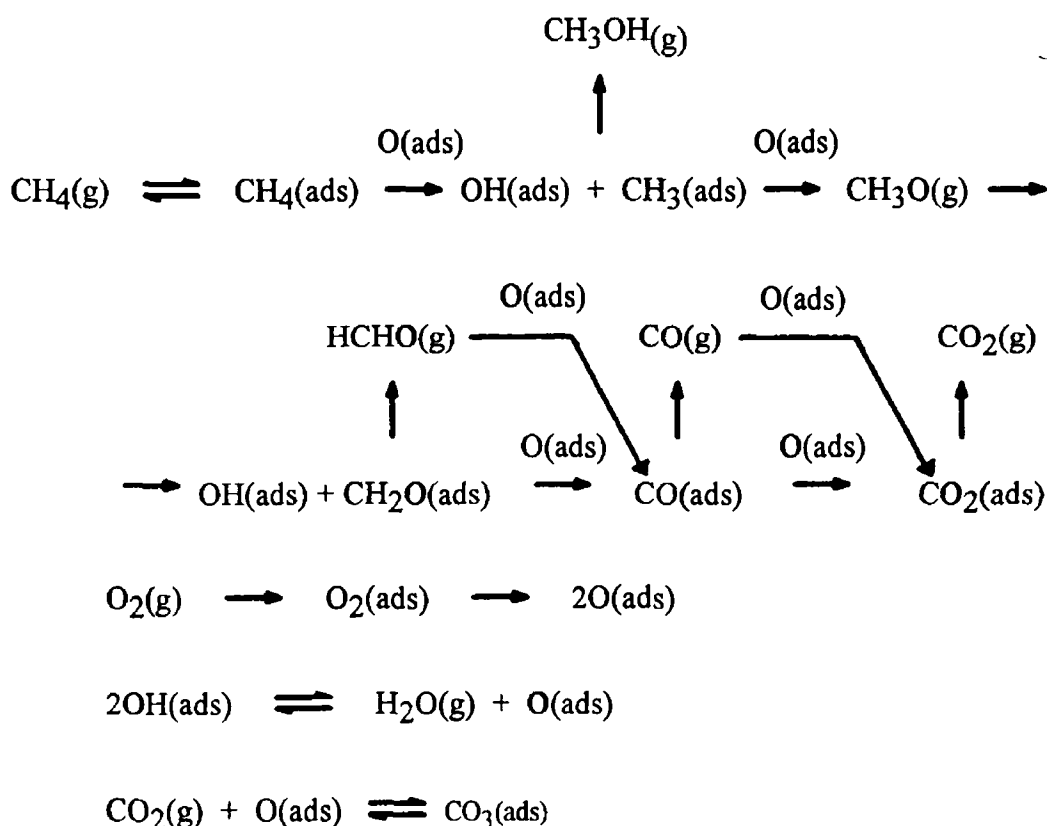
where r_{HCHO} represents the rate of formation of HCHO, k_3 and k_4 are the rate constants for reactions r3 and r4 respectively

$$r_{\text{CO}_2} = r\theta / (k_3/k_4 + \theta) \quad (\text{IV})$$

where r_{CO_2} represents the rate of formation of CO_2 (5)

According to Golodets (6) the experimental data on catalysis over metals and some metal oxides for CH_4 oxidation was described by equation (IV) when θ approximated to unity. On the basis of equations (III) and (IV) decreasing catalytic activity was expected when θ decreased. This also explained the decrease in CH_4 oxidation in the presence of more reactive molecules such as CH_3OH . As the substances interacted more strongly than CH_4 with adsorbed oxygen, this would have led to decreasing θ and hence a decrease in the rate of CH_4 oxidation according to equations (III) and (IV).

A more detailed scheme for the mechanism of the heterogeneous oxidation of CH_4 was also proposed by Golodets (6) involving seven independent routes. The mechanism is shown below



In contrast to the previous reaction mechanism in the above case CH_4 was adsorbed before interacting with adsorbed O_2 but this adsorption was regarded as weak and reversible. The adsorption of CH_4 was assumed to take place in the Henry region so that the surface coverage with CH_4 was negligibly small. Also the above scheme involved a progressive abstraction of H from CH_4 with the formation of adsorbed CH_3 species first rather than adsorbed CH_2 species. Mild oxidation products were unlikely due to the rapid oxidation of surface complexes and of the molecules CH_3OH or HCHO (6)

1.2 Oxidation of Higher Alkanes

Total oxidation of alkanes follows the generalised reaction:



In Table 1.1, the enthalpy changes for the total combustion of various alkanes in the gas phase are given (6). It should be noted that the enthalpy increase with the increasing molecular weight of the alkane while $-\Delta H^\circ_{298}$ per 1 g-atom of oxygen is approximately constant. The metals Pt and Pd have been found to exhibit high catalytic activity for the deep oxidation of alkanes, for example (34, 35, 36, 37, 39).

Table 1.1 : Enthalpy changes for the total gas phase combustion of a number of alkanes (6).

Oxidised Hydrocarbon R	Reaction	$-\Delta H^\circ_{298}$ kcal (mol R) ⁻¹	$-\Delta H^\circ_{298}$ kcal (g· atom O) ⁻¹
Methane	$CH_4 + 2O_2 = CO_2 + 2H_2O$	191.8	47.9
Ethane	$C_2H_6 + 3\frac{1}{2}O_2 = 2CO_2 + 3H_2O$	341.3	48.8
Propane	$C_3H_8 + 5O_2 = 3CO_2 + 4H_2O$	488.5	48.9
n-Butane	$C_4H_{10} + 6\frac{1}{2}O_2 = 4CO_2 + 5H_2O$	635.1	48.9
2-Methylpropane	$C_4H_{10} + 6\frac{1}{2}O_2 = 4CO_2 + 5H_2O$	633.1	48.8
n-Pentane	$C_5H_{12} + 8O_2 = 5CO_2 + 6H_2O$	782.1	48.9
2-Methylbutane	$C_5H_{12} + 8O_2 = 5CO_2 + 6H_2O$	780.1	48.8
2,2- Dimethylpropane	$C_5H_{12} + 8O_2 = 5CO_2 + 6H_2O$	777.4	48.6
Hexane	$C_6H_{14} + 9\frac{1}{2}O_2 = 6CO_2 + 7H_2O$	928.9	48.9
2-Methylpentane	$C_6H_{14} + 9\frac{1}{2}O_2 = 6CO_2 + 7H_2O$	927.2	48.9
3-Methylpentane	$C_6H_{14} + 9\frac{1}{2}O_2 = 6CO_2 + 7H_2O$	927.9	48.9
2,3- Dimethylbutane	$C_6H_{14} + 9\frac{1}{2}O_2 = 6CO_2 + 7H_2O$	926.4	48.8
2,2- Dimethylbutane	$C_6H_{14} + 9\frac{1}{2}O_2 = 6CO_2 + 7H_2O$	924.6	48.7

Hiam et al. (34) examined the oxidation of C_2H_6 , C_3H_8 , $n-C_4H_{10}$, and $i-C_4H_{10}$ alkanes over a Pt filament. The parameter which was measured was the

ignition temperature of each alkane as a function of reactant concentration for various hydrocarbon - O₂ mixtures. The temperature of the filament was increased until reaction occurred. Reaction caused a change in the filament resistance which could be measured. For C₃H₈ the ignition temperature varied from 558K at a hydrocarbon mole fraction of 5.2×10^{-3} to 493K at a hydrocarbon mole fraction of 23.1×10^{-3} . For *n*-C₄H₁₀ the ignition temperature varied from 500K at a mole fraction of 4.2×10^{-3} to 453 K at a hydrocarbon mole fraction of 18.7×10^{-3} . Kinetic data for the oxidation of C₂H₆ and *i*-C₄H₁₀, in addition to the alkanes mentioned above was also determined. The activation energies for the oxidation of C₂H₆, C₃H₈, *n*-C₄H₁₀ and *i*-C₄H₁₀ were reported as 27.3, 17.0, 17.0 and 10.2 kcal mole⁻¹ respectively. The differences in activation energy were thought to reflect the differences in the dissociation energy of the C-H bond during the sorption process. It was concluded that the identical value for the activation energy for both C₃H₈ and *n*-C₄H₁₀ indicated that an identical rate determining step was involved, such as the abstraction of hydrogen from the CH₂ group rather than from a primary carbon atom, as in the case of C₂H₆. In the case of *i*-butane a tertiary carbon atom with its more loosely bound hydrogen atom was believed to be responsible for the marked decrease in activation energy. For the series of alkanes studied the catalytic oxidation rate over Pt was calculated. The rate constants were found to be 4.7×10^{-2} , 46, 140 and 17 cm sec⁻¹ for C₂H₆, C₃H₈, *n*-C₄H₁₀ and *i*-C₄H₁₀ respectively. The low value for *i*-C₄H₁₀ compared with *n*-C₄H₁₀ was attributed to the role of side chain oxidation for *i*-C₄H₁₀ (34).

A mass spectrometer was used to analyse the effluent stream from the reaction vessel which indicated that formation of CO₂ was the only carbon-containing product following ignition. No intermediate oxidation products were detected and this absence was believed to indicate that under their reaction conditions the entire process occurs on the surface of the catalyst (34).

The study was extended to higher alkanes (35). A similar technique was used as above involving measurement of the catalyst ignition temperature, at which the transition from a region of kinetic control, where the kinetics of the reaction controlled the oxidation process, to one of diffusion control, where the diffusion of reactants to and from the surface of the catalyst controlled the reaction. The concentration of the organic reactant was kept at less than 2 vol% of the total gas mixture and the order of reaction was determined in each case for the organic reactant. Since the O₂ content of the gas mixture was kept in excess, the order of reaction with respect to O₂ could not be determined. Again Pt samples in the form of a wire were used, but in addition Pd filaments were also examined (35).

Over Pt, the oxidation of the alkanes *n*-C₈H₁₈, 2,2,4 trimethylpentane (2,2,4 TMP) and 2,3,4 trimethylpentane (2,3,4 TMP) led to the formation of the

reaction products CO_2 , CO and H_2O (as determined by GC and mass spectrometry) and exhibited first order reaction kinetics with respect to the alkane (35). The activation energies for the above reactions were determined to be 17.6, 13.9 and 13.7 kcal mole^{-1} respectively. The oxidation of C_3H_8 , $n\text{-C}_8\text{H}_{18}$ and 2,2,4 TMP over Pd was also studied (35). In this case the activation energies were determined to be 24.4, 26.0 and 39.4 kcal mole^{-1} respectively. The differences in activation energy were related to the C-H bond strengths present in the molecule implying that the primary process in the reaction mechanism was the abstraction of hydrogen. It was concluded that as the activation energy reached a constant or near constant value for the higher alkanes, despite the increase in chain length, then the oxidation mechanism of these compounds have an identical step, namely the abstraction of a H atom from a secondary C atom which is energetically less expensive than abstraction from a primary C atom. The formation of the radical initiates the oxidation process by oxygen atoms chemisorbed on neighbouring sites. It was concluded that complete oxidation was favoured when the metal surface has a fractional coverage with both reactants, hydrocarbon and O_2 . Again the differences in activity between Pt and Pd were attributed to variations in the oxygen surface coverage exhibited by the two metals (35).

Barnard and Mitchell (36) examined the oxidation of $n\text{-C}_7\text{H}_{16}$ on Pt/SiO_2 . A standard flow apparatus was used, with total reactant flow rates in the region of between 25 and 250 $\text{cm}^3\text{min}^{-1}$, and analysis was by GC. Again the rate controlling step was assumed to be the surface reaction between molecularly adsorbed oxygen and the hydrocarbon. A Hougen-Watson rate equation was found to describe the oxidation process (36), i.e.

$$r = (k K_{\text{O}_2} K_R p_{\text{O}_2} p_R) / \{ 1 + K_{\text{O}_2} p_{\text{O}_2} + K_R p_R \}$$

where k = the rate constant of reaction (moles min^{-1}), K_{O_2} = adsorption equilibrium constant for O_2 (atm^{-1}), K_R = the adsorption equilibrium constant for $n\text{-C}_7\text{H}_{16}$, p_{O_2} and p_R = the partial pressures of O_2 and $n\text{-heptane}$ respectively. The values for k , K_{O_2} and K_R were determined to be 9.21×10^{-5} moles min^{-1} , 13.8 atm^{-1} and 20 atm^{-1} respectively. Since K_{O_2} and K_R were approximately equal, it was concluded that the bonding strengths of O_2 and $n\text{-C}_7\text{H}_{16}$ were approximately the same (36).

As already stated Yao (30) examined the oxidation of C_1 to C_4 alkanes at 473K to 773K over Pd, Pt and Rh catalysts. The results indicated that with an increase in alkane chain length the reaction rate increased over each metal and it was concluded that H abstraction was the slow step in the oxidation reaction, because the ease in breaking the C-H bond increases in the same order. For

catalysts in the form of wires, the rate over Pd was an order of magnitude higher than over Rh, while the kinetic parameters for the four alkanes over Pt were different than over the other two metals. The results obtained for the activation energies of the oxidation reactions in the temperature range between 523K and 673K over the wire catalyst samples are shown in Table 1.2

Table 1.2 Activation energies (kcal mole⁻¹) for the oxidation of hydrocarbons over wire catalyst samples (30)

Catalyst (Wire)	Activation Energies for the Oxidation of Hydrocarbons Between 523K and 673K (kcal mole ⁻¹)		
	C ₂ H ₆	C ₃ H ₈	C ₄ H ₁₀
Pd	22	23	26
Rh	18	22	21
Pt	26	22	25

For Al₂O₃ supported catalyst samples the kinetic parameters were similar to those for wire samples. However the rate per surface precious metal atom over each Al₂O₃ supported sample was less than that over the corresponding wire. It was found that the deactivation by the Al₂O₃ support for each precious metal was less for CH₄ than for the larger alkanes. This was consistent with the theory that more adjacent sites are needed for the adsorption of the larger alkanes. CeO₂/Al₂O₃ supported Pt and Pd samples were less active than the corresponding samples without CeO₂. From chemisorption measurements it was found that in general highly dispersed metal sites were not active for alkane oxidation (30)

Otto et al (37) examined the structure sensitivity of C₃H₈ oxidation over Al₂O₃ supported Pt catalysts, ranging in loading from 0.03 wt% to 30 wt% Pt. The samples were calcined in air at 873K prior to reduction in H₂ at 673 K. For the reaction studies a recirculation batch reactor was used and analysis of the reaction was carried out using a mass spectrometer. Initially a mixture of 1.5 mol% C₃H₈ and 15 mol% O₂ was used with Ar as the carrier gas. The oxidation reaction was found to be first order with respect to C₃H₈ and with excess O₂, independent of the O₂ concentration. The conversion of C₃H₈ was examined as a function of Pt particle size. C₃H₈ oxidation activity increased with increasing Pt particle size. The rate constant for the reaction was found to vary between 1.25 x 10⁻³ min⁻¹ over a 0.03 wt% Pt sample to 8.04 x 10⁻³ min⁻¹ over a 30 wt% Pt sample. When dispersion data, obtained using CO chemisorption measurements (based on a CO/Pt ratio of 0.7), was taken into account the reaction rate per

surface atom was calculated to range from $1.15 \times 10^{-3} \text{ min}^{-1}$ to $9.20 \times 10^{-2} \text{ min}^{-1}$ respectively for the samples mentioned above. The apparent activation energy for the oxidation reaction was observed to be unaffected by the concentration of Pt in the samples over which reaction was occurring, remaining constant at $22.1 \pm 3.4 \text{ kcal mol}^{-1}$. Based on the measured reaction kinetics for the C_3H_8 oxidation, the energy associated with the slow step of the reaction mechanism remained the same, which implied that the removal of O_2 from the Pt did not affect the activation energy or that the reaction could not take place on highly dispersed Pt (37).

In the same study (37) the effects of Pt sintering and redispersion on the oxidation of C_3H_8 was also examined. A series of experiments were carried out in which a sample of highly dispersed Pt was sintered in order to observe if there was any increase in the C_3H_8 reaction rate with increasing Pt particle size. This was found to be the case, since over a 0.12 wt% Pt sample the reaction rate increased from $1.5 \times 10^{-3} \text{ min}^{-1}$ to $4.6 \times 10^{-3} \text{ min}^{-1}$ after the sample had been exposed in H_2 at 773 K for 63h. No measurement of Pt particle size was carried out but it was assumed that this increase in rate was due to Pt sintering as a previous TEM study (38) had indicated that heating in H_2 above 773K caused an increase in Pt particle size. The magnitude of the rate change depended on the temperature and time of exposure. Sequential C_3H_8 oxidation isotherms (i.e. after each treatment in H_2) indicated that following the increase in activity due to sintering, there was a decrease in activity which, because of its very gradual nature, could not be explained by poisoning of the metal surface with oxygen. The decrease was attributed to redispersion of Pt under reaction conditions leading to a more dispersed but less active Pt phase (37).

Finally a theoretical reaction site density calculation for three different reaction mechanisms was carried out. These were an Eley-Rideal mechanism (where C_3H_8 molecules from the gas phase reacted with surface oxygen), a mechanism involving a rapid adsorption of C_3H_8 followed by a slow dissociation step and a Langmuir-Hinshelwood mechanism. The latter mechanism was found to be consistent with the empirical data for the amount of surface Pt, where the C_3H_8 was sparsely adsorbed on suitable sites or ensembles, thus explaining the increase in oxidation rate with Pt particle size. It was suggested that surface oxygen facilitated the dissociation of C_3H_8 molecules (37).

Volter et al (39) examined the effects of catalyst pretreatment and reaction conditions with respect to the oxidation of $n\text{-C}_7\text{H}_{16}$ over $\text{Pt}/\text{Al}_2\text{O}_3$. Two types of sample were prepared, one containing 0.5 wt% Pt prepared from a chlorine containing precursor salt and one containing 0.1 wt% or 0.5 wt% Pt, with no chlorine present. A catalyst sample of mass 0.1g was used in a continuous flow system, through which a flow of air or O_2 saturated with 10 Torr $n\text{-C}_7\text{H}_{16}$ was

passed. During a reaction run the sample was heated initially to 623K in O₂ or air and then the *n*-C₇H₁₆ was added. The temperature was then decreased in 10K steps and conversion at each step was determined by GC after 20min. When the lowest temperature was reached at which reaction occurred then the sample was heated up step by step until the original temperature was reached (39)

Calcination in Ar or air was found to have a major effect on the activity of chlorine containing samples. Conversion increased with increasing temperature of calcination, up to 1173K, and also prereduction in H₂ at 773K for samples calcined at low temperature was a means of activating chlorine containing samples. However for chlorine free Pt samples calcination up to 1173K had no effect on conversions *n*-C₇H₁₆. However the addition of chlorine to a sample which had been precalcined at 773K and which was subsequently recalcined at 823K after chlorine addition, led to combustion being poisoned. Similar treatment of a sample precalcined at 1273K had no effect on the combustion activity (39)

A model was proposed for the surface of the catalyst samples where two types of active site were present for *n*-C₇H₁₆ combustion - a Pt (IV) surface complex, formed from the oxidation of highly dispersed Pt in air or O₂ at 773 K, and a poorly dispersed metallic crystalline Pt phase formed from the decomposition of the surface complex due to heating at higher temperatures. The Pt(IV) species was believed to be much less active for combustion. Increasing the calcination temperature would increase the amount of crystalline Pt and thus, as was determined for the chlorine containing Pt samples, the activity would increase. The fact that the activity for the chlorine free samples was nearly independent of calcination temperature was believed to indicate that the number of active sites remained constant and that there was a larger amount of crystalline Pt present initially. However it was also pointed out that the fact that the activity was independent of the thermal treatments may have indicated that a heterogeneous - homogeneous reaction mechanism was occurring over the chlorine free Pt samples. In that case the small amount of crystalline Pt present in the samples would suffice to bring about combustion (39)

After calcination, the dispersion of chlorine free samples was much lower than the chlorine containing samples and the thermal stability of chlorine free samples was found to be distinctly lower than those containing chlorine. The influence of the ratio of O₂ to hydrocarbon was tested by oxidation experiments in pure O₂ or in air. O₂ was found to cause a poisoning effect in some cases. In pure O₂ a chlorine containing Pt sample which was calcined at 773K displayed a low activity for *n*-C₇H₁₆ combustion while in air the identical catalyst was much more active, which implied that activity decreased with increasing O₂ partial pressure. However this effect only occurred with well dispersed samples. For

poorly dispersed Pt samples there was little difference when O₂ or air was used. Again this was explained by different states of Pt being present. With combustion in air a reducing effect of *n*-C₇H₁₆ caused the oxidised Pt to be reduced to active zerovalent crystalline Pt, while combustion in an O₂ atmosphere which was more oxidising led to the formation of the less active Pt(IV) surface complex (39).

Under certain conditions (when the furnace temperature was decreased from 623K to 451K and held constant and using a certain mass of sample) the combustion of *n*-C₇H₁₆ was found to undergo periodic oscillations. The frequency of these oscillations was determined to be 0.8 h⁻¹ and one cycle varied from 10 to 95 % conversion, while the sample temperature varied from 413 to 463K. The only reaction product was CO₂. Again the presence of two types of Pt were used to explain this phenomenon, alternating formation and reduction of Pt(IV). The sample was thought to undergo self heating during increased conversion due to the exothermic combustion and this, allied with a decrease in the amount of *n*-C₇H₁₆ in the reaction atmosphere and hence an excess of O₂ in the reaction mixture, led to the formation of oxidic Pt which was less active. This caused a drop in temperature and *n*-C₇H₁₆ conversion. When the latter reached a minimum, the amount of *n*-C₇H₁₆ in the reaction mixture reached a maximum, the surface reduction effect reached a maximum and the less active Pt(IV) oxide phase was reduced to active crystalline zerovalent Pt and the cycle began once more (39).

However the oxidation of alkanes over Pt has been found to depend on the support as well as the particle size. Hubbard et al (40) found that the rate of C₃H₈ oxidation depended not only on the metal particle size but also on the support material used (Al₂O₃ or ZrO₂). Samples were prepared by multiple impregnation followed by drying at 393K for 2h and calcination at 873K for 20h. The concentration of Pt used ranged from 0.02 to 1.5 wt % Pt. Sample pretreatment, prior to activity analysis using a recirculating batch reactor, involved reduction in H₂ at 673K followed by exposure to O₂ at 773K for 20h. Analysis of reaction products was by mass spectrometry. As with previous studies (37, 41) the oxidation reaction over the Pt/ZrO₂ catalysts was found to be first order with respect to C₃H₈ and the apparent activation energy (17.8 ± 3.5 kcal mol⁻¹ for Pt/ZrO₂, 22.1 ± 3.4 kcal mol⁻¹ for Pt/γ-Al₂O₃) was also found to be in agreement with the values obtained in previous studies for C₃H₈ oxidation over Pt (30, 34, 37, 41). Over the concentration range of Pt used (0.02 to 1.5 wt%) the rate constant decreased by a factor of 20, from 152 × 10⁻³ min⁻¹ for the sample containing 0.02 wt% Pt to 6.55 × 10⁻³ min⁻¹ for the 1.5 wt% Pt sample. Therefore for a given amount of Pt supported by ZrO₂ the rate was fastest over highly dispersed metal and decreased with increasing particle size. It was concluded that ZrO₂ did not inhibit the catalytic activity of highly dispersed Pt.

whereas $\gamma\text{-Al}_2\text{O}_3$ interacted strongly with the latter species and deactivated it. It was proposed that highly dispersed Pt was very active for C_3H_8 oxidation provided an inert support was used. Alternatively, it was pointed out that there could have been a synergistic catalytic enhancement of Pt by a weakly interacting ZrO_2 (40).

In a subsequent study (42) the same authors used C_3H_8 as a model reaction to study the influence of several effects including the Pt concentration and the support material used. The Pt loadings used were 0.03 - 10 wt% Pt/ $\gamma\text{-Al}_2\text{O}_3$, 0.04 - 1.5 wt% Pt/ ZrO_2 and 0.10 - 4.76 wt% Pt/ SiO_2 . They found that for highly dispersed Pt activity decreased in the order

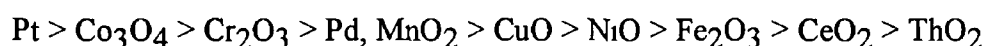
$$\text{Pt/ZrO}_2 > \text{Pt/SiO}_2 > \text{Pt/Al}_2\text{O}_3$$

As expected the activities of the catalysts of high dispersion were more dependent on the support material than samples with low dispersions, since in the former cases the majority of the metal atoms were in direct contact with the support. Thus as the Pt particle size grew the metal support interaction effects decreased. For the three supports examined catalysts with low dispersions ($< 12\%$) exhibited the same specific rate constant for the oxidation of C_3H_8 . However for catalysts with dispersions of 100% the specific rate was 30 times greater over Pt/ ZrO_2 than Pt/ Al_2O_3 . The specific rate was 20 times greater over Pt/ SiO_2 than over Pt/ Al_2O_3 for catalysts with a dispersion of 77%. The activity data indicated that a large fraction of the Pt in contact with $\gamma\text{-Al}_2\text{O}_3$ was deactivated by a metal support interaction. The change in catalyst activity by the support material appeared to be primarily due to a modification in the reaction site density as changes in the apparent activation energy were not observed (42).

Kooh et al (43) investigated the effects of catalyst composition and structure on the rate of $n\text{-C}_7\text{H}_{16}$ oxidation over Pd/ Al_2O_3 , Pt/ Al_2O_3 and Pt/ ZrO_2 catalysts. The precious metal was deposited on the support by either incipient wetness impregnation or ion exchange. All samples were calcined in air at 773K and 1173K for 2h. The rate of $n\text{-C}_7\text{H}_{16}$ oxidation was measured in a fixed bed microreactor loaded with between 0.1 and 0.7g of catalyst pellets and analysis of the reaction products was carried out by gas chromatography using a thermal conductivity detector. The only observed reaction product was CO_2 . For both Pt and Pd catalysts turnover frequencies were obtained and plots of the logarithm of the turnover frequency versus time indicated that for both ZrO_2 and Al_2O_3 supported catalysts there were two sites of high and low intrinsic activity, labelled A and B respectively. On A sites the turnover frequencies for $n\text{-C}_7\text{H}_{16}$ oxidation were found to depend on the composition of the metal (i.e. Pt or Pd) and the

metal particle size At 410K, Pt crystallites were eight times more active than Pd particles of the same size range For both Pt and Pd crystallites, particles larger than 50 Å in diameter were twenty times more active than crystallites smaller than 20 Å in diameter For B sites Pt crystallites were ten times more active than Pd crystallites of the same particle diameter and activity was four times higher on large Pt crystallites rather than smaller ones At the temperatures used in the study, up to 673K, carbon fouled the metal surface and the amount of deactivation depended on the metal particle size For example the coke formation and deactivation rate was much lower on particles of less than 20 Å in diameter than on particles of greater than 50 Å in diameter Another factor which was observed to influence the rate of deactivation was the support composition Using the Al₂O₃ support (83m²g⁻¹) instead of the ZrO₂ support (40m²g⁻¹) for a 5 wt% Pt sample, increased the carbon deposition per surface Pt atom by a factor of five and decreased the deactivation rate by a factor of 5 The kinetics of coke formation and catalyst deactivation were found to differ and it was concluded that carbon formed on the metal particles and migrated slowly to the support Increasing the support surface area (and hence decreasing the density of the metal crystallites) increased the diffusion of carbon to the support The faster the carbon migrated from the metal to the support, the more slowly the metal was poisoned by the carbon (43)

In a study on hydrocarbon oxidation over metal and metal oxide catalysts Moro-oka et al (41) examined the oxidation of C₃H₈ A flow system at atmospheric pressure was used and a gas composition of 50 vol% O₂, 48 vol% N₂ and 2 vol% hydrocarbon was passed through the system The samples examined were Pt, Pd, CuO, Co₃O₄, NiO, MnO₂, Fe₂O₃, Cr₂O₃, CeO₂ and ThO₂ The use of support materials was not reported Irrespective of the catalyst employed the only reaction product of the oxidation reaction was CO₂ Values for both reaction orders and apparent activation energies are given in Table 1 3 The oxidation reaction was found to be approximately first order with respect to C₃H₈ and independent of the O₂ concentration As a measure of activity the reaction rate at 573K was calculated using the activation energies and these are also given in Table 1 3 The order of decreasing activity, for the catalyst samples studied was



However it should be noted that no account was taken of the active surface area of each of the above catalyst samples so that the comparisons are qualitative rather than quantitative

Table 1 3 · Kinetic parameters obtained in C₃H₈ oxidation over Catalysts

(41)

Catalyst	Reaction order in C ₃ H ₈	Reaction order in O ₂	Temperature Range (K)	Apparent Activation Energy (kcal mol ⁻¹)	Log V ₅₇₃ [*] (V in mole (m ² s ⁻¹)
Pt	0 83	-0 09	493-533	17 0	-5 09
Pd	1 30	-1 60	610-641	36 3	-6 99
CuO	0 54	0 16	582-636	28 7	-7 13
Co ₃ O ₄	0 94	0 30	548-614	24 5	-6 76
NiO	0 89	0 40	623-689	26 2	-8 33
MnO ₂	1 01	0 00	567-631	28 3	-7 01
Fe ₂ O ₃	0 68	0 22	668-698	35 9	-8 83
Cr ₂ O ₃	0 78	0 17	556-614	21 9	-6 88
CeO ₂	0 67	0 25	656-723	27 8	-9 21
ThO ₂	-----	-----	646-691	36 8	-9 26

*Note V₅₇₃ represents the reaction rate at 573K calculated from apparent activation energies

A correlation was observed between the activity for hydrocarbon oxidation and the heat of formation of the catalyst oxide per unit oxygen atom, ΔH_O . An example is shown in Fig 1 3 for C₃H₈ oxidation (41). Catalyst samples with higher values for ΔH_O exhibited lower oxidation activity. It appeared that the slow step in of the oxidation reaction mechanism depended on ΔH_O . It was believed that there was a different reaction mechanism over the metals Pt and Pd than over the metal oxide catalysts. Over the latter the slow step in the reaction was the surface reaction between adsorbed oxygen and adsorbed hydrocarbons, while for Pt and Pd the slow step was thought to be the adsorption of oxygen (41)

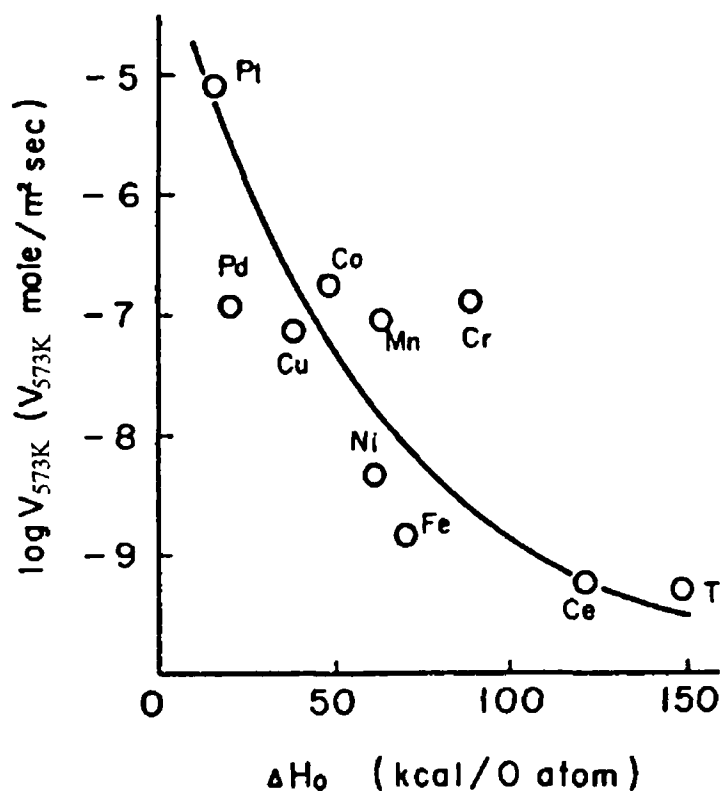


Fig 1.3 : Correlation between activity for C_3H_8 oxidation and heat of formation of catalyst oxide (41).

Yao et al (44, 45) examined the oxidation of a number of hydrocarbons including C_2H_6 and C_3H_8 over NiO and $\alpha-Cr_2O_3$ crystals. A continuous flow reactor system was used and analysis of the reaction was carried out using a mass spectrometer. The hydrocarbons were completely oxidised to CO_2 and the kinetics of the reaction were studied by measuring the rate of production of CO_2 using a reactant composition of 4 % O_2 , 1 % hydrocarbon and 0.1 % H_2O . Over NiO crystals the rate of reaction of C_2H_6 was 0.018 and 0.0053 $cm^3(m^2min)^{-1}$ at 623K and 573K respectively, while for C_3H_8 the corresponding values were 0.038 and 0.0084 $cm^3(m^2min)^{-1}$. The specific reaction rate described by the empirical power law

$$\text{rate of } CO_2 \text{ produced} = k p_{O_2}^b p_R^c (p_{H_2O})^a$$

where k , p_{O_2} and p_R have been described previously, p_{H_2O} represents the partial pressure of H_2O and b , c , and a represent the order of reaction with respect to O_2 , alkane and H_2O respectively. For the oxidation of C_2H_6 the values of a , b , and c were determined to be 0.27, 0.44 and 0.50 respectively while for C_3H_8 the

corresponding values were 0.26, 0.29 and 0.53. From Arrhenius plots the apparent activation energy for the oxidation of C_2H_6 and C_3H_8 over NiO was determined to be $17 \text{ kcal mole}^{-1}$ and $21 \text{ kcal mole}^{-1}$ respectively and were independent of the reactant gas composition. A change in slope was observed in the Arrhenius plots which was believed to indicate a shift in the rate determining step or reaction mechanism (44).

In the case of $\alpha\text{-Cr}_2\text{O}_3$ four samples were studied (45). A Cr_2O_3 powder from Johnson Matthey Co. Ltd., composed of randomly shaped crystals, was used. The second sample consisted of crystals prepared by the method of flux growth from the aforementioned powder and consisted of well defined polyhedral crystals of $\alpha\text{-Cr}_2\text{O}_3$. The third sample was prepared by the thermal decomposition of $K_2\text{Cr}_2\text{O}_7$ and the crystals were thin platelets with distinctive hexagonal appearance. The fourth sample was the third sample ground into a powder and sintered to constant area at 1123K. Over these samples the kinetic data suggested that at high concentrations, O_2 and hydrocarbon were competing for the same active sites. The oxidation kinetics for C_2H_6 and C_3H_8 were found to be quite similar over the four $\alpha\text{-Cr}_2\text{O}_3$ catalysts. The rates of reaction for oxidation were measured at 573K using a gas composition of 1% O_2 , 0.1% hydrocarbon and 0.3% H_2O . The specific reaction rates and determined apparent activation energies, over the various Cr_2O_3 samples, for C_2H_6 and C_3H_8 are given in Table 1.4. The catalytic selectivity and reaction kinetic parameters were determined to be dependent on the morphological structure of the catalyst surface with the sample consisting of well defined polyhedral crystals appearing to be most active. The reason for this enhanced activity was not explained (45).

Nitadori et al. (46) examined the effects of varying the A or B ion in perovskites, of the form ABO_3 , on the reaction rate for the oxidation of C_3H_8 . They found that reaction rates over LaCoO_3 were up to 2 orders of magnitude higher than over LaFeO_3 . It was determined that, with exception of Sr^{2+} , variation of the A ion caused oxidation rates to differ by less than 1 order of magnitude. Substitution of some of the A ions with Sr^{2+} i.e., $A_{1-x}\text{Sr}_x\text{BO}_3$, led to an increase in the rate of oxidation of C_3H_8 by 1 order of magnitude compared with catalysts which did not contain Sr^{2+} . $\text{La}_{0.8}\text{Sr}_{0.2}\text{CoO}_3$ was found to be the most active catalyst (46).

Table 1 4· The rate of oxidation and apparent activation energies for hydrocarbons over α -Cr₂O₃ crystals (45)

Catalyst	Hydrocarbon	Rate* (cm ³ STP/min-m _g)	Apparent Activation Energy (kcal mol ⁻¹)
α -Cr ₂ O ₃ (Randomly shaped crystals)	C ₂ H ₆	0 0013	21 0
	C ₃ H ₈	0 0087	24 7
α -Cr ₂ O ₃ (Well-defined polyhedral crystals)	C ₂ H ₆	0 0080	21 3
	C ₃ H ₈	0 0240	27 5
α -Cr ₂ O ₃ (Thin hexagonal platelet crystals)	C ₂ H ₆	0 0014	nd
α -Cr ₂ O ₃ (sintered to constant area)	C ₂ H ₆	0 0002	nd
	C ₃ H ₈	0 0036	nd

* Note Rate at 1% O₂, 0 1% hydrocarbons, 0 3% H₂O

nd Not determined

More recently Barnard et al (47) studied the activity of LaCoO₃ for the oxidation of C₃H₈ and CO Catalysts were prepared by the simultaneous oxidation/coprecipitation of La(II) and Co(II) nitrates The catalysts were heated at 673K for 1h and then at 873K for 1h in air Activity measurement was carried out in a fixed bed reactor using a gas mixture containing 0 104 vol% C₃H₈, 0 983 vol% CO, 1 44 vol% O₂ and 97 5 vol% He The activity for CO and C₃H₈ oxidation increased linearly with the surface area of the catalyst For a high surface area perovskite (32m²g⁻¹), 578K was determined to be the temperature at which 50% C₃H₈ conversion occurred, while for the sample with an area of only 6m²g⁻¹ this temperature was 80K higher The activities, represented as turnover numbers, for CO and C₃H₈ oxidation were 5 x 10⁻³ and 6 x 10⁻⁴ molecules oxidised per atom of surface Co per second (47)

Stein et al (48) examined the total oxidation of C₅ and C₆ alkanes over a number of metal oxide catalysts A pulse microcatalytic technique was used and the temperature required to obtain 80 % conversion of the hydrocarbon in the gas

phase was used as a measure of catalytic activity. Again no account of the differences in the surface area of the active phase was taken into account. The hydrocarbons examined were $n\text{-C}_5\text{H}_{12}$, 2-methyl butane (2 MB), $n\text{-C}_6\text{H}_{14}$ and 2,3-dimethyl butane (2,3 DMB). Several metal oxides were used and details of the results for the activity of each of these catalyst samples for the hydrocarbons mentioned above are given in Table 1.5

Table 1.5. Values reported for specific surface areas and hydrocarbon conversion over metal oxides (48)

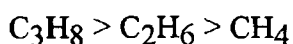
Catalyst	Specific surface area (m^2g^{-1})	Temp to Attain 80% Conversion (K)			
		$n\text{-C}_5$	2-MB	$n\text{-C}_6$	2,3-DMB
Co_3O_4	11.3	460	518	453	476
Mn_2O_3 + Mn_3O_4	3.2	623	645	523	548
NiO	6.2	603	613	558	560
Cr_2O_3	14.0	568	558	560	563
Fe_2O_3	13.9	558	690	603	570
TiO_2	10.2	683	748	538	628
CeO_2	9.3	628	685	570	646
ThO_2	55.7	638	670	618	638
Al_2O_3	87.6	655	783	626	658
CuO	0.5	743	763	655	685
WO_3	3.6	763	873	723	843
Pb_3O_4	0.6	748	803	639	773
MgO	90.3	758	868	628	753
SiO_2	421.0	808	838	693	788
BeO	nd	743	793	688	788
V_2O_5	1.0	860	870	811	860
ZnO	0.5	798	923	628	833
CaO	nd	773	873	713	868
ZrO_2	0.7	795	873	729	873

nd = Not determined

With the exception of Cr_2O_3 and Fe_2O_3 , $n\text{-C}_6\text{H}_{14}$ was the most easily oxidised over the oxide catalysts examined. 2-MB was the most difficult to oxidise over all the oxide catalysts except Co_3O_4 , Cr_2O_3 and Zr_2O_3 . For all the hydrocarbons examined the most active oxide sample was found to be Co_3O_4 . From Table 1.5 it can be observed that the catalyst samples can be grouped on the basis of activity. The most active catalysts were found to be Co_3O_4 , $\text{Mn}_2\text{O}_3 + \text{Mn}_3\text{O}_4$, NiO and Cr_2O_3 , whereas Fe_2O_3 , TiO_2 , CeO_2 , ThO_2 , Al_2O_3 and CuO had moderate activity for hydrocarbon oxidation. WO_3 , Pb_3O_4 , MgO , SiO_2 , BeO , V_2O_5 , ZnO , CaO and ZrO_2 were determined to have low activity for the oxidation of the hydrocarbons studied (48).

Other workers have studied the oxidation of alkanes over unsupported and supported metal oxides (49, 50). Economy et al (49) found that BaCr_2O_3 supported on $\gamma\text{-Al}_2\text{O}_3$ (specific surface area 80 to $120\text{m}^2\text{g}^{-1}$) was active for the total oxidation of both $i\text{-C}_4\text{H}_{10}$ and $n\text{-C}_4\text{H}_{10}$. In the range 473K to 673K the activation energies were determined to be 10.3kcal mol^{-1} and 12.3kcal mol^{-1} respectively. Complete conversion of $i\text{-C}_4\text{H}_{10}$ to CO_2 occurred between 620K and 720K for space velocities of 2200h^{-1} , 4600h^{-1} , and 7200h^{-1} . The activity of the catalyst was attributed to the presence of small amounts of Cr ions in lower oxidation states. It was determined that the valence of the Cr varied between 5.2 and 5.8 upon heat treatment at different temperatures in the reaction mixture. It was suggested that at the lower valence values the predominant species was Cr^{5+} with small amounts of Cr^{6+} behaving as lattice imperfections while at the higher values Cr^{5+} represented the defect structure while the Cr^{6+} species predominated (49). Johnson et al (50) found that samples of hopcalite ($\text{MnO}_2 + \text{CuO}$) was active for the total oxidation of $n\text{-C}_6\text{H}_{14}$, $n\text{-decane}$ ($n\text{-C}_{10}\text{H}_{22}$) and 2,2-dimethyl butane at hydrocarbon concentrations ranging from 20 to 125mg cm^{-3} . At 620K conversions were determined to be 97%, 96% and 98% respectively, in an excess oxygen atmosphere (50).

Accomazzo and Nobe (10) found that a $\text{CuO-Al}_2\text{O}_3$ (composition 1:1) was effective in the oxidation of CH_4 , C_2H_6 and C_3H_8 . Correlations were found between the oxidation activity of the catalyst and both the polarisability and the ionisation potential of the hydrocarbons. As the polarisability of the hydrocarbon increased, its reactivity over the catalyst sample also increased, whereas for increasing ionisation potentials the opposite was the case. Activity decreased in the sequence



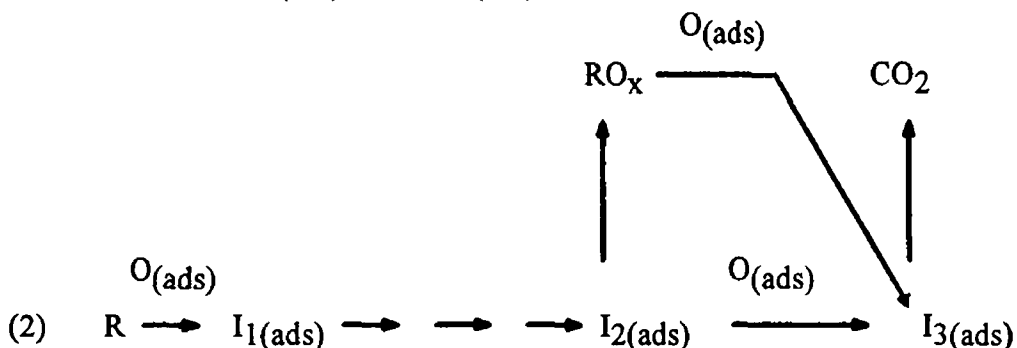
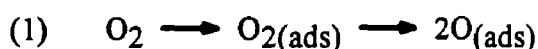
In the oxidation of CH_4 , C_2H_6 and C_3H_8 the orders with respect to the hydrocarbon were 0.9, 0.7, and 0.6 respectively (10)

Golodets (6) summarised the trends observed in the oxidation of alkanes on metal oxides. For alkanes the reactivity increases with the number of C-atoms but decreases with the degree of branching of the C-atom skeleton (for an alkane of the same C-atom number). Furthermore it was stated that the deep oxidation of an alkane, R, over metal oxides could be described by a power rate law

$$r = K p_R^b p_{\text{O}_2}^c$$

where r , K , p_{O_2} have been described previously, p_R is the partial pressure of the alkane, R, and b and c are the reaction orders with respect to the alkane and O_2 respectively. Typical values of b were 0.5 - 1.0 and those for c were close to zero.

A reaction mechanism was suggested (6) for the reaction at high temperatures, when oxidation was observed to occur and when surface organic complexes would be destroyed rapidly as follows



where $\text{I}_1(\text{ads})$, $\text{I}_2(\text{ads})$, and $\text{I}_3(\text{ads})$ represent surface intermediates. The structure and composition of the intermediate $\text{I}_1(\text{ads})$ is of fundamental importance in the comparison of the reactivity of different alkanes on a catalyst surface. The intermediates $\text{I}_2(\text{ads})$ and $\text{I}_3(\text{ads})$ were believed to be carbonate-carboxylate and formate type complexes respectively (6).

In the first step in the above reaction scheme (6) negatively charged ions of $\text{O}(\text{ads})$ formed as electrons were transferred from the catalyst surface. In step (2) of the above mechanism the oxidised molecules were positively charged during their interaction with the catalyst as electron transfer occurred in the opposite direction. This theory was reinforced by the correlations between reactivity and both polarisability and ionisation potential of alkanes over metal oxides observed

by Accomazzo and Nobe (11) since it indicated that electron transfer or displacement occurred from the alkane to the catalyst together with the formation of positively charged alkane ions

In the above reaction scheme (6) although the possible identity of I_1 was not given, some experimental work has been carried out in this area. As part of their studies on hydrocarbon oxidation over NiO and Cr_2O_3 crystals Yao et al (44, 45) carried out isotope studies with deuterated alkanes in order to obtain information on the adsorbed state of the hydrocarbon on the crystal surface and to get information on the rate determining step. The rates for the oxidation of normal and deuterated C_2H_6 were determined alternatively to ensure comparability and the values obtained indicated that the rate determining step was either the adsorption of C_2H_6 as the radical C_2H_5 , with the breaking of a C-H bond (if chemisorption of the C_2H_6 molecule was the slow step) or the interaction of adsorbed O_2 and either gas phase or adsorbed C_2H_6 through attack at the C-H bond

1.3 References

- (1) J J Spivey, Catalysis, **8**, 158 (1989)
- (2) D L Trim, Appl Catal, **7**, 249 (1983)
- (3) L D Pfefferle and W C Pfefferle, Catal Rev -Sci Eng, **29**, 219 (1987)
- (4) F Dywer, Catal Rev -Sci Eng, **6**, 261 (1972)
- (5) M F Zwinkels, S G Jaras and P G Menon, Catal Rev -Sci Eng, **35**, 319 (1993)
- (6) G I Golodets, Heterogeneous Catalytic Reactions Involving Molecular Oxygen, Studies in Surf Sci Catal, **15**, Elsevier, Amsterdam(1983)
- (7) G C Bond, Heterogeneous Catalysis Principles and Applications, Clarendon Press, Oxford, U K , (1974)
- (8) V D Sokolovskii, Catal Rev -Sci Eng, **32**, 1 (1990)
- (9) C F Cullis and B M Willat, J Catal, **83**, 267 (1983)
- (10) M A Accomazzo and K Nobe, Ind Eng Chem Process Des Dev, **4**, 425 (1965)
- (11) R B Anderson, K C Stein, J J Feenan and L Hofer, Ind Eng Chem, **53**, 809 (1961)
- (12) W P Yant and C O Hawk, J Am Chem Soc, **49**, 1454 (1927)
- (13) G Kainz and H Horwatitish, Microchim Acta, **7** (1962)
- (14) R Mezaki and C C Watson, Ind Eng Chem Process Dev Res, **5**, 62 (1966)
- (15) O P Ahuja and G P Mathur, Can J Chem Eng, **45**, 367 (1967)
- (16) J G Firth and H B Holland, J Chem Soc Faraday Trans I, **65**, 1121 (1969)
- (17) C Kemball, Proc Roy Soc, **A217**, 376 (1953)
- (18) V S Salnikov, T V Sorokine and P G Tsyrumikov, React Kin Catal Lett, **30**, 209 (1986)
- (19) J R Anderson and P Tsai, Appl Catal, **19**, 141 (1985)
- (20) P E Marti, M Maciejewski and A Baiker, J Catal, **139**, 494 (1993)
- (21) H Arai, T Yamada, K Eguchi and T Seiyama, Appl Catal, **26**, 265 (1986)
- (22) R Doshi, C B Alcock, N Gunasekaran and J J Carberry, J Catal, **140**, 557 (1993)
- (23) H M Zhang, Y Teraoka and N Yamazoe, Appl Catal, **41**, 137 (1988)
- (24) M Machida, K Eugchi and H Arai, J Catal, **120**, 377 (1989)
- (25) R F Hicks, H Qi, L Young and R G Lee, J Catal, **122**, 280 (1990)
- (26) P Briot, A Auroux, D Jones and M Primet, Appl Catal, **59**, 141 (1990)
- (27) P Briot and M Primet, Appl Catal, **68**, 301 (1991)
- (28) T R Baldwin and R Burch, Appl Catal, **66**, 337 (1990)
- (29) T R Baldwin and R Burch, Appl Catal, **66**, 359 (1990)
- (30) Y Yao, Ind Eng Chem Prod Res Dev, **19**, 293 (1980)
- (31) F M Ribiero, M Chow and R A Dalla Beta, J Catal, **146**, 537 (1994)
- (32) S H Oh, P J Mitchell and R M Siewert, J Catal, **132**, 287 (1991)

- (33) C F Cullis, D E Keane and D L Trim, J Catal, 19, 378 (1970)
- (34) L Hiam, H Wise and S Chaikin, J Catal, 10, 272 (1968)
- (35) A Schwartz, L Holbrook and H Wise, J Catal, 21, 199 (1971)
- (36) J A Barnard and D S Mitchell, J Catal, 12, 386 (1968)
- (37) K Otto, J M Andino and C L Parks, J Catal, 131, 243 (1991)
- (38) H C Yao, M Sieg and H K Plummer Jr , J Catal, 59, 365 (1979)
- (39) J Volter, G Lietz, H Spindler and H Lieske, J Catal, 104, 375 (1968)
- (40) C P Hubbard, K Otto, H S Gandhi and K Y S Ng, J Catal, 139, 268 (1993)
- (41) Y Moro-oka, Y Morikawa and A Ozaki, J Catal, 7, 23 (1967)
- (42) C P Hubbard, K Otto, H S Gandhi and N Y S Ng, J Catal, 144, 484 (1993)
- (43) A B Kooh, W-J Han, R Glee and R F Hicks, J Catal, 130, 374 (1991)
- (44) Y-F Y Yao and J T Kummer, J Catal, 28, 124 (1973)
- (45) Y-F Y Yao, J Catal, 28, 139 (1973)
- (46) T Nitadori, T Ichiki and M Misono, Bull Chem Soc Jpn, 61, 621 (1988)
- (47) K R Barnard, K Foger, T W Turney and R D Williams, J Catal, 125, 265 (1990)
- (48) K S Stein, J J Feenan, L J E Hofer and R B Anderson, Ind Eng Chem, 52, 671 (1960)
- (49) J Economy, D I Meloon and R L Ostrozyński, J Catal, 4, 446 (1965)
- (50) J E Johnson, J G Christian and H W Carhart, Ind Eng Chem, 53, 900 (1961)

CHAPTER 2

Thermal Stability of "Saffil" Fibre

2 Introduction

This chapter outlines the results of a study carried out on the fibrous alumina material "Saffil". The aim of the study was to investigate the thermal stability of the material by measuring specific surface areas and pore volumes and also to examine methods of increasing the stability of the fibre by the addition of cations. The Saffil fibre was used as the support material for heterogeneous oxidation catalysts and, in use, these catalysts could reach high temperatures during reaction and loss of surface area of the support material could lead to a drop in activity. In this section the properties of alumina, Al_2O_3 will be examined.

Alumina, Al_2O_3 , is one of the most extensively used support materials for heterogeneous supported metal catalysts. This is largely due to the fact that it is inexpensive, reasonably stable and can be obtained in a wide range of surface areas (1). Al_2O_3 is the only known oxide of aluminium but there are many polymorphs and hydrated species whose nature is dependent on the preparation conditions (2). The adsorptive and catalytic properties of Al_2O_3 have been extensively studied and a mass of empirical data on preparation and properties was available by 1945 (3). The existence of a number of different phases of Al_2O_3 is well known, including $\gamma\text{-Al}_2\text{O}_3$, $\eta\text{-Al}_2\text{O}_3$, $\delta\text{-Al}_2\text{O}_3$, $\theta\text{-Al}_2\text{O}_3$, $\chi\text{-Al}_2\text{O}_3$, $\varepsilon\text{-Al}_2\text{O}_3$, $\kappa\text{-Al}_2\text{O}_3$ and $\alpha\text{-Al}_2\text{O}_3$ (3 - 9). Known as the transition aluminas, they can be prepared by a number of methods, e.g. by the calcination of alumina hydrates (4).

The various Al_2O_3 phases have been classified in the terms of the temperatures at which they are formed from aluminium hydroxides (3). The first class consists of aluminas of the form $\text{Al}_2\text{O}_3 \cdot n\text{H}_2\text{O}$, where n is less than 0.6 and greater than 0, produced by dehydration at temperatures not exceeding 873K. This class is referred to as the γ -group and to it belongs the phases χ -, η - and $\gamma\text{-Al}_2\text{O}_3$. The other class consists of the high temperature aluminas, nearly anhydrous Al_2O_3 phases, obtained by heating at temperatures between 1173K and 1273K, and in it belongs the κ , θ and δ phases (3).

Al_2O_3 phases have also been classified on the basis of their crystallographic structures (3). The structure of the Al_2O_3 phases are based to a greater or lesser extent on the hexagonal close packed oxygen lattice, with Al ions in the octahedral and Tetrahedral interstices. Three types of Al_2O_3 phases have been identified. Firstly, the α -series Al_2O_3 phases with hexagonal close packed lattices of the form ABAB, for example $\alpha\text{-Al}_2\text{O}_3$, see Fig 2.0. The β -series are made up of phases with an alternating class packed lattice of the form ABAC - ABAC or ABAC - CABA. It comprises mostly of alkali or alkaline earth oxides containing $\beta\text{-Al}_2\text{O}_3$, $\kappa\text{-Al}_2\text{O}_3$ and $\chi\text{-Al}_2\text{O}_3$. Finally, Al_2O_3 phases with cubic close packed lattices, schematically represented by ABC-ABC, belong to the γ -series. This last class can be further subdivided into the low temperature or γ -group, i.e. $\eta\text{-Al}_2\text{O}_3$ and $\gamma\text{-Al}_2\text{O}_3$, and the δ - or high temperature group,

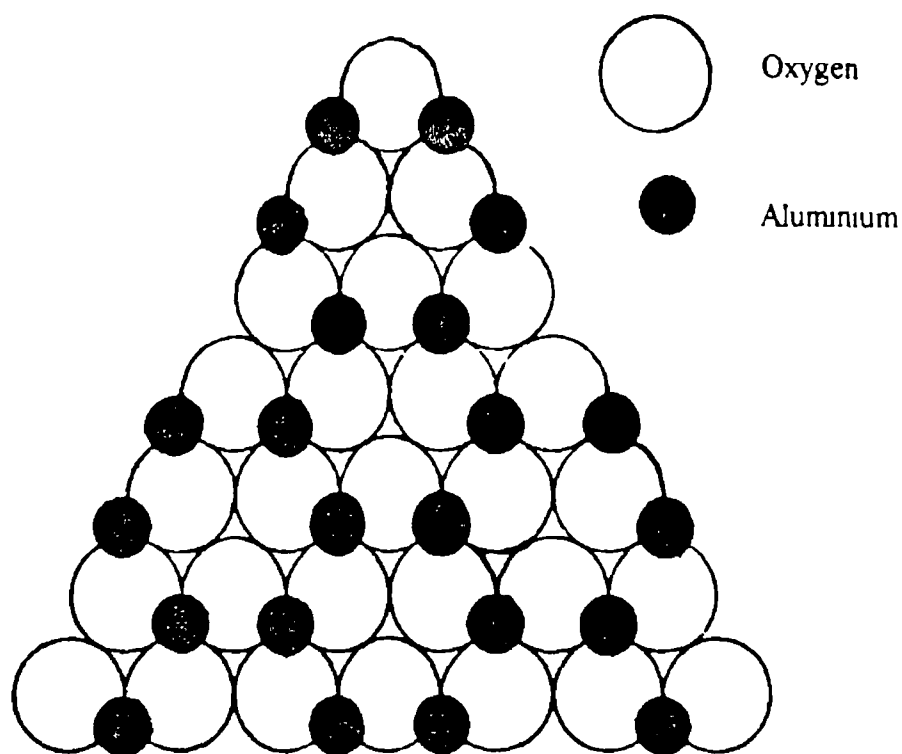


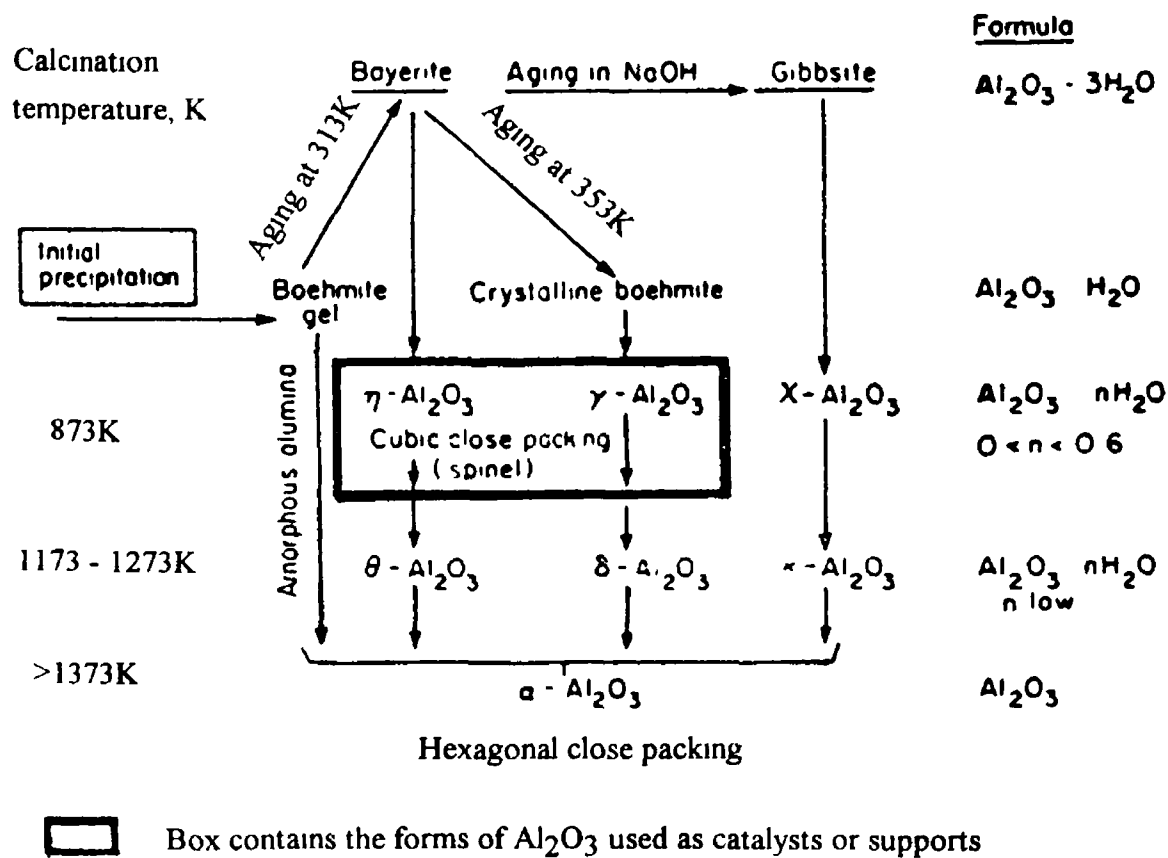
Fig.2.0 : The structure of $\alpha\text{-Al}_2\text{O}_3$

i.e. $\delta\text{-Al}_2\text{O}_3$ and $\theta\text{-Al}_2\text{O}_3$ (3)

Some of the phase transformations of Al_2O_3 are illustrated in Fig 2.1. The α -phase is the thermodynamically stable form and all other phases are converted to this phase upon heating above approximately 1473K in air (1). $\alpha\text{-Al}_2\text{O}_3$ exists in nature as the mineral corundum, where its occurrence in rocks is widespread (4). Pure $\alpha\text{-Al}_2\text{O}_3$ can be prepared industrially by the ignition of $\text{Al}(\text{OH})_3$ or $\text{AlO}(\text{OH})$ at high temperatures (10).

As already mentioned, other phases of Al_2O_3 are normally formed by the dehydration of hydroxides of aluminium. Bayerite, $\text{Al}(\text{OH})_3$, is one such trihydroxide from which both $\eta\text{-Al}_2\text{O}_3$ and $\gamma\text{-Al}_2\text{O}_3$ can be formed. It has a structure which consists of a lattice with double layers of hydroxyl ions and two thirds in the form ABABAB. Consequently the atoms of the third layer are placed above the atoms of the first layer, with the double layers held together by hydrogen bonding between adjacent layers of hydroxyl groups. The distance between the two double layers AB has been found to be 2.64Å and the shortest O-O distance between adjacent layers has been determined to be 3.13Å (3). Heating bayerite at ca 353K can lead to the formation of boehmite, an aluminium oxyhydroxide, $\text{AlO}(\text{OH})$, which in turn can be converted to the γ -, δ - or α -phases, depending on the temperature of calcination. However, calcining bayerite at, for example, 873K leads to the formation of $\eta\text{-Al}_2\text{O}_3$, which in turn can be transformed to the θ -phase and, at temperatures above 1373K, to the α -phase (3).

Fig 2.1 . Important phase transformations of Al_2O_3



The structure of $\gamma\text{-Al}_2\text{O}_3$ is defect spinel in type, which is slightly trigonally distorted (11) The general formula for a spinel is AB_2X_4 In the normal spinel, 8 metal atoms (A) occupy the tetrahedral sites and 16 metal atoms (B) occupy the octahedral positions The structure can be regarded as built up of alternate cublets (10) as illustrated in Fig 2 2 Inverse and disordered spinels are said to have a defect structure because all the crystallographically identical sites within the unit cell are not occupied The unit cell for $\gamma\text{-Al}_2\text{O}_3$ is composed of thirty two O atoms and twenty one and a half Al atoms, with the O lattice built up by a cubic close packed stacking of the O layers (11) as shown in Fig 2 3 From work with single crystal electron diffraction studies Lippens and de Boer (12) determined that the O lattice is fairly well ordered

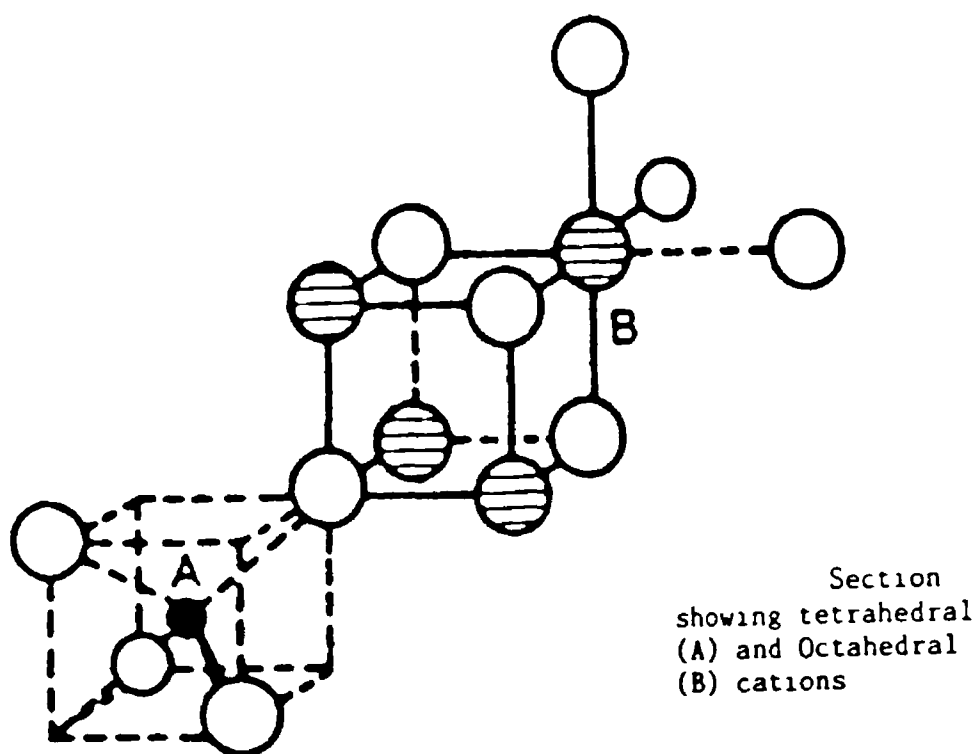


Fig 2 2 Spinel structure of type AB_2X_4 (2)

As with $\gamma\text{-Al}_2\text{O}_3$, $\eta\text{-Al}_2\text{O}_3$ has a trigonally distorted spinel structure, although this distortion is less pronounced than in the γ -phase (11) The unit cell is similar to that for $\gamma\text{-Al}_2\text{O}_3$, but stacking faults are more frequent in the O lattice for the η -phase, hence structurally the main difference between the γ - and η -phases is the slightly higher occupation of the tetrahedral positions in the γ -phase, and the lower packing density of the O in $\eta\text{-Al}_2\text{O}_3$ (11)

The structure of $\delta\text{-Al}_2\text{O}_3$ has been studied (13, 14, 15) This phase has been deduced to have a lattice consisting of three Al_2O_3 spinel cells forming a super structure containing an integer number of Al ions It has been proposed that the vacant positions

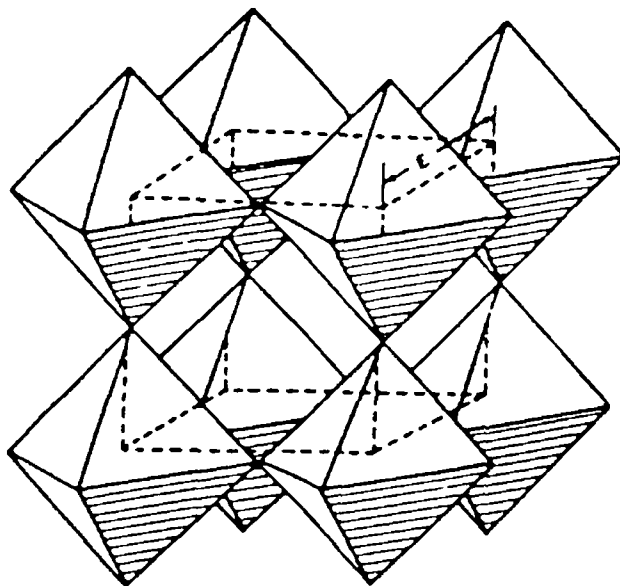


Fig 2.3 : Diagram showing the least dense packing for $\gamma\text{-Al}_2\text{O}_3$ (29)

are ordered parallel to the C-axis, on a 4-fold screw axis (3) The unit cell dimensions of $\delta\text{-Al}_2\text{O}_3$ which have been reported vary but typical values are $a = b = 7.95\text{\AA}$ and $c = 23.48\text{\AA}$ (3)

$\theta\text{-Al}_2\text{O}_3$ is monoclinic in structure and has been found to be isomorphous with $\beta\text{-Ga}_2\text{O}_3$ (3), the structure of which has been determined by Geller (16) The lattice parameters for the θ -phase have been determined to be $a = 11.24\text{\AA}$, $b = 5.72\text{\AA}$, $c = 11.74\text{\AA}$, $\beta = 103^\circ 20'$ The O lattice is nearly cubic close packed, with Al atoms mostly in the tetrahedral positions (3)

Aluminas may also be formed from gibbsite, see Fig 2.1 Gibbsite is the most well known trihydroxide of Al_2O_3 , being the main constituent of bauxites found in north and south America (4) Upon heating this compound at progressively higher temperatures the phases formed are firstly $\chi\text{-Al}_2\text{O}_3$, then $\kappa\text{-Al}_2\text{O}_3$ and finally $\alpha\text{-Al}_2\text{O}_3$ The crystal structure of gibbsite has been found to be based on a double layer of closely packed hydroxyl ions, with $2/3$ of the octahedral holes being filled with Al ions (17) The lattice is deformed due to the alterations of occupied and empty octahedral sites, the vacant octahedral sites being bigger than those which are filled (3) The structure of gibbsite is shown in Fig 2.4 The stacking of the double layers can be represented by ABBA ABBA etc, and are held together by H-bonding The distance between A and B is 2.03\AA compared with 2.81\AA for the distance between two adjacent A or B layers (3)

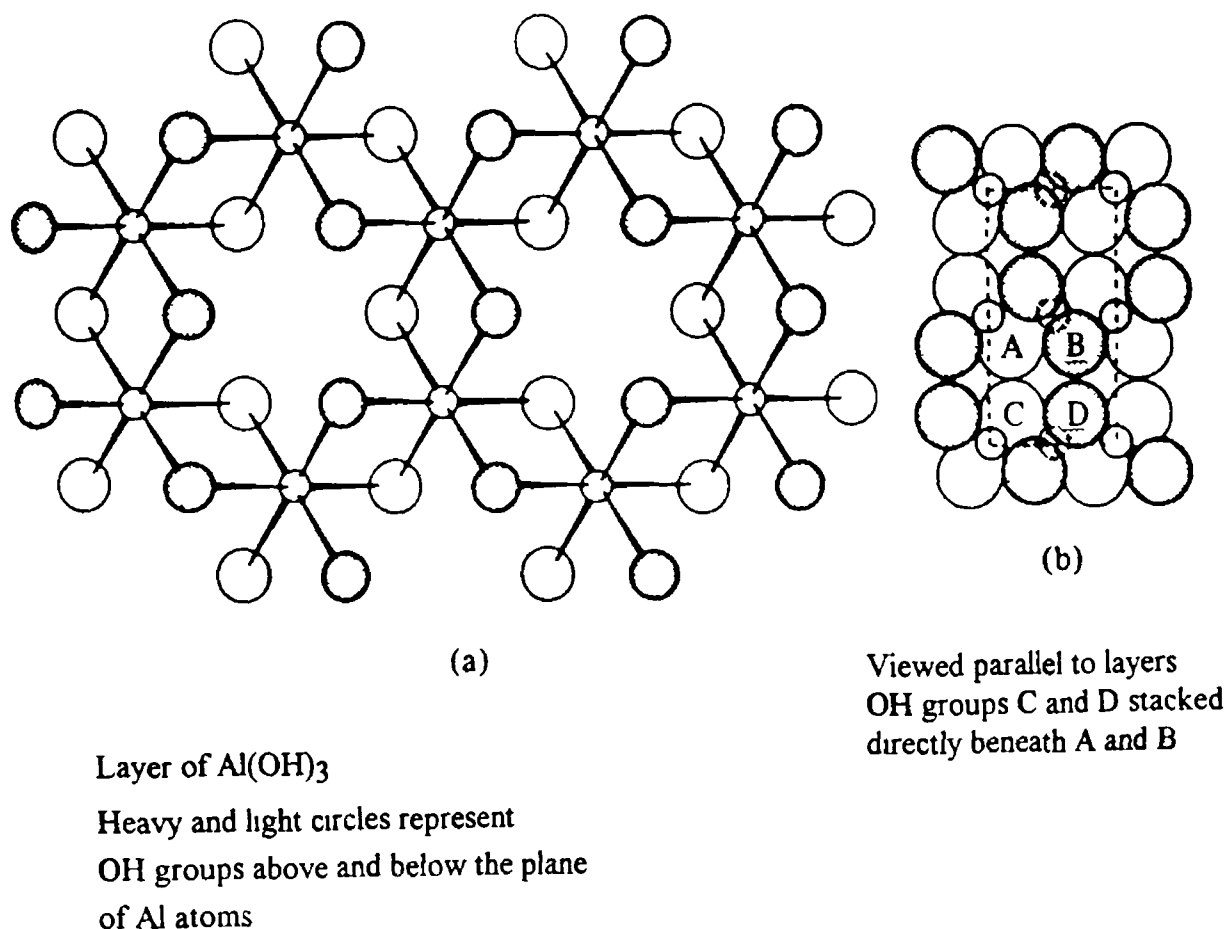


Fig 2 4 • Structure of Gibbsite (10)

The structures of χ - and κ - Al_2O_3 have also been determined (3) χ - Al_2O_3 has a hexagonal lattice structure, which is very nearly cubic, with a trigonal deformation. There is a one dimensional disorder in the O layers stacking perpendicular to the C-axis similar to that in the η -phase, but much stronger for the χ -phase. The dimensions of the unit cell have been reported to be $a = 5.56\text{\AA}$ and $c = 13.44\text{\AA}$ (3). The other phase, κ - Al_2O_3 , also has a hexagonal lattice with $a = 9.71\text{\AA}$ and $c = 17.86\text{\AA}$. The stacking sequence of the O layers for κ - Al_2O_3 has been found to be very like that of mica and can be represented by the sequence ABAC - ABAC or ABAC - CABA (3).

The surface structure of the Al_2O_3 γ - Al_2O_3 and η - Al_2O_3 phases have been studied, both in terms of importance as a support material and for catalytic activity (11). Since the simplest surface model is one in which a single crystallographic face is preferentially exposed, Knozinger and Ratnasamy (11) reviewed surface models of

alumina and proposed idealised surface models for the (111)-plane, (110)-plane and the (100)-plane. The (111)-face of Al_2O_3 (11) is illustrated in Fig. 2.5. There are two different types of layer with two different cation distributions in the spinel lattice parallel to the (111)-plane, designated A and B layers for simplicity. The A layer consists of twenty four cation positions, with eight in octahedral sites and the remaining sixteen in the tetrahedral interstices. In the case of the B-layer, the cations are in the twenty four octahedral positions. The (110)-plane also consists of two different cation layers (11) as illustrated in Fig. 2.6. The C-layer contains an equal number of cations aligned in the tetrahedral and octahedral interstices between rows of oxygen atoms. The cation positions are only in the octahedral interstices for the D-layer. For the (100)-plane of Al_2O_3 , the configuration is a square lattice of atoms where only octahedral cation positions are possible (11).

Knozinger and Ratnasamy (11) identified five different types of hydroxyl groups which could be present in these planes. Their structures are illustrated and some of their characteristics are given in Table 2.0. For the A-layer in the surface parallel to the (111)-plane two types of hydroxyl configuration can occur. Type Ia, is a terminal hydroxyl group co-ordinated to a single tetrahedral cation and type IIa is a bridging hydroxyl group linking a tetrahedral and octahedral Al cation. Type IIa occurs three times as frequently as type Ia. For the B-layer two hydroxyl configurations are again possible. Both are hydroxyl bridging groups, with type IIb being a hydroxyl group linking two octahedral cation positions and type III where the hydroxyl group is co-ordinated to three cations in octahedral interstices. Type IIb occurs three times more frequently than type III. Taking into account vacant cation positions in the octahedral interstices, a fifth type of hydroxyl group, co-ordinated to a single cation in an octahedral site, can occur (11).

For the C and D-layers parallel to the (110)-plane of the lattice, type Ia and type IIb occur on top of the C-layer and type Ib on top of the D-layer. Only type Ib hydroxyl can occur on the top of a layer parallel to the (100)-plane of the spinel lattice. The occurrence and relative concentrations of the five hydroxyl configurations is dependent on the relative contributions of the different crystal faces present (11).

Peri (18) developed a model for the surface of $\gamma\text{-Al}_2\text{O}_3$ based on the (100)-plane being predominantly exposed, with Al ions in octahedral sites being positioned immediately under each surface hydroxyl of a fully hydroxylated surface. The model was based on a number of previous studies (19, 20, 21,). The five hydroxyl bands which were observed in the $\gamma\text{-Al}_2\text{O}_3$ infra red spectrum during dehydroxylation were proposed to be due to hydroxyl groups in distinct lateral surface environments. For example, the high wavenumber band at 3800cm^{-1} was thought to be due to a hydroxyl group with four oxide nearest neighbours (but only four exposed five co-ordinated Al^{3+} ions) and the band in between 3800cm^{-1} and 3700cm^{-1} was due to hydroxyl groups located at one, two or three nearest neighbour oxide ions (18).

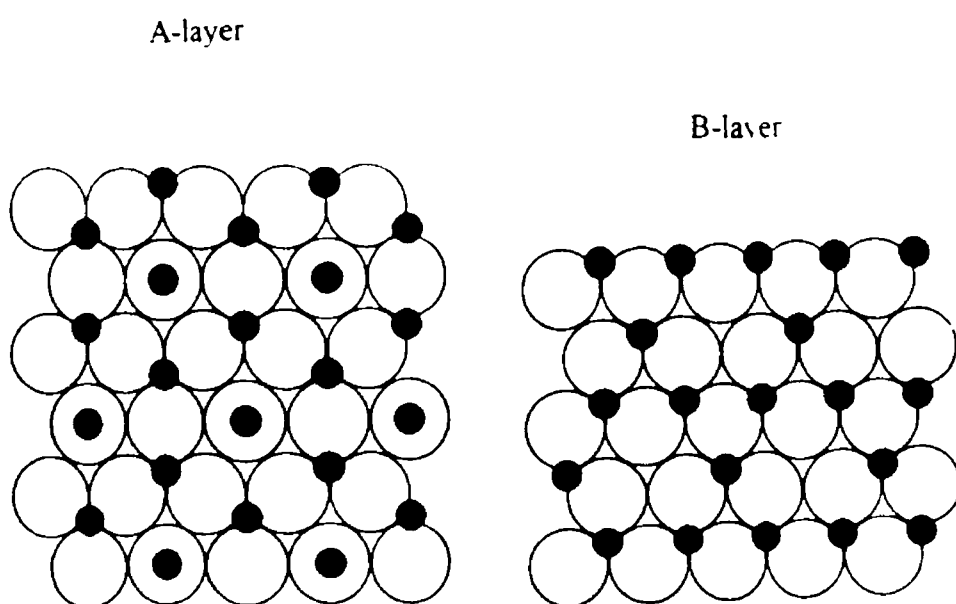


Fig 2.5 : (111) - Face of Al_2O_3 spinel lattice (11)

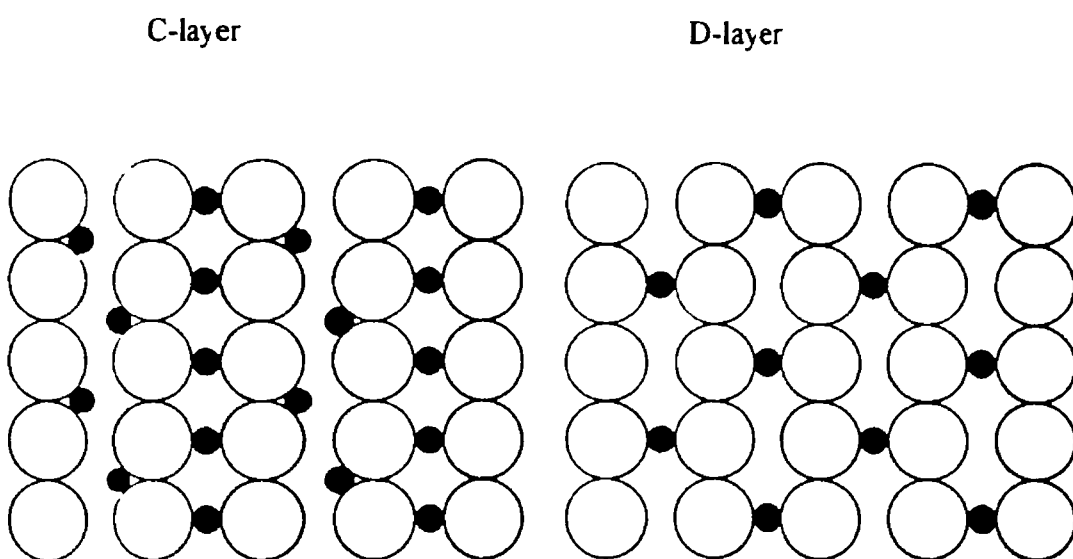
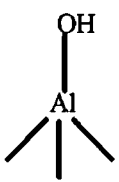


Fig 2 6 · (110) - Face of Al_2O_3 spinel lattice (11)

Table 2 0 The Five Different Types of Hydroxyl Groups on Al₂O₃(11)

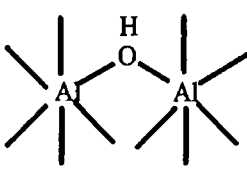
Configuration Crystal Face Net Charge at OH $\nu(\text{OH}) \text{ cm}^{-1}$



Type Ia (111), (110) - 0.25 3760 - 3780




Type IIa (111) + 0.25 3730 - 3735



Type IIb (111), (110) 0 3740 - 3745



Type III (111) + 0.5 3700 - 3710



Type Ib (110), (100) - 0.5 3785 - 3800
3795 - 3800

hydroxyl groups located at one, two or three nearest neighbour oxide ions (19)

However, there are a number of drawbacks to Perr's model (11, 18) Firstly the surface of $\gamma\text{-Al}_2\text{O}_3$ maybe more complex than only the (100)-plane being exposed, with a number of crystal planes being present As the model can only be applied to square lattices with equivalent hydroxyl groups on the surface, it is not applicable to the (111) - plane (11) Also Knozinger and Ratnasamy (11) pointed out that the assumption that the number of nearest neighbour oxide ions in the surface was the dominant factor controlling IR stretching frequencies of hydroxyl ions was incorrect It should only have been a minor factor as an inductive effect was unlikely since this is usually not transmitted through more than two bands Knozinger and Ratnasamy (11) related the hydroxyl stretching frequency to the net charge on the group in question Thus hydroxyl groups of type Ib with net charge of -0.5 had a frequency of approximately 3800cm^{-1} while type III hydroxyl had a frequency of 3700cm^{-1} in the IR spectrum and a charge of +0.5 (as shown in Table 2.0) Since five OH bands appear in the IR spectrum for the dehydroxylation of $\gamma\text{-Al}_2\text{O}_3$ up to 1273K it has been concluded that a combination of the (110) -, (111) - and (100) - planes are exposed in the surface of $\gamma\text{-Al}_2\text{O}_3$ (11, 12) Furthermore, the intensity of these bands is dependent on the relative surface concentration of three different hydroxyl configurations (3)

According to Lippens and Steggerda (3) the hydroxyl groups on the surface of Al_2O_3 behave as Bronsted acid sites When water is produced from the dehydration of two neighbouring hydroxyl groups, an Al atom is left on the surface, which, due to its electron deficient character, behaves as a Lewis acid site These Bronsted and Lewis acid sites have been considered to be responsible for the catalytic activity of Al_2O_3 (3) Knozinger and Ratnasamy (11) have pointed out that during the dehydroxylation process a Lewis base site in the form of a coordinatively unsaturated O atom is also produced However since $3.7 \times 10^{14} \text{ cm}^{-2}$ anion vacancies and coordinatively unsaturated atoms have already been formed at less than or equal to 573K and since catalytic activity of Al_2O_3 is developed only after dehydroxylation at temperatures above 573K , it has been concluded that Lewis acid and base sites, formed during the dehydroxylation process, are unlikely to be responsible for catalytic activity (11) Knozinger and Ratnasamy (11) proposed that between 573K and 673K special site configurations develop which possess the energetic and structural properties required as active sites These sites were believed to be defects in the partially dehydroxylated surface, i.e. with multiple vacancies and/or clusters of O atoms in certain environments depending on the crystal face in which they are exposed (11)

Janacek et al (22) examined the surface acidity of a number of Al_2O_3 samples prepared using different methods Acidity was measured by titration with n-butylamine and ranged from $3.9 \mu\text{mol m}^{-2}$ for Al_2O_3 prepared from AlCl_3 and NH_4CO_3 to $1.0 \mu\text{mol m}^{-2}$ for an Al_2O_3 sample prepared by the thermal decomposition of $\text{Al}(\text{OH})_3$ with

subsequent hydrothermal treatment in the presence of HNO_3 . The differences in acidity were suggested to be due to the different way of formation of primary $\text{Al}(\text{OH})_3$, when, because of the varying conditions during their formation, a different degree of polymerisation of structural units of $\text{Al}(\text{OH})_3$ was achieved, leading to different OH group surface concentrations. The structural phases of the Al_2O_3 used in the study were not determined (22)

The surface acidity of Al_2O_3 (phase not stated) modified by various cations and anions has also been reported (23) The added ions examined were SO_4^{2-} , F^- , PO_4^{3-} , Cl^- , Zn^{2+} , Mg^{2+} and Na^{2+} and acidity was again measured by titration with n-butylamine. The total acidity was determined for an untreated Al_2O_3 sample to be $2.1 \mu\text{mol m}^{-2}$, while the presence of anions led to an increase in total acidity by a factor of two or three. Although Zn^{2+} also increased acidity, the cations Na^+ and Mg^{2+} decreased acidity. The increase in acidity was greatest for bulky anions such as SO_4^{2-} and PO_4^{3-} . The reported results are given in Table 2.1. An attempt was also made to estimate the surface basicity of these Al_2O_3 samples by observing the colour changes of adsorbed acid-base indicators, but the technique was found to be lacking in sensitivity and estimation proved impossible (23)

According to Vit et al (24) there is little information on the basicity of Al_2O_3 as it is generally regarded as an acid catalyst. It has been pointed out that the surface concentration of basic sites may vary depending on factors such as preparation methods, the degree of rehydration and the measurement technique used (24) Vit et al (24) determined the surface concentration of basic sites on $\gamma\text{-Al}_2\text{O}_3$ using a displacement method based on the spectrophotometrically monitored displacement of pre-adsorbed benzoic acid by acetic acid in methanol. The data obtained is given in Table 2.2 and clearly demonstrates the dependence of surface basicity on calcination temperature. Maximum basicity was obtained after calcination at 793K (24) Specific surface area was also directly related to basicity.

When Al_2O_3 is used as a catalyst support, the active component is often introduced by ion exchange (25) One important factor governing this process is the isoelectric point of the support material. The isoelectric point of a solid is the pH at which the surface of the solid is electrically neutral (26) Parks (27) has reviewed work carried out on the isoelectric point of a number of solids including aluminium compounds up to 1965. Some of the results from these studies are given in Table 2.3. However, for a single crystallographic phase, values from 6.4 to 10 have been reported for the isoelectric point, depending on the method of preparation of the sample and the method of measurement. Subramanian et al (28) found that the isoelectric point of a commercially available $\gamma\text{-Al}_2\text{O}_3$ sample, produced by American Cyanamid, was dependent on the temperature at which the sample was analysed, as shown in Fig 2.7. At 296K a value of 7.2 was obtained, while at 355K a value of 8.2 was determined (28)

Table 2 1 · Surface Acidity of Ion Modified Al₂O₃ (23)

Ion	wt%	mmol ion g ⁻¹ Al ₂ O ₃	Specific Surface Area m ² g ⁻¹	Total Acidity μmol m ⁻²
SO ₄ ²⁻	4.85	0.53	239	5.2
F ⁻	2.61	1.41	183	4.1
PO ₄ ³⁻	3.00	0.33	223	2.9
Cl ⁻	0.99	0.28	216	2.6
Zn ²⁺	1.28	0.20	203	2.3
	2.12	0.33	210	2.4
	4.14	0.66	20	2.5
Mg ²⁺	0.89	0.37	240	1.8
Na ⁺	0.62	0.27	208	0.4
Untreated	-----	-----	209	2.1

**Table 2 2 Dependence of Basicity of Al₂O₃ Sample on Calcination
Temperature (24)**

Calcination Temperature (K)	Specific Surface Area (m ² g ⁻¹)	Basicity (μmol g ⁻¹)
283	101	78
723	259	245
793	285	326
853	171	156
983	138	107
1123	122	84

Table 2 3 Summary of Results for Isoelectric Points Reported in the Literature and Reviewed by Parks (27)

Compound	Isoelectric Point	Method of Preparation
α -Al ₂ O ₃	9 4	Flame Fusion Sapphire
	10	Commercial "Chromatographic Al ₂ O ₃
	8 4	Natural Corundum
	9 4	Natural Corundum
	9 4	Flame Fusion Sapphire
	6 4 - 6 7	α -Al ₂ O ₃ (Linde A abrasive)
γ -Al ₂ O ₃	8 0	From Thermal Treatment and Aging of Al Ethylate
	8 35	γ -Al ₂ O ₃
	7 20	Commercially Available γ -Al ₂ O ₃ (American Cyanamid)
α -AlOOH	< 2	Natural Bauxite
	8 8	From AlCl ₃ + NH ₄ OH at 291K
	7 6	From Na ₂ AlO ₃ + CO ₂
γ -AlOOH	2	Natural Diaspore
	7 5	From AlCl ₃ + NH ₄ OH at 343K
	5 4	From Na ₃ AlO ₃ + CO ₂
α -Al(OH) ₃	5 2	Natural Gibbsite
	4 9	From Aging of Na ₃ AlO ₃ (aq)
γ -Al(OH) ₃	9 2	From Hydrolysis of Purified Al(OC ₂ H ₅) ₂
	7 5	From AlCl ₃ + NH ₄ OH(aq) at 343K
	5 4	From Na ₃ AlO ₃ (aq) + CO ₂ (g)

Added cations and anions also influence the isoelectric point of Al₂O₃ (26) For an Al₂O₃ sample, whose phase was not reported, the addition of anions decreased the pH of the isoelectric point from 7 3 for an untreated sample to 5 6, 4 7 and 4 5 for the addition of F⁻, Cl⁻ and SO₄²⁻ respectively Cation addition, in the case of the ions Zn²⁺ and Mg²⁺ had little effect, but for Na⁺ a pH value for the isoelectric point of 9 7 was obtained (26)

The surface areas of some of the Al₂O₃ phases reported by various workers are given in Table 2 4, together with reported values of density It is important for a catalyst support material to have a high surface area on which the active phase can be distributed (25) For this reason the high surface area η - and γ -phases are used extensively as catalyst support materials (11) γ -Al₂O₃ has typical surface areas and densities ranging

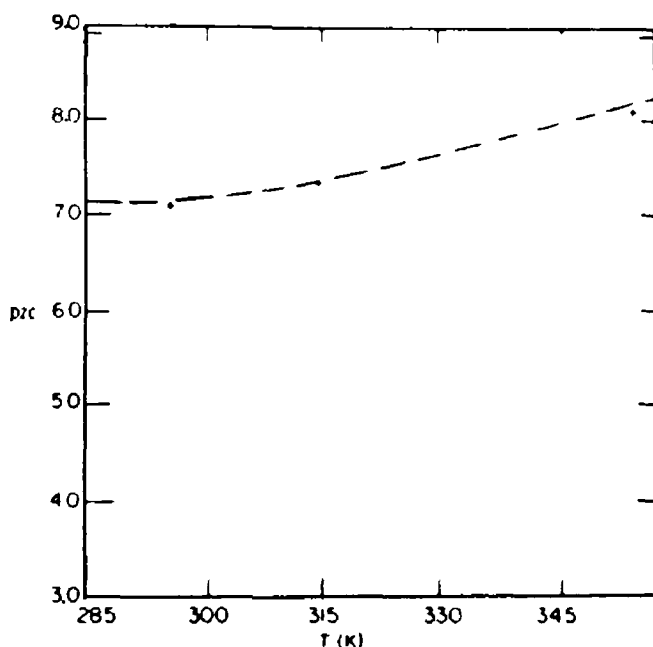


Fig 2.7 . Dependence of isoelectric point on temperature of measurement for Al_2O_3 (28)

from $129\text{m}^2\text{g}^{-1}$ to $>500\text{m}^2\text{g}^{-1}$ and 0.4 to $0.8\text{ cm}^3\text{g}^{-1}$ respectively. For the surface area of $\eta\text{-Al}_2\text{O}_3$ values as high as $250\text{m}^2\text{g}^{-1}$ have been reported (11). The higher temperature phases such as $\delta\text{-Al}_2\text{O}_3$ and $\theta\text{-Al}_2\text{O}_3$ have much lower surface areas, see Table 2.4. The α -phase normally has a low surface area compared to the other phases of Al_2O_3 , as low as 2 or $3\text{ m}^2\text{g}^{-1}$ (30). However, formation of a high surface area form of $\alpha\text{-Al}_2\text{O}_3$ has been reported by Russell and Cochrane (35). They found that upon heating diaspor (an aluminium oxyhydroxide, $\text{AlO}(\text{OH})$) at 873K , a material with a surface area of $85\text{m}^2\text{g}^{-1}$ was formed and was identified using x-ray diffraction to be $\alpha\text{-Al}_2\text{O}_3$. The transformation of phases to $\alpha\text{-Al}_2\text{O}_3$ is a subject to which a large body of research has been devoted as support surface area loss can lead to loss of activity for supported catalysts (36). The common features of the γ -, δ -, θ - and η -phases are the cubic close packing of the O ions, Al ions in the octahedral groups, with the θ and δ -phases being nearly dehydroxylated (37).

Soled (29) proposed a model for $\gamma\text{-Al}_2\text{O}_3$, taking hydroxyl groups as structural elements into account. He found that the formula $\text{Al}_{8/3-x}\square_x\text{O}_{4-y/2}(\text{OH})_y$ was consistent when $x = y$ and yielding the stoichiometry $\text{Al}_{2.5}\square_{0.5}\text{O}_3.5(\text{OH})_{0.5}$ where \square represents cation vacancies. According to Soled (29) the changes of the γ -, θ - and δ -phase to the $\alpha\text{-Al}_2\text{O}_3$ could be viewed as particle growth resulting from condensation of hydroxyl

Table 2 4 • Reported Surface Areas and Densities of Al₂O₃ Phases

Al ₂ O ₃ Phase	Density (g cm ⁻³)	Reference	Specific Surface Area (m ² g ⁻¹)	Reference
α	3 20	4	2 - 10	1, 4, 29
γ			> 500	1
			200	11
			190	28
			171 - 285	24
			129	30
χ	3 00	5	180	31
			200 - 250	32
δ	3 20	5	30	31
θ	3 56	4	37	4
			20	31
η	2 50 - 3 60	5	250	11
			220	33, 34

species and formation of water. This would account for the less dehydroxylated nature of γ-Al₂O₃ compared to the θ- or δ-phase, the former phase containing one mole of water per five moles of Al₂O₃ (37). The major modification of these phases during dehydroxylation is probably microporosity (37). Burtin et al (37) pointed out that the drawback with the above model for γ-Al₂O₃ is that the requirements of the spinel structure were not met by the Soled model (29) as the ratio between the trivalent and divalent cationic sites was not equal to two. Thus, the proposed the formula for γ-Al₂O₃ (37), was



where \square represents cation vacancies, $< >$ represents anionic vacancies of the spinel structure. Burtin et al. (37) proposed that upon high temperature treatment the removal of water by a dehydroxylation mechanism results in an increasing number of anion vacancies. Due to the defect structure of the spinel lattice for transition Al_2O_3 , cation vacancies are also present and the annihilation of these vacancies leads to the destruction of the spinel lattice and a structural re-arrangement proceeding exothermally (37). The above model for the transformation from γ - to α - Al_2O_3 is one which does not involve mechanisms of co-operative or diffusional atomic movements and is in agreement with the experimental results of Tucker and Hren (38). Their TEM data indicated that the transformation begins on the surface of isolated particles or the neck region of sintered particles where anion vacancies are preferentially located and as sintering generally occurs before transformation, vacancies are expected to occur more frequently at the neck between adjacent particles (38). Hence in the Burtin et al. (37) model the formation of α - Al_2O_3 would occur by a nucleation and growth mechanism. Nucleation would proceed in regions rich in cationic and anionic vacancies while growth would occur through an annihilation reaction between cationic and anionic vacancies at the reaction interface (37).

The transformation of Al_2O_3 phases to the α - Al_2O_3 has been examined by a number of other studies reviewed by Tucker and Hren (38). The mechanisms proposed include nucleation growth (39, 40), stacking fault growth i.e. nucleation at the surface and neck regions of particles (41, 42), synchro-shear (diffusionless co-operative atom movement) (43) and volume diffusion (44) for the γ -phase. For the θ -phase both sintering/synchro-shear (45) and nucleation growth (40) have been proposed.

A number of authors have studied the influence of sintering temperature on the surface area of Al_2O_3 , and have shown decreasing surface areas as the temperatures is increased (46, 47, 48). Gitzen (49) has pointed out that factors including particle size, heating rate and the presence of impurities can effect the transformations of Al_2O_3 . Burtin et al. (50) found that the greater the initial surface area of the Al_2O_3 sample the higher the rate of transformation to the α -phase, upon calcination at high temperature. Fig.2.8 (50) illustrates the specific surface area for two Al_2O_3 samples, with different initial specific surface areas, as a function of time after calcination at 1378K.

The atmosphere in which the Al_2O_3 sample is calcined can also have a large effect on the rate of surface area loss. The surface area loss of γ - Al_2O_3 during calcination is greatly accelerated by the presence of water vapour (46, 48, 51). In the region of 1273K, in the presence of steam, the γ -phase has been found to undergo rapid transformation to the α -phase (52). It has been suggested that the acceleration of the phase transformation is caused by adsorption/desorption of water molecules, leading to an acceleration of the surface diffusion of O anions (53) in a similar manner to the

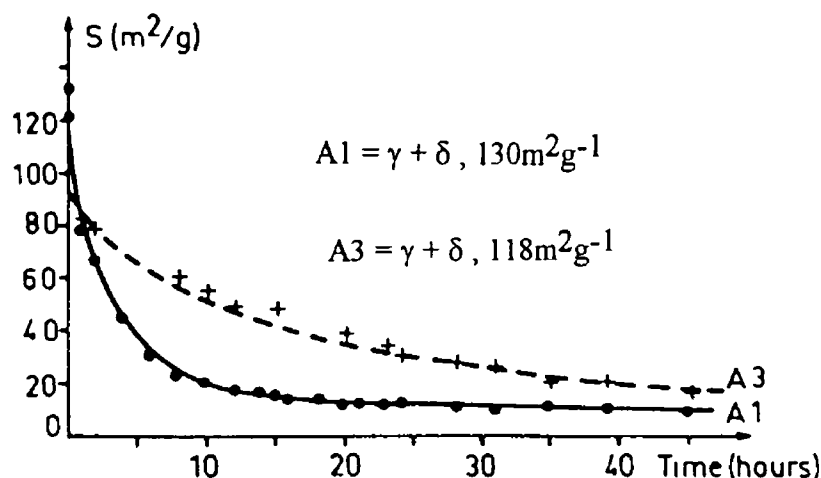


Fig 2.8 : Specific surface areas of two different Al_2O_3 samples versus time of calcination at 1378K (50).

mechanism suggested by Anderson and Morgan (54) for the effect of steam on the sintering of MgO . In that case sintering was thought to occur due to the mobility and rapidity of exchange of H_2O molecules on the surface. The adsorption and desorption of H_2O provided a mode of transport for the O^{2-} ion, so that an O ion from the surface could be removed in the desorbing H_2O molecule leaving the O^{2-} of the original H_2O in an adjacent position on the surface (54).

Additives to Al_2O_3 can affect phase transformation either by inhibiting or accelerating the process. It has been determined that metal oxides can inhibit the transformation of $\gamma\text{-Al}_2\text{O}_3$ to the α -phase by up to 523K (49). Alkaline earth metal ions have also been found to influence the thermal stability of transition Al_2O_3 (55), for example the stabilisation of Al_2O_3 by the addition of Ba (56) which resulted in Al_2O_3 which exhibited surface areas as high as $10\text{m}^2\text{g}^{-1}$ after calcination at 1873K. The stabilisation was believed to be due to the formation of stable barium hexa-aluminate, $\text{BaO} \cdot 6\text{Al}_2\text{O}_3$ (56).

The effects of cations on the thermal stability of Al_2O_3 have been reported but in some cases contradictory results have been obtained by different researchers for the effects of certain cations (50). Some of this work is summarised in Table 2.5.

Table 2 5 Studies on the Effect of Ions on the Phase Transformations of Al_2O_3

Inhibitors	Accelerators	Reference
	Fe^{3+}	43
La^{3+} , Zr^{4+} , Ca^{2+}	In^{3+} , Ga^{3+} , Mg^{2+}	50
Si^{4+}		55
Ba^{2+}		56
Th^{4+} , Sc^{3+} , Be^{2+} , Ce^{3+} , Sr^{2+} , Ca^{2+}	Fe^{3+} , Mn^{3+} , Mo^{3+} , Co^{3+} , Zn^{2+} , Y^{3+} , Mg^{2+} , La^{3+}	57
Cr^{6+}	Cr^{3+}	58
Mg^{2+} , Zr^{4+} , La^{3+}		59
	Ni^{2+}	60
La^{3+}		62, 63, 64, 65, 66
La^{3+} , Ce^{3+} , Cs^+ , Zr^{4+} , Ba^{2+} , Ca^{2+}		67
Ce^{3+}		68, 69

Young et al (60) examined the deactivation of $\text{Ni}/\text{Al}_2\text{O}_3$ supported catalysts and found that this was caused by transformation from γ - to α - Al_2O_3 of the support which was catalysed by the presence of Ni . This reaction was found to be complex, with the surface area of the support being stabilised initially but decreasing rapidly with increase in the time or temperature of calcination. At 1173K and 1223K the surface area of $\text{Ni}/\text{Al}_2\text{O}_3$ dropped slightly and then remained constant for 14h, after which time the surface area was observed to rapidly decrease. These effects were rationalised in terms of an initial substitution of divalent Ni in the trivalent Al lattice resulting in a decrease in the number of cation vacancies and a decrease in Al diffusion in the surface region and, therefore, an initial stabilisation. However dissolved Ni would diffuse away from the surface region into the bulk of the Al_2O_3 , the rate being strongly temperature dependent. The arrival of Ni at grain boundaries could form nucleation sites for transformation to the α -phase, a necessary precursor step for the rapid formation of that phase (60).

Kozlov et al (61) found that dispersed Pt on γ - Al_2O_3 lowered the temperature of the phase transformation of the support to the α -phase as illustrated in Fig 2 9. The effect was found to be proportional to Pt content (up to 3wt%)

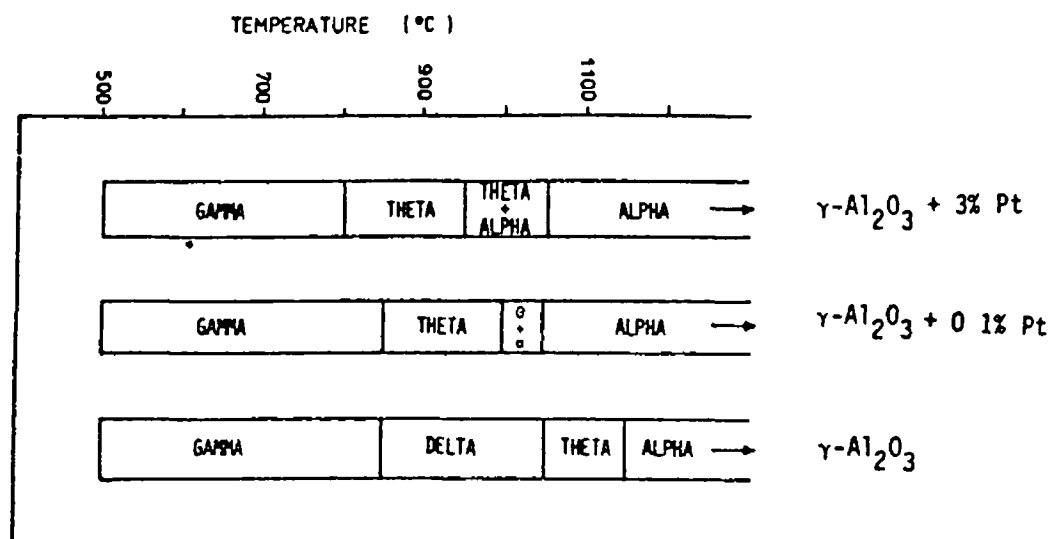


Fig 2.9 : The effect of Pt concentration on the transition temperature of $\gamma\text{-Al}_2\text{O}_3$ to the α -phase (61).

Burtin et al (50) examined the addition of a number of cations to $\gamma\text{-Al}_2\text{O}_3$ and found that Al^{3+} , Ga^{3+} and In^{3+} ions lowered the temperature of transformation to the α -phase to 1545K, 1549K and 1533K respectively, compared with 1553K for untreated $\gamma\text{-Al}_2\text{O}_3$. Similarly XRD measurements for conversion to $\alpha\text{-Al}_2\text{O}_3$ indicated that cations, in order of increasing acceleration for the transformation, were In^{3+} , Ga^{3+} , Al^{3+} and Mg^{2+} . On the other hand the cations Zr^{4+} , Ca^{2+} , Th^{4+} and La^{3+} were found to be inhibitors of the formation of $\alpha\text{-Al}_2\text{O}_3$, with La^{3+} increasing the temperature of transformation to 1657K. It was established that the concentration of the added element did not play a crucial role in the transformation mechanism, but that a threshold concentration was required to obtain a homogeneous solid solution in order to observe the real effect of the cations (50).

A kinetic model has been put forward to describe the effects of added cations on the transformation of $\gamma\text{-Al}_2\text{O}_3$ to the α -phase based on cation valency and distribution among divalent or trivalent sites (37). It was based on the equation -

$$\delta\lambda/\delta t = A[1 + \beta(5N - Z - 2)]$$

where $\delta\lambda/\delta t$ represents the rate of change of the fraction of α - Al_2O_3 formed, A is a constant related to a given fraction of α - Al_2O_3 formed (λ), N is the ratio of the number of trivalent or divalent sites occupied by added cations, which is dependent on the ionic radii of the cations concerned, β is the ionic fraction of the cation with respect to the Al cations and Z represents the valency of the cations (37)

Schaper et al (62) added La^{3+} to γ - Al_2O_3 , in order to improve thermal stability. In untreated γ - Al_2O_3 , the phase transformation to α - Al_2O_3 was found to proceed via a nucleation and growth mechanism. The addition of La^{3+} stabilised the γ - Al_2O_3 but decreased the initial specific surface area prior to the sintering test. The presence of La^{3+} was found to cause a decrease in the rate of surface diffusion due to the formation of a La compound on the surface forming physical barriers or impassable blocks. Using ESR spectroscopy, this compound was identified as lanthanum aluminate (LaAlO_3). The addition of La was found to postpone the transformation to the α -phase by 373K by decreasing the rate of nucleation.

Oudet et al (63, 64) also added La^{3+} to the Al_2O_3 supports, again to increase thermal stability. In agreement with Schaper and co-workers (62) they found that the addition of La led to the nucleation of a thermally stable LaAlO_3 perovskite type structure. As this compound was similar in crystallographic nature to γ - Al_2O_3 (both being face centred cubic related compounds) it was proposed that coherent interfaces formed between the microdomains of the γ - Al_2O_3 phase and the stable LaAlO_3 phase, thus ensuring the thermal stability of the support (63). For La doped Pt/ Al_2O_3 and Pt-Rh/ Al_2O_3 the microdomains influenced both the thermal stability of the Al_2O_3 and provided increased numbers of nucleation sites for metals during deposition. The LaAlO_3 microdomains strongly decreased the extent of coalescence of aggregates at high temperatures (64).

Bettman et al (65) pointed out that since La additions reported by Schaper et al (62) were lower than the concentration required to give a La_2O_3 monolayer, the blocks of LaAlO_3 must have been tiny and three dimensional in nature and spaced closely together in order to influence surface diffusion. Xie et al (66) investigated the structure of dispersed La_2O_3 supported on γ - Al_2O_3 , using XRD analysis. The concentration at which the La_2O_3 crystalline phase was no longer detectable was taken to be the amount required to give a two dimensional monolayer on top of the Al_2O_3 , $17.2 \mu\text{mole La m}^{-2}$. It was suggested that the resulting surface would be composed of patches of oxide ions sitting on oxygen ions of the substrate, without any cementing cations in between.

Bettman et al (65) also proposed a two dimensional overlayer over γ - Al_2O_3 , but their values for the saturation layer was half of the value of that reported by Xie et al (66). According to Bettman et al (65), for samples produced by the impregnation of Al_2O_3 with aqueous LaNO_3 beyond the two dimensional layer saturation, the crystalline

phase which developed was cubic La_2O_3 below approximately 973K and LaAlO_3 between approximately 1073K and 1273K

Dreeland and Finlayson (67) examined cation additions to a form of fibrous η - Al_2O_3 "Saffil", produced by ICI, in order to improve thermal stability at high temperatures, see Table 2 5 Of the cations examined, La^{3+} , Ce^{3+} and Cs^+ were found to be most effective, with low amounts of dopant more efficient than higher concentrations of cations for thermal stabilisation It was determined that the thermal stability of the untreated η - Al_2O_3 fibre was lower than any of the doped samples, at temperatures up to 1273K (67)

A number of workers have examined the effect of additives on the thermal stability of Al_2O_3 exposed to high temperatures in the presence of water vapour (51, 53, 55) In sintering experiments involving exposure at 1173K for 40 h under a partial steam pressure of 12 bar Schaper et al (53) found that the addition of 4-5 mol% La_2O_3 drastically decreased surface area loss of γ - Al_2O_3 After heat treatment undoped Al_2O_3 exhibited a surface area of $3\text{m}^2\text{g}^{-1}$, whereas the sample containing 5 mol% La_2O_3 had a surface area of $30\text{m}^2\text{g}^{-1}$ (53)

Beguin et al (55) investigated the influence of Si additions on the thermal stability of Al_2O_3 Si was introduced in the form of tetraethoxy silicon, $\text{Si}(\text{OC}_2\text{H}_5)_4$ Untreated Al_2O_3 as well as Si modified samples were aged under a flow of air at 1323K or 1493K for 24 h in the presence or absence of water vapour (21 vol%, the percentage corresponding to the amount of water vapour formed during combustion of a stoichiometric air + CH_4 mixture) At 1323K in steam the undoped Al_2O_3 was completely converted to the α -phase, the surface area dropping from $107\text{m}^2\text{g}^{-1}$ initially to $4\text{m}^2\text{g}^{-1}$ after heat treatment The stability of Al_2O_3 increased with the Si loading, with a Al_2O_3 sample containing 3wt% Si exhibiting a surface area of ca $50\text{m}^2\text{g}^{-1}$ after 24h at 1373K in steam As the stabilisation increased with increasing Si coverage (up to 3wt%) it was suggested that the surface species responsible for the sintering process was not present at the surface of the modified Al_2O_3 Furthermore, it was claimed that the formation of Si-O-Si or Si-O-Al bridges during the dehydroxylation process was at the origin of the stabilisation effect as their formation decreased the number of cationic vacancies (55)

In the following sections the work carried out on the characterisation of the Al_2O_3 fibre material "Saffil" will be detailed The thermal stability of the Al_2O_3 was determined and attempts to improve the thermal stability by the addition of different cations were investigated The Al_2O_3 fibre was to be used as a support for Pt oxidation catalysts and as part of the preparation procedure the support was normally prewashed in acid prior to impregnation with Pt Therefore the effects of acid washing on the surface area and thermal stability of the Al_2O_3 material were also examined

2 1 Experimental

2 1 1 Preparation of Al₂O₃ Samples

Acid Washing Treatment

The Al₂O₃ material used was produced by ICI(Runcorn) under the trade name "Saffil" The manufacturer quoted the composition as greater than 95% Al₂O₃ and less than 5% SiO₂ Impurities of Fe, Cr, Ni, Na, Mg, Ca and Cl were present in quantities of less than 2210 ppm The Al₂O₃ was claimed to be the η phase The Al₂O₃ was used, as supplied, in mat form The preparation methods for the Al₂O₃ sample pre-treated with water or acid are summarised in Table 2 6

Table 2 6 Pre-treatment Details for Al₂O₃

Sample Code	Treatment	Rinsing procedure	Drying
U	none	none	none
H	0 1MHCl (0 025dm ³ g ⁻¹ Al ₂ O ₃)	H ₂ O (2 5dm ³ g ⁻¹ Al ₂ O ₃)	340K for 16h
N	0 1MHNO ₃ (0 025dm ³ g ⁻¹ Al ₂ O ₃)	H ₂ O (2 5dm ³ g ⁻¹ Al ₂ O ₃)	340K for 16h
W	none	H ₂ O (2 5dm ³ g ⁻¹ Al ₂ O ₃)	340K for 16h

The acid washed samples were prepared using either 0 1M HNO₃ or 0 1M HCl The acid was supplied by Riedel de Haen, reagent grade In both cases the mats were sprayed with acid The Al₂O₃ mats were then washed with warm milli Q water in order to remove excess nitrate or chloride ions In the case of the HCl treatment, the washings from the water rinse were tested with silver nitrate to check that no chloride ions were present The water washed sample (W) was prepared by taking a 2g Al₂O₃ mat and rinsing with 5dm³ of warm water All samples were dried at 340K for 16h in an oven and then ground to powder form An untreated mat sample was also examined as a control In addition an untreated Al₂O₃ sample which had undergone calcination (see below) was acid washed as described above with HCl (Sample CH)

All samples in the acid pre-treatment study were calcined in static air at 1370K for various intervals of time, in a muffle furnace 1g samples were placed in porcelain crucibles and heated to 1370K at a rate of 250Kh⁻¹ After 24h at 1370K a small amount

of each sample was removed for surface area determination. After 45h all samples were removed from the furnace. After firing, samples were cooled to room temperature in a desiccator, prior to testing.

Impregnation with Cations

The preparation details for Al_2O_3 samples impregnated with cations is given in Table 2.7. Each sample is described by an alpha-numeric code. The first letter indicates the cation added, L = La^{3+} , C = Ce^{3+} and S = Si^{4+} . The second indicates whether the Al_2O_3 used was untreated, U, or pre-treated with HNO_3 , N. The third letter indicates whether the Al_2O_3 was dry, D, or pre-wetted prior to cation impregnation, W or heated at high temperature prior to cation addition, T. The fourth letter C indicates that the sample was calcined after impregnation below 800K to decompose the precursor salt. Finally, the numbers 1, 2 or 3 refer to the percentage wt% cation loading of either 0.5 wt%, 1.0 wt% and 3.0 wt% respectively.

In all cases ground Al_2O_3 Saffil fibre (either untreated, dried at 723K for 14h in an oven or pre-treated with HNO_3) was used. Impregnation was carried out by the addition of alcoholic solutions of either $\text{LaCl}_3 \cdot 7\text{H}_2\text{O}$ (Riedel de Haen, Analar), $\text{Ce}(\text{NO}_3)_3 \cdot 6\text{H}_2\text{O}$ (Riedel de Haen, Analar) or $\text{Si}(\text{OC}_2\text{H}_5)_4$ (Aldridge 99% pure) to the ground fibre. In the case of La and Ce additions, CH_3OH (Lab-Scan HPLC grade) was used as the solvent, while for Si, $\text{C}_2\text{H}_5\text{OH}$ (Riedel de Haen, reagent grade) was used as the solvent. After mixing for one hour, excess solvent was removed using either a rotary evaporator or by vacuum filtration using a sintered glass funnel to collect the impregnated Al_2O_3 fibre. After solvent removal the impregnated fibre was then dried at 340K for 16 h in an oven. For certain samples (denoted SUWC) impregnated with Si a heat treatment after drying, which involved heating in flowing air ($30\text{dm}^3\text{h}^{-1}$) at 770K for 12h, was carried out.

All samples were calcined at 1370K, with removal of portions of each sample after time intervals between 14 and 48h, certain samples were also calcined at 1370K in flowing air containing 10% H_2O including an untreated Al_2O_3 sample. In addition untreated Al_2O_3 samples were heated for 24h at temperatures from 873K to 1273K.

2.1.2 Surface Area Determinations

The surface area was determined using a Micromeritics Pulse Chemisorb 2700 (a schematic diagram of which is given in Fig. 2.10). The instrument consisted of a prep line for sample treatment prior to analysis and a test line connected to a TCD. Specific surface areas were determined using a single point method, results being obtained by N_2 adsorption at liquid N_2 temperatures ($< 75\text{K}$) from a 30% N_2 /70% He

Table 2 6. Preparation Details for Al₂O₃ Samples Impregnated with Cations

Sample Code	Cation	Loading wt%	Preparation Procedure	Heat Treatment
LUW1	La ³⁺	0.5	Solutions of MeOH containing LaCl ₃ 7H ₂ O were added to the powdered, prewetted Al ₂ O ₃ fibre. Solvent was removed using a rotary evaporator. Dried at 340K for 12h.	None
LUW2		1.0		
LUW3		3.0		
LUD1	La ³⁺	0.5	As for LUW samples except that the impregnation solution was added to dry Al ₂ O ₃ .	None
LUT1	La ³⁺	0.5	As above except that the Al ₂ O ₃ was dried at 823K for 1h prior to impregnation.	None
LUWC1	La ³⁺	0.5	As for LUW samples.	723K for 4h in static air.
CUW1	Ce ³⁺	0.5	As for LUW samples except that Ce(NO ₃) ₃ 6H ₂ O was used.	None
CUW2		1.0		
CUW3		3.0		
CNW2	Ce ³⁺	1.0	As above except that the Al ₂ O ₃ was treated with 0.1M HNO ₃ prior to impregnation.	None

Table 2 6 contd

Sample Code	Cation	Loading wt%	Preparation Procedure	Heat Treatment
CE	Ce ³⁺	20.0	As above except that excess solvent was removed by vacuum filtration, washed with milli Q H ₂ O and, after air drying for 15min under vacuum, dried in the normal manner	None
SUW1	Si ⁴⁺	0.5	Solutions of EtOH containing tetraethylorthosilicate were added to the powdered, EtOH prewetted Al ₂ O ₃ . Solvent was removed using a rotary evaporator, dried at 380K for 12h	None
SUW2		1.0		
SUW3		3.0		
SUWC1	Si ⁴⁺	0.5	As for SUW samples	770K for 12h under flowing air (30dm ³ h ⁻¹)
SUWC2		1.0		
SUWC3		3.0		

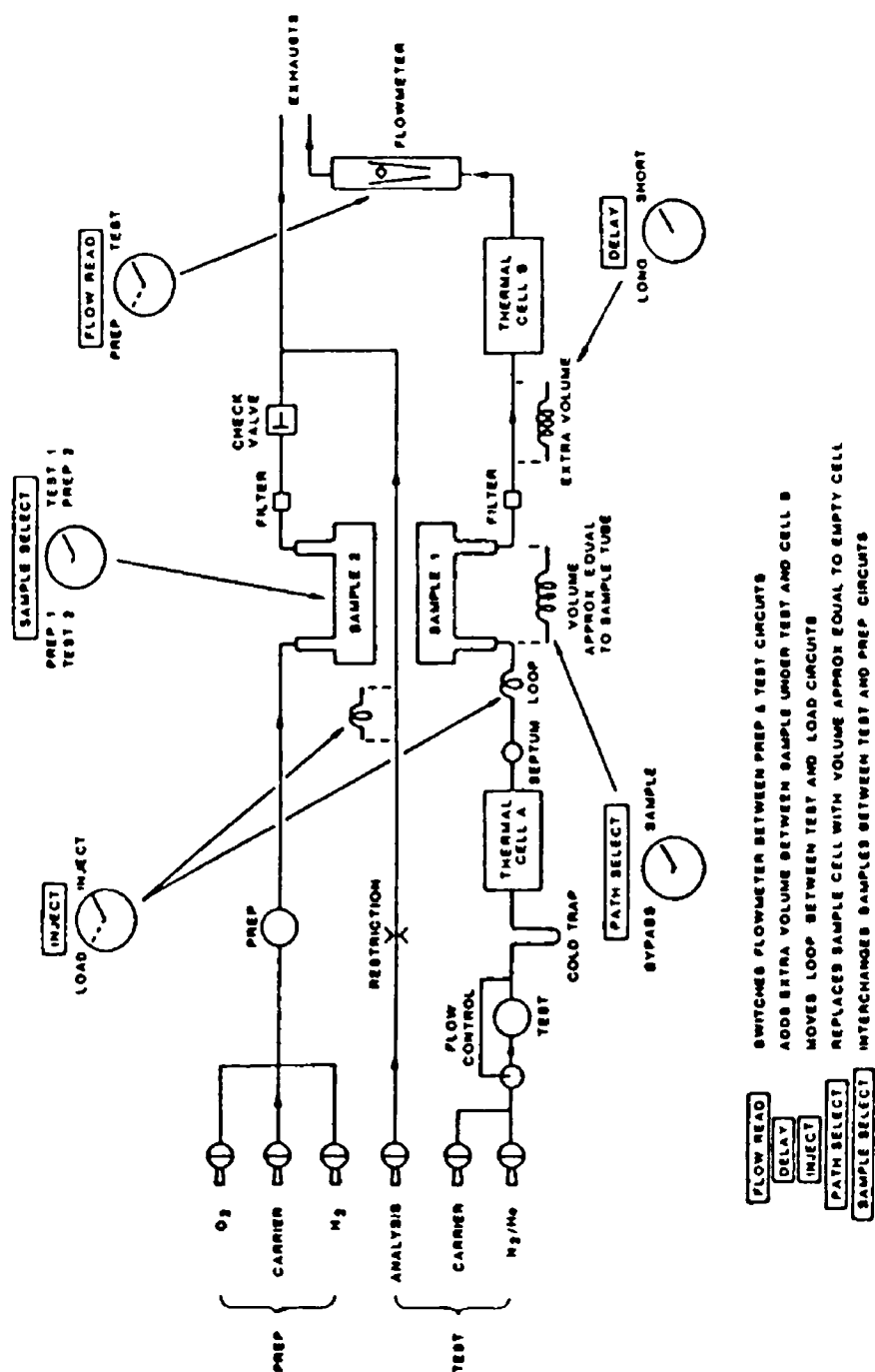


Fig 2 10 Schematic diagram of Pulse Chemisorb 2700

mixture The N₂ (Irish Industrial Gases Ltd , normal grade) and He (Air Products Ltd , normal grade) were passed through O₂ and H₂O traps prior to entering the instrument The gas ratio was obtained using two flow regulators Prior to analysis the instrument was calibrated using an empty sample holder placed on the test line, injecting slugs of N₂ (1cm³) into the system and calibrating the instrument to display the surface area occupied by 1 cm³ N₂ (see Appendix I) For analysis, 0.1g of sample was placed in a clean dry, pre-weighed sample tube which was then attached to the Pulse Chemisorb 2700 on the prep line The sample was then outgassed in the N₂/He mixture (15cm³ min⁻¹) at room temperature for 5 minutes, purged at 370K for 15 minutes and finally 530K for 1h The sample was then cooled to room temperature and switched to the test line via a four port valve (see Fig 2.10) Adsorption was brought about by immersion of the sample tube in a dewar flask containing liquid N₂, while desorption was brought about by heating the sample to room temperature The quantities of nitrogen adsorbed and desorbed were monitored using the thermal conductivity detector within the instrument Each sample underwent a minimum of two adsorption-desorption cycles during a single point analysis Differences of less than 5% were observed between adsorption and desorption peaks and successive adsorption peaks agreed within 1% Agreement between results obtained for the surface area of two different samples of the same material was within 5%

In order to check the accuracy of the single point method an untreated fibre sample (U) was examined by the above single point method and by a multipoint method The multipoint method was similar to the single point method except that analysis was carried out using different N₂/He gas mixtures ranging from 10% to 40% content) Additionally the instrument had to be calibrated to display the volume of N₂ adsorbed at each % N₂ content The basis of the calibration procedure is given in Appendix I For the multipoint method, differences of less than 4% were observed between adsorption and desorption peaks at a particular N₂ content and less than 1% for successive adsorption peaks at a particular N₂ content For surface areas of different samples of the same material, differences of less than 2% were observed The values obtained from the multipoint surface area determination on sample U are given in Table 2.7 and Graph 2 The value obtained for the surface area of the sample was 156 m²g⁻¹ for the multipoint method which was in good agreement with the value obtained using the single point method which was 154m²g⁻¹ Therefore the single point method was used for subsequent surface area determination All results were recorded on a Philips PM8261 xt Recorder

2.1.3 Total Pore Volume Measurements

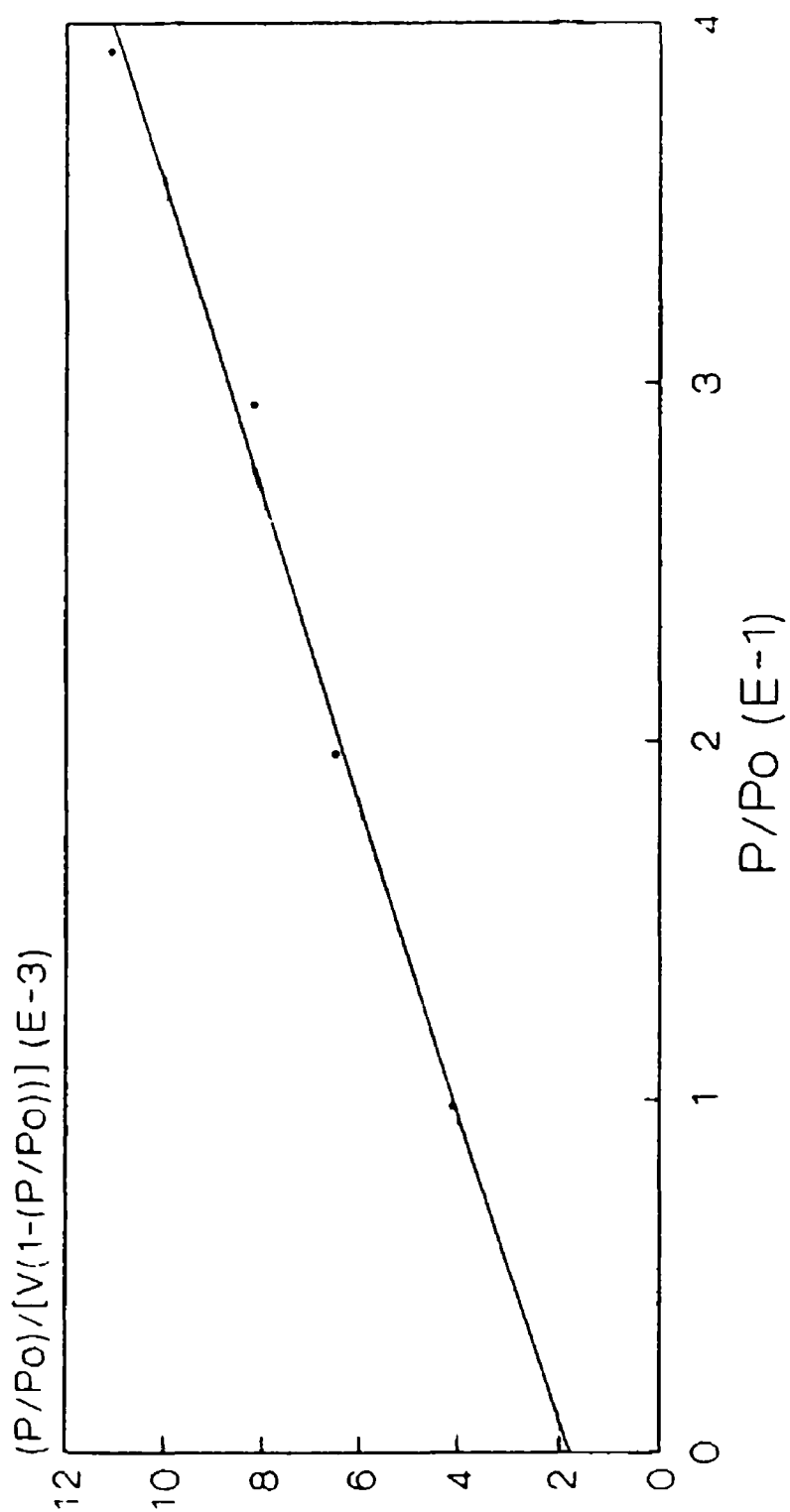
Total pore volume measurements were carried out using the Micromeritics Pulse Chemisorb 2700 The instrument was first calibrated by placing an empty sample holder

on the test line and injecting a 10cm³ volume of pure N₂ in a stream of 98% N₂/2% He at ambient conditions. The instrument was then adjusted to indicate the true volume of this gas when condensed as a liquid, the state in which it existed when filling the pores of a sample under these conditions. A ground sample (approximately 0.15g) was placed in the sample holder and attached to the prep line of the instrument and degassed in pure N₂ (Irish Industrial Gases, reagent grade) at 373K for 0.5h and then 523K for 1h before cooling to room temperature prior to analysis. The sample holder was immersed in liquid N₂ for 0.25h in order for N₂ to condense in all of the pores of the sample. Then a 98%N₂/2%He mixture was established over the sample and N₂ was then detected by the thermal conductivity detector so that the total pore volume was detected. The error for samples of the same material was typically $\pm 3\%$. Again the results were recorded using a Philips PM8261 xt Recorder.

Table 2.7 Surface Area Analysis

Sample Code	Sample Mass (g)	Nitrogen Content (%)	Specific Gas Volume (V) (cm ³ g ⁻¹ at STP)	P/Po* (x10 ⁻¹)	P/Po V(1-P/Po) (x10 ⁻³)	Specific Surface Area (m ² g ⁻¹)
U	0.0972	10	26.75	0.98	4.1	156.58
		20	37.55	1.96	6.5	
		30	50.41	2.94	8.2	
		40	58.23	3.92	11.1	

* $P/Po = (\% \text{Nitrogen Content} / 100) \times [\text{atm Pressure} / (\text{atm Pressure} + 15)]$



Graph 2. Adsorption isotherm according to the BET equation

2 1 4 X-Ray Diffraction Measurements

To determine the Al_2O_3 phases present x-ray diffraction measurements were carried out using a Philips 1400 series x-ray Diffractometer with a $\text{Cu K}\alpha$ source, $\lambda = 1.5405 \text{ \AA}$, operating with a voltage of 40KV and lamp current of 20mA. The scan rate was 1°min^{-1} and chart speeds of 1 cm min^{-1} or 2 cm min^{-1} were used. The range setting varied according to the intensities of the diffraction peaks, from $1 \times 10^3 \text{ cs}^{-1}$ to $1 \times 10^4 \text{ cs}^{-1}$. The powdered sample was placed in a rectangular sample holder, compressed manually using a cover slip, and then placed in the instrument.

2 1 5 Thermogravimetric Analysis

Thermogravimetric measurements were carried out in order to determine water loss from the Al_2O_3 using a Stanton Redcroft Thermogravimetric Analyser, TGA750. The results were recorded on a Linseis 6510 twin pen chart recorder. 10mg powdered samples were used. Samples were heated at a rate of 10 K min^{-1} up to 1173 K under static air.

2.2 Results and Discussion

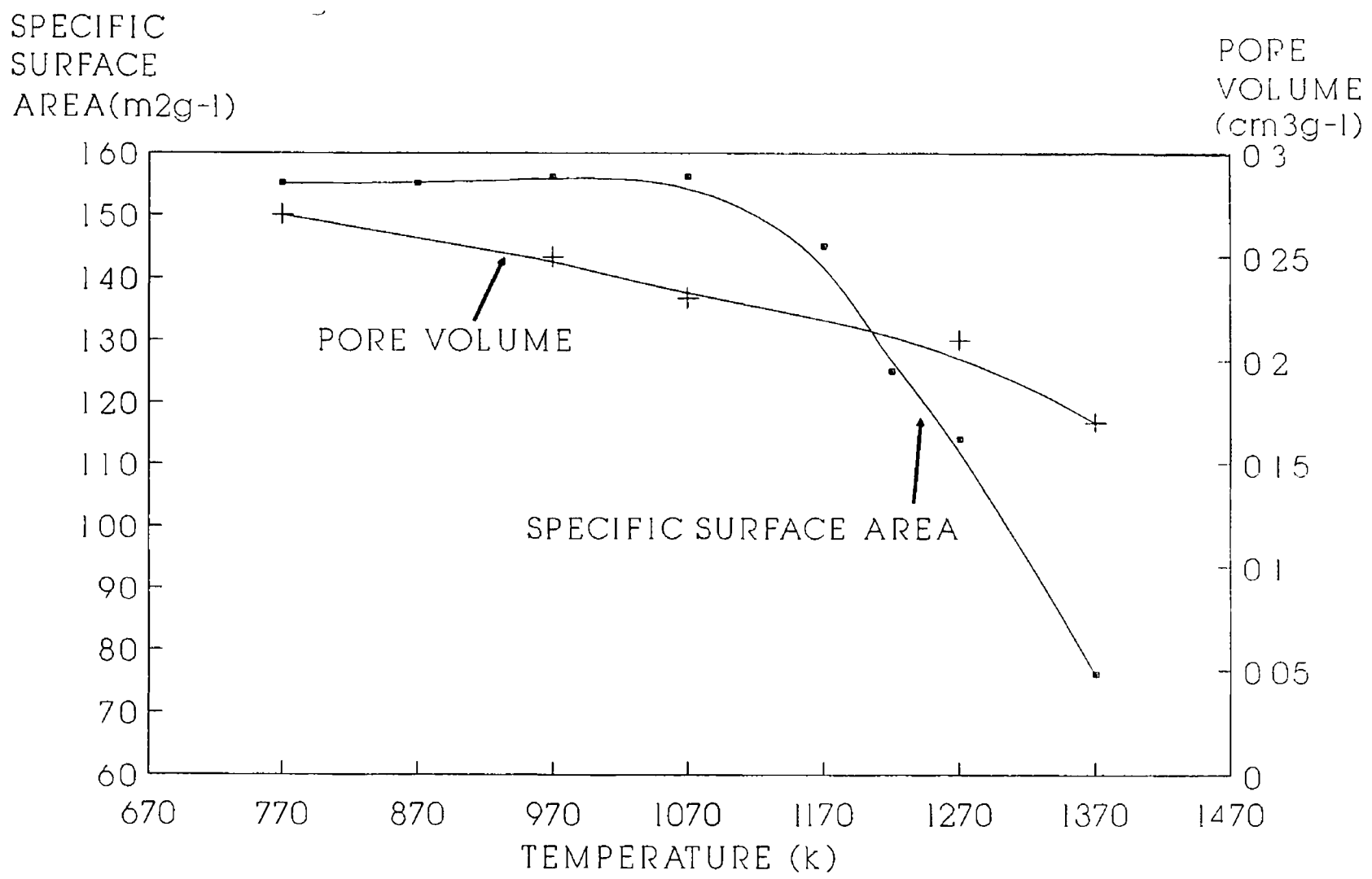
The specific surface areas for U heated for 24h at various temperatures are illustrated in Graph 2.1 together with pore volumes. No loss of surface area occurred up to 1070K but above this temperature the loss became significant, dropping from $155\text{m}^2\text{g}^{-1}$ for an uncalcined sample to $125\text{m}^2\text{g}^{-1}$ after calcination at 1220K for 24h. After 24h at 1370K the surface area dropped to $76\text{m}^2\text{g}^{-1}$, while the pore volume decreased to $0.17\text{cm}^3\text{g}^{-1}$, compared with $0.27\text{cm}^3\text{g}^{-1}$ for an uncalcined sample. Table 2.9 shows the change in surface area with time on calcination at 1370K for sample U and various other acid and H_2O treated samples. The surface area for sample U decreased rapidly at this temperature, with almost 40% surface area loss after 5h at 1370K, while further exposure up to 48h led to a decrease of another 10%.

Acid pre-treatment on the Al_2O_3 fibre had an effect both on the initial surface area and thermal stability. The initial surface area prior to calcination for sample H was $188\text{m}^2\text{g}^{-1}$ compared with $155\text{m}^2\text{g}^{-1}$ for sample U. However loss of surface area with time over the first 3h at 1370K was more rapid for sample H compared with sample U. After 3h at 1370K the surface area of sample H dropped by 54% to $86\text{m}^2\text{g}^{-1}$, while for sample U the drop was only 37% of its original value over the same time period. Sample N also had a higher initial surface area ($167\text{m}^2\text{g}^{-1}$) than sample U and the rate of surface area loss with time was slightly higher than that of U, dropping by 47% after 5h at 1370K, compared with the drop of 40% for sample U over the same time period.

Since the surface area of the Al_2O_3 fibre dropped upon heating at 1370K and acid treatment appeared to increase the Al_2O_3 surface area, a sample which had been precalcined at 1370K for 24h was treated with HCl in the usual manner. The surface area had been measured prior to acid treatment and was found to be $76\text{m}^2\text{g}^{-1}$. After the HCl treatment the surface area did not change. Therefore the HCl treatment did not affect the surface area of the untreated Al_2O_3 fibre but not the calcined fibre.

As the acid washed material was also rinsed with water, in order to examine the effect of rinsing with water, sample W was prepared. From the surface area results, the water washing process did not alter the surface area of the Al_2O_3 , with sample W having an initial surface area of $160\text{m}^2\text{g}^{-1}$, which was similar to the corresponding value for sample U, taking experimental error into account. The surface area of sample W dropped by 44% after 5h at 1370K, to $90\text{m}^2\text{g}^{-1}$ which again was in good agreement with the surface area of sample U after the same treatment. The striking feature from Table 2.8 is that although samples U, H, N and W exhibited different initial rates of surface area loss, after heating at 1370K for 48h the values for specific surface areas were very similar when experimental error is taken into account.

The untreated and acid pre-treated samples were examined by x-ray diffraction before and after heat treatment. Fig 2.11 illustrates the XRD pattern for $\eta\text{-Al}_2\text{O}_3$,



Graph 2.1 Specific surface area (m^2g^{-1}) and pore volume (cm^3g^{-1}) for sample U after heating for 24h at various temperatures

**Table 2 8 · Specific surface area for various Saffil samples
after calcination at 1370k for varying lengths of time**

Sample	Time of Calcination at 1370K (h)	Specific Surface Area (m ² g ⁻¹)
U	0	155
	1	100
	3	98
	5	87
	24	76
	48	73
W	0	160
	1	nd
	3	nd
	5	90
	24	83
	48	70
N	0	167
	1	nd
	3	nd
	5	88
	24	79
	48	73
H	0	188
	1	nd
	3	86
	5	nd
	24	81
	48	72

nd = not determined

γ - Al_2O_3 and α - Al_2O_3 from the powder diffraction files, while Fig 2 12 and Fig 2 13 shows the XRD patterns for sample U, H and N before and after calcination at various temperatures. The XRD pattern for sample U (Fig 2 12a) prior to heat treatment indicated that the predominant Al_2O_3 phase was η - Al_2O_3 with possibly γ - Al_2O_3 also present. This was concluded from the presence of diffraction peaks at $2\theta = 19.5^\circ, 32.4^\circ, 37.5^\circ, 45.9^\circ, 60.9^\circ, 67.05^\circ$ and 85° which, according to the powder diffraction files was indicative of either η - Al_2O_3 or γ - Al_2O_3 . From examination of peak intensities, with the 100% peak at 67.05° and the peak at 45.9° having a relative intensity of 69%, it appeared that η - Al_2O_3 was the predominant phase according to the powder diffraction files (see fig s 2 11a and 2 11b). Fig 2 12b illustrates the pattern for sample U heated to 1273K for 24h. The pattern was similar to that in Fig 2 12a for the uncalcined sample U, with no evidence for the formation of any new Al_2O_3 phases at 1270K. However, upon heating sample U for 24h at 1370K the XRD data pointed to the formation of a small amount of α - Al_2O_3 , see Fig 2 12c, due to diffraction peaks at $2\theta = 25.6^\circ, 35.1^\circ, 43.4^\circ, 52.6^\circ, 57.5^\circ$ and 68.2° which are in agreement with the values for α - Al_2O_3 in the powder diffraction files, both with regard to diffraction angle and relative peak intensities with respect to the peak at $2\theta = 43.4^\circ$ (see Fig 2 11c). Since, excluding the above peaks, the diffraction pattern was similar to that for uncalcined sample U and as the peak at 43.4° was only 16% of the intensity of the most intense peak in the diffraction pattern at $2\theta = 67.2^\circ$, it can be concluded that the major phase was still η - Al_2O_3 . There was no evidence for the presence of either δ - Al_2O_3 or θ - Al_2O_3 . A shoulder appeared at $2\theta = 46.5^\circ$ on the main peak at $2\theta = 45.5^\circ$ upon heat treatment at 1370K for 24h. Although the diffraction pattern for δ - Al_2O_3 also has a peak present at $2\theta = 46.5^\circ$ the relative intensity of the shoulder, 42%, to the peak at $2\theta = 45.5^\circ$, does not agree for δ - Al_2O_3 . If δ - Al_2O_3 were present then the relative intensities should have been 30% and 80% respectively.

Fig 2 13 represents the diffraction patterns for sample H and N prior to and also after heat treatment at 1370K for 24 h. Fig 2 13a and Fig 2 13b show the XRD data for sample H and N respectively prior to calcination. Both samples had diffraction patterns which were identical to sample U prior to calcination. However, subjection to heat treatment at 1370K for 24h led to the formation of α - Al_2O_3 in larger quantities than those formed by sample U after the same treatment. For sample H (Fig 2 13c) treatment at 1370K for 24h gave a diffraction pattern which contained diffraction peaks for α - Al_2O_3 , which were approximately three times greater in intensity than those which appeared in the diffraction pattern for sample U after the same treatment. In the case of sample N, the above calcination treatment gave diffraction peaks for α - Al_2O_3 (Fig 2 13d) whose intensities were twice as great as that of the intensities of the corresponding peaks for sample U after 24h at 1370K, see Fig 2 12c. Again, after calcination, there was no evidence for the presence of θ - Al_2O_3 or δ - Al_2O_3 in sample N or H although in both

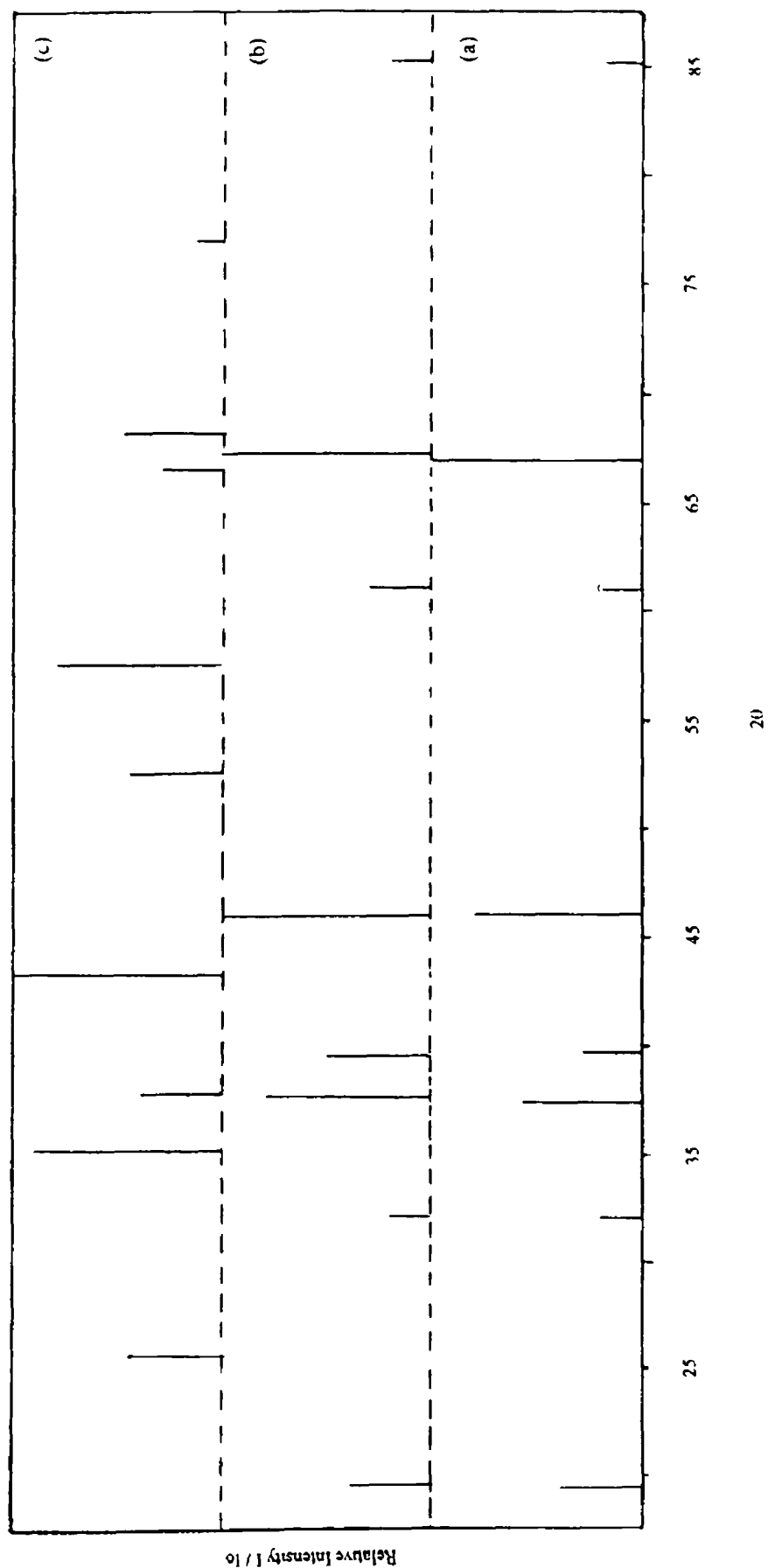


Fig.2.11 : X-ray diffraction pattern for (a) $\eta\text{-Al}_2\text{O}_3$, (b) $\gamma\text{-Al}_2\text{O}_3$ and (c) $\alpha\text{-Al}_2\text{O}_3$ from powder diffraction files

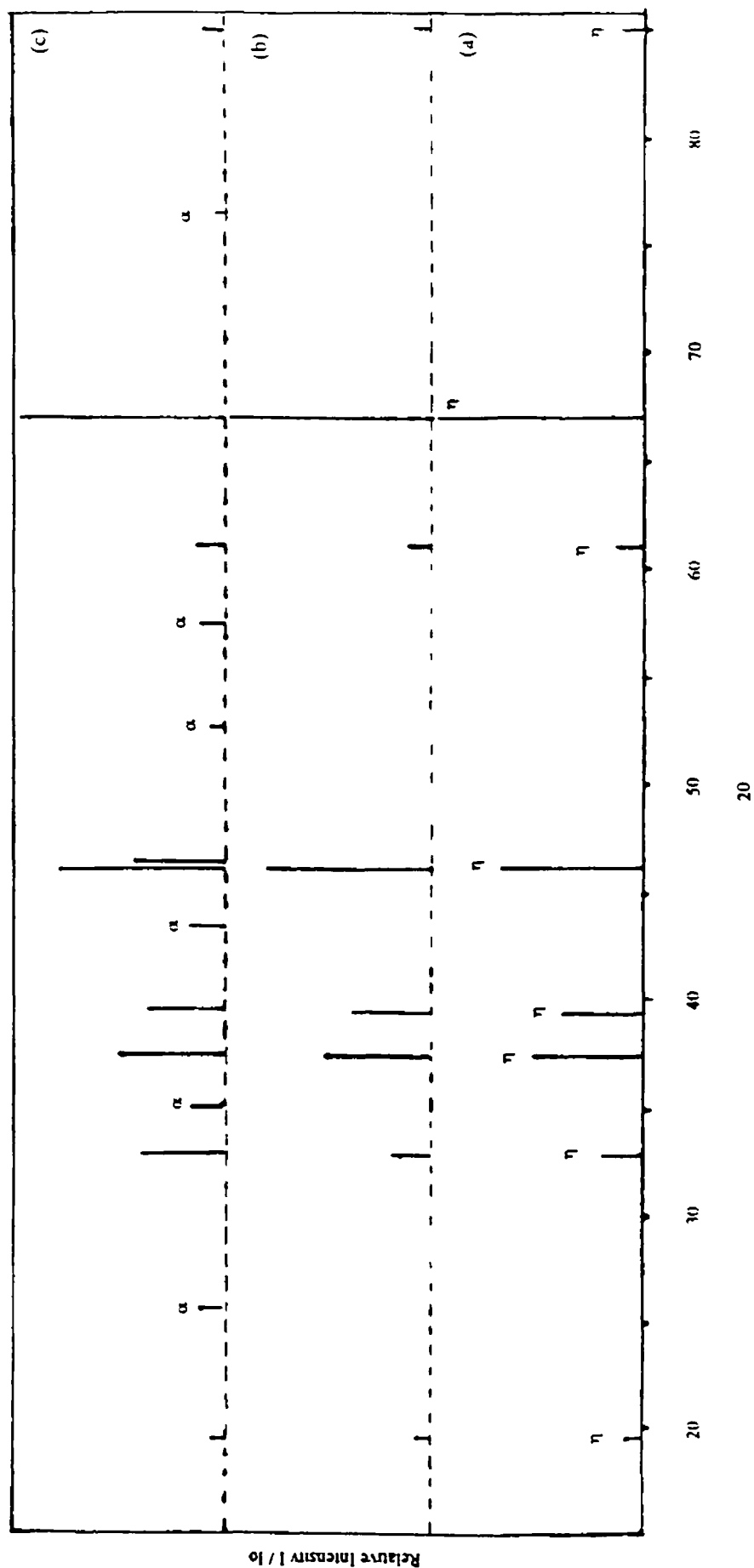


Fig 2 12 X-ray diffraction pattern for (a) U, (b) U after 24h at 1273K, (c) U after 24h at 1373K
 η = η -Al₂O₃ peak, α = α -Al₂O₃ peak

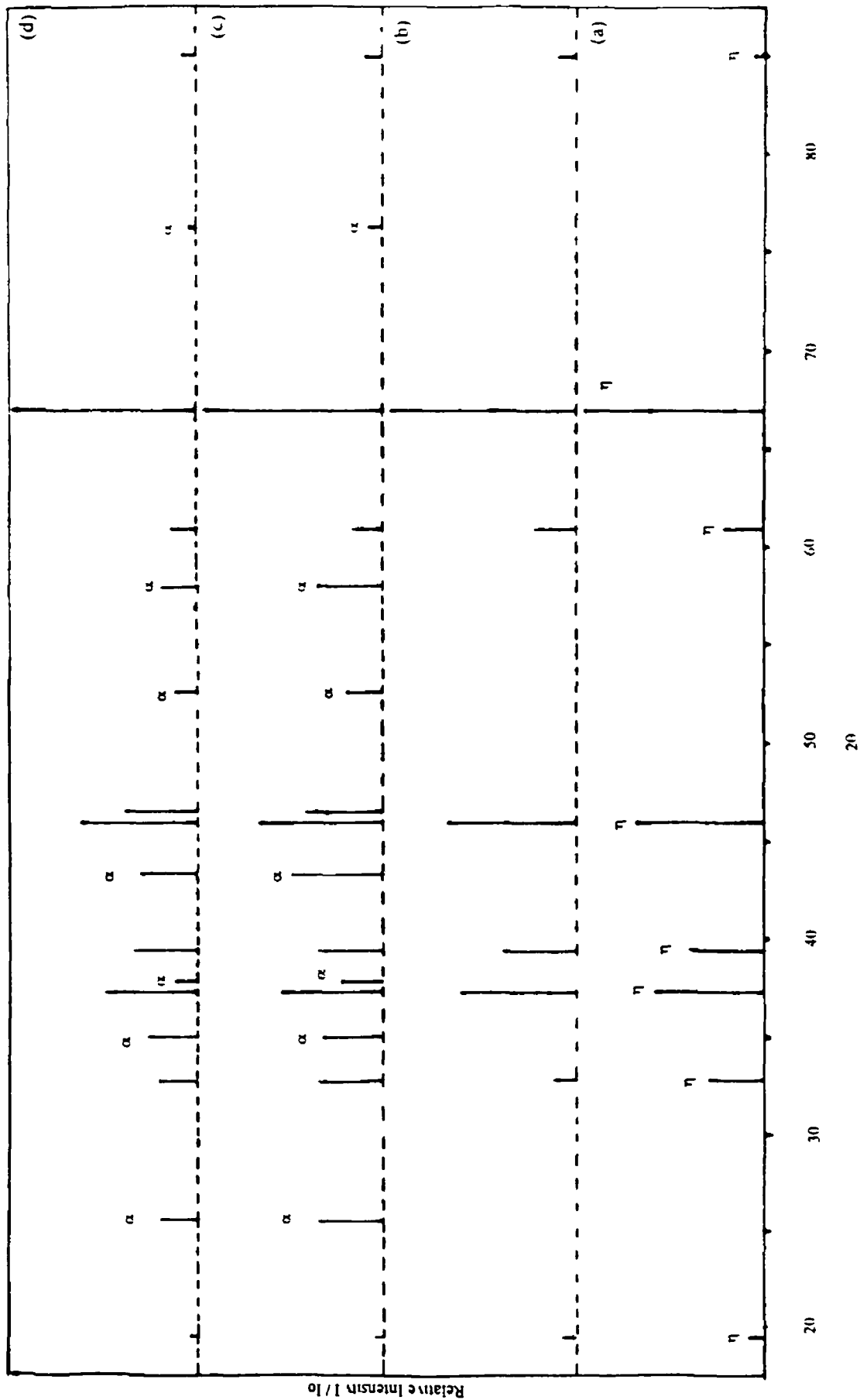


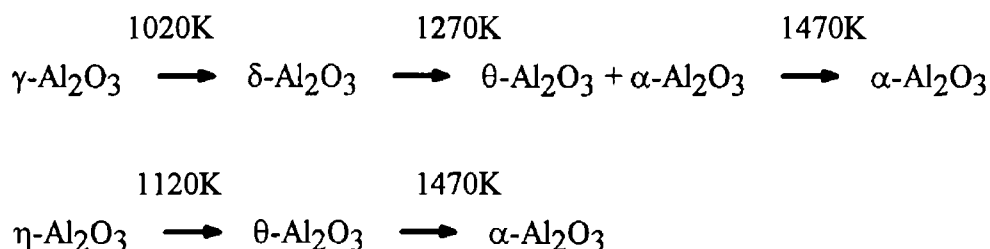
Fig 2 13 X-ray diffraction pattern for (a) H, (b) N, (c) H after 24h at 1373K, (d) N after 24h at 1373K. η = $\eta\text{-Al}_2\text{O}_3$ peak, α = $\alpha\text{-Al}_2\text{O}_3$ peak

cases a shoulder developed in the diffraction pattern at $2\theta = 46.5^\circ$ on the main peak at $2\theta = 45.5^\circ$

From the above results it is clear that acid pre-treatment of the Al_2O_3 fibre led to an increase of surface area compared with untreated fibre, with a higher rate of surface area loss initially at 1370K. The XRD data suggests formation of larger amounts of $\alpha\text{-Al}_2\text{O}_3$ in the acid treated samples heated at 1370K than in the equivalent untreated samples. However despite the differences in the initial rates of surface area loss at 1370K for samples U, H and N, after 48h at 1370K all samples exhibited similar surface areas.

The initial increase in the specific surface area of the acid treated fibre was probably due to a "break up" or fracturing of the Al_2O_3 fibres caused by the strength of the acid. The water rinsing of the acid treated fibre to remove excess chloride or nitrate did not appear to be responsible as sample W exhibited no increase in surface area compared with the untreated fibre.

According to X-ray diffraction data there was no evidence for the presence of $\theta\text{-Al}_2\text{O}_3$ or $\delta\text{-Al}_2\text{O}_3$ in any of the samples exposed to 1170K and above, which was in disagreement with Lippens et al (12) who stated that the phase transformations for $\eta\text{-Al}_2\text{O}_3$ and $\gamma\text{-Al}_2\text{O}_3$ occurred as shown below



However, if the above scheme was correct then the x-ray diffraction data might indicate that $\theta\text{-Al}_2\text{O}_3$ was present as well as $\eta\text{-Al}_2\text{O}_3$ in the fibre samples as, according to Lippens et al (12), 1370K would be too low a temperature for transformation of $\eta\text{-Al}_2\text{O}_3$ to $\alpha\text{-Al}_2\text{O}_3$. It is also possible that diffraction peaks due to small amounts of $\delta\text{-Al}_2\text{O}_3$ or $\theta\text{-Al}_2\text{O}_3$ could be masked by diffraction peaks for the other phases which were present in larger amounts i.e. $\gamma\text{-Al}_2\text{O}_3$, $\eta\text{-Al}_2\text{O}_3$ or $\alpha\text{-Al}_2\text{O}_3$.

The acid treatment also appeared to accelerate the phase transformation to $\alpha\text{-Al}_2\text{O}_3$. Burtin et al (50) found that increased surface areas facilitated phase transformations and this could be one reason why the acid treated Al_2O_3 samples contained more $\alpha\text{-Al}_2\text{O}_3$ than sample U after treatment at 1370K.

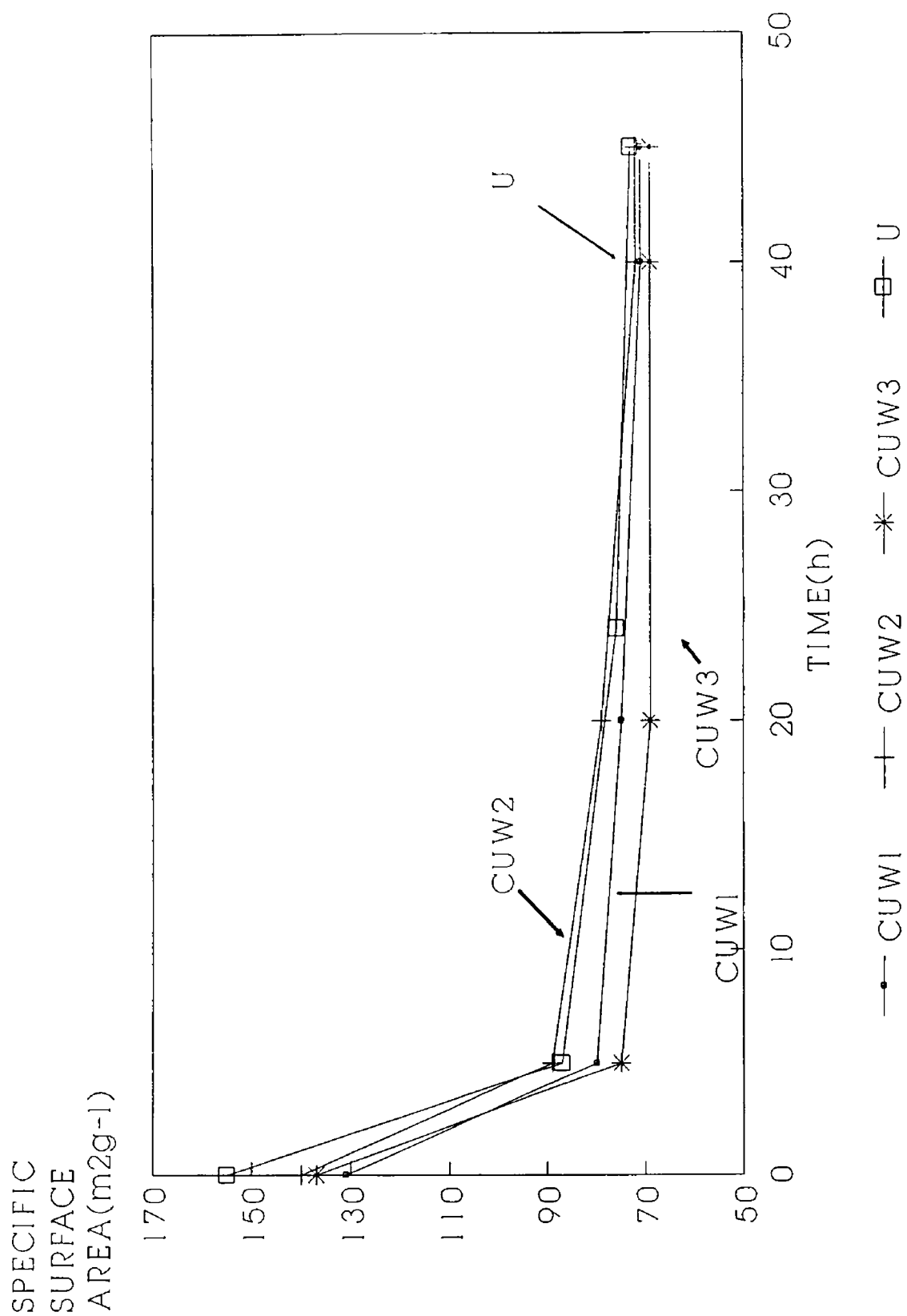
It has been pointed out already that a model has been postulated which describes the transformation of Al_2O_3 to the α -phase in terms of an annihilation reaction between anionic and cationic vacancies and that particle nucleation would be increased in areas rich in cationic and anionic vacancies (37). It is possible that the increased amount of $\alpha\text{-Al}_2\text{O}_3$ in the acid pre-treated Al_2O_3 samples, compared with untreated Al_2O_3 after

calcination at 1370K, may have been due to removal of soluble Al^{3+} cations, producing cationic vacancies and hence accelerating the phase transformation. Ananin et al (70) found that the treatment of a partially hydrated Al_2O_3 surface in aqueous HCl led to the detachment of Al^{3+} cations not stabilised by hydroxyl groups.

The surface areas of sample U, H and N after long periods of exposure at 1370K (>24h) were quite similar despite the fact that the X-ray diffraction data indicated there was wide variations in the amount of $\alpha\text{-Al}_2\text{O}_3$ formed in each sample. Therefore, it may be that the surface area loss is not primarily due to phase transformation in this case. The Al_2O_3 fibre material used (Saffil) is highly porous with an average pore diameter of approximately 6nm, according to the manufacturer. The results indicated that the surface area loss was accompanied by a loss in pore volume, see Graph 2.1, and it is possible that the major cause of surface area loss was due to pore loss rather than phase transformation. The results for the surface area of the Al_2O_3 samples impregnated with cations, after aging at 1370K appears to be in agreement with this theory.

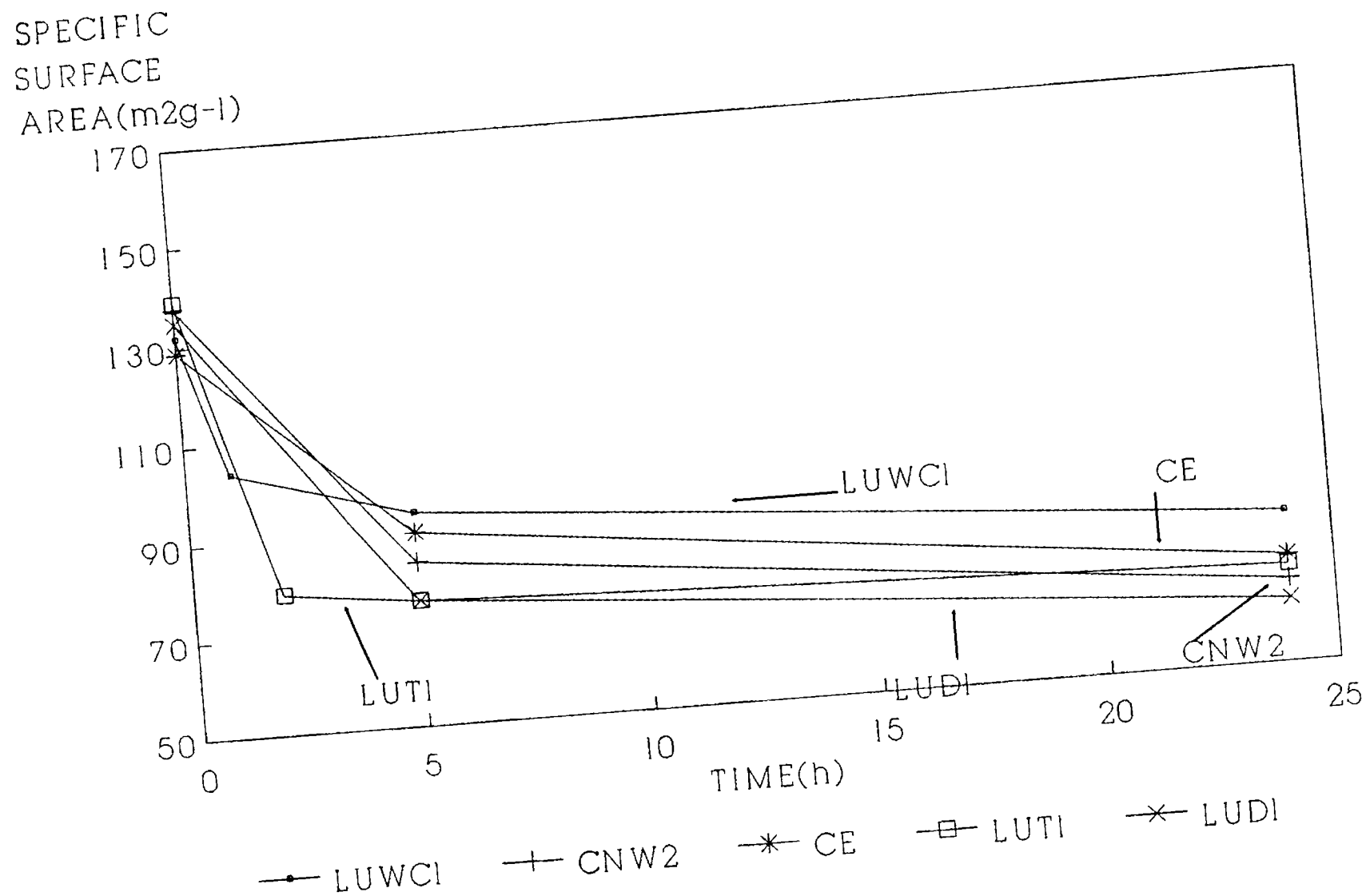
The effects of cation addition to the Al_2O_3 material with respect to surface area before and after heat treatment at 1370K are illustrated in Graph 2.2, 2.3, 2.4, 2.5 and 2.6. Initially the surface area of the Al_2O_3 material dropped from $155\text{m}^2\text{g}^{-1}$ to between $141\text{m}^2\text{g}^{-1}$ and $127\text{m}^2\text{g}^{-1}$ upon cation addition. This was probably due to pore filling by the cation solution. Graph 2.2 illustrates the results for the surface area of certain cerium doped Al_2O_3 samples before and after calcination at 1370K for different lengths of time. It is obvious from this graph that for CUW1, CUW2 and CUW3 the addition of cerium had no stabilising effect on surface area irrespective of the amount of cation added during preparation. For example, after 45h at 1370K sample CUW1 had a surface area of $72\text{m}^2\text{g}^{-1}$ while CUW3 had a surface area of $69\text{m}^2\text{g}^{-1}$ after the same treatment. This compared with a specific surface area of $73\text{m}^2\text{g}^{-1}$ for sample U after 45h at 1370K. In order to ascertain if the ineffectiveness of the cerium additions towards thermal stabilisation was due to cation concentrations being too low a sample was prepared with a nominal cerium loading of 20wt%, CE, and the surface area values for this sample after various periods of time at 1370K are given in Graph 2.3. From these results it would appear that the addition of large amounts of cerium accelerated, rather than decelerated the rate of surface area loss, as CE had a specific surface area of $72\text{m}^2\text{g}^{-1}$ after only 24h at 1370K.

Graph 2.3 also illustrates the results for sample CNW2, which was a HNO_3 pre-treated Al_2O_3 sample to which 1wt% cerium was added. This was prepared in order to determine whether the addition of cerium could inhibit the initial increased rate of surface area loss exhibited by acid pre-treated Al_2O_3 samples. Again the results indicated that cerium addition did not decrease the rate of surface area loss, with CNW2 having a surface area of $67\text{m}^2\text{g}^{-1}$ after 24h at 1370K.



Graph 2.2 . Specific surface area (m²g⁻¹) versus time (h) at 1370K for CUW1, CUW2 and CUW3.

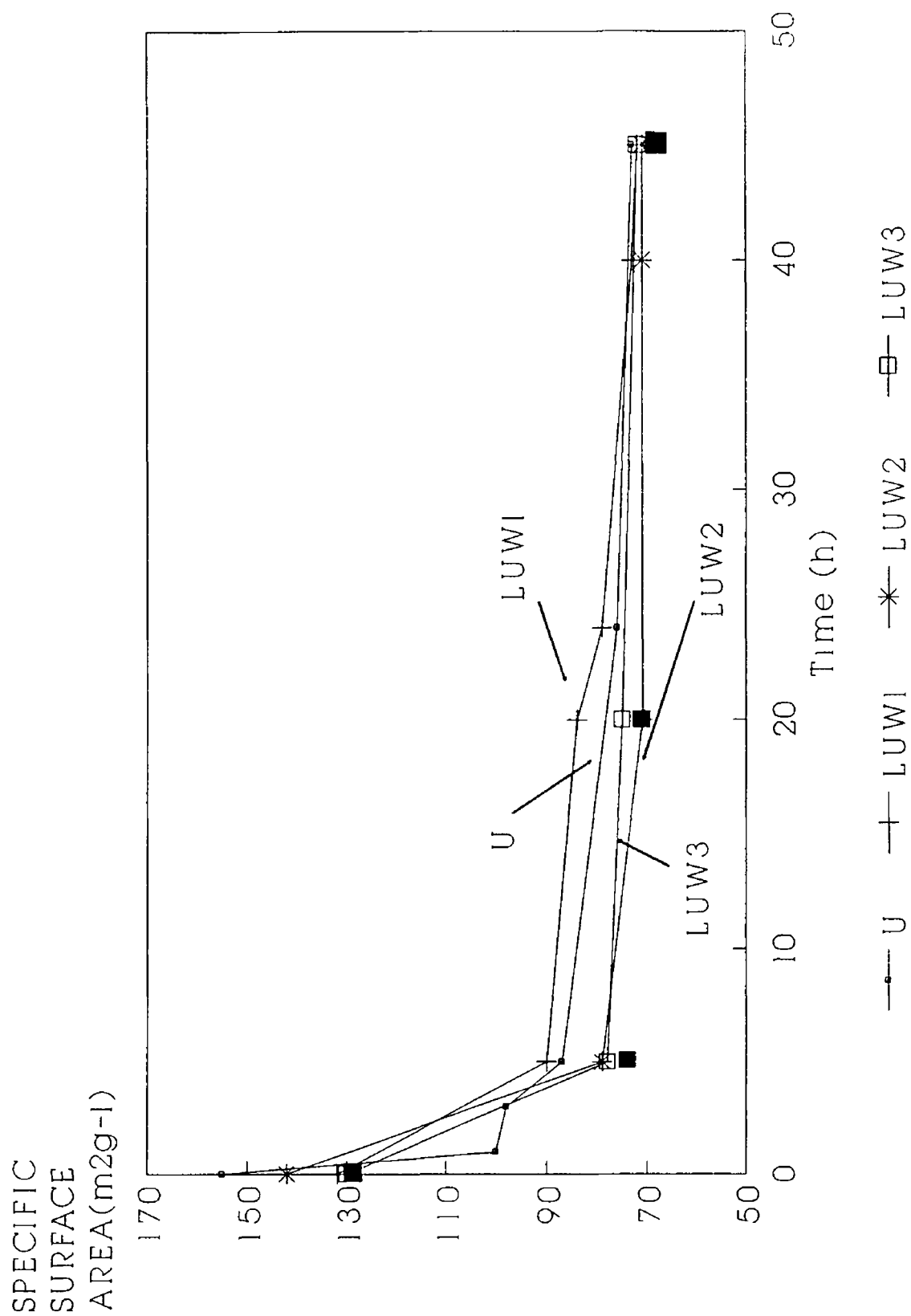
Graph 2 3 Specific surface area (m^2g^{-1}) versus time (h) at 1370K for LUT1, LUDI, LUWCI, CE and CNW2



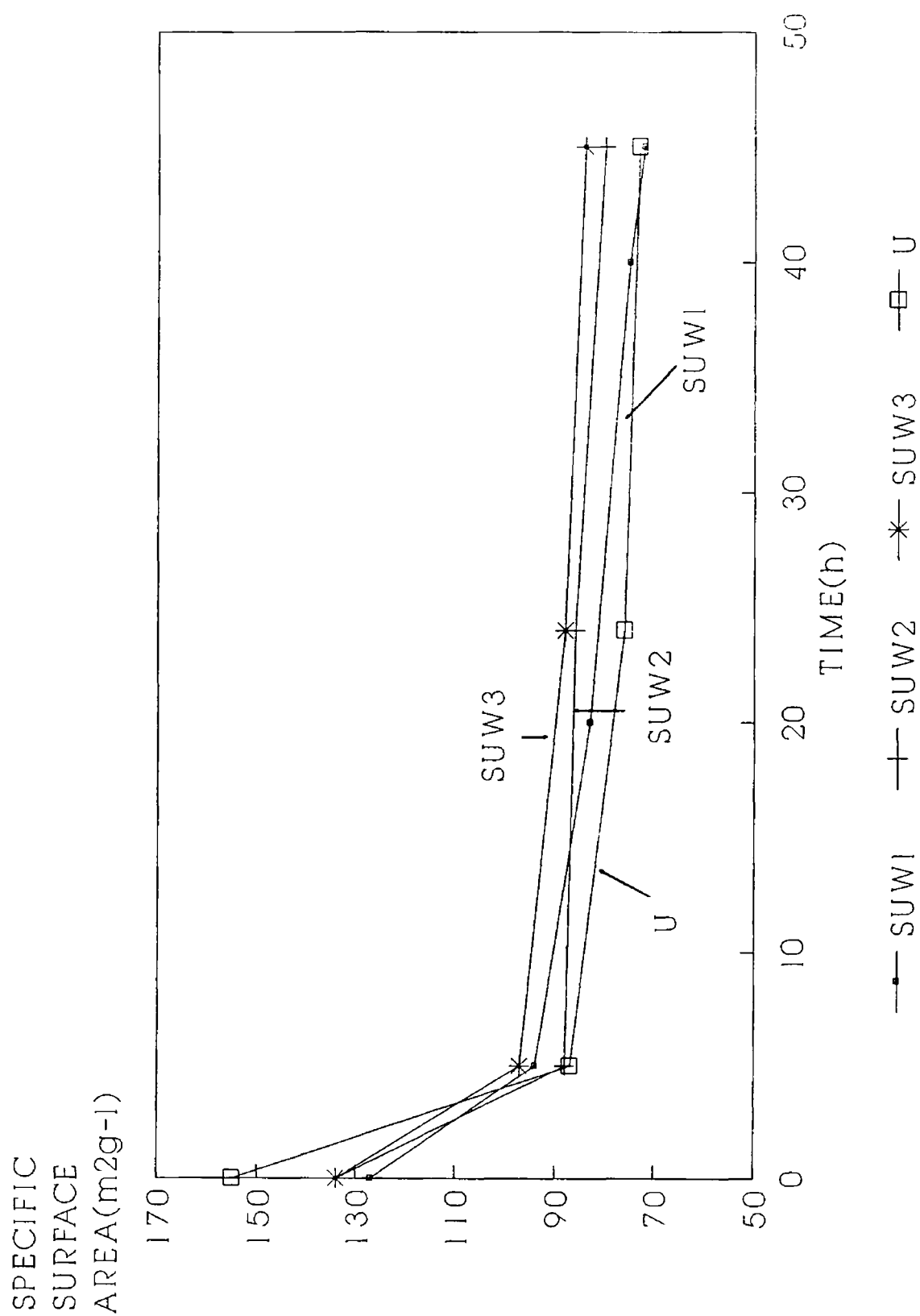
The surface area changes at 1370K with time for Al_2O_3 samples with various lanthanum additions are shown in Graph 2 3 and 2 4. The addition of 0.5wt% lanthanum had a slight effect on surface area loss at 1370K, with LUW1 having a specific surface area of $78 \text{ m}^2\text{g}^{-1}$ after 45h. However additions of lanthanum at higher weight loadings had no effect on thermal stability, with samples LUW2 and LUW3 having specific surface areas of $71 \text{ m}^2\text{g}^{-1}$ and $72 \text{ m}^2\text{g}^{-1}$ respectively after 45h at 1370K.

The LUW samples were prepared using powdered Al_2O_3 prewetted with methanol prior to impregnation with the methanolic lanthanum containing solutions. In order to examine whether prewetting the Al_2O_3 prevented the uptake of some of the lanthanum, a sample was prepared using dry Al_2O_3 , sample LUD1. In addition, a sample was prepared using Al_2O_3 dried at 823K for 1h and then prewetted with methanol, sample LUT1. This was prepared in order to exclude the possibility of occluded water effecting the uptake of the cation solution by the Al_2O_3 . Thermogravimetric analysis of the Al_2O_3 material indicated that there was approximately a 12% weight loss up to 773K, which was probably due to water loss. The specific surface areas of both LUD1 and LUT1 before and after exposure at 1370K are illustrated in Graph 2 3. It is clear from the data that neither sample had increased thermal stability compared with the other lanthanum impregnated samples or the untreated Al_2O_3 . Calcination of the lanthanum impregnated samples at a lower temperature, i.e. 723K for 4h, in order to decompose the lanthanum chloride salts which would be present after impregnation, had no effect on the thermal stability of the Al_2O_3 at 1370K, as can be observed from the data determined for sample LUWC1, illustrated in Graph 2 3.

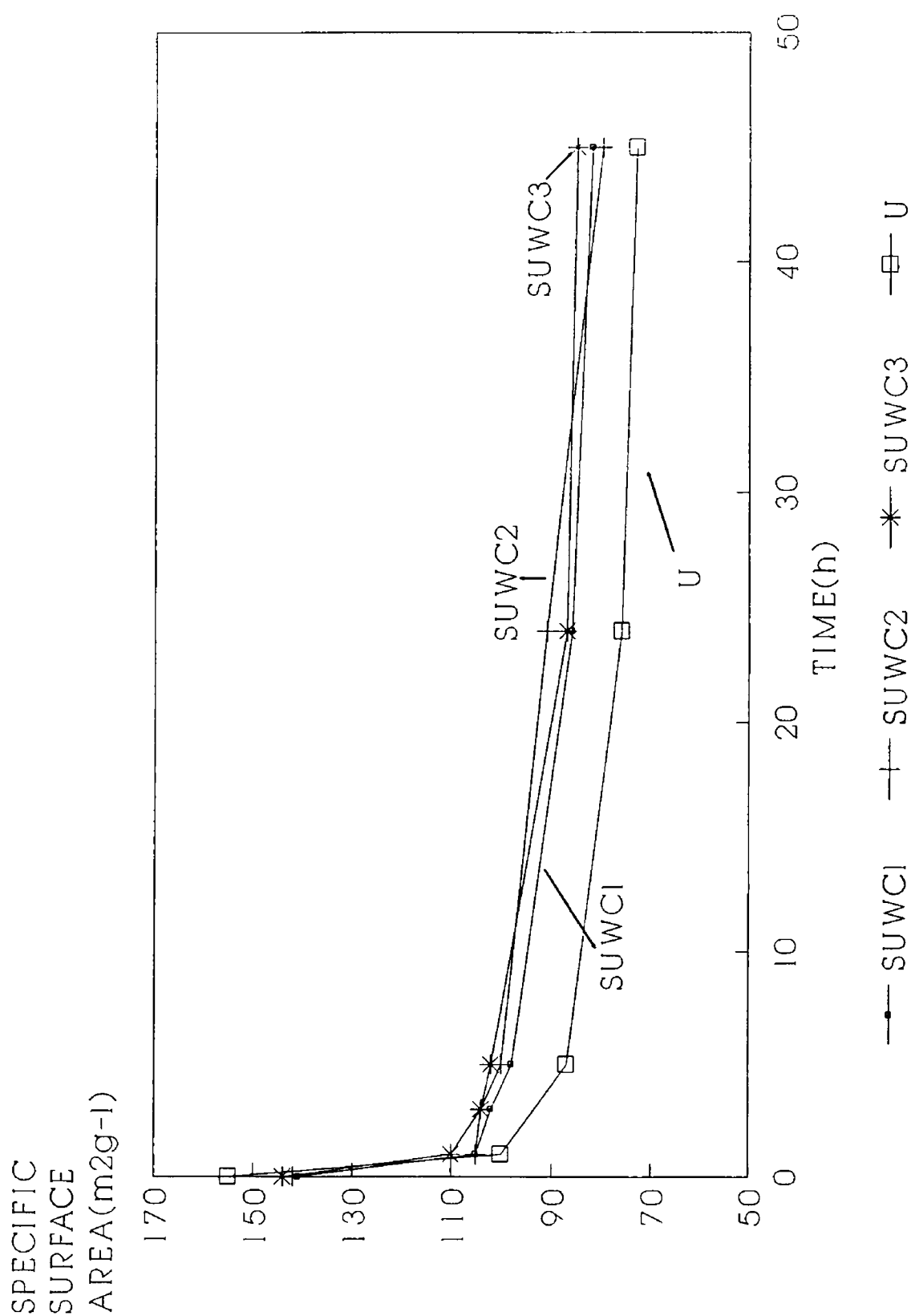
In previous work it has been reported that the addition of silicon to Al_2O_3 has a beneficial effect on thermal stability (55). To this end silicon was added to the Al_2O_3 and the results for specific surface areas are given in Graph 2 5 and 2 6. Samples containing 1wt% and 3wt% silicon, (Graph 2 5) appeared to have slightly more thermal stability than the untreated Al_2O_3 , with samples SUW2 and SUW3 having specific surface areas of 80 and $84 \text{ m}^2\text{g}^{-1}$ respectively after 45h at 1370K, compared with a specific surface area of $73 \text{ m}^2\text{g}^{-1}$ exhibited by sample U after the same treatment. Lower concentrations of silicon had no effect on thermal stability (see Graph 2 5, SUW1). Graph 2 6 contains results for Al_2O_3 to which silicon had been added and also underwent a heat treatment in flowing air ($30 \text{ dm}^3\text{h}^{-1}$) at 770K for 12h in order to break down the precursor compound in accordance with the method of Begum et al (55). The specific surface area of sample SUWC1 at $86 \text{ m}^2\text{g}^{-1}$ after 45h at 1370K was greater than the specific surface area of the corresponding sample which had not undergone an air treatment during preparation sample SUW1. However the specific surface areas of samples SUWC2 and SUWC3 after 45h at 1370K differed little from those of SUW2 and SUW3 after a similar exposure at 1370K, indicating that for silicon additions greater than 0.5wt% the calcination process during preparation had no effect on thermal stability.



Graph 2 4 Specific surface area (m²g⁻¹) versus time (h) at 1370K for U, LUW1, LUW2 and LUW3



Graph 2 5 Specific surface area (m²g⁻¹) versus time (h) at 1370K for SUW1, SUW2, and SUW3



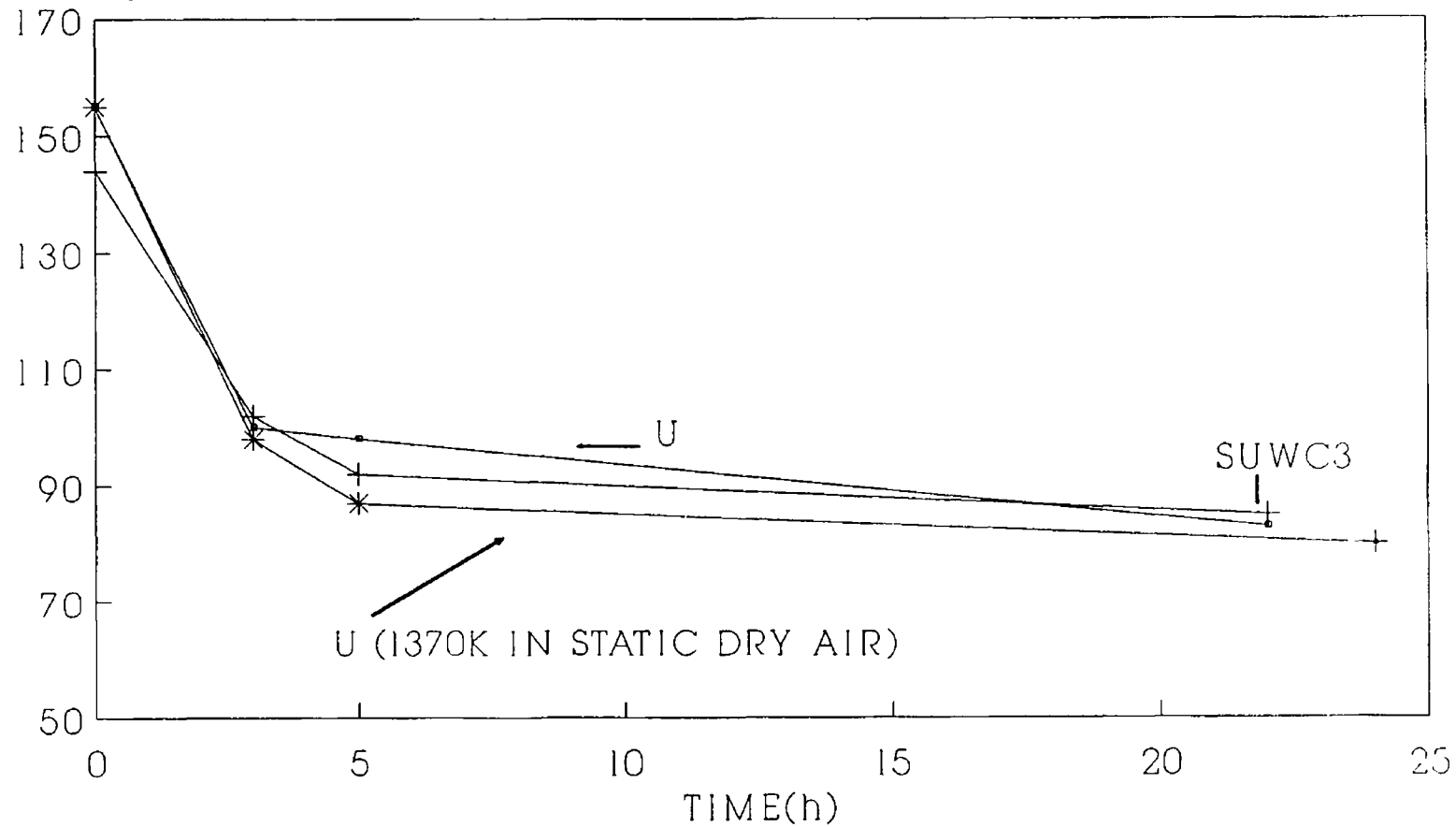
Graph 2.6 Specific surface area (m^2g^{-1}) versus time (h) at 1370K for SUWC1, SUWC2 and SUWC3

The effect of heating at 1370K in the presence of water vapour upon the surface areas of both sample U and SUWC3 was examined and the results obtained for specific surface areas are given in Graph 2 7, together with the results for sample U exposed at 1370K in a dry static air atmosphere. It is clear from the data presented in Graph 2 7 that the presence of water vapour did not decrease the thermal stability of the Al_2O_3 . Both Johnston (51) and Begum et al (55) found that the presence of water vapour greatly increased the rate of γ - to α - Al_2O_3 transformation.

X-ray diffraction measurements were carried out on some of the cation treated Al_2O_3 samples after heat treatment at 1370K for 24h. Fig 2 14 is a graphical representation of the x-ray diffraction patterns for (a) SUW3, (b) LUW3 and (c) CUW3 after 24h at 1370K. The patterns for SUW3 and LUW3 were very similar to that for sample U prior to calcination (see Fig 2 12a) i.e. the major phase appeared to be η - Al_2O_3 and/or γ - Al_2O_3 . There was no evidence for the presence of α -, θ -, δ - Al_2O_3 or any lanthanum or silicon species. Begum et al (55) claimed that the absence of diffraction peaks typical of a crystalline form of silicone for Si doped Al_2O_3 samples suggested a strong interaction of the Si with the Al_2O_3 starting material. The diffraction pattern for sample CUW3 after 24h at 1370K (see Fig 2 14c) was similar to those described above except that the presence of CeO_2 was also indicated by the diffraction peaks at $2\theta = 28.6^\circ$, 47.4° and 56.4° . There should have been a peak at $2\theta = 33.1^\circ$ but this may have been masked by the broad peak at $2\theta = 32.9^\circ$. Figure 2 14d represents the diffraction pattern for sample SUWC3 after calcination for 24h at 1370K in steam. It is clear from the pattern that even in steam the presence of silicon prevents phase transformations.

From the X-ray diffraction data it is clear that the addition of La^{3+} , Ce^{3+} or Si^{4+} to the Al_2O_3 material is effective in the prevention of the formation of α - Al_2O_3 at 1370K. However according to the specific surface area data, the addition of cations did not prevent or greatly decrease the rate of surface area loss at 1370K compared with the untreated Al_2O_3 , despite the fact that in untreated Al_2O_3 low surface area α - Al_2O_3 was formed. Therefore as with the acid pre-treatment study, it would appear that the major cause of surface area loss in this material was not due to phase transformation to α - Al_2O_3 , but due to loss of pores.

SPECIFIC
SURFACE
AREA(m^2g^{-1})



—●— U(steam) —+— SUWC3 —*— U(dry air)

Graph 2 7 Specific surface area (m^2g^{-1}) versus time (h) at 1370K for sample U, Sample U aged in steam and SUWC3 aged in steam

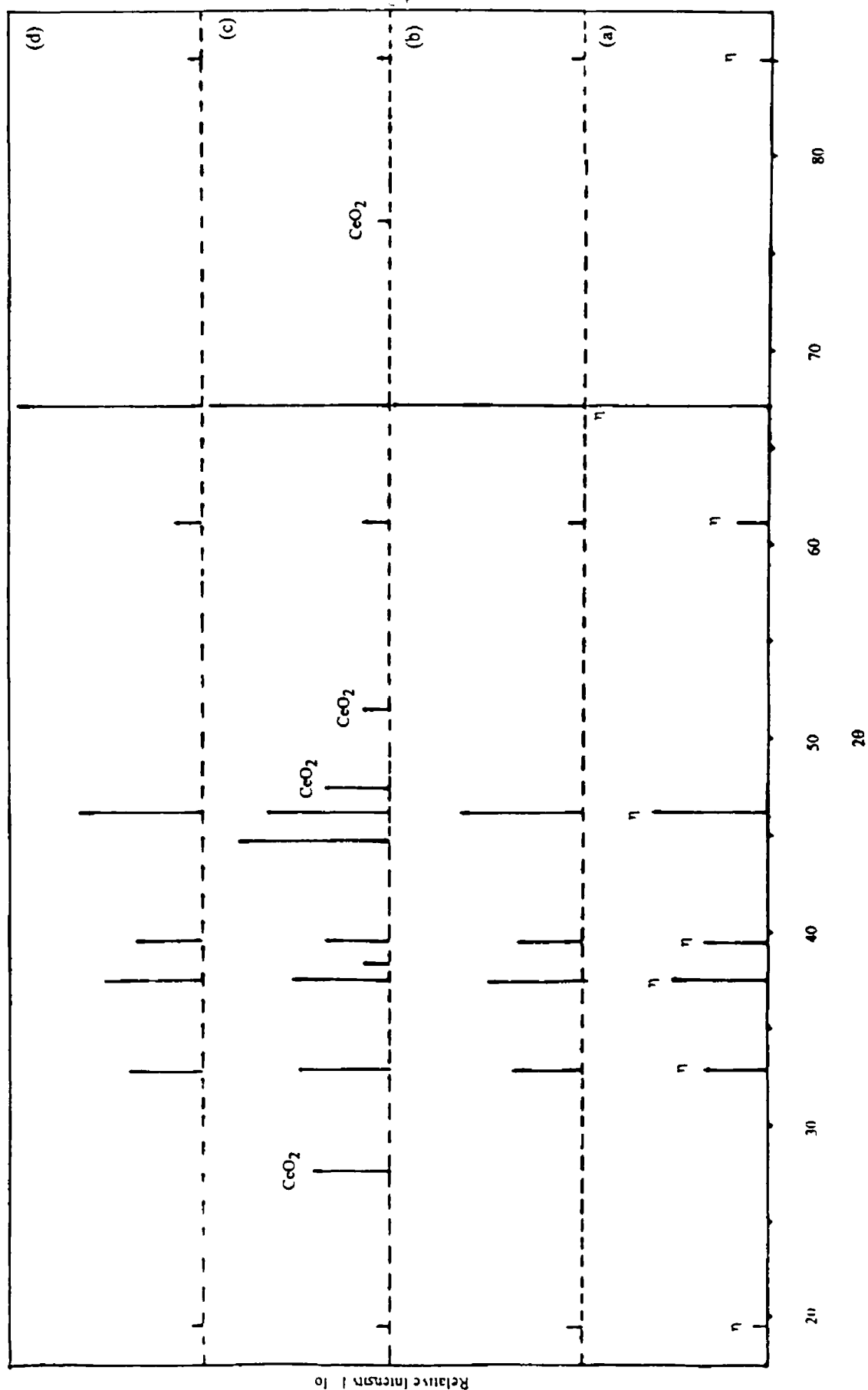


Fig 2 14 X-ray diffraction pattern for (a) SUWC3 after 24h at 1373K, (b) LUW3 after 24h at 1373K, (c) CUW3 after 24h at 1373K, (d) SUWC3 aged in steam for 24h

2.3. Conclusions

A number of conclusions can be drawn from this study on the thermal stability of the Al_2O_3 fibre material, "Saffil". From surface area and pore volume results it was concluded that the uncalcined Al_2O_3 had a high surface area ($155\text{m}^2\text{g}^{-1}$) and pore volume ($27\text{cm}^3\text{g}^{-1}$). X-ray diffraction measurements indicated that the material was predominantly composed of $\eta\text{-Al}_2\text{O}_3$ although $\gamma\text{-Al}_2\text{O}_3$ may also have been present. Thermogravimetric analysis showed that the Al_2O_3 material underwent a weight loss of up to 12% on heating up to 773K, probably due to the loss of occluded water. The surface area of the Al_2O_3 fibre was stable up to 1070K but at temperatures greater than or equal to 1170K the surface area and pore volume dropped. The x-ray diffraction pattern for the Al_2O_3 fibre calcined at 1370K indicated that the material was still predominantly $\eta\text{-Al}_2\text{O}_3$ (possibly with some $\gamma\text{-Al}_2\text{O}_3$ also present). There was also a small amount of $\alpha\text{-Al}_2\text{O}_3$ present. There was no evidence for $\delta\text{-}$ or $\theta\text{-Al}_2\text{O}_3$ although there was a diffraction peak at $2\theta = 46.5^\circ$ but, because of its relative intensity, this could not be assigned to either of the latter two phases.

Treatment of the untreated fibre with H_2O had no effect but acid treatment increased the surface area, up to $167\text{m}^2\text{g}^{-1}$ and $188\text{m}^2\text{g}^{-1}$ respectively for HNO_3 and HCl treated fibre. However acid treated Al_2O_3 lost surface area more quickly over the first 24h at 1370K than the untreated fibre, with XRD data indicating more of the α -phase being present in the former samples than in the untreated fibre calcined in the same way. This may be due to removal of soluble Al^{3+} cations by the acid treatment leading to increased cation vacancies and hence accelerated transformation to the α -phase. However after 48h at 1370K the surface area of acid treated and untreated Al_2O_3 samples was similar despite differences in the amount of α -phase present which might indicate that transformation to the α -phase was not the primary cause of surface area loss. The material was manufactured so that it contained a certain amount of Si ($< 5\%$) and thus the untreated fibre was probably resistant to phase transformation.

Addition of cations La^{3+} , Ce^{3+} or Si^{4+} to the untreated Al_2O_3 fibre had little effect on the surface area loss at 1370K, irrespective of the cation or preparation technique used. However, XRD data indicated that cation addition did prevent the formation of $\alpha\text{-Al}_2\text{O}_3$ at 1370K. In the case of a Ce treated samples calcined at 1370K the XRD pattern also indicated the presence of CeO_2 but there was no XRD evidence for La or Si compounds on Al_2O_3 treated with these cations and heated at 1370K.

From the above evidence it would appear that the surface area loss at 1370K for "Saffil" was not primarily due to the formation of $\alpha\text{-Al}_2\text{O}_3$. Since the surface area loss was accompanied by loss of total pore volume, the major loss of surface could have been due to loss of pores.

2 4 References

- (1) D L Trim and Stanislaus, Appl Catal, 21, 215 (1986)
- (2) F A Cotton and G Wilkinson, Basic Inorganic Chemistry, Ch 15, Wiley, New York (1976)
- (3) B C Lippens and J J Steggerda, Physical and Chemical Aspects of Aspects of Adsorbents and Catalysts (Ed B G Linsen) Ch 4, Acad Press, London and New York, (1970)
- (4) J W Newsome, H W Heiser, A S Russell and H C Stumpf, Alumina Properties, Alumina Co of America (1960)
- (5) H C Stumpf, A S Russell, J W Newsome and C M Tucker, Ind Eng Chem, 42, 1398 (1950)
- (6) M B K Day and V J Hil, J Phys Chem, 57, 946 (1953)
- (7) R Tertian and D Papee, C R Acad Sci Paris, 241, 1575 (1955)
- (8) J F Brown, D Clark and W W Elliott, J Chem Soc, 84 (1953)
- (9) T Sato, J Appl Chem, 12, 9 (1962)
- (10) N N Greenwood and A Earnshaw, Chemistry of the Elements, Pergamon Press, Oxford (1986)
- (11) H Knozinger and P Ratnasamy, Catal Rev -Sci Eng, 17, 31 (1978)
- (12) B C Lippens and J H de Boer, Acta Crystallographic, 17, 1312 (1964)
- (13) H P Rooksby and C J M Rooymans, Clay Miner Bull, 4, 234 (1961)
- (14) R Tertian and D Papee, J Chim Phys, 55, 341 (1958)
- (15) B C Lippens and J H de Boer, J Catal, 3, 44 (1961)
- (16) S Geller, J Chem Phys, 33, 676 (1960)
- (17) H D Megan, Z Kristallorg, A 87, 185 (1934)
- (18) J B Peri, J Phys Chem, 69, 226 (1965)
- (19) J B Peri and R B Hannan, J Phys Chem, 64, 1526 (1960)
- (20) J B Peri, Actes Congr Intern Catalyse, 2e Paris, 1, 1333 (1961)
- (21) J B Peri, J Phys Chem, 69, 211 (1965)
- (22) L Janacek, M Safarova, R A Shkrabina and K Jiratova, React Kinet Catal Lett, 27, 357 (1985)
- (23) K Jiratova and L Beranek, Appl Catal, 2, 125 (1982)
- (24) Z Vit, L Nondek and J Malek, Appl Catal, 2, 107 (1982)
- (25) S Lee and R Aris, Catal Rev -Sci Eng, 27, 207 (1985)
- (26) K Jiratova, Appl Catal, 1, 165 (1981)
- (27) G A Parks, Chem Rev, 65, 177 (1965)
- (28) S Subramanian, J A Schwarz and Z Hejase, J Catal, 117, 512 (1989)
- (29) S Soled, J Catal, 81, 252 (1983)
- (30) C P Haung and W Stumm, Surf Sci, 32, 287 (1972)

- (31) Y Vonobev, R A Shkrabina, E M Moroz, V B Fenelov, R V Zagrafskaya, T D Kambarova and E A Levitskii, J Kinet Catal, 22, 1275 (1981)
- (32) J H de Boer, Angew Chem, 70, 383 (1958)
- (33) C Morterra, A Zecchina, S Coluccia and A Chiorino, J Chem Soc, Faraday Trans I, 73, 1544 (1977)
- (34) C Morterra, A Chiorino, G Ghiotti and E Garrone, J Chem Soc, Faraday Trans I, 75, 271 (1979)
- (35) A S Russell and C N Cochrane, Ind Eng Chem, 42, 1336 (1950)
- (36) D H Trimm, Appl Catal, 7, 249 (1983)
- (37) P Burtin, J P Brunelle, M Pijolat and M Soustelle, Appl Catal, 34, 239 (1987)
- (38) D S Tucker and J J Hren, Mat Res Soc Symp Proc, 31, 337 (1984)
- (39) F W Dynis and J W Halloran, J Am Ceram Soc, 65, 442 (1982)
- (40) H Yanagida, G Yamaguchi and J Kubota, J Ceram Soc Jpn, 74, 371 (1966)
- (41) D S Tucker, J Am Ceram Soc, 68, C-163 (1985)
- (42) D S Tucker, E J Jenkins and J J Hren, J Electr Microsc Techn, 2, 29 (1985)
- (43) G C Bye and G T Simpkin, J Am Ceram Soc, 57, 367 (1984)
- (44) J Beretika and M J Ridge, J Chem Soc A, 12, 2106 (1967)
- (45) J R Wynnycki and C G Morris, Met Trans B, 16, 345 (1985)
- (46) W S Brey and K A Kreiger, J Am Chem Soc, 71, 3637 (1949)
- (47) D S Maciver, H H Tobin and R T Barth, J Catal, 2, 485, (1963)
- (48) D Aldcroft, G C Bye, J G Robinson and K S W Sing, J Appl Chem, 18, 301 (1968)
- (49) W H Gitzen, Alumina as a Ceramic Material, The Amer Ceram Soc, Columbus, Ohio (1970)
- (50) P Burtin, J P Brunelle, M Pijolat and M Soustelle, Appl Catal, 34, 225 (1987)
- (51) M Johnston, J Catal, 123, 245 (1990)
- (52) D J Harris, D J Young and D L Trimm, Proc 10th Aus Chem Eng Conf, P 175, Sydney, August (1982)
- (53) H Schaper, D J Amesz, E B M Doesburg and L L Van Reijen, Appl Catal, 9, 129 (1984)
- (54) P J Anderson and P L Morgan, J Chem Soc, Faraday Trans I, 60, 930 (1964)
- (55) B Beguin, E Garbowski and M Primet, J Catal, 127, 595 (1991)
- (56) M Machida, K Eguchi and H Arai, J Catal, 103, 385 (1987)
- (57) V J Vereschagin, V Yu Zelinskii, T A Khabas and N N Kolova, Zh Prikl Khim (Leningrad), 55, 1946 (1982)
- (58) T Tsuchida, R Furuichi, T Ischi and K Itoh, Thermochimica Acta, 64, 373 (1983)

- (59) H Schaper and L L Van Reijen, Proc 5th Int Roundtable Conf Sintering, Portoroz, Yugoslavia, 7-10th September, 1981, p 173, Elsevier, Amsterdam (1982)
- (60) D J Young P Udaja and D L Trim, in, B Delmon and G F Forment(Eds) Catalyst Deactivation, Studies in Surf Sci Catal, 34, p 331, Elsevier, Amsterdam (1980)
- (61) N S Kozlov, M Ya Lazarev, L Ya Mostovaya and I P Stremok, J Kinet Catal, 14, 1130 (1983)
- (62) H Schaper, E B M Doesburg and L L Van Reijen, Appl Catal, 7, 211 (1983)
- (63) F Oudet, A Vejux and P Courtine, J Catal, 114, 112 (1988)
- (64) F Oudet, A Vejux and P Courtine, Appl Catal, 50, 79 (1989)
- (65) M Bettman, R E Chase, K Otto and W H Weber, J Catal, 117, 447 (1989)
- (66) Y Xie, M Qian and Y Tang, Sci Sin Ser, B6, 27, 549 (1984)
- (67) M J Dreelan and O E Finlayson, Proc Roy Ir Acad, 89B, 411 (1989)
- (68) H C Yao and Y F Yu Yao, J Catal, 86, 254 (1984)
- (69) R Gaugin, M Graulier and D Papee, Adv Chem Ser, 143, 147 (1975)
- (70) V N Ananin, A I Trokímetz, L Shaverdina and M Zaretskii, React Kinet Catal Lett, 27, 139 (1985)

CHAPTER 3

Preparation and Characterisation of Pt/Al₂O₃ Catalysts

3 Introduction

Different methods of preparation can have major effects on the properties of supported metal catalysts. As impregnation of the metal salt onto the support normally involves an ion exchange route, the surface acid/base properties of the support would be important. The effect of pre-treating the support with acid is investigated in this chapter, for Pt/Al₂O₃ systems with regard to Pt dispersion, Pt surface area or Pt concentration. The effects of other preparation variables (i.e. impregnation method, pH of the impregnating solution and drying temperature after impregnation) on Pt/Al₂O₃ catalysts were also examined. In this section literature on the preparation of Pt/Al₂O₃ catalysts will be reviewed.

Due to economic considerations, a large body of research has been carried out on preparation methods for supported metal catalysts. Lee and Aris (1), who have published a review on the distribution of active ingredients on supported pelleted catalysts, claimed that in the past most of the work was empirical in nature and catalyst preparation was considered more an art than a science. However, it is clear from the literature, that, studies are now aimed at understanding the scientific basis of the art of catalyst preparation. In their review, Lee and Aris (1) formulated mathematical models describing the impregnation and drying steps in the preparation of supported catalysts, using langmuir adsorption kinetics, the concept of capillarity and the principles of transport phenomena in porous media.

The aim of any preparation technique for supported metal catalysts is to obtain a highly dispersed, stable, metallic component on the support so that the surface area of the metal component is maximised. The properties of these catalysts are in close relation to the state of dispersion of the active elements. Impregnation of the support with an aqueous solution of a compound containing the appropriate catalytic component is an important, and frequently used method, of preparing this type of catalyst. The support is normally of high surface area and the four supports most frequently used are Al₂O₃, SiO₂-Al₂O₃, active carbon and molecular sieves (2). In its simplest form, the impregnation method involves three steps -

- (a) contacting the support with impregnating solution for a certain period of time
- (b) drying the support to remove the imbibed liquid
- (c) activation of the catalyst

There are two main impregnation techniques used i.e. incipient wetness and wet impregnation.

In wet impregnation the pre-wetted support is immersed in the metal salt solution and the metallic ions in the solution are adsorbed onto the support surface. With incipient wetness impregnation, the dry support is immersed in just enough metal salt

solution to saturate the pores of the support and metal moves into the support pores by solvent imbibition. In both cases, the resulting catalyst is dried and the catalytic component activated by calcination and/or reduction.

A number of preparation variables are thought to have a major effect on the dispersion of the supported metal. These include the metal precursor salt, the metal loading, the calcination temperature, and, if used, the reduction temperature (1)

Brunelle (2) examined the preparation of catalysts by metallic complex adsorption on mineral oxide supports. His analysis was based on the principals of surface polarisation versus pH and the adsorption of counter ions by electrostatic attraction. He concluded that the three most important parameters which appeared to regulate these adsorption phenomena were the isoelectric point of the oxide support, the pH of the aqueous solution and the nature of the metallic complex. He stated that an oxide in contact with a solution whose pH is below the oxide's isoelectric point tends to be charged positively and to be surrounded by compensating anions. The same oxide in a solution of pH above its isoelectric point polarizes negatively and tends to be surrounded by positive cations. Depending on the metallic complex, anionic or cationic, the pH of the impregnating solution can be adjusted to obtain maximum sorption of metal complexes on the oxide surface. For example, for Pt impregnation onto Al_2O_3 one of two conditions are required for adsorption, (a) an anionic precursor, such as a H_2PtCl_6 solution, with a pH lower than the pH of the isoelectric point of Al_2O_3 (approximately pH 7 - 8), (b) a cationic precursor, such as a $\text{Pt}(\text{NH}_3)_4(\text{OH})_2$ solution, with a pH greater than 8.

Palmer and Vannice (3) examined the effects of several preparation variables on the dispersion of supported platinum catalysts. In their study, two different salts were used for impregnation, $\text{H}_2\text{PtCl}_6 \cdot 6\text{H}_2\text{O}$ and $[(\text{NH}_3)_4\text{Pt}(\text{NO}_3)_2]$, together with four support materials, $\eta\text{-Al}_2\text{O}_3$, SiO_2 , $\text{SiO}_2\text{-Al}_2\text{O}_3$ and carbon. They used two different preparation methods, incipient wetness and wet impregnation. They found that the catalysts prepared using H_2PtCl_6 had a metal dispersion equal to, or better than, those which were prepared with $[(\text{NH}_3)_4\text{Pt}(\text{NO}_3)_2]$, using either impregnation technique on each of the supports. Of the supports examined, they found that greatest dispersion was achieved on $\eta\text{-Al}_2\text{O}_3$, while lower dispersion occurred on activated carbon and $\text{SiO}_2\text{-Al}_2\text{O}_3$, in agreement with a study by Cusumano et al (4) who found that impregnation of $\text{SiO}_2\text{-Al}_2\text{O}_3$ with H_2PtCl_6 , as compared with impregnation on Al_2O_3 , produced catalysts of lower dispersion. Also, $\text{SiO}_2\text{-Al}_2\text{O}_3$ supported catalysts were insensitive to the salt used for impregnation and the deposition method (3). Finally, Palmer and Vannice (3) found that the incipient wetness technique was superior to the excess solution technique for all the supports examined, with the exception of $\text{SiO}_2\text{-Al}_2\text{O}_3$.

A number of other studies have examined the effect of the Pt precursor salt on catalyst dispersion, (5, 6, 7). However, much of this research involved comparisons

between the effectiveness of different Pt salts rather than determining mechanisms of adsorption of the precursor onto the support. Modelling of impregnation kinetics has been carried out for the adsorption of hydrochloric acid (HCl), perhenic acid (HReO₄) and H₂PtCl₆ on γ -Al₂O₃ (8). The rate constants for the adsorption of HCl, HReO₄ and H₂PtCl₆ on γ -Al₂O₃ were calculated to be 0.032, 0.128 and 0.800 min⁻¹ respectively.

The sorption of ammonium hexachloroplatinate [(NH₄)₂PtCl₆] and ammonium tetrachloroplatinate [(NH₄)PtCl₄] on γ -Al₂O₃ has been examined (9). It has been determined that at the pH of impregnation, i.e. pH 3-4, these salts are in the form of unhydrolysed ions, PtCl₆²⁻ and PtCl₄²⁻ respectively. Evidence was obtained for two different sorption mechanisms: one involved anion exchange with surface hydroxyl groups of γ -Al₂O₃, the other mechanism involved ligand removal, where the active sites of the support surface entered the Pt co-ordination sphere, removing chloride ions into the solution. It was also determined that the quantity of metal sorbed by the support appeared to be lower for Pt (II) (by ca. 20%) than for Pt (IV). This has been attributed to the higher reactivity of the octahedral complexes of Pt (IV) compared with the square planar complexes of Pt (II).

Where there is no chemical interaction between the Pt salt and the support, then the size and distribution of Pt crystallites ultimately depends on the physical properties of the support, i.e. the porosity, surface area, etc. Dorling et al (10) suggested a model for the impregnation process for H₂PtCl₆ on SiO₂. They proposed that during drying, the impregnating solution concentrated as the solvent was removed by evaporation. A point was reached where crystallisation of the metal salt occurred, providing a nucleus in the pores of the support that still contained solution. Further drying caused the Pt particles to crystallise out in an amount dependent on the volume of solution in the pore at the onset of crystallisation. Increasing the concentration of the impregnating solution increased the number of pores which contained a crystallite of Pt, until the number of Pt crystallites equalled the number of pores. Therefore, up to a certain Pt concentration, the number of Pt crystallites increased and the mean crystallite size varied slowly, but beyond this Pt concentration the number of crystallites would remain constant and the crystallites increased in size due to nucleation.

Pt salts can also be adsorbed onto supports by ion exchange, i.e. the adsorption of Pt(NH₃)₄²⁺ ions from dilute [Pt(NH₃)₄]Cl₂ solutions by SiO₂ has been described in terms of exchange with surface H⁺ ions and it has been demonstrated that the amount of Pt taken up can be controlled through the adjustment of the pH (11). It was determined that at pH 8 the value for the adsorption of Pt(NH₃)₄²⁺ on SiO₂ was approximately 0.12 mmol Pt(NH₃)₄²⁺ g⁻¹ SiO₂ while at pH 9 the corresponding value was approximately 0.3 mmol g⁻¹ SiO₂ (11). Dorling et al (10) also established that the

amount of $\text{Pt}(\text{NH}_3)_4^{2+}$ adsorbed from the solution was related to the number of available exchange sites on the silica

The solvent used for the metal precursor salt solution used during impregnation can also have a major effect on metal dispersion of supported catalysts. The solvent can effect the rate of impregnation, in addition to the amount of metal precursor adsorbed on the support (12). This can be explained in terms of the ability of solvents to compete with the metal precursor in adsorption onto the support. Machek et al (12) carried out a number of studies in this area, in particular they carried out a study on the effects which occurred when acetone or water were used as solvents for H_2PtCl_6 during the impregnation of active carbon and $\gamma\text{-Al}_2\text{O}_3$ supports. They determined that aqueous solutions of H_2PtCl_6 gave uniform Pt distributions on $\gamma\text{-Al}_2\text{O}_3$, while, when acetone was used, non-uniform platinum distributions were obtained. The opposite situation was found to be the case for the active carbon support. They related this phenomenon to the heats of wetting of the solvents on the support, i.e. the greater the heat of wetting the lower the competition with the metal precursor salt for the adsorption sites on the support.

Competitive adsorption can also improve the dispersion of platinum supported catalysts. Pt in $\text{Pt}/\text{Al}_2\text{O}_3$ catalysts is often found near the external surface of the porous support, when a catalyst is prepared by impregnating with a H_2PtCl_6 solution. This is because, as the solution penetrates the pore, the metal salt is removed completely from the liquid, so that, if the time for metal salt diffusion from the liquid to the pore wall is short, compared to solution penetration, then the metal salt will be deposited in the region of the pore first in contact with the solution. A competitive adsorber can improve the Pt distribution because, during solution penetration, the metal salt penetrates further into the pore, as it is unable to occupy sites upon which the competitor adsorbs (1, 13).

Maatman (13) found that the addition of a variety of different acids and salts to H_2PtCl_6 solutions increased the dispersion and activity of platinum on an $\eta\text{-Al}_2\text{O}_3$ carrier. These included HCl and HNO_3 and the salts $\text{Al}(\text{NO}_3)_3$, NH_4NO_3 , and NaNO_3 . The acids gave uniform distributions of Pt on the support while the nitrate salts were less efficient, with Pt only near the external surface of the Al_2O_3 pellets used (13).

A number of studies have been carried out with regard to two component impregnations (H_2PtCl_6 and a competitor) on an Al_2O_3 support (14, 15, 16). Summers and Hegedus (15) examined the performance and durability properties of Pt/Pd oxidation catalysts supported on Al_2O_3 pellets for automotive emission control. The form of the Al_2O_3 used was not reported. To assess the importance of metal location on the pellets five catalysts were prepared, namely - Pt(exterior)/Pd(interior), Pd(exterior)/Pt(interior), Pt(exterior)/Pd(exterior), Pt(exterior) and Pd(exterior). To achieve the first two catalyst configurations competitive adsorbates were used. HF was used with PdCl_2 to produce a subsurface layer of Pd (by blocking the Al_2O_3 sites near

the surface) Similarly to achieve an inner core of Pt, citric acid was used as a competitive adsorbate with H_2PtCl_6 . It was determined that improvements in both the steady state and light off performance of catalysts for the oxidation of CO and propylene when the catalysts were impregnated by an outer shell of Pt and an inner shell of Pd (15)

Shyr and Ernst (16) examined the effect of competitive adsorbates on the impregnation of $\gamma\text{-Al}_2\text{O}_3$ spherical beads with H_2PtCl_6 . The competitive adsorbates studied included HCl, HF, HNO_3 , acetic acid, citric acid, tartaric acid, AlCl_3 , NaCl, NaF, NaBr, NaNO_3 , Na_3PO_4 , Na benzoate and Na citrate. Radial Pt profiles were examined by electron probe microanalysis of bead cross sections. Nine distinctly different types of profiles were determined, shown in Fig 3 0. After 22h impregnation only with H_2PtCl_6 and acetic acid was a uniform distribution of Pt through the beads achieved (16)

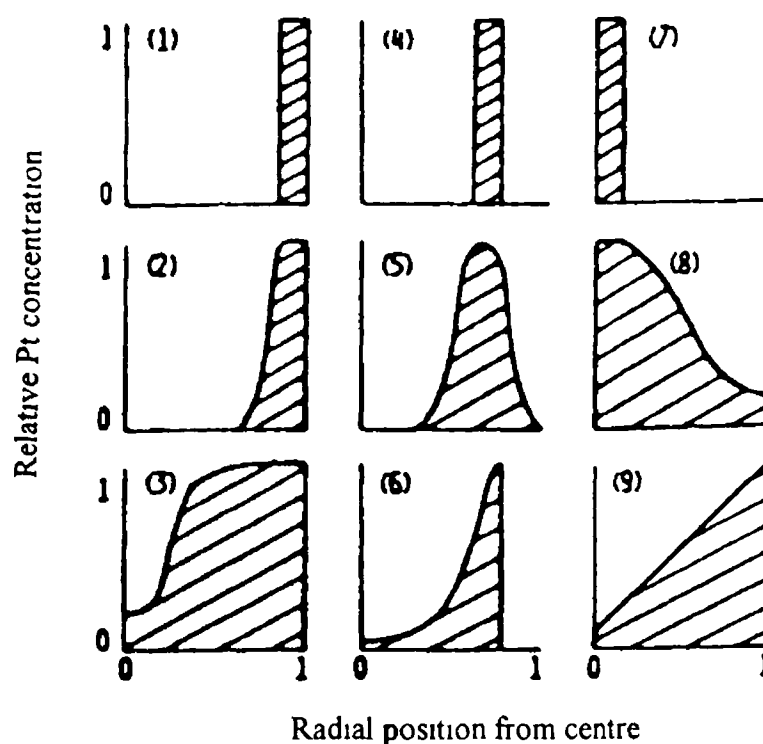
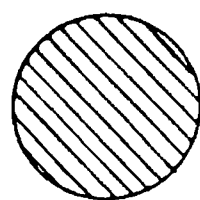
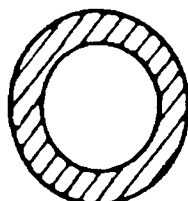


Fig 3 0 The nine Pt distributions in Al_2O_3 beads determined by Shyr and Ernst (16)

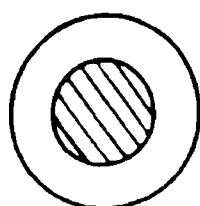
A study was carried out by Jianguo et al (17) on competition between H_2PtCl_6 and acids, including citric and lactic acid, for adsorption of pelleted $\eta\text{-Al}_2\text{O}_3$ supports. It was determined that the adsorption isotherms for the organic acids mentioned above obeyed the langmuir adsorption isotherm on $\eta\text{-Al}_2\text{O}_3$. They found that using these acids with a Pt impregnating solution, the platinum phase would be concentrated in different areas of a $\eta\text{-Al}_2\text{O}_3$ pellet, i.e. when lactic acid was used as a competitive adsorbate during impregnation Pt was distributed either in a broadened region at the external surface of the pellet or homogeneously. On the other hand, use of citric acid caused Pt to be distributed in the centre of $\eta\text{-Al}_2\text{O}_3$ pellet, see Fig 3.1



(A) Homogeneous Pt distribution
(Lactic Acid as competitor)



(B) Egg shell Pt distribution
(Lactic acid as competitor)



(C) Egg Yolk Pt distribution
(Citric acid as competitor)

Fig 3.1 The effect of competitive adsorbates on Pt distribution in Al_2O_3 beads determined by Jianguo et al. (17)

Castro et al (18) found that during competitive adsorption of HCl and H_2PtCl_6 on Al_2O_3 pellets, low concentrations of HCl ($< 0.1\text{M}$) gave a inhomogeneous distribution of Pt throughout the pellet. They concluded that incomplete Pt penetrations were due to strong HCl and H_2PtCl_6 interactions with the surface,

together with low amounts of impregnant which were not sufficient to saturate the surface

It has also been established that, using inorganic salts such as NaNO_3 , NaCl , $\text{Ca}(\text{NO}_3)_2$ and CaCl_2 , the adsorption of H_2PtCl_6 on $\gamma\text{-Al}_2\text{O}_3$ can be altered by changing the ionic strength of their aqueous phase, which, in turn, changes the platinate ion activity. It has been determined that by increasing the ionic strength of the electrolyte the amount of metal adsorbed decreased. For example with the addition of the monovalent salts NaNO_3 and NaCl measurable Pt adsorption occurred on $\gamma\text{-Al}_2\text{O}_3$ up to a salt concentration of 0.1M, while for the divalent salts $\text{Ca}(\text{NO}_3)_2$ and CaCl_2 (which had three times the ionic strength of the monovalent salts) no measurable Pt adsorption occurred past an electrolyte concentration of 0.03M (19)

After impregnation with the metal precursor and drying, catalysts may be calcined in oxygen or air, at temperatures above 773K, in order that the catalyst precursor is converted to its active form. Depending on the catalyst, a reduction treatment in H_2 at high temperature may be carried out to bring about activation. High temperature treatments can cause sintering of the active phase, decreasing the surface area of the active component. Sintering of metals and especially sintering of Pt has been widely studied (20). The influence of treatment conditions, (temperature and atmosphere), and the metal, (nature of the metal loading), on the activation energies of sintering have been determined (20)

Bournonville, et al (21) found that the Pt surface area on chlorinated Al_2O_3 increased as the temperature of calcination increased up to 773K. Beyond that temperature, the surface area decreased, see Fig 3.2. No comparison was made with Pt supported on unchlorinated Al_2O_3 . To obtain high metal dispersions, calcination in air was required prior to reduction in H_2 (21), as illustrated in Fig 3.3

The presence of chloride ions can decrease the rate of sintering of Pt. In another study, Bournonville and Martino (22) found that if a chlorine content of higher than 1 wt% was present on the $\gamma\text{-Al}_2\text{O}_3$ support, Pt in $\text{Pt}/\text{Al}_2\text{O}_3$ catalysts did not sinter at relatively high temperatures (up to 773K) in an oxidising atmosphere, while in H_2 the rate was decreased when chlorine was present compared with when chlorine was not present. It was proposed, that in oxidising atmospheres at high temperatures, the formation of chloroplatinum aluminates would reduce sintering and that the formation of complexes, such as $\text{PtCl}_2(\text{AlCl}_3)$, could bring about a redispersion of the active phase, (because these complexes are volatile at high temperatures). In a H_2 atmosphere at high temperatures (773 - 973K) they concluded that it was difficult to know the nature of migrating species, as the surface atoms adsorbed H_2

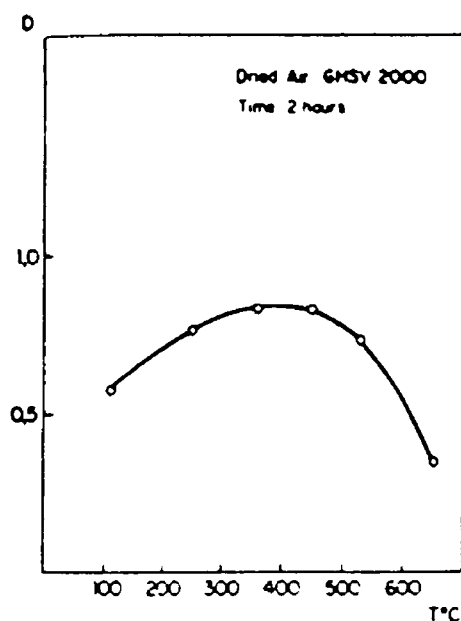


Fig 3 2 · The effect of calcination temperature on Pt dispersion (D) in catalysts prepared with chlorinated supports (21).

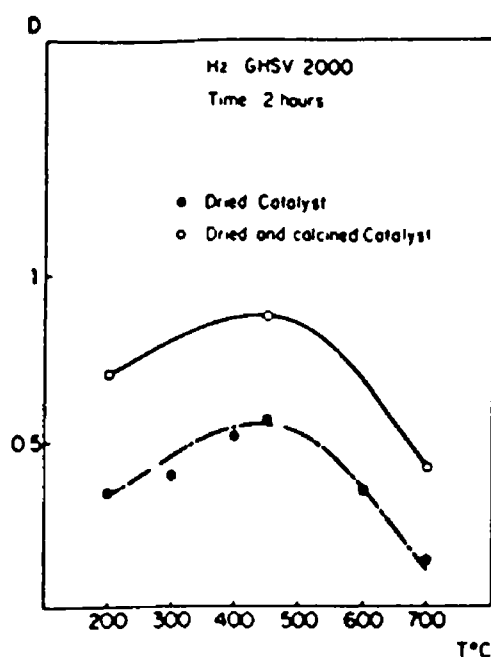


Fig.3.3 The effect of reduction temperature on Pt dispersion (D) in catalysts prepared with chlorinated Al_2O_3 supports(21).

The results of the study indicated that the presence of chlorine on the support increasing the support acidity, enhanced the interaction between the support and the Pt moiety, thus reducing its mobility on the surface (22)

The redispersion phenomenon for Pt/Al₂O₃ catalysts in an oxidising atmosphere has been explained by two different theoretical models (23)

- (a) the crystallite migration model
- (b) the molecular migration model

The first model envisaged sintering to occur by migration, collision and coalescence of metal crystallites on the support surface (23) Since this model always predicted a decrease in dispersion, an additional process had to be incorporated into the model to explain increases in dispersion observed during treatment at low temperatures (< 873K) in O₂ (23) Ruckenstein and Pulvermacher (24) attributed the increase in dispersion to changes in interfacial energies The latter depended on the atmosphere in which a thermal transformation was carried out and the change in the balance of the interfacial energies caused crystallites to split into smaller crystallites, resulting in higher dispersion (24)

In the second model, the molecular migration model, sintering occurred by the dissociation of atomic or molecular species from metal crystallites, followed by migration of these species over the support surface The species which migrated were then captured by trapping sites on the surface of the support (25) This model explained both increases and decreases in dispersion depending on the treatment involved In the case where the migrating species were caught by sites on the support that have large enough metal-support interactions or if the colliding molecular species caused the nucleation of new crystallites, then an increase in dispersion occurred (23) This mechanism involves vapour phase transport and surface migration (26) It is believed that on the formation of Pt/O species a change in surface tension occurs on the Al₂O₃ support which enables the Pt/O species to "wet" the Al₂O₃ surface, hence becoming more mobile However this is restricted as the Pt/O species become trapped on strong binding sites on the Al₂O₃ surface (23)

Pt/Al₂O₃ systems have been reported to exhibit strange behaviour when exposed to high temperatures in certain atmospheres For example Dautzenberg and Walters (27) found that with Pt/Al₂O₃ catalysts (up to 2wt% Pt) heat treatment in H₂ at 823K or above resulted in a decrease in H₂ chemisorption Using TEM and XRD analysis it was determined that this behaviour was not due to Pt agglomeration, but rather a certain fraction of the Pt becoming what was termed "inaccessible" It was also determined that this phenomenon could be reversed by oxidation in air at temperatures below 773K (27) It has been proposed that this may be due to a strong metal support interaction (SMSI) effect (28) The SMSI effect was first described by Schwab more than six decades ago (29) Interest in the interaction between metal particles and the oxide support was awakened by studies carried out by Tauster et al (30, 31) They studied

group VIII metals supported on transition metal oxides, and established that when reduced in hydrogen at high temperature, the metals exhibited anomalously low uptakes of H₂ and CO at room temperature. This phenomenon was termed "strong metal support interaction" and early explanations for the SMSI effect very often involved electron transfer from the support to the metal particle (32, 33), but more recent work (34) has pointed to the fact that the dramatic changes in catalytic properties observed are not exclusively due to electron transfer. Metals in the SMSI state have lower activities for structure insensitive reactions, much lower activities for hydrogenolysis reactions and in certain cases (i.e. Pt/TiO₂ compared with Pt/SiO₂) significantly higher activities and different selectivities for the CO/H₂ reaction (35).

Bond and Burch (35) reviewed the research carried out on the SMSI effect up to 1982 and concluded that the strong metal support interaction phenomenon was almost exclusive to titanium oxide (TiO₂) systems. They claimed that for insulator oxides of a single element, e.g. Al₂O₃, SiO₂ and MgO, that the direct influence upon the geometric and electronic properties of small metal particles was usually small (35). However as already stated evidence has been found for SMSI effects in insulator oxide supported catalytic systems (27, 28, 36, 37, 38, 39, 40). Gonzalez-Tejeda et al (36) found evidence for SMSI effects and suggested that for Pt/Al₂O₃ catalysts, Pt particles could decompose into an atomic form incorporated into the support, after reduction in H₂ at 723K. Den Otter and Dauzenberg (37) found that, upon heating in H₂ at 1123K, Pt/Al₂O₃ catalysts exhibited a decrease in H₂ chemisorption, although hardly any agglomeration of the particles took place, and they concluded that a surface Pt alloy was formed.

Similar findings were reported by Kunimori et al (38) and they proposed the formation of a surface alloy of the form



Using the technique of temperature programmed reduction, together with transmission electron microscopy and catalytic activity measurements, Ren-Yuan et al (39) found that, for Pt/Al₂O₃ systems during reduction, the metal combined intimately with the support. They proposed the formation of a Pt/Al₂O₃ alloy and also that on increasing the reduction temperature, the metal support interaction would be strengthened through the transformation of the Pt rich alloy to an Al₂O₃ rich one on the surface and a diffusion of some of the Pt atoms into the sublayers of the support. Huizinga et al (40) also obtained results which appeared to demonstrate a substantial interaction between Pt oxide and Al₂O₃.

Despite the evidence indicating a strong metal-support interaction for oxide supports other than group IVB oxide supports some researchers have found evidence to

the contrary. For example, Menon and Froment (41) claimed that the suppression of H_2 chemisorption in Pt/Al_2O_3 catalysts was not due to strong metal support interactions. Instead, the effect was due to self inhibition brought about by strongly adsorbed H_2 . Recently Alekseev et al (42) found that although Pd/SiO_2 catalysts doped with Ti, Zr or Hf exhibited SMSI behaviour with regard to H_2 chemisorption and catalytic activity, undoped Pd/SiO_2 did not exhibit SMSI phenomena.

The following sections in this chapter detail the investigation of the effects of preparation variables on the characteristics of Pt/Al_2O_3 catalysts and on their catalytic activity for the complete oxidation of $i-C_4H_{10}$. The effect of pre-treatment of the support with acid prior to impregnation (a technique used for washing the support material) was examined. Pt/Al_2O_3 catalysts prepared using Al_2O_3 fibre mats as the support were compared with similar catalysts supported on powdered Al_2O_3 . The influence of the pH of the impregnating solution was also examined. For catalysts supported on mats the distribution profiles of Pt deposited on the support during impregnation was determined and the effect of drying temperature, after impregnation, on the Pt distribution profiles was investigated.

the contrary. For example, Menon and Froment (41) claimed that the suppression of H_2 chemisorption in Pt/Al_2O_3 catalysts was not due to strong metal support interactions. Instead, the effect was due to self inhibition brought about by strongly adsorbed H_2 . Recently Alekseev et al (42) found that although Pd/SiO_2 catalysts doped with Ti, Zr or Hf exhibited SMSI behaviour with regard to H_2 chemisorption and catalytic activity, undoped Pd/SiO_2 did not exhibit SMSI phenomena.

The following sections in this chapter detail the investigation of the effects of preparation variables on the characteristics of Pt/Al_2O_3 catalysts and on their catalytic activity for the complete oxidation of $i-C_4H_{10}$. The effect of pre-treatment of the support with acid prior to impregnation (a technique used for washing the support material) was examined. Pt/Al_2O_3 catalysts prepared using Al_2O_3 fibre mats as the support were compared with similar catalysts supported on powdered Al_2O_3 . The influence of the pH of the impregnating solution was also examined. For catalysts supported on mats the distribution profiles of Pt deposited on the support during impregnation was determined and the effect of drying temperature, after impregnation, on the Pt distribution profiles was investigated.

3.1 Experimental

3.1.1 Catalyst Preparation

The specifications of the Al_2O_3 material used (ICI Saffil fibre) as the support material were given in Sec 2.1.1. A series of $\text{Pt}/\text{Al}_2\text{O}_3$ catalysts were prepared as detailed in Table 3.0. Two preparation methods were used. In method A, the dry Al_2O_3 mat was spray impregnated with an excess volume of an aqueous solution ($25\text{cm}^3\text{g}^{-1}$ Al_2O_3) of $\text{H}_2\text{PtCl}_6 \cdot 6\text{H}_2\text{O}$ (Johnston Matthey). After impregnation the sample was dried at 310K for 16h. In method B, the Al_2O_3 fibre was first ground into a powder using a mortar and pestle and then an aqueous solution of $\text{H}_2\text{PtCl}_6 \cdot 6\text{H}_2\text{O}$ ($25\text{cm}^3\text{g}^{-1}$ Al_2O_3) was added to the powdered Al_2O_3 in a round bottomed flask. Excess solvent was removed using a rotary evaporator and the sample was then dried at 310K for 16h. For all catalyst samples prepared the concentration of the impregnating solution was adjusted to give a nominal Pt loading of 5wt%. All samples were calcined, after drying, at 900K for 0.25h in a preheated muffle furnace.

Samples were also prepared with pre-treated Al_2O_3 supports prepared in the same manner as that described in Sec 2.1. Both 0.1M HNO_3 (Riedel de Haen, GPR grade) and 0.1M HCl (Riedel de Haen, GPR grade) were used for pre-treatment and also milli Q H_2O .

To investigate the effect of the pH of the impregnating solution, an untreated Al_2O_3 support was spray impregnated (method A) with a $\text{H}_2\text{PtCl}_6 \cdot 6\text{H}_2\text{O}$ solution of pH4. The pH was adjusted by the addition of 0.1M NaOH (Riedel de Haen, GPR grade).

To determine the influence of drying temperature four samples were prepared using different drying procedures. Two catalyst samples were prepared using method A, one with an untreated support and one with a HNO_3 pre-treated support, and were dried at 350K for 16h prior to calcination. Two further samples, prepared identically to the two described above, were dried at 390K for 16h and calcined in the normal manner.

Table 3 0 Preparation Details for Pt/Al₂O₃ Samples Used In Study

Sample Code	Impregnation Method *	Impregnating Solution pH	Al ₂ O ₃ Support pre-treatment	Drying Temp for 16h after Impregnation
**Pa(U)T1	A	1	untreated	310K
Pa(W)T1	A	1	H ₂ O	310K
Pa(C)T1	A	1	HCl	310K
Pa(N)T1	A	1	HNO ₃	310K
Pb(U)T1	B	1	Untreated	310K
Pb(N)T1	B	1	HNO ₃	310K
Pa(U)4T1	A	4	Untreated	310K
Pa(U)T2	A	1	Untreated	350K
Pa(N)T2	A	1	HNO ₃	350K
Pa(U)T3	A	1	Untreated	390K
Pa(N)T3	A	1	HNO ₃	390K

*Note A = spray impregnation, B = wet impregnation

** Pa(U)T1 = Pt/Al₂O₃ catalyst prepared by method A (a), using untreated support fibre (U) and dried at 310K (T1)

3 1 2 Estimation of Nitrate Uptake by the Al₂O₃ Support Material

In order to estimate the uptake of NO₃⁻ by the Al₂O₃ fibre during pre-treatment with 0.1M HNO₃ prior to impregnation two experiments were carried out in which the washings from the pre-treatment process were monitored potentiometrically for the presence of NO₃⁻. In the first experiment the pre-treatment and water washing was carried out in a normal air atmosphere. The Al₂O₃ fibre mat was pre-treated with an 1 x 10⁻³M HNO₃ (Riedel de Haen) solution. The mat was then rinsed in the normal manner with milli Q H₂O (as described in Section 2.1) and the washings were combined and retained. The concentration of NO₃⁻ was determined from comparison of the potential obtained using a Orion Model EE-N Nitrate Electrode and the potentials obtained for a standard curve of various NO₃⁻ concentrations, ranging from 10⁻¹ to 10⁻⁴ M.

The second experiment was essentially the same as the first except that during pre-treatment 1.43 x 10⁻³ M NO₃⁻ was used and after pre-treatment any NO₃⁻ present in the washings was trapped in cold H₂O, under an N₂ atmosphere to prevent loss of NO₃⁻. The apparatus used in the experiment is illustrated in Fig 3.4.

For both experiments a blank run was carried out in which the Al₂O₃ mat was washed with milli Q H₂O and the washings analysed. In these cases a concentration of less than 10⁻¹ M NO₃⁻ was found in the washings.

3 1 3 H₂ Chemisorption Measurement

The instrument used for H₂ chemisorption measurement was the Micromeritics Pulse Chemisorb 2700. A schematic diagram of the instrument is given previously in Fig 2.10, Sec 2.1.2. The operation of the instrument for chemisorption measurement is based on a pulse technique. A known volume of pulses of adsorbate gas are injected into an inert carrier gas stream flowing over the reduced catalyst. By determining the number of pulses, together with the fraction of each pulse adsorbed, the amount of gas chemisorbed by the catalyst to obtain monolayer coverage on the exposed metal surface can be calculated.

The gases used for the catalyst pre-treatment and measurement were purified before entering the instrument. Ar (normal grade, Air Products Ltd) was purified using a BOC Rare Gas Purifier, which contains titanium granules at 970K to remove N₂ and O₂, a copper furnace to remove hydrocarbons, H₂ and CO, and a molecular sieve at ambient temperature to remove H₂O and CO₂. The specified purity of the gas leaving

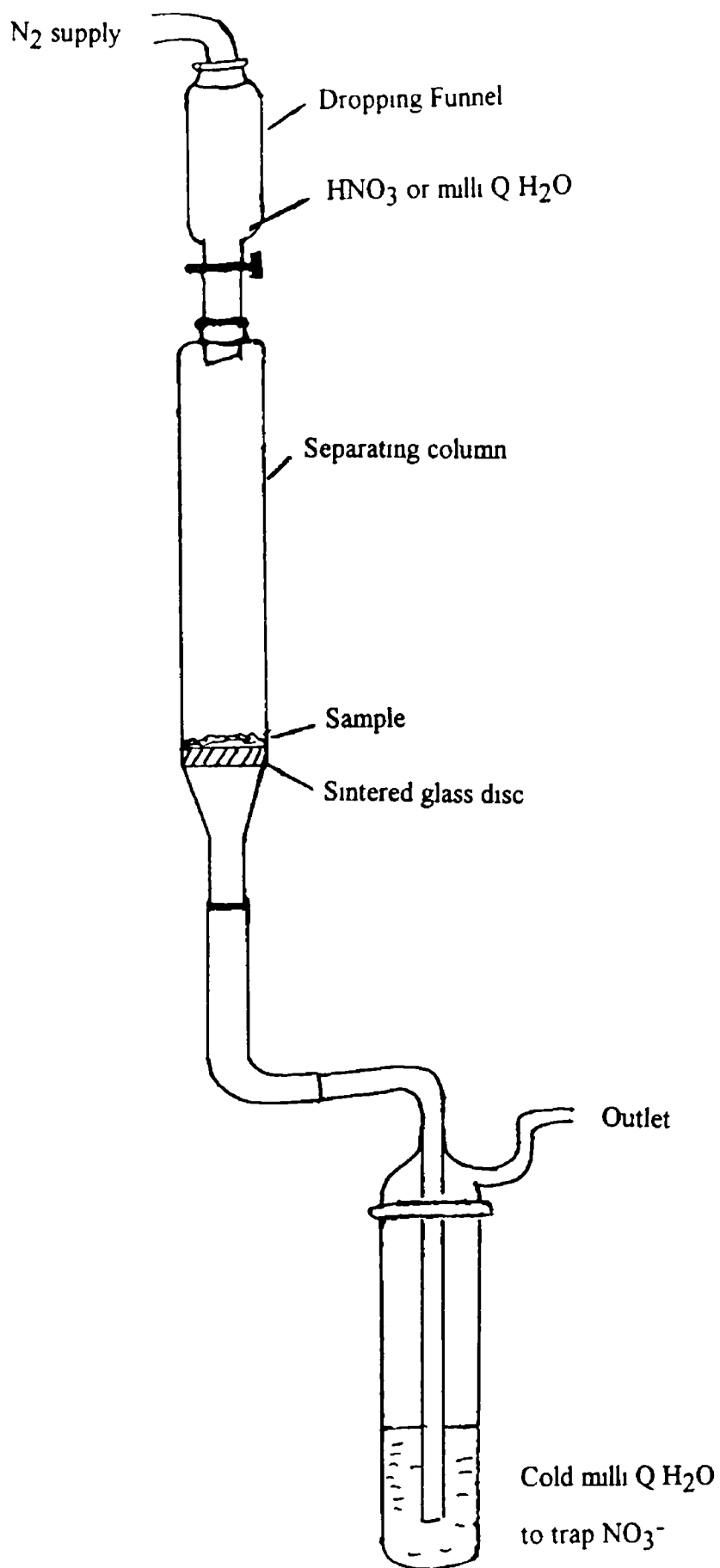


Fig 3 4 : Apparatus for trapping NO₃⁻ in cold H₂O prior to NO₃⁻ determination

the purifier was 99.995%. H₂ (CP grade, Air Products Ltd.) was purified using a Johnston Matthey EP1 Hydrogen Purifier, which operates by the principle of diffusion of H₂ through a palladium alloy membrane, allowing only the passage of H₂, and the specified purity of the gas exiting the purifier was 99.9999%.

Treatment of the catalyst sample prior to and during analysis was as follows. The catalyst sample, which was powdered, was placed in a preweighed, clean sample tube. The sample tube was then attached to the instrument. Sample pre-treatment (purging and reduction) were carried out on the prep. line of the instrument. The sample was purged in Ar (15cm³min⁻¹) at 285K for 0.25h, 370K for 0.5h and 520K for 1h. It was then reduced in H₂ (15cm³min⁻¹) at 520K for 1h, followed by 670K for 2h. The sample was finally purged in Ar at 670K for 0.25h. After pre-treatment the sample was switched to the test line of the instrument via a four way switching valve. Testing involved injection of successive H₂ pulses (48μl) over the sample. Non-adsorbed H₂ was analysed by a thermal conductivity detector within the Pulse Chemisorb 2700. Adsorption was carried out at a temperature of 305K and desorption was brought about by heating the sample to 670K for 15min. Each analysis consisted of at least two adsorption/desorption cycles. After testing, the sample tube was reweighed in order that the sample mass could be determined.

The difference between adsorption results for successive cycles was ±4%. The difference between adsorption results for different samples of the same catalyst was ±3%. The accuracy of the analysis method was examined by the measurement of the uptake of H₂ by the silica supported platinum standard catalyst, Europt-1. The average uptake was found to be 145μmol H₂ g⁻¹ and this compared with previous results from an international study of between 160 and 190μmol H₂ g⁻¹ (43). However it must be noted that the latter results were obtained using a volumetric static flow technique (43).

3.1.4 Atomic Absorption Spectroscopy

The Pt content of the samples was estimated after acid digestion by flame atomic absorption spectroscopy. A mass of catalyst was used to give Pt contents of the order of 20ppm after digestion. Each sample was digested by first adding the minimum amount of HF (GPR grade, Riedel de Haen), approximately one or two drops, in order to break up the support material. Then 5cm³ of freshly prepared aqua regia was added and the sample was then heated to near dryness. Approximately 1cm³ of concentrated HCl (GPR grade, Riedel de Haen) was used to redissolve each sample. The digested samples were made up to 100cm³ in volumetric flasks after the addition of HCl and LaCl₃ (BDH, Spectrosol). The latter compounds were added to prevent interference problems, with all solutions prepared containing concentrations of 0.1M HCl and 200ppm La³⁺. A

standard curve was prepared with solutions containing Pt concentrations within the linear working range of 0 to 150ppm Pt

Atomic absorption measurements were obtained in triplicate Analysis was carried out using an Instrumental Laboratory Spectrophotometer 357 The instrumental conditions used during analysis are given in Table 3 1

Table 3 1 Instrumental Conditions For Atomic Absorption Spectroscopy

Light Source	Pt / hollow cathode lamp
Lamp Current	6 mA
Wavelength	265 9 nm
Slit Width	160 μ m
Band Pass	0 5 nm
Burner Head	Single Slot
Flame Description	Air-acetylene, oxidising, fuel lean, blue

For Pt analysis standard solutions were prepared containing known amounts of Pt and were acid digested in the same manner as the other catalyst samples in order to estimate the possible Pt loss during the digestion process The error due to digestion was found to be $\pm 8\%$ The difference in the value for Pt content between duplicate samples, was determined experimentally to be $\pm 3\%$

In order to measure the distribution of Pt on an Al_2O_3 mat, a mat was spray impregnated with a solution containing sufficient Pt to give a 5wt% Pt loading, dried, calcined at 900K in static air for 0 25h and divided into nine sections In addition three sections were divided transversely into top, middle and bottom sections after calcination The division of the impregnated mat is illustrated in Fig 3 5

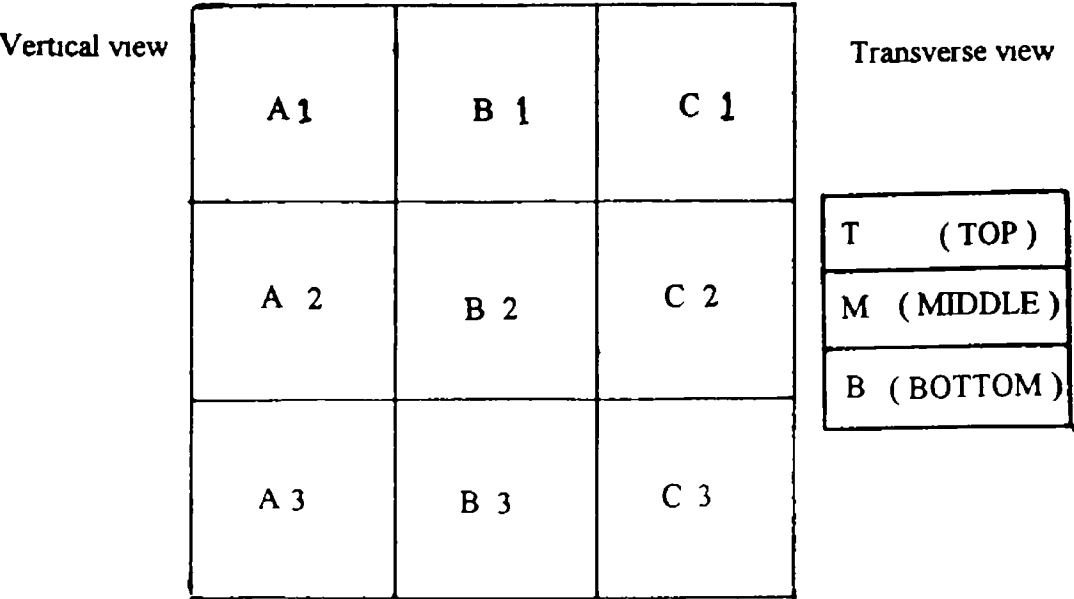


Fig 3 5 : Division of mat for Pt analysis

3.1.5 Activity Measurements

A schematic diagram of the activity unit used for the measurement of reactivity is illustrated in Fig 3.6. The activity unit was designed to allow the controlled flow of various gas mixtures over heated catalysts. The sample holder was attached to the activity unit by two cajon fittings with o-ring seals. The sample holder was designed so that the catalyst sample was supported on a sintered glass disc and the gas passed through the sample from the top.

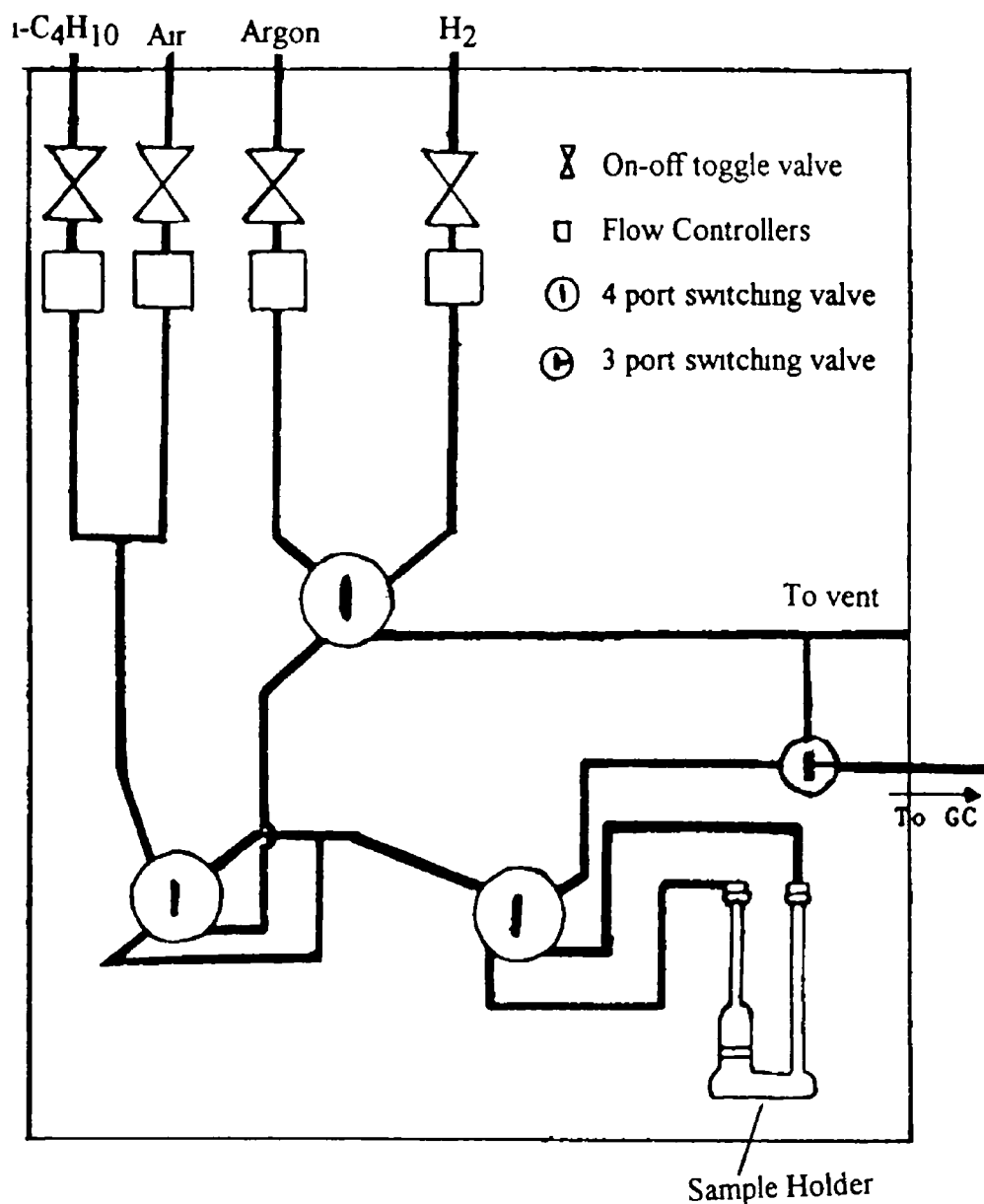


Fig 3.6 Activity unit for catalyst testing

Analysis of the reaction products was carried out using a Pye Unicam Pu 4450 gas chromatograph with an FID detector and the results were integrated using a Hewlett Packard 3390A integrator. The instrumental conditions used for gas chromatographic analysis are given in Table 3.2. The system allowed the separation of hydrocarbons but neither CO nor CO₂ could be analysed using this system due to the lack of a TCD detector. The detectability of the system was typically of the order of $1 \times 10^{-11} \text{ g s}^{-1}$ for all hydrocarbons examined.

The reaction mixture used was an air (normal grade, IIG Ltd)/i-butane (CP grade, Air Products Ltd) mixture in stoichiometric ratio, $32 \text{ cm}^3 \text{ min}^{-1}$ air, $1 \text{ cm}^3 \text{ min}^{-1}$ butane. The hydrocarbon content of the gas mixture before reaction was determined using GC by by-passing the sample via the four-way valve. The i-butane gas used had a composition of 99.6% i-butane, 0.3% methane, 0.03% ethane, 0.01% propane.

Table 3.2 Instrumental Conditions for GC Analysis

Detector	Flame ionisation detector
Column	2m, 6mm i.d., glass
Packing	Porapak Q
Temperatures	Column 445K Injector 470K Detector 490K
Carrier Gas	Nitrogen (normal grade, IIG)
Detector Gases	H ₂ (normal grade, Air Products Ltd) Air (normal grade, IIG)
Flow Rates	Carrier $30 \text{ cm}^3 \text{ min}^{-1}$ H ₂ $33 \text{ cm}^3 \text{ min}^{-1}$ Air $330 \text{ cm}^3 \text{ min}^{-1}$

Reaction runs were carried out as follows. A pre-weighed sample of ground catalyst (approximately 0.04g) was placed in a sample holder and the holder was attached to the activity unit as described above. The sample was treated prior to reaction in one of two ways. In the first method, the sample was immediately exposed to the reaction mixture for five minutes at room temperature prior to raising the furnace temperature. In the second method, involving reduction, the sample was prereduced as follows: the sample was purged in argon ($20 \text{ cm}^3 \text{ min}^{-1}$) at room temperature for 5 minutes, 370K for 0.5h, and 520K for 1h. This was followed by reduction in H₂ ($20 \text{ cm}^3 \text{ min}^{-1}$) at 520K for 1h and then at 670K for 2h. Finally, after reduction, the

sample was purged in argon ($20\text{cm}^3\text{min}^{-1}$) at 670K for 0.25h and then cooled to room temperature prior to reaction

Furnace temperature was increased to 420K and if no reaction occurred at that temperature, the temperature was raised in 50K increments until reaction occurred. Samples of the gas mixture passing over the catalyst were injected into the gas chromatograph (via a gas sampling valve) and reaction was detected by a decrease in the area of the i-butane peak. At each temperature, samples of the product gases were analysed by GC until a steady state was reached (i.e. little change in the area of the i-butane peak after several successive injections). At that point the temperature was raised by 50K and the products again analysed until a steady state was reached. The maximum sample temperature used was 670K. After reaction at this temperature the sample was cooled to room temperature in argon. Then a second reaction run was carried out in a similar manner to the first run. It should be noted that, other than cooling to room temperature in argon, no sample treatment was carried out prior to the second reaction run.

3.1.6 DSC Activity Measurements

Catalytic activity measurements were also carried out using a Stanton Redcroft DSC 700. The instrument was connected to gas supplies as illustrated in Fig 3.7, air (normal grade, IIG Ltd), i-butane (Air Products Ltd) and nitrogen (normal grade, IIG Ltd). For normal activity runs, air and i-butane were passed through the DSC in a 32:1 stoichiometric ratio. The flow rates used were $0.6\text{cm}^3\text{min}^{-1}$ i-butane and $19.2\text{cm}^3\text{min}^{-1}$ air. The gas mixture was passed through the DSC at room temperature for at least 0.16h prior to analysis. Both the sample and reference material ($\alpha\text{-Al}_2\text{O}_3$) were loaded into aluminum crucibles and placed in the DSC head prior to analysis. Identical masses of sample and reference were used and normally 1mg samples were used. The standard temperature programme used was to heat the catalyst and reference at 10K min^{-1} up to 573K and hold at that temperature for 0.5h, prior to cooling to room temperature. Normally three successive reaction runs were carried out. The DSC and temperature traces were recorded on a Linseis L6510 twin pen chart recorder.

In order to examine the reproducibility and sensitivity of the DSC trace, a number of experiments were carried out in which the activity run conditions were varied and the effects of these changes on the DSC and temperature traces were noted. The conditions affected included the composition of the reactant mixture and the sample / reference masses used. The effluent gases from the DSC were also analysed using a flame ionisation detector in a GC and for certain runs a CO_2 analyser (Analytical Development Co. Ltd) was also fitted to the outlet of the DSC furnace. The details of these experiments together with the results are given in section 3.2 of this chapter.

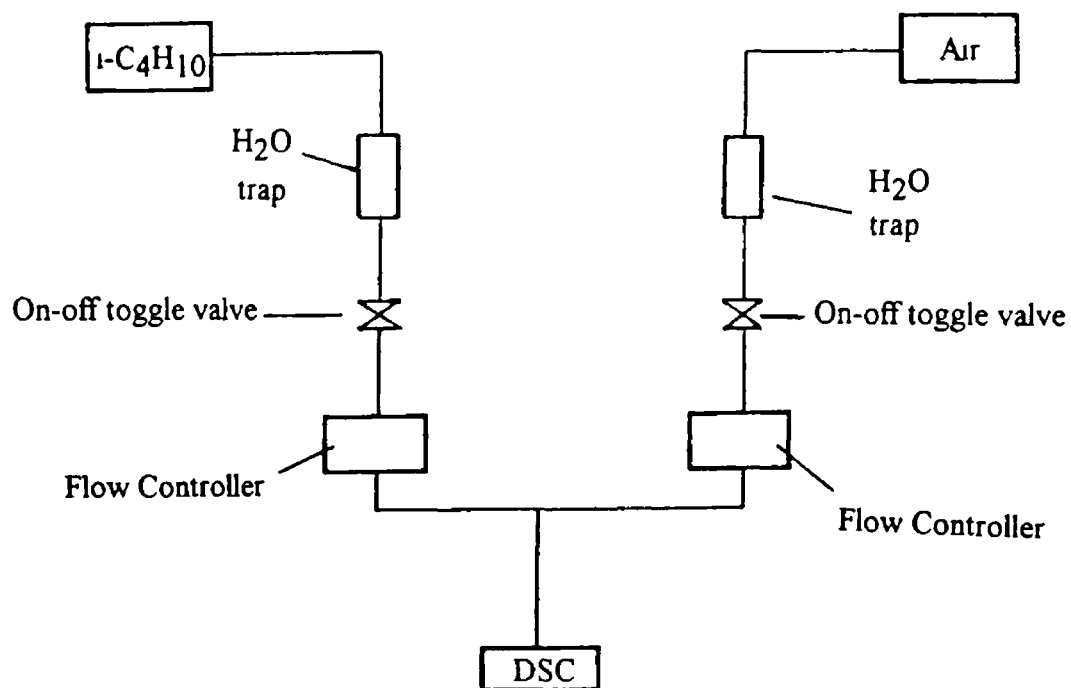


Fig 3 7 Activity unit used with DSC analysis.

3.2 Characteristics of DSC activity measurement

A typical DSC activity trace is shown in Fig 3 8 for 1mg of 5% Pt/Al₂O₃ sample where a 1 32 butane air mixture, with a total inlet flow rate of 19 8 cm³ min⁻¹, was used Both the DSC signal and the sample temperature are recorded Catalytic activity results in the production of an exothermic trace by the DSC Initially the temperature of the sample increases linearly with the heating rate of the furnace However, as the DSC signal increases with activity at a certain point, marked "A" in Fig 3 8 the temperature of the sample rapidly increases above the heating rate of the furnace, before increasing linearly again with the same furnace heating rate, at a higher temperature than that of the DSC furnace If the furnace temperature is then decreased a trace similar to that shown in Fig 3 9 is obtained The DSC signal decreases as the sample temperature drops indicating that activity can not be maintained independently of the furnace temperature

In order to find out the relationship between the activity traces and the actual activity of the sample, a GC and CO₂ analyser were used to monitor the effluent gas stream from the furnace Using these techniques it was observed that CO₂ appeared in the effluent stream at approximately 0 8 to 1 min prior to the temperature jump, labelled point "B" in Fig 3 8 This was about 9min after the beginning of the DSC exotherm, point C in Fig 3 8 The appearance of CO₂ in the effluent gas stream corresponded to a drop in the level of butane coming from the furnace outlet as determined by GC The production of CO₂ indicated that the oxidation of i-butane was occurring

The exotherm indicated by the DSC signal is very similar to the light off characteristics of a car exhaust catalysts illustrated by Trimm (44) and shown in Fig 3 10 Trimm (44) pointed to three distinct regions in the performance graph for oxidation catalysts, illustrated as regions 1, 2 and 3 in Fig 3 10 Comparing Fig 3 10 with the DSC exotherm obtained from an activity run, i e Fig 3 8, the similarity between the two diagrams can be observed Therefore, it is probable that the region where the DSC signal increases slowly, region C in Fig 3 8, is the kinetic controlled region Light off is represented by the rapid increase in the DSC signal, region A in Fig 3 8 Finally, the point where the DSC signal stabilises at a higher level, region D in Fig 3 8, represents the situation where the reaction reaches a steady state The rapid increase in sample temperature (above the heating rate of the DSC furnace), corresponding to the region in which the DSC signal increases rapidly, is likely to represent the light off of the catalyst sample

With most of the Pt/Al₂O₃ catalyst samples a second sample temperature jump and a second DSC exotherm, was observed, see Fig 3 11 The magnitude of these features were smaller than the initial temperature increases and DSC exotherms It is possible that these samples may contain two distinct sites for oxidation of butane, one

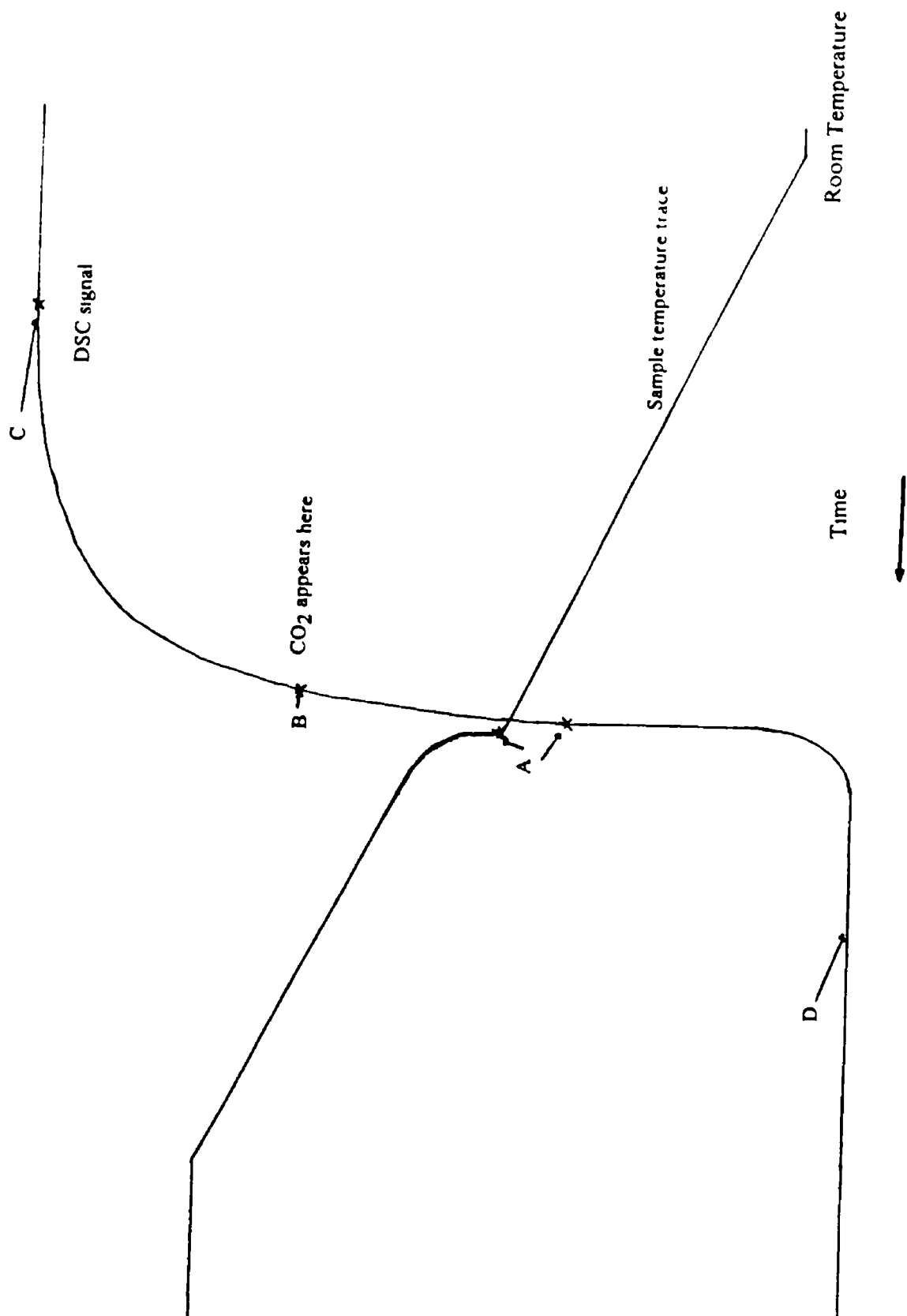


Fig 3 8 A typical DSC activity trace for 1mg 5%Pt/Al₂O₃ sample with a 1 32 butane.air mixture, with a total inlet flow rate of 19 8cm³min⁻¹, heating rate 10Kmin⁻¹

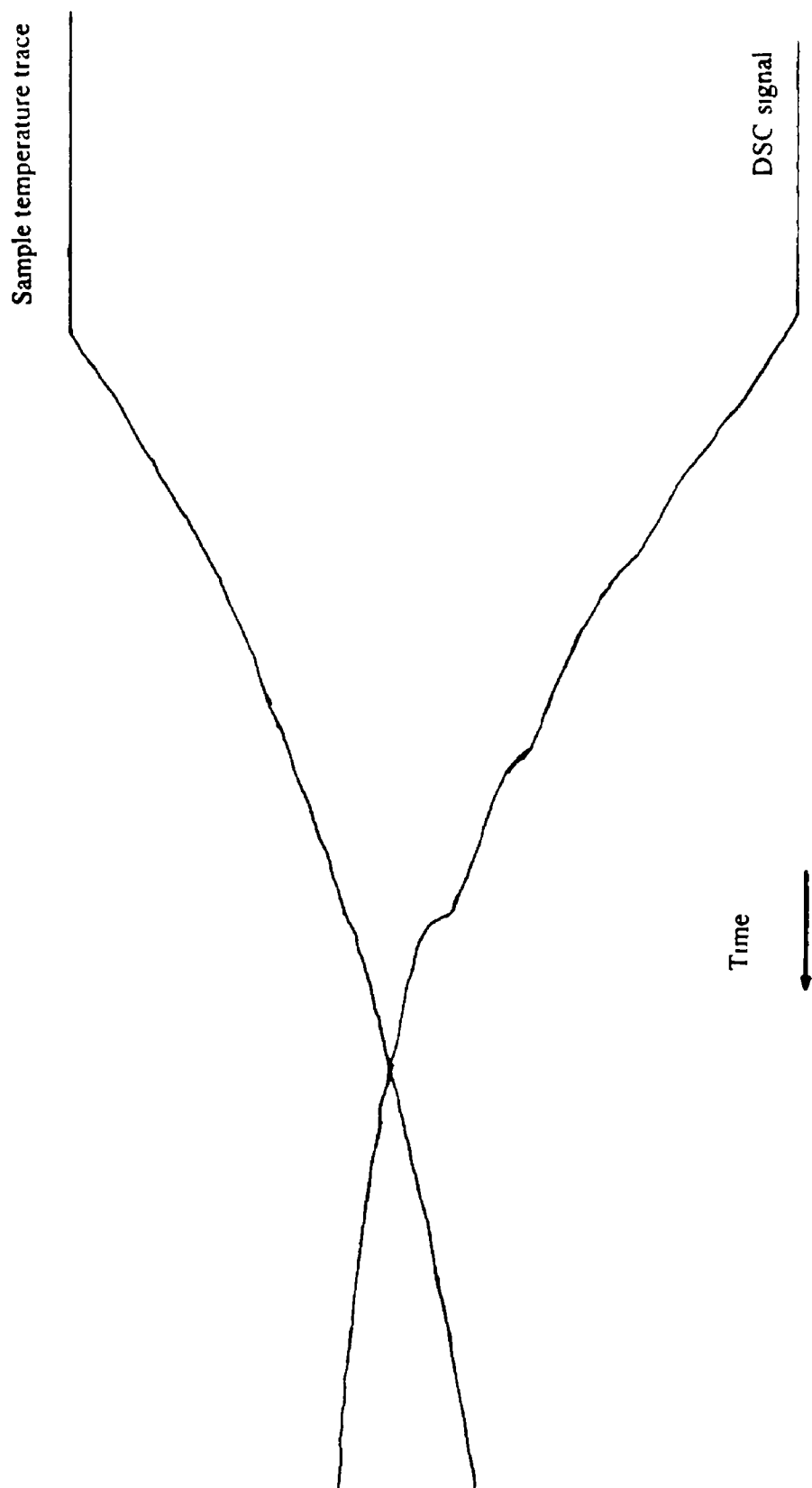


Fig.3.9 : As for Fig.3.8 except the temperature of the DSC Furnace was decreased

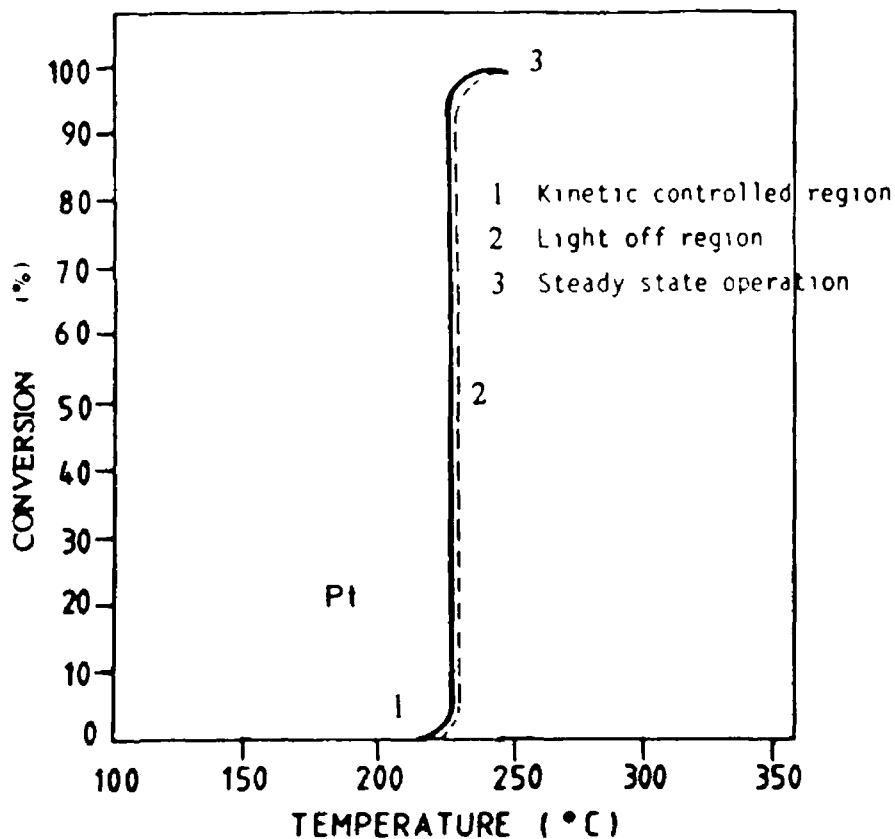


Fig 3.10 · The light off characteristics of a car exhaust catalyst illustrated by Trimm (44)

type of site may be active at lower temperatures while the other type might require a higher temperature, brought about by the light off of the catalyst before activity occurs

However Wise et al (45) reported a similar phenomenon for the oxidation of isopropyl alcohol using a similar heat flux technique They obtained a trace with two consecutive "run away" exothermic reactions with increasing catalyst temperature They concluded this to be due to the formation of a stable intermediate product which in that case was acetone (45)

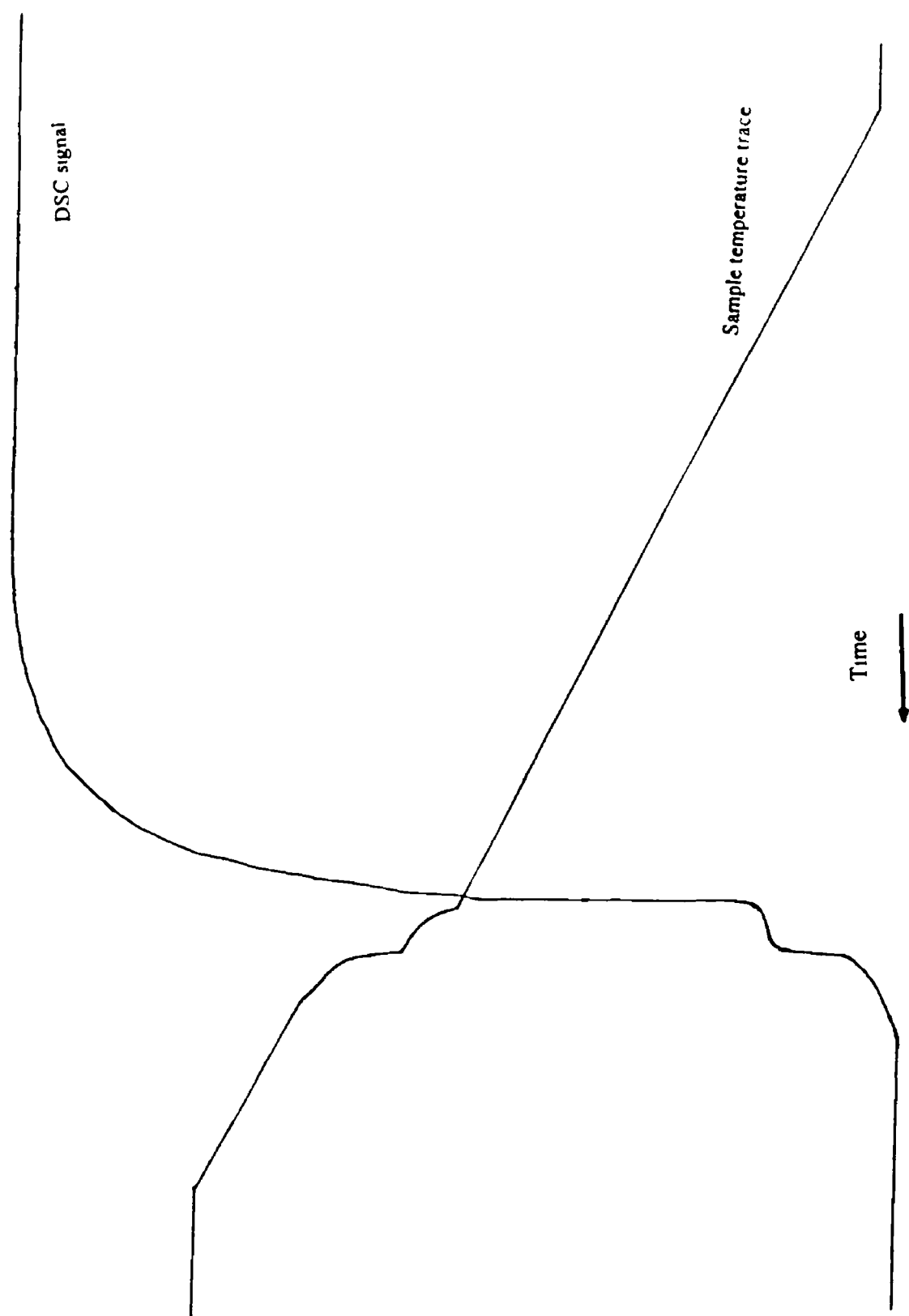


Fig 3 11 : DSC trace for sample which exhibited two temperature jumps during an activity run

3.2.1 The Effect of Experimental Conditions on DSC Measurement

A series of experiments were carried out to examine the relationship between the catalyst sample mass and reactant gas composition on the extent of reaction, the light off temperature and the shape of the DSC profiles. Each experiment consisted of at least two activity runs and was carried out twice with different samples of the same catalyst, 5% Pt/Al₂O₃. The difference in light off temperature (LOT) values between runs was less than $\pm 2\%$, while the corresponding value for the variation in exotherm magnitude was on average less than or equal to $\pm 2\%$. The difference in LOT values obtained during identical experiments using different samples of the same catalyst was also on average less than $\pm 2\%$. For experiments using catalyst sample masses of less than or equal to 1mg the variation in exotherm magnitude was less than or equal to $\pm 2\%$ while for larger samples (i.e. 5 and 10 mg) this increased to on average $\pm 4\%$.

Effect of sample weight on the DSC activity Measurements

The results for the effects of the variation of sample mass are given in Table 3.3. In a standard DSC activity run 1mg catalyst samples were used. For a 5% Pt/Al₂O₃ sample of that mass the size of the exotherm was determined to be 840 mV. The drop in butane was found to be 36% and the sample temperature trace contained two temperature increases at 473K and 500K. The magnitude of these temperature increases was 24K and 18K respectively. Catalyst masses ranging from 0.7mg to 10mg were examined. Due to sample handling difficulties it was not possible to examine catalyst masses of lower than 0.7mg. In general increasing catalyst mass up to 5mg brought about a significant increase in the size of the DSC exotherm and an increase in i-butane conversion. Further increasing the catalyst mass to 10mg resulted in a small increase in the amount of butane converted (1%), although there was a substantial increase in the magnitude of the exotherm (71mV) compared with that found using a 5mg sample.

Table 3 3 Effect of Sample Mass Variations on DSC Activity Measurements
(Reactant Mixture Composition was $0.6\text{cm}^3\text{min}^{-1}$ $i\text{-C}_4\text{H}_{10}$, $19.2\text{cm}^3\text{min}^{-1}$ air
prior to entry into DSC)

Sample Mass (mg)	Light off Temp (K)	Extent of Temp Jump(K)	$i\text{-C}_4\text{H}_{10}$ Drop(%)	Exotherm (mV)	Size (mW)	Calculated (mW)	Value* (%)
0.7	433, 457	34, 6	34	756	378	387	33
1.0	423, 453	24, 18	36	840	420	410	37
5.0	423, 453	24, 10	45	864	432	512	38
10.0	423, 469	44, 2	46	936	468	524	41

* Note The values for calculated exotherm size (mW) were determined assuming an outlet flow rate of $i\text{-C}_4\text{H}_{10}$ of $0.38\text{cm}^3\text{min}^{-1}$ and the figures for $i\text{-C}_4\text{H}_{10}$ conversion obtained from GC analysis. Calculated values for % $i\text{-C}_4\text{H}_{10}$ conversion were determined from the determined exotherm size (mW) and assuming an outlet flow rate of $0.38\text{cm}^3\text{min}^{-1}$.

The DSC lineariser converts the amplified differential temperature input from the DC amplifier to a calorimetric analogue output proportional to the rate of evolution or adsorption of heat in mW. Table 3 3 gives values for the size of the DSC exotherms in mW calculated from the experimentally determined values in mV. Combustion of butane yields 2877kJmol^{-1} of energy and $1\text{W} = 1\text{JS}^{-1}$. It is possible to calculate the work evolved by the combustion of a certain flow rate of butane in mW. The calculated values for the work produced by the determined values for the amount of butane consumed during reaction are also given in Table 3 3. It is also possible, from the DSC exotherm (mW), to calculate the theoretical % butane conversion represented by the exotherm. Again these values are given in Table 3 3. All the above calculations are given in appendix II.

Fig 3 13 graphs the exotherm size (mV) and % butane conversion as a function of catalyst mass. The amount of butane conversion was not directly related to catalyst mass. The mass of catalyst sample should effect the amount of butane converted during the oxidation reaction. With a greater sample mass, more active sites ought to be available for the reaction leading to increased butane conversion. However, in any heterogeneous catalytic process, reaction on the catalyst surface cannot occur at a rate greater than the rate at which reactants can be transported to the surface or at which products can be removed from the catalyst surface (46). This limitation was first pointed out by Wagner (47) and implies that beyond a certain value, the rate of reaction cannot be increased simply by increasing the number of active sites. In the case of these DSC activity measurements, due to the dimensions of the sample crucible or holder used

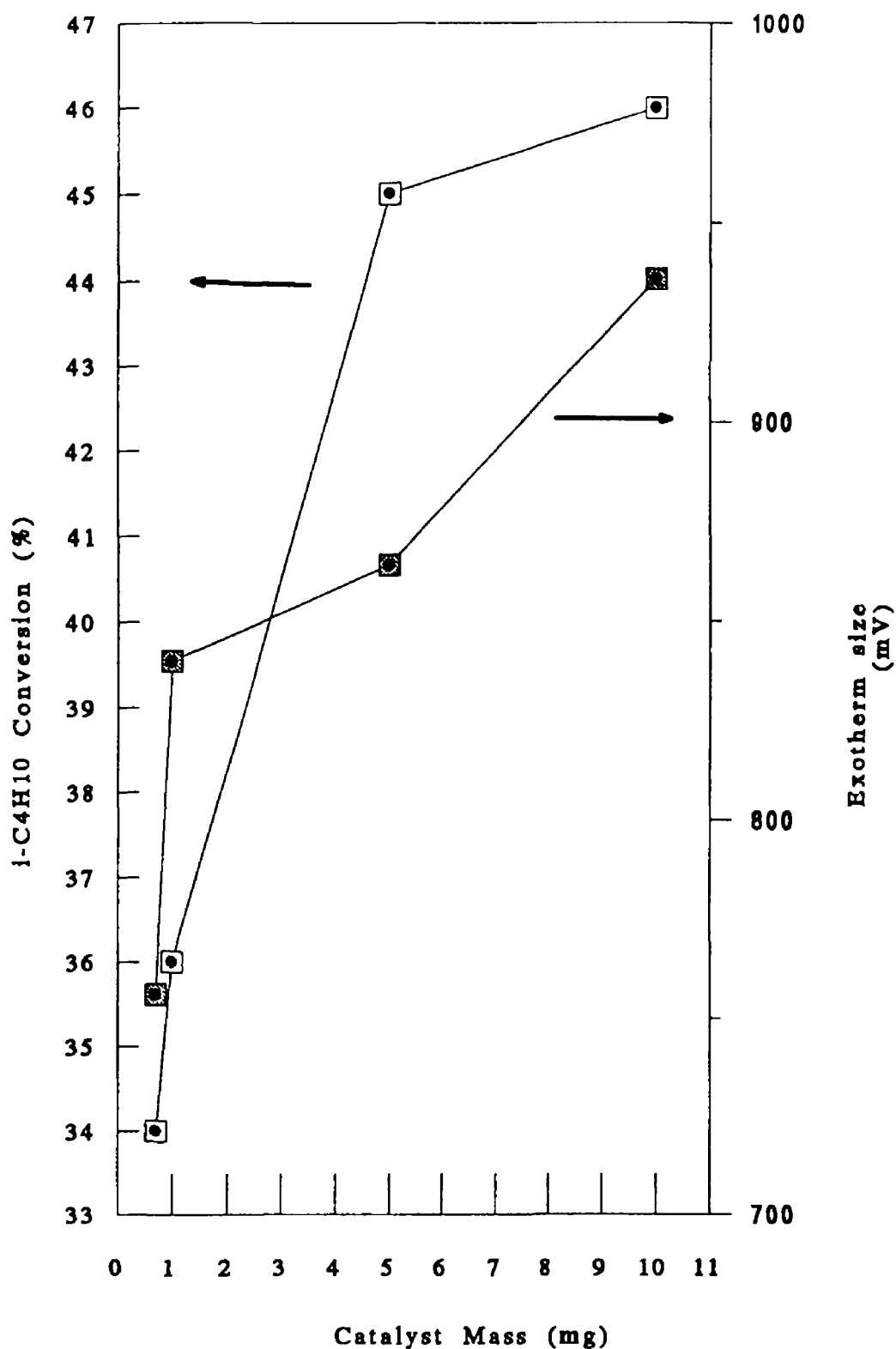


Fig 3 12 Graphs of the exotherm size (mV) and % butane conversion as a function of catalyst mass

in the DSC furnace, limitations of transport of reactants to the catalyst surface could have affected activity. As the sample holder is cylindrical in shape and open only at the top, to allow loading of the sample, the reactant gases pass over, rather than through, the sample holder, see Fig 3.14. Therefore despite diffusion of reactants through the sample, increasing catalyst mass would not increase activity. This could explain why the % butane conversion over the 5mg and 10mg samples was identical, when experimental error was taken into account. However for sample masses of 5mg and lower the general relationship of increasing exotherm size and $i\text{-C}_4\text{H}_{10}$ conversion with increasing sample mass held.

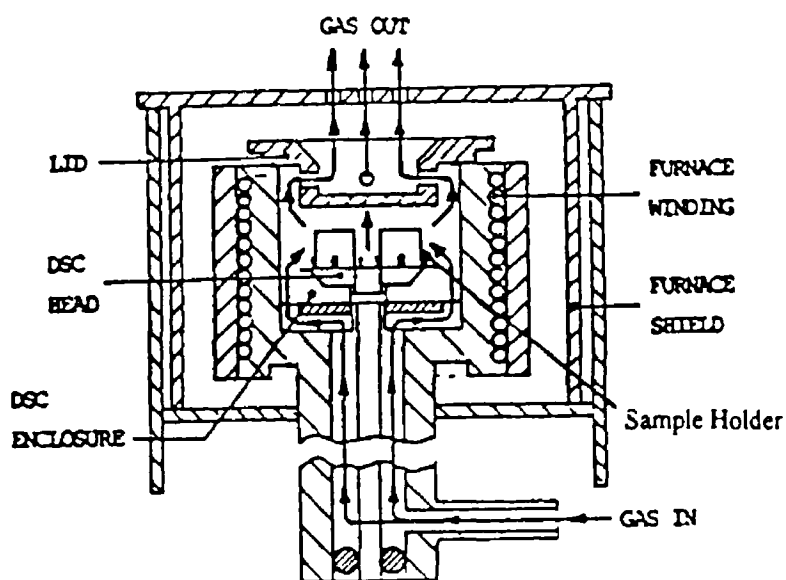


Fig.3.13 Sample holder arrangement in DSC (48)

From Table 3.3 it is clear that for the activity runs carried out with lower masses of catalyst sample, i.e. 0.7 mg and 1 mg, the size of the exotherms was in good agreement with the theoretical values calculated from the % butane conversions determined by GC analysis. However, for activity runs with larger sample masses the magnitude of the exotherms was not in agreement with the theoretical values calculated from % butane conversions determined by GC analysis. With regard to the accuracy of the results for the activity runs over the 5 mg and 10 mg catalyst samples it is more

probable that the GC data for the conversion of butane during reaction is more accurate than the DSC results for the magnitude of the exotherm produced during reaction. Sample preparation and packing in the sample holder are important in obtaining good reliable DSC results. With larger sample masses differences in the packing of samples may have caused the lower than expected DSC exotherm size.

The Effect of Flow Rate and the Fuel / Air Ratio on the DSC trace

A series of experiments were carried out over 1mg 5%Pt/Al₂O₃ samples to examine the effect of variations in the total flow rate and composition of the reactant gas mixture on the butane reaction, the light off temperature and the magnitude of the DSC exotherm produced. The results of these experiments are given in Tables 3.4 and 3.5.

From the results it is evident that variations in the overall flow rate and in the composition of the reactant gas mixture had no effect on the light off temperature. However, there were slight variations in the values for the second temperature increase, depending on the composition of the reactant gas mixture. For all the activity runs the first sample temperature increase was in the region of 470K. Depending on the flow rate and the butane air ratio, the second sample temperature increase ranged from 500K to 543K. There was no trend with regard to the overall flow rate or the gas mixture composition and the temperature at which this second temperature increase occurred.

The results indicate that changes in the overall flow rate of the reactant gas mixture did influence both the fraction of butane converted during reaction and the magnitude of the exotherms exhibited during the activity run. In the case of gas mixtures with butane air ratios of 1/28 and 1/35, the overall flow rate was altered by the addition of N₂. In both cases the activity run carried out using the lower flow rate exhibited a higher % conversion of butane and DSC exotherms larger in magnitude than the respective values obtained from activity runs carried out using a higher overall flow rate of reactants. This drop in butane conversion and in the size of the exotherm with higher overall flow rates is probably due to the resultant drop in the residence time of the reactant gases on the catalyst sample surface.

In contrast, decreasing the flow rate of the reactant gas mixture by dropping the individual flow rates of the reactants, whilst still maintaining the butane / air ratio, brought about an increase in the % conversion of butane (compared with the total amount of butane passing over the catalyst), and a decrease in the size of the exotherm.

Table 3.4: Effects of variation of Reactant Gas Composition on DSC Activity Measurements

C ₄ H ₁₀ :Air Ratio	Flow Rate (inlet) (cm ³ min ⁻¹)				i-C ₄ H ₁₀ Drop (%)	Exotherm Size (mW)	Light off Temp. (K)
	Air	i-C ₄ H ₁₀	N ₂	Total			
1:15	9.0	0.6	--	9.6	20	508	477, 539
1:28	16.8	0.6	--	17.4	42	888	473, 543
1:28	16.8	0.6	2.4	19.8	33	796	471, 515
1:32	9.8	0.3	--	10.1	46	532	473, 514
1:32	19.2	0.6	--	19.8	36	840	473, 503
1:35	14.0	0.4	--	14.4	43	732	469, 503
1:35	14.0	0.4	5.4	19.8	32	584	473, 542

Table 3.5 : Theoretical Calculated Values For % i-C₄H₁₀ drop and Exotherm Size Determined Respectively From Exotherm Size and % i-C₄H₁₀ Drop.

Butane:Air Ratio	Outlet Flow Rate (cm ³ min ⁻¹)	i-C ₄ H ₁₀ Drop (%)	Exotherm (mW)	Theoretical Value % i-C ₄ H ₁₀ Drop*	Theoretical Value for Exotherm size# (mW)
1:15	5.9	20	254	23	221
1:28	10.7	42	444	40	465
1:28	12.2	33	396	36	366
1:32	6.3	46	266	47	262
1:32	12.2	36	420	38	398
1:35	9.0	43	366	49	322
1:35	12.2	32	292	40	230

Note : The values for calculated exotherm size (mW) were determined assuming an outlet flow rate of i-C₄H₁₀ of 0.38cm³min.⁻¹ and figures obtained for % i-C₄H₁₀ conversion from GC.

* Note : Calculated values for % i-C₄H₁₀ conversion were determined from the determined exotherm size (mW) and assuming an outlet flow rate of 0.38cm³min.⁻¹

The explanation for the differences in butane conversion and exotherm size runs as follows. The increase in the fraction of butane converted in the case of the run with the lower flow rates of butane and air is again due to the increased residence time of the gases on the catalyst surface. On the other hand, the drop in the size of the exotherm

exhibited by the same activity run is caused by the lower amount of butane passing over the sample

The ratio of butane to air also had an effect on the activity of the catalyst. Decreasing the flow rate of air, thus changing the butane air ratio, whilst maintaining the flow rate of butane and overall flow rate of the gas mixture at 19.8 cm^3 using N_2 , caused a decrease both in the magnitude of the exotherm and the fraction of butane converted during reaction. Therefore, from the values quoted from Table 3.5, it is clear that, as expected, deviations in the reactant gas mixture composition away from the stoichiometric butane air ratio led to a decrease in the conversion of butane over catalysts during reaction for runs where the same overall flow rate was used.

The exotherm sizes were in reasonable agreement with the GC results for butane conversion considering that there was a drop in total flow rate of approximately $38\% \pm 4\%$ from the gas inlet of the furnace and the outlet. The magnitudes of the exotherms in mW are listed in Table 3.5. Theoretical values for the amount of butane converted (%) during reaction, calculated from the magnitude of the exotherms and from the flow rate of gas from the outlet of the furnace, are also given. The detailed calculations which yielded these values are given in appendix II. The values for the theoretical butane conversions calculated from the size of the exotherms are in reasonable agreement with the determined butane conversions, the largest discrepancy being 8% higher than the determined GC value for the activity run carried out with a 1.35 butane air ratio. On average, the actual GC results for butane conversion differed by $\pm 4\%$ from the calculated values. Theoretical values for the magnitude of the exotherms are listed in Table 3.5, calculated from the GC results for butane conversion and the outlet gas flow rates. Theoretical exotherm sizes, calculated from the determined butane conversions, differed from the actual values by approximately $\pm 30\text{ mV}$.

52

3.3 Results and Discussion

Pt content was determined using atomic absorption spectroscopy and the results are given in Tables 3.6 and 3.7. The correlation coefficient for the regression analysis on the results for the Pt standard curve was 0.9970. All catalysts were prepared with a nominal 5wt% Pt loading, but the results indicated some differences in the Pt content.

From the results it is clear that the method of impregnation affected the uptake of Pt by the Al_2O_3 support. Sample Pb(U)T1, prepared using impregnation method B, where the powdered Al_2O_3 support was soaked in the impregnating solution and excess solvent was removed using a rotary evaporator, exhibited the highest Pt uptake, nearly 6wt%. In comparison sample Pa(U)T1 prepared by method A, spray impregnation, had a determined Pt uptake which was ca. 1.5wt% lower than the Pt uptake for the former catalyst. Impregnation of the support material with a solution of pH 4 also resulted in a decrease in Pt uptake, as can be observed from the value for the Pt uptake determined for Pa(U)4T1 compared to Pa(U)T1.

Pre-treatment of the support material also influenced the uptake of Pt. Washing the Al_2O_3 support with milliQ H_2O or HCl caused a drop in the uptake of Pt during impregnation compared with the catalyst with the unpre-treated Al_2O_3 support. On the other hand HNO_3 pre-treatment led to an increase in the Pt uptake. The order with regard to Pt uptake for the samples in the pre-treatment study was as follows -

$$\text{Pa(C)T1} < \text{Pa(W)T1} < \text{Pa(U)T1} < \text{Pa(N)T1}$$

In the study of the effects of drying temperature after impregnation, drying at 350K after impregnation gave maximum Pt uptake while at higher or lower drying temperatures the Pt uptake dropped. For the drying temperature study the determined Pt loading followed the trend -

$$\text{Pa(U)T2} > \text{Pa(U)T1} > \text{Pa(U)T3}$$

The Pt content of catalysts with HNO_3 pre-treated supports were more affected by the drying temperature than catalysts with untreated supports. For Pa(N)T2 the Pt content was 2% lower than the Pt loading for Pa(N)T1. There was a difference of nearly 2% between the determined Pt loading between sample Pa(U)T2 and Pa(N)T2.

For all of these samples the catalyst mat was powdered and from this a random sample was taken for digestion and analysis by atomic absorption spectroscopy.

Table 3 6 Results for Atomic Absorption Measurements

SAMPLE CODE	DETERMINED Pt LOADING (ppm)	NOMINAL LOADING(ppm)	% Pt LOADING DETERMINED (wt%)
Pa(U)T1	24 86	28 60	4 34
Pa(W)T1	17 75	22 65	3 92
Pa(C)T1	19 17	26 80	3 58
Pa(N)T1	16 33	16 95	4 82
Pb(U)T1	34 81	29 40	5 92
Pb(N)T1	16 53	17 01	4 85
Pa(U)4T1	19 17	24 45	3 92
Pa(U)T2	30 54	31 95	4 78
Pa(N)T2	23 44	41 90	2 79
Pa(U)T3	33 39	39 30	4 25

In order to measure the distribution of Pt on an Al_2O_3 mat impregnated in a similar manner to Pa(U)T1, a mat which had been impregnated, dried and calcined was divided into nine equal sized rectangles. The results for the AA analysis of each section are given in Table 3 7. A diagram of the mat is given in Fig 3 5. In addition, three sections were divided transversely into top, middle and bottom sections denoted by the initial T, M or B respectively (see Fig 3 5). Samples A1, B2 and C1 were separated into top, middle and bottom sections.

In the case of these samples, the highest Pt loading was determined to be on the top surface, 6 7%, 7 2% and 6 9% respectively. The bottom sections of these samples had a lower Pt loading than the top sections, although higher than the middle sections. For samples A1 and C1, the overall Pt loading was approximately 5%. Sample B2 which was the centre section of the mat (see Fig 3 5), had a lower overall Pt loading, 3 3wt%. Pt loadings for the other samples examined ranged from 2 2wt% for sample B1, up to 6 3wt% for sample B3. The total Pt loading for the complete mat was determined to be 4 8wt%. The results point to an uneven distribution of Pt on the mat, with high Pt loadings on the top of the mat and a very low concentration of Pt in the middle of the mat (when the mat is viewed transverse). Taking into account the determined Pt loading for each of the mat segments, the overall Pt loading for the complete mat was 4 8wt%.

Table 3.7 Analysis of Distribution of Pt Upon an Untreated Al₂O₃ Mat After Spray Impregnation Overall Pt content 4.8wt%.

Sample	Pt Content (wt%)	
	Each piece	Overall
AT1	6.7	5.3
AB1	5.2	
AM1	3.7	
BT2	7.2	3.3
BB2	2.8	
BM2	2.6	
CT1	6.9	5.1
CB1	3.8	
CM1	2.6	
B1		2.2
A2		4.8
C2		5.8
A3		4.5
B3		6.3
C3		5.9

The results for nitrate determination for the washings from the pre-treatment of the Al₂O₃ mat with 0.1M HNO₃ and milliQ water in Table 3.8 and 3.9. These determinations were carried out in order to elucidate how much NO₃⁻ was retained on the Al₂O₃ mat after HNO₃ pre-treatment. Table 3.8 represents the results from the first experiment where the acid pre-treatment and water washing procedure was carried out under a normal air atmosphere. The mat was pre-treated with an overall nitrate concentration of 1×10^{-3} M NO₃⁻. From a standard curve of nitrate solutions, the concentration of nitrate in the washings from the pre-treatment procedure was 3.27×10^{-4} M, indicating that 67% of the nitrate was retained by the mat. However, in order to obtain a more accurate estimate of the nitrate uptake the same experiment was carried out in a closed system, under nitrogen and the nitrate was trapped in cold water. Again

from a standard curve of nitrate solutions of different concentrations, in this case the amount of NO_3^- in the washings was determined to be $6.8 \times 10^{-4}\text{M}$, see Table 3.9. Taking into account the fact that the original concentration applied to the mat was in this case $1.43 \times 10^{-3}\text{M}$, it would appear that up to 52% of the nitrate applied was retained by the mat.

Table 3.8 Determination of Nitrate Uptake For HNO_3 Pre-treated Mat Under Normal Atmosphere

NO_3^- Concentration (M)	Log Concentration	Average Voltage (mV)
1×10^{-4}	-4.0	-25.1
5×10^{-4}	-3.3	-36.2
1×10^{-3}	-3.0	-64.2
5×10^{-3}	-2.3	-77.5
1×10^{-2}	-2.0	-102.5
1×10^{-1}	-1.0	-142.5

Correlation Coefficient = 0.984

Unknown = -39.0 mV

Therefore the concentration of unknown from the standard curve = $3.27 \times 10^{-4}\text{ M}$

Table 3.9 : Determination of Nitrate Uptake For HNO_3 Pre-treated Mat Under N_2 Atmosphere

NO_3^- Concentration	Log Concentration	Voltage (mV)
1×10^{-4}	-4.0	-39.2
1×10^{-3}	-3.0	-92.0
5×10^{-3}	-2.3	-129.4
1×10^{-2}	-2.0	-144.0
1×10^{-1}	-1.0	-196.5

Correlation Coefficient = 0.9998

Unknown = -83.8mV

Therefore concentration of NO_3^- , from standard curve , = $6.8 \times 10^{-4}\text{ M}$

The results from the H₂ chemisorption analysis are given in Table 3 10 Values for Pt surface area, dispersion and particle diameter ranged from 138 4m²g⁻¹ Pt, 53 5% and 2 06nm respectively for Pa(N)T1 to 21 56m²Ptg⁻¹Pt, 9 0% and 12 97nm respectively for Pb(U)T1 Again the method of impregnation affected the characteristics of the catalyst Spray impregnation, method A, resulted in a catalyst which exhibited much higher uptake of H₂, Pa(U)T1, than the sample which was prepared by impregnation method B, sample Pb(U)T1 Spray impregnating with an impregnating solution of pH 4, Pa(U)4T1, also caused a drop in H₂ uptake compared with Pa(U)T1

Pre-treatment of the support with acid or milli Q H₂O also affected the H₂ uptake exhibited by the catalysts Pre-treatment with HNO₃ produced an increase in H₂ uptake compared with catalyst with untreated supports while treatment with HCl or milli Q H₂O produced a drop in H₂ uptake Even samples prepared using impregnation method B showed an increase in H₂ uptake when the support was pre-treated with HNO₃ The trend for H₂ uptake values for samples dried at temperature T1 determined from chemisorption was -

$$\text{Pa(N)T1} > \text{Pa(U)T1} > \text{Pb(N)T1} > \text{Pa(W)T1} > \text{Pa(C)T1} > \text{Pb(U)T1}$$

From the chemisorption measurements on the catalyst samples prepared to examine the effects of drying temperature after impregnation, the drying temperature had a marked effect on the H₂ uptake of catalysts Samples Pa(N)T2 and Pa(N)T3 had H₂ uptakes which were respectively 35% and 80% lower than Pa(N)T1 Samples Pa(U)T2 and Pa(U)T3 had almost identical H₂ uptake values, approximately 43% lower than the value for Pa(U)T1 The overall pattern for H₂ chemisorption for samples prepared in study on the influence of drying temperature after impregnation was

$$\text{Pa(U)T1} > \text{Pa(U)T3} \approx \text{Pa(U)T2}$$

$$\text{Pa(N)T1} > \text{Pa(N)T2} > \text{Pa(N)T3}$$

The results for the activity for the Pt/Al₂O₃ samples for *i*-butane conversion obtained using the GC method are given in Table 3 11 The extent of butane conversion is given in terms of a percentage of the overall amount of butane present prior to reaction For comparison between catalyst samples the extent of conversion is also expressed in terms of the percentage of the total amount of butane present, per gram of sample, see Table 3 11 For the majority of samples which were examined, the temperature region at which activity occurred during the first reaction run (producing a decrease in the amount of butane in the effluent gas stream

Table 3 10 H₂ Chemisorption Measurements For Catalyst Samples

Sample Code	H ₂ Adsorbed (cm ³ g ⁻¹)	Dispersion * (%)	Pt Surface Area*		Pt Particle Size* (nm)
			(m ² Pt g ⁻¹ sample)	(m ² Pt g ⁻¹ Pt)	
Pa(U)T1	0 926	32 0	4 18	83 66	3 34
Pa(W)T1	0 378	13 0	1 71	34 18	8 18
Pa(C)T1	0 304	10 5	1 38	27 52	10 16
Pa(N)T1	1 537	53 5	6 92	138 40	2 02
Pb(U)T1	0 253	9 0	1 08	21 56	12 97
Pb(N)T1	0 544	19 0	2 46	49 14	5 69
Pa(U)4T1	0 649	22 5	2 93	58 68	4 77
Pa(U)T2	0 503	17 5	2 27	45 42	6 16
Pa(N)T2	0 997	34 5	4 51	90 14	3 10
Pa(U)T3	0 529	18 5	2 39	47 82	5 85
Pa(N)T3	0 279	9 5	1 26	25 25	11 08

*Note Calculated assuming a nominal Pt loading of 5wt%

from the activity unit) was normally at the same or at a higher temperature region as that exhibited in the second run. Pre-treatment prior to the first reaction run had a major effect on the activity of catalyst samples during that run. In all but one case the reduction in H₂ prior to reaction resulted in an increase in the temperature required for the oxidation reaction to be initiated, compared with similar catalyst samples which did not undergo this H₂ pre-treatment. The exception to this was sample Pa(C)T1, where reaction over the reduced sample started at a lower temperature (between 420K and 470K) than over the unreduced sample (where activity was observed between 470K and 520K). From the first reaction run, the trend with regard to the temperature region in which activity was observed, i.e. the temperature range in which light off occurred, over samples reduced prior to reaction was, in order of increasing temperature, as shown below

$$\text{Pa(C)T1} < \text{Pa(U)T1} = \text{Pa(W)T1} = \text{Pa(U)4T1}$$

Table 3 11 GC Activity Measurements For Catalyst Samples

Sample Code	pre-treatment prior to Run1	Sample Temp (K)	i-C ₄ H ₁₀ Conversion			
			Run1		Run2	
			%	%g ⁻¹ sample (x10 ³)	%	%g ⁻¹ sample (x10 ³)
Pa(W)T1	none	420	0	0 000	0	0 000
		470	0	0 000	2	0 039
		520	39	0 756	39	0 756
		570	39	0 756	40	0 775
		620	39	0 756	40	0 775
		670	40	0 775	41	0 795
Pa(W)T1	Reduced in H ₂	420	0	0 000	38	0 728
		470	0	0 000	40	0 766
		520	0	0 000	41	0 785
		570	38	0 728	42	0 805
		620	38	0 728	42	0 805
		670	38	0 728	42	0 805
Pa(U)4T1	none	420	0	0 000	0	0 000
		470	nd	nd	23	0 263
		520	13	0 352	25	0 678
		570	23	0 623	30	0 813
		620	23	0 623	55	1 491
		670	23	0 623	55	1 491
Pa(U)4T1	Reduced in H ₂	420	0	0 000	0	0 000
		470	0	0 000	0	0 000
		520	0	0 000	3	0 073
		570	22	0 537	23	0 561
		620	23	0 561	23	0 561
		670	23	0 561	23	0 561
Pa(U)T1	none	420	0	0 000	0	0 000
		470	80	1 699	80	1 699
		520	80	1 699	80	1 699
		570	83	1 762	84	1 783
		620	84	1 783	84	1 783
		670	86	1 826	nd	nd

Table 3 11 Contd

SAMPLE CODE	pre- treatment prior to Run1	Sample Temp (K)	1-C ₄ H ₁₀ Conversion			
			Run1		Run2	
			%	%g ⁻¹ sample (x10 ³)	%	%g ⁻¹ sample (x10 ³)
Pa(U)T1	Reduced in H ₂	420	0	0 000	0	0 000
		470	0	0 000	0	0 000
		520	0	0 000	89	1 914
		570	83	1 785	89	1 914
		620	90	1 935	90	1 935
		670	89	1 914	90	1 935
Pa(N)T1	none	420	0	0 000	0	0 000
		470	nd	nd	0	0 000
		520	0	0 000	82	1 962
		570	82	1 962	82	1 962
		620	82	1 962	82	1 962
		670	82	1 962	83	1 970
Pa(C)T1	none	420	0	0 000	0	0 000
		470	0	0 000	33	0 679
		520	27	0 556	40	0 823
		570	26	0 535	62	1 276
		620	28	0 576	64	1 317
		670	28	0 576	64	1 317
Pa(C)T1	Reduced in H ₂	420	0	0 000	0	0 000
		470	23	0 488	24	0 510
		520	24	0 510	nd	nd
		570	21	0 446	32	0 679
		620	21	0 446	nd	nd
		670	21	0 446	57	1 210

Note nd = not determined

For samples which were not reduced prior to activity analysis pre-treatment of the support increased the temperature at which light off occurred compared with the unpre-treated sample. In this case the order with regard to the temperature range at which activity was observed to occur was

$$\text{Pa(U)T1} < \text{Pa(W)T1} = \text{Pa(C)T1} = \text{Pa(U)4T1} < \text{Pa(N)T1}$$

In general the temperature range at which activity over the catalyst began was lower for the second reaction run compared to the first reaction run. The exception to this rule was a sample of catalyst Pa(U)T1 which, when not reduced in H₂ prior to run 1 exhibited activity in the same temperature range for both run 1 and run 2 between 420K and 470K.

For catalyst samples which underwent the reductive treatment prior to run 1, the catalysts prepared with HCl and milli Q H₂O pre-treated supports exhibited a lower light off temperature than the untreated sample during run 2. The pattern as regards the initial exhibition of activity at a particular temperature range, listed in order of increasing temperature was as shown below -

$$\text{Pa(W)T1} < \text{Pa(C)T1} < \text{Pa(U)T1} = \text{Pa(U)4T1}$$

On the other hand for samples which were not treated in H₂ prior to run 1, the order for the temperature region in which activity was observed during the second reaction run was -

$$\text{Pa(U)T1} < \text{Pa(C)T1} = \text{Pa(U)4T1} = \text{Pa(W)T1} < \text{Pa(N)T1}$$

For all the samples which were examined the extent of conversion of 1-butane increased as the temperature was raised. However, for most of the catalyst samples examined this increase in the conversion occurred until a point was reached where the extent of conversion changed little despite further increases in the sample temperature. Also, in general the magnitude of 1-butane conversion over the catalyst during the second activity run was greater than conversions which were determined from the first run. This could suggest a change in the nature of the surface of the sample during the first reaction run. For the first reaction run for samples reduced in H₂, reaction over Pa(U)T1 at 670K was greater than over the H₂O pre-treated sample or over the HCl pre-treated sample. Unfortunately activity over Pa(N)T1, after the sample was reduced in H₂, was not examined.

Under the conditions mentioned above the trend for 1-butane conversion (%g⁻¹sample) was

$$\text{Pa(U)T1} > \text{Pa(W)T1} > \text{Pa(U)4T1} > \text{Pa(C)T1}$$

The corresponding pattern for samples not reduced prior to activity analysis was -

$$\text{Pa(N)T1} > \text{Pa(U)T1} > \text{Pa(W)T1} > \text{Pa(U)4T1} > \text{Pa(C)T1}$$

Another point to be made about the magnitude of 1-butane conversion over the samples is that during the first analysis, when catalytic activity occurred, higher 1-butane conversions (%g⁻¹ sample) took place over sample Pa(U)T1, when reduced in H₂, than over unreduced samples of the same catalyst, when catalytic activity occurred. The opposite was true for samples Pa(U)4T1 and Pa(C)T1.

During the second reaction run, the order for 1-butane conversion at 670K over samples which were not reduced prior to run 1 was as follows -

$$\text{Pa(N)T1} > \text{Pa(U)T1} > \text{Pa(U)4T1} > \text{Pa(C)T1} > \text{Pa(W)T1}$$

On the other hand for samples reduced prior to run 1, the trend during the second run for 1-butane conversion (%g⁻¹ sample) was -

$$\text{Pa(U)T1} > \text{Pa(C)T1} > \text{Pa(W)T1} > \text{Pa(U)4T1}$$

In summary it can be said that pre-treatment with HCl or milli Q H₂O resulted in catalysts which exhibited lower activity (%g⁻¹ sample) than the untreated catalyst. In the case of catalyst samples which were not reduced in H₂ prior to activity measurement, the HNO₃ pre-treated sample exhibited the greatest 1-butane activity.

For the second reaction run, in the temperature regions where activity was determined to occur, the 1-butane conversions were greater in magnitude over unreduced samples of catalysts Pa(C)T1 and Pa(U)4T1, than over the corresponding samples which were not reduced in H₂ prior to run 1. On the other hand, the amount of 1-butane conversion over samples of Pa(W)T1, reduced in H₂ prior to run 1, was greater than unreduced samples.

Over most of the catalyst samples the oxidation of 1-butane led to the production of methane (for example over an unreduced sample of Pa(U)T1 there was a 200% increase in CH₄ in the reaction mixture during reaction at 670K). The exception to this was reaction over reduced and unreduced samples of Pa(C)T1 and unreduced Pa(N)T1.

samples which resulted in a decrease in the amount of methane in the reaction mixture. There were in general lower quantities of methane produced when samples were reduced prior to run 1 were utilised, compared with reaction over unreduced samples. The temperature of the catalyst sample had no discernible effect on the amount of methane in the reaction mixture, the amount of methane fluctuating up and down as the temperature of the reactor was increased.

The activity results for the catalysts determined using the DSC method are given in Table 3.12. Since these results represent data from the second DSC activity run carried out on these samples direct comparison can be made with the results obtained for the second activity run for unreduced samples determined using the GC method given in Table 3.11. The reason for the use of the second activity run results was because the light off temperature was normally higher and the size of the exotherm was lower during run 1 compared with run 2. Runs subsequent to the second DSC run normally gave the same light off temperatures and exotherm magnitudes. For the majority of the samples examined, the values for the light off temperature obtained using the DSC method were in the same temperature regions as those in which activity was observed using the GC method. The exception were samples of Pa(N)T1 and Pa(U)4T1 where there was considerable disagreement between the DSC and GC values for the temperature at which activity occurred (see Tables 3.11 and 3.12). For sample Pa(N)T1, the light off temperature determined by the DSC method was 458K while using the GC method, activity was not observed to occur until the temperature was in the region of above 470K. In contrast, for sample Pa(U)4T1 the temperature at which activity was observed to occur was considerably lower when determined using the GC method than the light off temperature for the same sample observed using the DSC method.

Taking the magnitude of the exotherm produced during the DSC activity measurement as a rough guide to the amount of butane conversion occurring, then the greatest conversion occurred over sample Pa(U)T1, while the lowest conversion occurred over sample Pa(U)4T1. Impregnation by method A produced a more active catalyst than the corresponding catalyst produced by method B. In disagreement with the GC results, the DSC results indicated that pre-treatment of the support prior to impregnation led to a decrease in activity, with Pa(U)T1 exhibiting the largest exotherm.

Table 3 12 DSC Activity Measurements for Catalyst Samples for Run 2

SAMPLE CODE	LIGHT OFF TEMPERATURE (K)		EXOTHERM SIZE		THEORETICAL i-C ₄ H ₁₀ CONVERSION * (%)
			(mV)	(mW)	
Pa(U)T1	433	(547)	840	420	38
Pa(C)T1	473	(547)	656	328	30
Pa(W)T1	447	(549)	648	324	29
Pa(N)T1	458	(583)	820	410	37
Pb(U)T1	443		801	401	36
Pb(N)T1	463		784	392	35
Pa(U)4T1	555	(590)	584	292	26

* Note The values for calculated exotherm size (mW) were determined assuming an outlet flow rate of i-C₄H₁₀ of 0.38cm³min⁻¹

With regard to the magnitude of the exotherm exhibited by the catalysts in the pre-treatment study prepared by impregnation method A the observed pattern was

$$\text{Pa(U)T1} > \text{Pa(N)T1} > \text{Pa(C)T1} > \text{Pa(W)T1}$$

From the activity data obtained using the DSC method theoretical results for % butane conversion, based on the magnitude of the exotherm and the "outlet" flow rate of butane prior to the activity run, were calculated and are also given in Table 3 12. There was a big difference in the theoretical values for butane conversion from the DSC exotherm and those obtained by the GC method. The butane conversion (%g⁻¹) was higher for the DSC method than indicated by the GC method. However it is difficult to compare results from each method as the nature of each method is essentially different. In the GC method the sample was placed on a sintered glass frit in a "U" tube. In the case of the DSC method, the sample is placed in a crucible and the gas is passed over, rather than through, the sample. Therefore, it might be expected that in the GC method more of the active sites of the sample may be available to the gas stream and this led to the higher i-butane conversion than that observed with the DSC method.

As already described in section 3.2, there was a second temperature jump observed in some of the DSC traces. This was much smaller than the first temperature jump associated with the light being in the region of 5 to 10K compared with 30 - 50K for the first increase. The temperature at which this second increase or jump occurred ranged between 30K and 130K above the first temperature jump, depending on the

sample involved For sample Pa(W)T1, the difference in temperature between the main increase in sample temperature due to reaction and the secondary increase was 102K while for Pa(N)T1 the difference was 75K Since this secondary increase occurred at different temperatures depending on the sample, it is possible that this second increase in the sample temperature might represent the light off of different sites, active at higher temperatures If this was the case then the quantity of these high temperature sites must be small as the associated temperature increase of the sample was only 5 to 10K

A number of conclusions can be drawn from the chemisorption results given in Table 3 10 The values for Pt particle diameter from chemisorption measurements were calculated from the value of the Pt surface area per gram of Pt in the sample and these results were calculated assuming a nominal loading of 5wt% Table 3 13 shows results recalculated from chemisorption measurements, taking into account the AAS determined Pt loadings for each sample It is obvious from the table that the trends mentioned previously in Table 3 10 with regard to Pt dispersion which were calculated assuming a 5wt% loading are ostensibly the same as those for the recalculated results The exception is Pa(N)T2, where the determined low value for Pt loading resulted in much higher values for Pt dispersion etc

Table 3 13 Recalculated H₂ Chemisorption Results Using AAS Determined Pt Loadings

Sample Code	Determined Pt loading (wt%)	Dispersion (%)	Pt Surface Area (m ² Ptg ⁻¹ Pt)	Pt Particle Size (nm)
Pa(U)T1	4 34	37 0	96 43	2 90
Pa(W)T1	3 92	17 0	43 58	6 0
Pa(C)T1	3 58	15 0	38 38	7 30
Pa(N)T1	4 82	55 5	144 13	1 94
Pb(U)T1	5 92	7 0	19 32	14 45
Pb(N)T1	4 85	19 5	50 70	5 52
Pa(U)4T1	3 92	29 0	74 83	3 74
Pa(U)T2	4 78	18 0	47 96	5 83
Pa(N)T2	2 79	62 0	161 51	1 73
Pa(U)T3	4 25	22 0	56 26	4 97

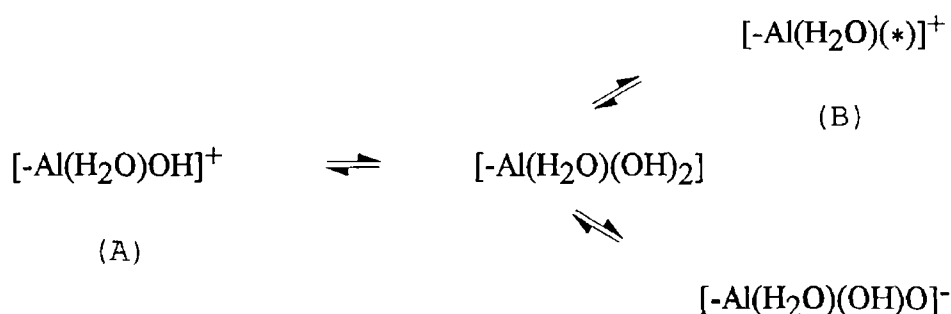
It should also be noted that the figures calculated for Pt particle size determined by H₂ chemisorption should be regarded with caution Scholten et al (49) has pointed

out that the calculation of metal particle size from chemisorption results, has as its basis, a theoretical scenario where the particles are free spherical or nearly spherical particles or a collection of free cubic particles, which in reality may not be the case. Duivenvoorden et al (50) found that H₂ chemisorption could not be used for the accurate estimation of metal particle size in certain catalytic systems. They examined catalysts such as Pt/Al₂O₃ using both H₂ chemisorption and EXAFS (extended X-ray absorption fine structure) analysis, and found that in some cases the chemisorption stoichiometry exceeded unity. Lemaitre et al (51) have pointed out that, although H₂ chemisorption on Pt is instantaneous at ambient temperatures and readily reaches complete monolayer coverage on exposed Pt surfaces, the main disadvantages of the method are the possibility of dissolution, the formation of hydrides and misleading results due to residual H₂ in the catalyst after reduction at high temperature.

Taking the foregoing provisos into account it should be noted that since the samples have undergone the same reduction treatment prior to analysis and are only slightly different in composition, comparison of the H₂ chemisorption results is a valid basis for discussion.

It has already been pointed out that sample Pa(N)T1 had a high uptake of H₂ compared with sample Pa(U)T1 and had a determined Pt loading close to the nominal 5wt%. It would appear that the HNO₃ pre-treatment of the Al₂O₃ support was responsible for these improvements. The water rinsing process after the acid treatment did not remove all the nitrate ions (NO₃⁻) from the support material. The nitrate determinations indicated that 33% and 48% of the nitrate added to the Al₂O₃ was present in the washings depending on which method of NO₃⁻ determination was used. The more accurate method would appear to indicate that as much as 52% of the nitrate was retained on the Al₂O₃ surface.

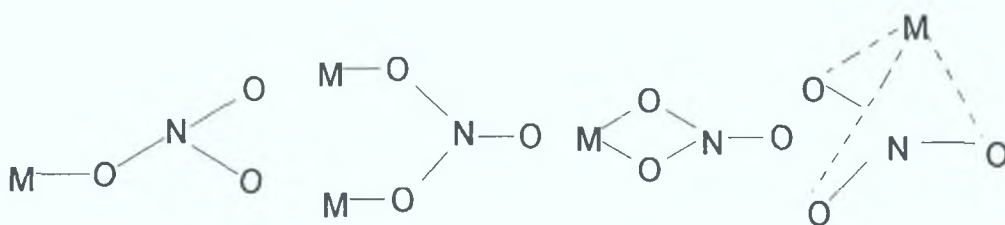
Studies have been carried out on the adsorption of other mineral acids and aqueous electrolytes on Al₂O₃ by Jacimovic et al (52) and Ahmed (53). In these types of solutions the occurrence of charged or neutral species at the oxide solution interface is due to the formation of metal-aquo complexes, as follows



(Where * represents an anion such as Cl⁻)

In species A, the anions do not replace the surface hydroxyl groups but stay outside the primary hydration shell of the surface as counter ions. In species B, the anions replace the hydroxyl ions and are thus attached directly to the metal cation in an analogous situation to ion exchange with these hydroxyl groups. Sivasanker et al. (54) have studied the adsorption and retention of chloride ions on both η - Al_2O_3 and γ - Al_2O_3 . They found that chloride ions exchanged with hydroxyl ions on the Al_2O_3 surface and were directly linked to surface Al^{3+} cations as illustrated in case B above.

It is possible that in the same way nitrate ions exchange with surface hydroxyl groups and link to surface Al^{3+} ions on the Al_2O_3 mat. The nitrate ion is planar with all N-O bond distances close to 1.22 Å (55). Metal nitrates illustrate the variety of ways in which the nitrate ions can be bound to metals, some of which are shown below (56):



Thus in a similar manner to the theory put forward by Sivasanker et al. (54) nitrate ions probably ion exchange with hydroxyl groups of the Al_2O_3 mat. Since such a large amount of nitrate was retained by the Al_2O_3 mat, even after extensive washing with milli Q water, it would appear that the nitrate ions are strongly bound to the Al_2O_3 fibre surface. The increase in Pt uptake during impregnation may have been brought about by a change in the acidity of the support by the presence of NO_3^- . This may have resulted in the support becoming more receptive to the adsorption of anionic species in a similar manner to effect of chlorine on Al_2O_3 reported in the literature (57).

The next question to be considered is why the H_2 uptake of the Pt/ Al_2O_3 sample prepared with the HNO_3 pre-treated Al_2O_3 i.e. Pa(N)T1 was increased compared with the other samples. It would appear that the increase in the uptake is not brought about by an interaction between nitrate adsorbed on the Al_2O_3 surface and H_2 , as an Al_2O_3 sample pre-treated with 0.1M HNO_3 but which was not impregnated with Pt, did not adsorb detectable amounts of H_2 .

Therefore, the effect of HNO_3 pre-treatments on the Al_2O_3 must be to improve the dispersion and increase the surface area of Pt. It is possible that the concentration of the nitrate used resulted in the blocking of some, but not all of the adsorption sites for Pt on the Al_2O_3 surface and acted in a similar manner to a competitive adsorbate. Maatman (13) proposed the use of additives to compete with Pt salts for adsorption

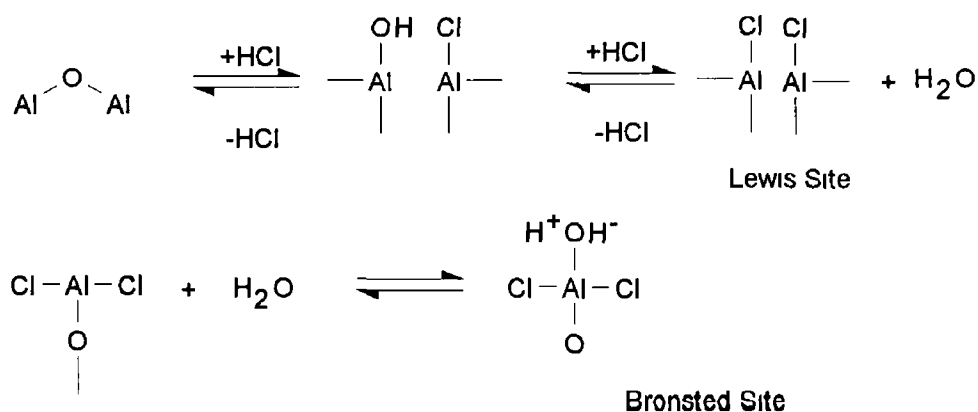
sites on Al_2O_3 in order to obtain a more dispersed Pt phase. In results discussed later in this work (Sec 4.3) it is interesting to note that increasing the concentration of the HNO_3 used for Al_2O_3 pre-treatment brought about a decrease in Pt uptake during impregnation for certain Pt samples. In that case the majority of the Pt adsorption sites on the Al_2O_3 support may have been blocked by nitrate species.

It is unlikely that during impregnation the Pt binds to Al_2O_3 bound nitrate sites on the support surface. Even if this indeed was the case the calcination procedure, 900K for 0.25h, would result in the decomposition of nitrate species on the surface and hence a loss in the amount of adsorbed Pt.

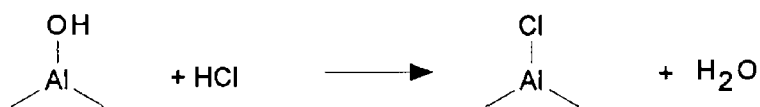
From the results sample Pa(C)T1 had a lower Pt uptake and a lower H_2 uptake (even taking into account the Pt loading determined by AAS) than either Pa(U)T1 or Pa(N)T1. Pa(C)T1 had the support pre-treated with 0.1M HCl prior to Pt impregnation. It would appear that not only did the HCl pre-treatment decrease the uptake of Pt but also the Pt which was deposited on the support surface was poorly dispersed, with a smaller exposed Pt surface area.

The addition of chloride in catalyst preparation has been dealt with in the literature. The presence of chloride in Pt/ Al_2O_3 catalyst preparation has been found to be important as chlorine has been found to alter the acidity of the Al_2O_3 thus making it more receptive towards the adsorption of anionic species (57). Also chloride is used as a competitive adsorbant, competing with Pt anions for adsorption sites on the Al_2O_3 , thus resulting in improved Pt dispersion (58), contrary to the present results. Finally, chlorine addition is thought to improve the resistance to the sintering of Pt (23) and have a prohibiting effect on coking (59).

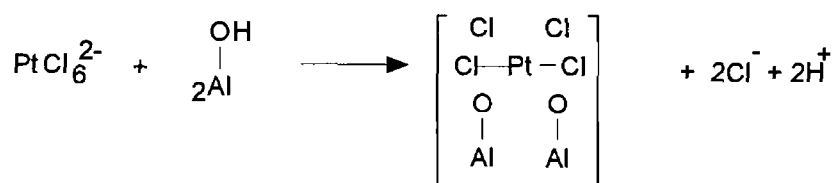
Enhancement of the acidity of Al_2O_3 can be brought about by the presence of impurities found in Al_2O_3 produced by the Bayer method (60) or can be deliberately induced by the incorporation of halogens such as chlorides or fluorides (60). The formation of acidic sites on chlorinated Al_2O_3 has been postulated to occur as follows (59) -



Sivasanker et al (54) proposed an ion-exchange type mechanism for the adsorption of HCl as has already been mentioned. It was proposed that the chloride ions ion-exchange with Al_2O_3 surface hydroxyl groups and link directly to surface Al^{3+} cations (54). It can be represented as -



A competitive adsorbant is often added to an impregnating solution to improve the distribution of Pt in Pt/ Al_2O_3 catalysts and HCl is commonly used as a competitive adsorbate (58) but other halogen containing reagents such as HF, CCl_4 , and AlCl_3 have also been studied (16). Van den Berg and Rijn ten (58) found from the adsorption isotherms for HCl and $\text{H}_2\text{PtCl}_6 \cdot 6\text{H}_2\text{O}$ on $\gamma\text{-Al}_2\text{O}_3$ at 298K, that at low concentrations ($<0.05 \text{ mol (dm}^3\text{)}^{-1}$) the adsorption strengths of chloride and $\text{PtCl}_5\text{OH}^{2-}$ anions were similar. The concentration of anion which is adsorbed depends on the number of adsorption sites present and thus depends on the structure and texture of the Al_2O_3 involved. Hence anions will have different adsorption isotherms on different forms of Al_2O_3 (18). For example, the simultaneous adsorption of chloride and Pt anions on $\gamma\text{-Al}_2\text{O}_3$ and $\eta\text{-Al}_2\text{O}_3$ has been investigated by Sivasanker et al (54). They found that at a given chloride ion concentration in aqueous solution the $\gamma\text{-Al}_2\text{O}_3$ adsorbed and retained less chloride ions than the η -form (54). Castro et al (18) have pointed out that even when $\text{H}_2\text{PtCl}_6 \cdot 6\text{H}_2\text{O}$ is used alone, the released chloride ions from the adsorption process can become fixed upon the Al_2O_3 surface. They represented the adsorption of the Pt chloride anion as shown below -



Since the released chloride is also adsorbed by the surface the adsorption of one molecule of chloroplatinic acid would occupy four surface sites.

Therefore, in contradiction to the present results, the pre-treatment of the Al_2O_3 support might have been assumed to increase the uptake of Pt, since it has been pointed out (61) that the presence of anions on Al_2O_3 can lead to a total increase in acidity by a factor of three, and possibly increase Pt dispersion. One possibility is that the Al_2O_3

surface was saturated with chloride, which was not removed by the rinsing process, blocking most of the surface adsorption sites leading to lower Pt uptakes during impregnation and causing a decrease in Pt dispersion if the PtCl_6^{2-} anions could not displace the Cl^- from the Al_2O_3 surface

The HCl and water washing treatment may have resulted in another change in the physical state of the Al_2O_3 surface which prevented Pt uptake during impregnation. It is possible that the number of surface sites was decreased by the treatment, by the removal of soluble Al^{3+} cations. Ananin et al (62) found that treatment of a partially hydrated Al_2O_3 surface with aqueous HCl led to the detachment of Al^{3+} cations. Thus, rather than blocking the adsorption site, the number of sites would be reduced by the removal of Al^{3+} leading to the decrease in Pt uptake. Also the removal of Al^{3+} cations could lead to loss of surface area of the support material at high temperatures. It has already been pointed out in the previous chapter of this work that the phase transformations of Al_2O_3 at high temperature are thought by some (63) to be brought about by the annihilation of cation and anion vacancies. It has also been shown in Ch 2 of this work that at high temperatures surface area loss of the Al_2O_3 fibre was accelerated by the HCl pre-treatment. Kozlov et al (64) found that the phase transformation of Al_2O_3 at temperatures at and above 1073K was accelerated by the addition of Pt dispersed on the surface of Al_2O_3 and that the effect was proportional to Pt concentration and that the transformation occurred via an intermediate, $\theta\text{-Al}_2\text{O}_3$. Deactivation due to metal-catalysed phase transformations of $\gamma\text{-Al}_2\text{O}_3$ has also been reported by Young et al (65) where nickel was found to accelerate support surface area loss at high temperature. Therefore, it may be that after pre-treatment of the Al_2O_3 with HCl, loss of surface area may have occurred during the calcination of this sample caused by a combination of the effect of the pre-treatment technique and a metal catalysed phase transformation. However, the temperature of calcination at 900K and the short period of time for which calcination was carried out (only 0.25h) would appear to preclude against this theory. It is unlikely that phase transformations would have occurred at such a low temperature and over such a short period of time. In the literature mentioned above (64, 65) the phase transformation were all observed at temperatures above 1073K.

The atomic absorption spectroscopy results indicated that sample Pa(U)4T1 also had a reduced uptake of Pt. This sample was prepared using a chloroplatinic impregnating solution, the pH of which was adjusted to four using NaOH. As already pointed out Brunelle (2) stated that an oxide in contact with a solution, whose pH is below the isoelectric point of that oxide, tends to be charged positively, surrounded by compensating anions and for Al_2O_3 the adsorption of an anionic precursor from a solution was facilitated by the pH of the solution being below pH7, the isoelectric point of Al_2O_3 (66). Since in this case the pH of the solution was four rather than one, the surface of the Al_2O_3 should be less positively charged than a surface pre-treated with a

chloroplatinic acid solution of pH 1 and hence the adsorption of $(\text{PtCl}_6)^{2-}$ anions would be decreased. Also the NaOH would have reacted with the $\text{H}_2\text{PtCl}_6 \cdot 6\text{H}_2\text{O}$, neutralising some of it and forming a sodium chloroplatinate salt, thus decreasing the amount of $(\text{PtCl}_6)^{2-}$ anions available for adsorption. Even taking into account the lower Pt loading, the uptake of H_2 measured by chemisorption was approximately 22% lower than that determined for sample Pa(U)T1. Thus it may be that the higher impregnating solution pH altered the surface sites on the Al_2O_3 surface so that the Pt was poorly dispersed. As a visual inspection of the catalyst mat after calcination indicated that in many places the surface of the mat was metallic silver/grey in colour, it did appear that the addition of NaOH to the impregnating solution had caused an alteration of the surface composition of the catalyst. All the other catalyst samples were dark brown in colour after calcination. It is possible that a Na compound was deposited on the surface which decreased the uptake of H_2 by the catalyst sample in question.

Rinsing the support in milli Q H_2O and drying prior to Pt impregnation also influenced Pt uptake and dispersion. Sample Pa(W)T exhibited a lower Pt loading and a much lower H_2 uptake than a similar sample prepared using an untreated Al_2O_3 mat. Contamination of the support during the water washing treatment leading to low Pt uptake and depressed H_2 chemisorption appears unlikely since milli Q grade water was used during rinsing. It could be that the rinsing treatment physically damaged the surface of the support material since 5dm^3 of warm water were poured on a mat of mass 1g. The fibre material may have been damaged by this abrasive treatment. However, according to N_2 physisorption surface area measurements, previously given in Ch.2 of this work, there was no decrease in surface area after water rinsing and since the Pt anions exchange with hydroxyl groups on the Al_2O_3 surface, Pt uptake during impregnation would not be expected to be inhibited. With regard to the decreased H_2 uptake, it would appear that the treatment either suppressed the uptake of H_2 by the addition of some contaminating substance or brought about a very poorly dispersed supported Pt surface. The presence of contaminants on the surface due to the water treatment, although unlikely for the reasons stated previously, could also explain a decreased uptake of Pt due to blocking of adsorption sites on the Al_2O_3 material. However this would appear to be unlikely as the catalyst sample prepared with the HNO_3 pre-treated support material also underwent a water rinsing treatment prior to impregnation (in order to remove excess NO_3^-) and appeared to be unaffected by pre-treatment with regard to Pt uptake and H_2 chemisorption. Sintering of Pt or loss of support surface area during calcination also appears improbable as an explanation for the depression of H_2 chemisorption. Although water washed Al_2O_3 did show accelerated surface area loss at 1173K compared with the untreated Al_2O_3 support material, the temperature at which calcination was carried out was quite low, 900K, and would not be

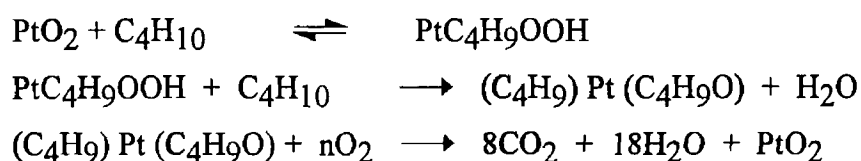
expected to bring about a change in the surface area of the support allied to the short time of exposure, 0.25h

A part of the study was involved with the examination of the effect of drying on the distribution of Pt on the Al_2O_3 support. The atomic absorption spectroscopy analysis on the mat divided into nine segments indicated that upon drying Pt spray-impregnated on the mat migrated to the surfaces of the mat. Also drying at 350K or 390K for 16h after impregnation appeared to cause poor Pt dispersions and this was more pronounced for catalysts with supports pre-treated with HNO_3 compared with unpre-treated supports. It appeared from a visual inspection of each of the catalyst mats, that drying at 350K or 390K for 16h caused Pt migration towards the edge of the Al_2O_3 mat. This was confirmed by the atomic absorption results for the Pt concentration of different areas of sample Pa(N)T3. The concentration of Pt was found to be higher at the edges of the mat than at the centre of the Al_2O_3 mat. Pt migration during drying is well known and has been dealt with in the literature. Van den Berg and Rijntjen (58) compared slow and fast drying and also found that fast drying led to non-uniform distribution of impregnant. Lee and Aris (1) reviewed research carried out on the effect of drying, and they claimed that the drying process could be described in terms of four distinct stages. The first stage, known as the pre-heated period, involves the entire wet body being warmed by the drying medium. The second stage occurs when the temperature has reached a constant level. As the liquid vaporises at the support surface, a meniscus forms across each pore developing capillary forces that draw liquid to the surface. During the first two stages, the dominant mechanism of moisture transport is capillary flow. In the third stage, capillary flow decreases and vapour diffusion becomes comparable to capillary flow. As capillary flow decreases more liquid vaporises within the interior of the support. In the final stage, the transport of liquid is completely dominated by vapour diffusion, the temperature of the support rises and the external surface becomes completely dry. From the above mechanism, it would appear that with fast drying of the $\eta\text{-Al}_2\text{O}_3$ supported catalysts examined in this study, capillary forces dominated the migration of impregnant and that the process was similar to the first two stages of the above drying mechanism. This process appeared to be accelerated with higher drying temperatures and resulted in a poorly distributed Pt on the Al_2O_3 surface.

The use of a different impregnation method for catalyst preparation was also studied. The powdered Al_2O_3 support material was immersed in an impregnating solution and dried using a rotary evaporator, described as method B in Sec 3.1. This method of impregnation was similar to the soak impregnation method described by a number of workers (1). Although catalysts prepared by this method were found to exhibit high Pt loadings, the values for H_2 chemisorption and hence Pt dispersion and Pt surface area were much lower than those for the corresponding samples prepared by the spray impregnation method, method A. It is probable that this was due to the fact that

during solvent removal, using a rotary evaporator, the Al_2O_3 powder was deposited on the sides of the round bottom flask. As the impregnating solution vaporised, despite the fact that the flask was rotating, the remainder was concentrated on one particular area of the surface of the flask, (due to the angle that the flask was held at) so that some of the powdered support was coated with more solution than the rest of the support. This would, therefore, have led to a nonhomogeneous distribution of Pt on the surface of the Al_2O_3 support and would have resulted in a poor Pt dispersion.

From the GC activity results in Table 3.11 it appears that the oxidation of *i*-butane over some of the catalysts examined, was not a simple deep oxidation involving the production of only carbon dioxide and water. Reaction over Pa(W)T1 and Pa(U)4T1 resulted in the production of CH_4 , as well as *i*-butane oxidation. A more complicated reaction than that proposed by Salmikov et al (67) appears to have occurred. They put forward the theory that the mechanism involved peroxide compound formation due to adsorption of molecular oxygen on the Pt/ Al_2O_3 catalyst surface. This would be followed by H_2 abstraction during the reaction of adsorbed peroxides with butane leading to the formation of adsorbed reactive radicals as in the scheme shown below.



From the GC study, the reduction in H_2 of catalyst samples prior to analysis had an effect on catalytic activity, in general causing a decrease in activity, and although samples with a highly dispersed Pt phase (as measured by H_2 chemisorption determination) gave high *i*- C_4H_{10} conversions, in general dispersions could not be correlated with % conversions of *i*- C_4H_{10} . It is difficult to make correlations between the Pt dispersions and activity measurement on samples which did not undergo prereduction in H_2 , as the surface of these catalyst samples would be fundamentally different after reduction. However even for samples reduced prior to activity measurement there was no direct correlation between activity and dispersion. The increase in activity after prereduction in H_2 compared with an unreduced sample for Pa(C)T1 and Pa(W)T1 is in agreement with results reported by Volter et al (68) who examined the oxidation of *n*-heptane over various Pt/ Al_2O_3 samples. They found that for chloride containing catalyst samples, prereduction in H_2 at 773 K prior to reaction measurement produced a more active oxidation catalyst than the corresponding samples.

which did not undergo a reductive treatment. This was despite the fact that the samples should have undergone reoxidation during heating prior to reaction. To a lesser extent prereduction was found to have a similar effect on non-chloride containing samples. They also found that calcination in O_2 at increasingly higher temperatures led to a decrease in Pt dispersion but an increase in oxidation activity for n-heptane. Similar results were obtained by Otto et al (69) during an examination of the effect of Pt particle size on the oxidation activity of Pt/ Al_2O_3 for the total oxidation of propane, C_3H_8 . Yao et al (70) found that Pt wires were more active for CH_4 oxidation than well dispersed Pt phases in supported catalyst samples. Volter et al (68) claimed that in Pt/ Al_2O_3 samples highly dispersed Pt was transformed into an oxidised surface complex $[Pt(IV)]_s$ by calcination in O_2 or air at 773K and that heating above this temperature led to a decomposition of this phase, the degree of decomposition increasing with increasing temperature. The product of this decomposition was a poorly dispersed crystalline Pt phase. They proposed a model involving dual active sites for hydrocarbon oxidation but where the poorly dispersed crystalline phase was much more active than the $[Pt(IV)]_s$ surface complex. They concluded that reduction in H_2 or calcination at higher temperatures led to an increase in the amount of crystalline Pt phase which in turn led to an increase in catalytic activity. Hicks et al (71) proposed that for CH_4 combustion over Pt/ Al_2O_3 a similar model applied i.e. a dispersed Pt phase, which was converted to PtO_2 under reaction conditions, and a crystalline phase, which was covered by an adsorbed layer of O_2 during reaction and which was 10 to 100 times more active for CH_4 oxidation than the dispersed phase. Otto et al (69) also concluded that propane oxidation was favoured on a crystalline Pt phase, with the reaction being expedited by a favourable ensemble of active Pt sites, more likely to form on larger crystals.

Therefore it could be concluded that the increase in activity of the catalyst samples examined in this study during run 2 compared with run 1 could be due to the decomposition of a $[Pt(IV)]_s$ surface complex and the formation of larger amounts of the more active crystalline phase due to the high temperatures to which the catalysts were exposed when reaction under oxidising conditions occurred during run 1.

For the total oxidation of CH_4 over Pt/ Al_2O_3 (72) or Pd/ Al_2O_3 (73 , 74) it has been determined that catalytic activity could be increased by activation in the reaction mixture at elevated temperatures, i.e. 873K (72). In the case of Pt this effect has been related to an increase in Pt particle size during activation, with the reactivity of chemisorbed O_2 increasing with Pt particle size (72). Therefore the observed increase in activity from run one to run two may be due to an increase in Pt particle size. It is unlikely that a redispersion of the Pt phase occurred during reaction as this should have led to a decrease in activity under reaction conditions according to the literature (68, 69, 70). H_2 chemisorption analysis after activity measurements would only give limited information as the catalyst sample would have to be reduced in H_2 at elevated

temperatures prior to H₂ uptake measurement and thus the surface would be fundamentally different from the surface present during the second activity run

In disagreement with Volter et al (68) the activity of the majority of the samples did not increase with prereduction in H₂. In fact in some cases reduction brought about a decrease in activity. In this study prereduction was at a temperature 100K lower than that used in the study by Völter et al (68), (673K as opposed to 773K), so the temperature may not have been high enough to produce more Pt crystallites to increase activity. In their study Volter et al (68) found that the activity of the Pt/Al₂O₃ samples with lower amounts of chloride present were less affected by prereduction in H₂ than samples containing higher amounts of chloride. This might explain why sample Pa(C)T1 had higher activity after prereduction in H₂ while the other samples did not exhibit this behaviour.

Turnover numbers (TON) for each catalyst sample were calculated from the data given in Tables 3 10 and 3 11, and the results of these calculations are given in Table 3 14. These values were calculated by dividing the percentage i-butane conversion per gram of catalyst sample, by the number of determined Pt surface sites per gram of sample (obtained by H₂ chemisorption measurement). They therefore, represent a measure of the activity per active site, if each Pt atom on the surface is an active site. At 670K during the first run the pattern for the turnover numbers for the samples in the pre-treatment study reduced prior to this run was as follows

$$\text{Pa(U)T1} > \text{Pa(W)T1} > \text{Pa(C)T1} > \text{Pa(U)4T1}$$

For unreduced samples the trend for turnover numbers decreased as shown below

$$\text{Pa(C)T1} > \text{Pa(W)T1} > \text{Pa(U)T1} > \text{Pa(N)T1} > \text{Pa(U)4T1}$$

During the second activity run, the pattern for unreduced samples and samples reduced prior to run one, change compared with those shown above for run one. For samples reduced prior to run one during the second run the trend as regards TONs was

$$\text{Pa(C)T1} > \text{Pa(U)T1} \approx \text{Pa(W)T1} > \text{Pa(U)4T1}$$

However, for samples which were unreduced, the order for TON during run 2 was

$$\text{Pa(C)T1} > \text{Pa(W)T1} > \text{Pa(U)T1} > \text{Pa(N)T1} > \text{Pa(U)4T1}$$

Table 3 14 Pt Surface Areas and Turnover Numbers for Catalyst Samples

Sample	Pre-treatment*	Temp	Pt Surface Area (m ² g ⁻¹)	Turnover Number (% per Pt atom) x 10 ⁻¹⁷	
		(K)		Run1	Run2
Pa(U)T1	R	520	4 18	0 00	3 85
		570		3 81	3 85
		620		3 89	3 89
		670		3 85	3 89
Pa(U)T1	NR	470	4 18	3 42	3 42
		520		3 42	3 42
		570		3 59	3 59
		620		3 59	3 55
		670		3 59	3 68
Pa(C)T1	R	470	1 38	3 48	3 63
		520		3 63	nd
		570		3 21	4 84
		620		3 21	nd
		670		3 21	8 62
Pa(C)T1	NR	470	1 38	0 00	4 69
		520		3 83	5 68
		570		3 70	8 81
		620		3 98	9 09
		670		3 98	9 09
Pa(N)T1	NR	520	6 92	0 00	2 74
		570		2 74	2 74
		620		2 74	2 74
		670		2 74	2 78

*Note R represents reduced in H₂ at 673K prior to activity measurement and NR represents not reduced

Note nd = not determined

Table 3 14. Contd

Sample	Pre-treatment*	Temp	Pt Surface Area (m ² g ⁻¹)	Turnover Numbers (% per Pt atom) x 10 ⁻¹⁷	
		(K)		Run1	Run2
Pa(W)T1	R	420	1 71	0 00	3 49
		470		0 00	3 67
		520		0 00	3 76
		570		3 48	3 85
		620		3 48	3 85
		670		3 48	3 85
Pa(W)T1	NR	470	1 71	0 00	0 20
		520		3 61	3 61
		570		3 61	3 70
		620		3 61	3 70
		670		3 70	3 80
Pa(U)4T1	R	520	2 93	0 00	0 02
		570		1 44	1 50
		620		1 50	1 50
		670		1 50	1 50
Pa(U)4T1	NR	470	2 93	0 00	1 16
		520		0 66	1 81
		570		1 16	2 17
		620		1 16	3 89
		670		1 16	3 89

*Note R represents reduced in H₂ at 673K prior to activity measurement and NR represents not reduced

Note nd = not determined

Despite the low H₂ uptake values determined by chemisorption measurement for Pa(C)T1, the activity results for this catalyst compared well with the activities of the other samples examined. In fact the TON for reduced and unreduced samples of Pa(C)T1 were either as high as or higher than the corresponding values for the other catalysts examined during the first reaction run. During run 2, the TONs exhibited by Pa(C)T1 were appreciably higher than the TONs of any of the other catalyst samples.

including Pa(U)T1 and Pa(N)T1. This was in sharp contrast to both the H₂ chemisorption and the atomic absorption spectroscopic results which indicated that this sample had a low Pt loading and a low Pt surface area and dispersion. Thus it might have been expected that the sample could have exhibited a lower activity than some of the other samples examined. However, the higher value of the TONs exhibited by this sample were caused by the lower number of Pt surface sites which were determined to be present by chemisorption measurement as opposed to a much greater level of 1-butane conversion during reaction compared with other samples. Therefore, the HCl treatment of support during catalyst preparation affected the TONs by either suppressing H₂ chemisorption and hence decreasing the estimated number of Pt surface sites or by affecting the surface morphology of the Al₂O₃ support in a manner which led to the formation of a smaller number of more active Pt sites than would have been obtained using untreated Al₂O₃ or Al₂O₃ treated in a different way, as discussed previously.

It is interesting to note that after the first reaction run the activity of Pa(C)T1 increased dramatically during run 2 (in some cases butane conversion actually doubled compared with run one). This appears to be due to the method of preparation of the catalyst. It is probable that the HCl treatment caused an increase in chloride ion concentration on the Al₂O₃ support, despite the water washing process to remove Cl⁻ ions (see Sec 2.1). During the first reaction run, at high temperatures (i.e. 670K), in the oxidising environment, it is unlikely that the presence of a higher chloride ion concentration may have caused a redispersion of the Pt phase, by a mechanism similar to that by Bournonville and Martino (22), i.e. through the formation of volatile complexes such as PtCl₂(AlCl₃). A redispersion of the Pt phase during the final stages of the first reaction run should have resulted in smaller Pt particles. This in turn should have caused a reduction in activity exhibited by this sample during run 2, compared with the first run (68, 69, 70, 71). It is therefore more likely that the oxidative treatment at the high temperatures of reaction might have led to a larger amount of the more active crystalline phase reported by Völter et al (68).

The light off temperatures from the DSC activity measurement indicated that, there was an optimum particle size for low light off temperatures, above or below which the temperature of light off was increased. Similarly, with two exceptions, the exotherm size did not increase linearly with H₂ uptake exhibited by samples, but again there appeared to be the same optimum particle size which gave highest activity. The GC activity results indicated that for samples Pa(W)T1, Pa(U)4T1, Pa(C)T1 and to a lesser extent Pa(U)T1 above a certain temperature there was a dramatic increase in butane conversion (in some cases up to 50% higher) compared with the magnitude of butane conversion at the initial temperature range at which activity was observed. In the DSC activity traces for these samples there was also evidence for a second sample temperature increase at a temperature higher than the initial light off temperature, although the

magnitude of the second increase was only about 25% of the initial increase due to the first light off. There was also indications of a second corresponding small exotherm within the main DSC exotherm but again it was only a fraction of the magnitude of the total exotherm.

Although there are differences in the magnitude of the effect recorded by the different methods of activity measurement, it would appear that at a distinct temperature there is an increase in activity compared with initial activity. This could indicate a second less active type of site which operates at a higher temperature than the sites responsible for the initial light off.

Another possibility is that at the higher temperature a secondary reaction is taking place. As stated previously Wise et al. (45) obtained similar results for the oxidation of isopropyl alcohol which were attributed to the formation of a stable intermediate, acetone, which subsequently decomposed to form deeper oxidation products. In the present study GC results indicated that there were trace amounts of CH_4 , C_2H_6 and C_3H_8 in the i-butane gas stream prior to reaction. Although over Pa(W)T1 and Pa(U)4T1 the amount of CH_4 increased during reaction, over the other catalysts examined, using the GC flame ionisation detector, there were no traces of other organic products in the effluent gas stream during or after reaction. It still must be regarded as one of the more likely explanations for the phenomenon observed. The possibility that this second temperature jump represents the occurrence of heterogeneous-homogeneous combustion, i.e. chemically initiated gas phase oxidation can be ruled out although this phenomenon is well reported in the literature. For example, it has been found that peroxy species produced on bismuth molybdate catalysts desorbs to initiate gas phase propylene oxidation (44), while similar intermediates have been proposed in the oxidation of benzene over vanadia (75). However, the fact that the second temperature increase was at different temperatures for different catalyst samples and also that the difference in temperature between the first major sample temperature increase (associated with light-off) and the second sample temperature depended on the catalyst sample which was used, indicated that heterogeneous-homogeneous reaction was not responsible for the second sample temperature jump. If a particular species was formed on the catalyst surface to initiate gas phase oxidation then it might be expected that this would occur at approximately the same temperature after light off on each of the catalysts. Thermally initiated gas phase oxidation can also be ruled out because, firstly, the second temperature jump occurred at different temperatures which were dependent of the catalyst sample used. If thermally initiated gas phase oxidation was responsible it would be expected that the sample temperature increase resulting would be dependent on the particular temperature of the furnace rather than the catalyst sample used. Secondly, a blank activity run was carried out in which no catalyst was present and the temperature of the DSC furnace was increased linearly to 623K, with the reactant gases (butane and

air) flowing through the system. The DSC signal remained constant throughout the activity run, with no indications of either an exotherm or an endotherm, implying that no thermally initiated gas phase oxidation had occurred up to 623K.

Although the butane conversions were lower from the DSC activity measurements than those obtained from the GC activity measurements when the actual masses of the catalyst samples are taken into account the activity results for *i*-butane conversion from the DSC method are an order of magnitude higher than those obtained by the GC method. This is an unexpected conclusion. In the DSC method the reactant gases were passed over the catalyst sample whereas in the case of the GC method they were passed through the sample. Thus it might have been expected that higher activity would have been exhibited by samples using the GC method since the catalyst is more accessible to the reactant gases using this method.

3.4 Conclusions

Pre-treatment of the Al_2O_3 support affected the uptake of Pt during impregnation, the amount of H_2 chemisorbed by the catalyst and the activity for 1- C_4H_{10} oxidation. Pre-treatment of the Al_2O_3 support with HNO_3 caused up to 50% of the NO_3^- used for pre-treatment to be retained on the support. This caused an increase in Pt uptake during impregnation (possibly brought about by a change in the acidity of the support) and higher Pt dispersions compared with catalysts prepared with untreated support material. The increase in dispersion may have resulted from the blocking of some but not all of the Pt adsorption sites on the Al_2O_3 by NO_3^- . On the other hand pre-treatment with H_2O or HCl led to decreases in Pt uptake during impregnation and decreased dispersions of Pt compared with catalysts prepared with untreated supports.

Spray impregnation produced catalysts which had higher Pt dispersions than catalysts prepared by wet impregnation. Drying at temperatures of 350K or 390K for 16h after impregnation led to a drop in dispersion compared with identical catalysts dried at 310 K for 16h. Drying at the later temperature resulted in a non-homogeneous distribution of Pt on the Al_2O_3 support when it was in mat form, with Pt more concentrated at the edges of the mat.

With regard to the oxidation of 1- C_4H_{10} it was determined that in general pre-reduction in H_2 caused a decrease in catalytic activity. However the HCl and H_2O pre-treated samples exhibited an increase in catalytic activity after pre-reduction. The untreated Pt/ Al_2O_3 had the lowest light off temperature, followed by the H_2O and HNO_3 pre-treated catalysts while the HCl pre-treated sample had an even higher light off temperature than any of the afore mentioned catalysts according to the DSC activity measurements. For unreduced catalysts the greatest % C_4H_{10} per gram catalyst occurred over the HNO_3 pre-treated and the untreated catalyst, with lower conversions over the H_2O and the HCl pre-treated catalysts. However when the Pt surface area of the catalysts was taken into account (determined by H_2 chemisorption measurement) reaction over the HCl pre-treated Pt/ Al_2O_3 catalyst produced the highest turn over numbers (TON), followed, in order of decreasing TONs, by the H_2O pre-treated catalyst, the untreated catalyst and finally the HNO_3 pre-treated catalyst. The large TONs for the HCl and H_2O pre-treated catalysts were due to the low uptakes of H_2 during chemisorption measurement rather than increased catalytic

activity

For most of the catalysts examined there appeared to be an increase in activity compared with initial activity at a distinct temperature. This may have been due to the presence of different active sites on the surface of the catalyst or due to the occurrence of a secondary reaction. Thermally initiated gas phase oxidation could be ruled out as a possible explanation.

3 5 References

- (1) S Lee and R Aris, Catal Rev -Sci Eng., 27, 207 (1985)
- (2) J Brunelle, Pure and Appl Chem., 50, 1211 (1978)
- (3) M Palmer Jr and M Vannice, J Chem Tech Biotechnol., 30, 205 (1980)
- (4) J Cusumano, W Dembinski and J Sinfelt, J Catal., 5, 471 (1966)
- (5) R Maatman and C D Prater, Ind Eng Chem., 49, 253 (1957)
- (6) J Roth and T Reichard, J Res Inst Catal., Hokkaido Univ , 20,185 (1972)
- (7) J Summers and A Auser, J Res Inst Catal., Hokkaido Univ , 52, 455 (1978)
- (8) D Do, Chem Eng Sci , 40, 1871 (1985)
- (9) N Kozlov, A Yanchunk and L Mostovaya, React Kinet Catal Lett., 19, 337 (1982)
- (10) T Dorling, B Lynch and R Moss, J Catal., 20, 190 (1970)
- (11) H Benesi and R Curtis, J Catal., 10, 328 (1968)
- (12) V Machek, J Hanika, K Sporka, V Ruzicka, J Kunz and L Janacek, in, G Poncelet, P Grange, and P A Jacobs (Eds), Preparation of Catalysts III, Studies in Surf Sci Catal ,16, p 69, Elsevier, Amsterdam (1983)
- (13) R Maatman, Ind Eng Chem., 51, 913 (1959)
- (14) E Michalko, U S Patent. 3 259 454 (1966)
- (15) J C Summers and L L Hegedus, J Catal., 51, 185 (1978)
- (16) Y S Shyr and W R Ersnt, J Catal., 63, 425 (1980)
- (17) W Jianguo, Z Jiayu and P Li, in , G Poncelet, P Grange and P A Jacobs (Eds), Preparation of Catalysts III, Studies in Surf Sci Catal. , 16, p 57, Elsevier, Amsterdam (1983)
- (18) A Castro, O Scelza, E R Benvenuto, G Baronetti, S De Miguel and J Parera, in, G Poncelet, P Grange and P A Jacobs(Eds), Preparation of Catalysts III ,Studies in Surf Sci Catal. , 16, p 47, Elsevier, Amsterdam (1983)
- (19) M Heise and J Schwarz, J Colloid Interface Sci., 113, 56 (1986)
- (20) P Flynn and S Wanke, Catal Rev -Sci Eng., 12, 93 (1975)
- (21) J Bournonville, J Franck and G Martino,, in , G Poncelet, P Grange and P A Jacobs(Eds), Preparation of Catalysts III, Studies in Surf Sci Catal. , 16, p 81, Elsevier, Amsterdam (1983)
- (22) J Bournonville and G Martino, in, B Delmon and G F Forment(Eds), Catalyst Deactivation, Studies in Surf Sci Catal. , 34, p 159, Elsevier, Amsterdam (1980)
- (23) R Fiedorow and E J Wanke, J Catal., 43, 34 (1976)
- (24) E Ruckenstein and B Pulvermacher, J Catal., 29, 224 (1973)

- (25) P C Flynn and E J Wanke, J Catal, 34, 390 (1974)
- (26) P Wynblatt and N A Gjostein, Scr Met, 7, 969 (1973)
- (27) F M Dautzenberg and H B Walters, J Catal, 51, 26 (1978)
- (28) K Kunimori, T Ouechi and T Uchijima, Chem Lett, 12, 1513 (1980)
- (29) G Schwab and H Schultes, Z Phys Chem, Abt B9, 265 (1930)
- (30) S J Tauster and S C Fung, J Catal, 55, 29 (1978)
- (31) S J Tauster, S C Fung and R Garten, J Amer Chem Soc, 100, 170 (1978)
- (32) J A Horsely, J Amer Chem Soc, 101, 2870 (1979)
- (33) C C Kao, C C Tsai and Y W Chung, J Catal, 73, 136 (1982)
- (34) P K deBokx, R L Bonne and J W Geus, Appl Catal, 30, 33 (1987)
- (35) G C Bond and R Burch, Catalysis, Roy Soc Chem 6, 27, Alden Press, Oxford (1983)
- (36) L Gonzalez-Tejuca, K Alka, S Nemba and J Turkevich, J Phys Chem, 81, 1399 (1977)
- (37) G Den Otter and F M Dautzenberg, J Catal, 53, 116 (1978)
- (38) K Kunimori, Y Ikeda, M Soma and T Uchijima, J Catal, 79, 185 (1983)
- (39) T Ren-Yuan, W Rong-An and L Li-Wu, Appl Catal, 10, 163 (1984)
- (40) T Huizinga, J Van Grondelle and R Prins, Appl Catal, 10, 199 (1984)
- (41) P Menon and G Froment, Appl Catal 1, 31 (1981)
- (42) O S Alekseev, V I Zaikovskii and Y I Ryndin, Appl Catal, 63, 37 (1990)
- (43) G C Bond and P B Wells, Appl Catal, 18, 225 (1985)
- (44) D L Trimm, J Catal, 7, 249 (1983)
- (45) H Wise, A Schwartz and L L Holbrook, J Catal, 199 (1979)
- (46) L D Pfefferle and W C Pfefferle, Catal Rev -Sci Eng, 29, 219 (1987)
- (47) C Wagner, Chem Tech Berlin, 18, 28 (1945)
- (48) Stanton Redcroft DSC 700 Instruction Manual, Stanton Redcroft Ltd, London (1987)
- (49) J Scholten, A Pijpers and A Hustings, Catal Rev -Sci Eng, 27, 151 (1985)
- (50) F Duivenvoorden, B Kip, D Koningsberger and R Prins, J Phys Colloq, 1, 227 (1986)
- (51) J Lemaitre, P Menon and F Delannay, in, F Delannay (Ed), Characterisation of Heterogeneous Catalysts, Ch 7, Marcel Dekker Inc , N Y (1984)
- (52) L Jacimovic, J Stevovic and S Veljkovic, J Phys Chem, 76, 3625 (1972)
- (53) S M Ahmed, J Phys Chem, 73, 3546 (1969)
- (54) S Sivasanker, A V Ramaswamy, and P Ratnasamy, in, B Delmon, P Grange, P Jacobs and G Poncelet (Eds), Preparation of Catalysts II, Studies in Surf Sci Catal, 3, p 185, Elsevier, Amsterdam (1979)

- (55) A Wells, Structural Inorganic Chemistry, Oxford University Press, London (1962)
- (56) K Jones, Comprehensive Inorganic Chemistry, Pergamon Press, 2, 380 (1975)
- (57) E Santacesaria, S Carra and J Adam, Ind Eng Chem Prod Res Dev , 16, 1 (1977)
- (58) G H Van den Berg and H Th Rjnten, in, B Delmon, P Grange, P Jacobs and G Poncelet(Eds), Preparation of Catalysts II, Studies in Surf Sci Catal , 3, p 265, Elsevier, Amsterdam (1979)
- (59) B J Cooper and D L Trimm, in B Delmon and G F Froment(Eds), Catalyst Deactivation, Studies in Surf Sci Catal , 6, p 63, Elsevier, Amsterdam (1980)
- (60) C N Satterfield, Heterogeneous Catalysis in Practice, McGraw-Hill, New York (1980)
- (61) K Jiratova and L Beranek, Appl Catal , 2, 125 (1982)
- (62) V N Ananin, A I Trokhmetz, L Shaverdina and M Zaretski, React Kinet Catal Lett , 27, 1 (1985)
- (63) P Burtin , J P Brunelle, M Pijolat and M Soustelle, Appl Catal , 34, 239 (1987)
- (64) N S Kozlov, M Ya Lazarev, L Ya Mostovaya and I P Stremok, J Kinet Catal , 14, 1130 (1973)
- (65) D J Young, P Udaja and D L Trimm, in, B Delmon and G Froment(Eds) Catalyst Deactivation, Studies in Surf Sci Catal , 6, p331, Elsevier, Amsterdam, (1980)
- (66) K Jiratova, Appl Catal , 1, 165 (1981)
- (67) V S Salnikov, T V Sorokineand P G Tsyrunikov, React Kinet Catal Lett , 30, 209 (1986)
- (68) J Volter, G Lietz, H Spindler and H Lieske, J Catal , 104, 375 (1987)
- (69) K Otto, J M Andino and C L Parks, J Catal , 131, 243 (1991)
- (70) Y -F Y Yao, Ind Eng Chem Prod Res Dev , 19, 293 (1980)
- (71) R F Hicks, H Qi, M L Young and R G Lee, J Catal , 122, 280 (1990)
- (72) P Briot, A Auroux, D Jones and M Primet, Appl Catal , 59, 141 (1990)
- (73) P Briot and M Primet, Appl Catal , 68, 301 (1991)
- (74) T R Baldwin and R Burch, Appl Catal , 66, 337 (1990)
- (75) C Daniel, J R Mounier and D W Kuelks, J Catal , 31, 360 (1973)

CHAPTER 4

Study of Pt-Sn/Al₂O₃ and Pt/SnO₂ Catalysts

4 Introduction

This chapter deals with work carried out on Pt-Sn/Al₂O₃ and Pt/SnO₂ catalysts involving both characterisation and i-butane activity measurement. Although Pt-Sn/Al₂O₃ samples have been used as reforming catalysts (1) and Pt/SnO₂ samples are known to be efficient low temperature CO oxidation catalysts (2) little work has been carried out on the oxidation of hydrocarbons such as butane over Pt-Sn catalyst samples. Production of an efficient bimetallic oxidation catalyst where the addition of Sn led to a smaller amount of precious metal being required would be commercially important. It was therefore decided to examine a number of Pt-Sn catalysts and to determine their activity for i-C₄H₁₀ oxidation. In this section a summary of the pertinent literature on Pt-Sn catalysts is given.

4.1 Pt-Sn/Al₂O₃ Systems

Catalysts in which Pt together with a second metal, such as Re, Ir or Sn, are dispersed on an Al₂O₃ support are commonly used by the petroleum industry for reforming reactions (1). For example for the conversion of n-hexane to benzene or lower hydrocarbons it has been found that the addition of Sn to Al₂O₃ or SiO₂ supported Pt catalysts drastically lower the rates of reactions producing carbonaceous catalyst poisons, brought about through polymerisation of extensively dehydrogenated surface species, hence increasing stability (3).

A large body of work has been carried out in order to elucidate the state of the metallic components upon reduction in H₂ for Pt-Sn catalysts. For this system there is disagreement in the literature as to the oxidation state of Sn upon reduction. The studies which produced evidence against the formation of metallic Sn and Pt-Sn alloys, will first be examined here.

Muller et al. (4) carried out a surface study on Pt-Sn bimetallic reforming catalysts, using H₂ and O₂ adsorption measurements using a microbalance at temperatures of 723K and 296K. A series of catalysts with varying Pt (0 - 0.35wt%) and Sn (0 - 1.4wt%) contents were prepared using aqueous solutions of SnCl₂ and H₂PtCl₆ to impregnate the γ -Al₂O₃ support. They were calcined at 803K for 2h in air. The adsorption results indicated that Sn, even after reduction in H₂ at 783K, was tightly bound to the Al₂O₃ support and that the Sn was present as Sn(II). Evidence for this was the lack of irreversible adsorption of O₂ at room temperature on reduced Sn/Al₂O₃ samples. Electron microdiffraction measurements also indicated that no metallic Sn or Pt-Sn alloys were present in reduced Pt-Sn/Al₂O₃ samples. Pt, on the other hand, was reduced to the metallic state. It was established that the amount of O₂ adsorbed on the Pt-Sn/Al₂O₃ catalysts was proportional to both the Pt and Sn contents and a scheme was put forward for the transition from the reduced to the oxidised state for the Pt-Sn samples (4), shown in Fig.4.0.

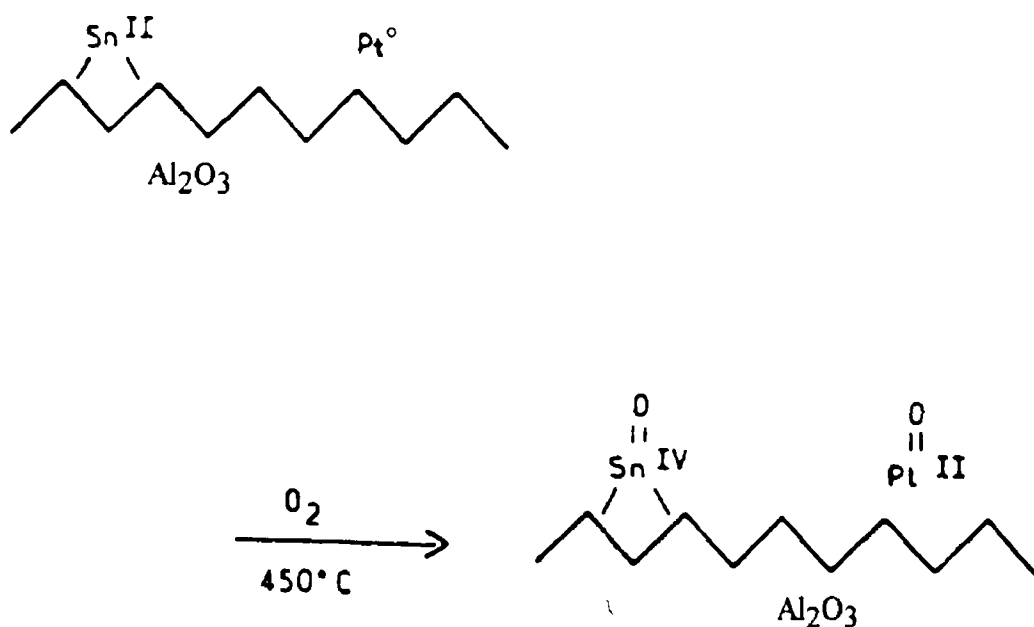


Fig.4 0 . Scheme proposed for the transition from the reduced to the oxidised state for Pt-Sn samples (4).

Bacaud et al (5) found that at low Pt loadings (0.35 wt%) and Sn loadings of between 0.2 wt% and 0.4 wt% formation of Sn(II) occurred upon reduction in H_2 . However at higher Pt loadings (i.e. 1 wt%) the whole of the Sn was reduced. In a more recent study (6) evidence for the presence of Pt-Sn alloys was found in samples prepared by the successive impregnation of SnCl_4 and, after calcination at 673K in air, H_2PtCl_6 . The Pt and Sn loadings ranged from 0.31wt% to 1.15wt% and 0.20wt% to 4.00wt% respectively. The samples were then either calcined in air at 673K for 1h or analysed without a second calcination step. Mossbauer spectroscopy and temperature programmed reduction (TPR) were used to analyse the samples. Reduction in H_2 at 773K for 1h resulted in the formation of the alloys PtSn_4 and PtSn . Sn(II) and Sn(IV) were also found to be present on the catalyst surface. Calcination after Pt addition had little effect on the results.

Burch (7) examined a series of Pt-Sn/ Al_2O_3 catalysts containing 0.3wt% Pt and varying amounts of Sn (0.3 - 5.0wt%), prepared by exposing industrial Pt/ Al_2O_3 catalysts to acetone solutions of $\text{SnCl}_4 \cdot 5\text{H}_2\text{O}$ and calcining in air at 770K for 2h or by heating to 770K at 10Kmin^{-1} and holding at that temperature for 2h. TPR, H_2 chemisorption and monitoring reoxidation in O_2 after reduction in H_2 , were the techniques used to characterise the samples. It was determined that although Pt catalysed the reduction of Sn, the average oxidation state was +2, after reduction in H_2 at temperatures up to 960K, and that irrespective of the length of reduction time no further reduction took place, see TPR profiles in Fig 4 1.

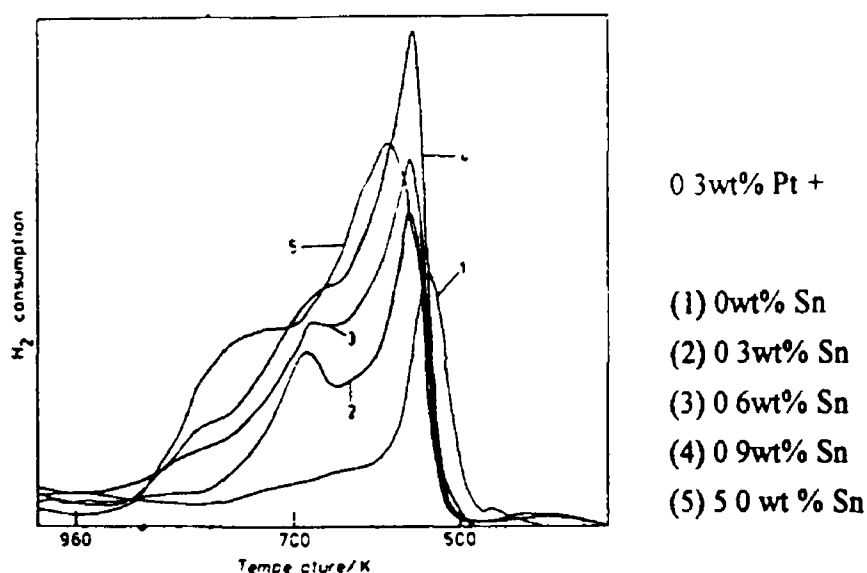


Fig 4.1 . TPR profiles of Pt-Sn/Al₂O₃ samples produced by Burch et al. (7)

It was established that although the average oxidation state of Sn was independent of Sn content, the adsorption of H₂ by the sample increased with the amount of Sn present, indicating that the Pt dispersion was increased by the addition of Sn. Burch (7) concluded that no Pt-Sn alloys were formed during reduction, that there was a strong interaction between Sn(II) and the Al₂O₃ support which prevented the formation of metallic Sn, and that the special properties of Pt-Sn/Al₂O₃ catalysts might be caused by a change in the electronic properties of the Pt by an interaction with Sn(II) ions on the support surface.

TPR and the adsorption of H₂ and O₂ were techniques which were also used by Lieske and Volter (8) to examine the state of Sn in reduced Pt-Sn/Al₂O₃ reforming catalysts. A range of samples were prepared with Sn contents up to 12 wt% and Pt contents of either 0.5 or 1.0 wt%. Preparation involved impregnation with HCl solutions of H₂PtCl₆ and SnCl₂ and calcination by heating at 773 K for 1 h. For Sn/Al₂O₃ samples both Sn(IV) and Sn(II) were determined to be present on the support surface. With high Sn loadings (10 wt%), however, a small part of the Sn oxide was reduced to the metallic state, shown by the adsorption of O₂ at room temperature after reduction. Similarly for bimetallic Pt-Sn/Al₂O₃ samples, with large Sn contents, although the main part of the Sn existed as carrier stabilised Sn(II), a minor part of the Sn was reduced to Sn(0), forming bimetallic clusters with Pt. TPR profiles were used to calculate the change in the valence state of the Sn, see Fig 4.2. With Pt-free samples the value for the valence state was determined to +2 (due to the formation of Sn(II)), whereas with Pt-containing samples a value for the change in valence of Sn greater than 2 was obtained, indicating the formation of some metallic Sn.

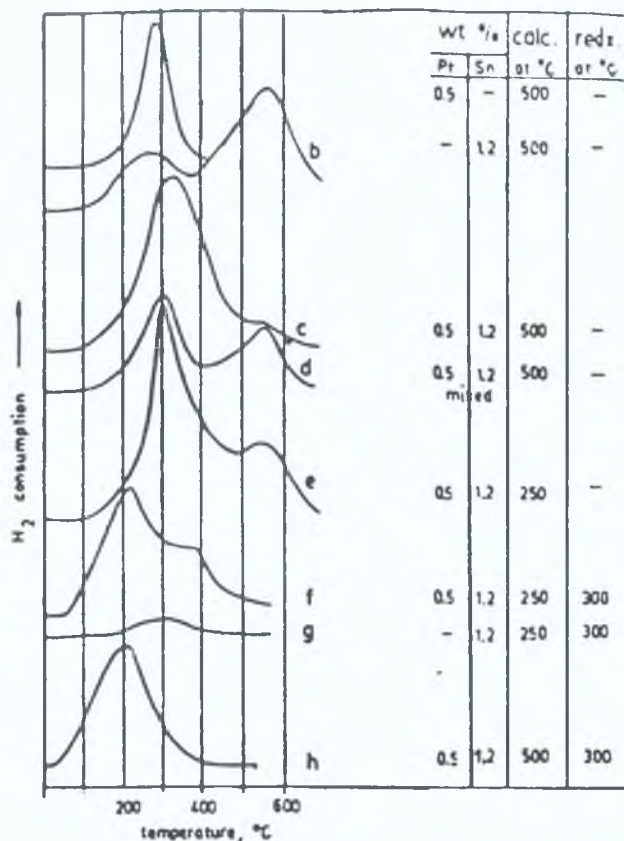


Fig.4.2 : TPR profiles for Pt-Sn/Al₂O₃ catalysts obtained by Lieske and Volter (8).

TPR profiles were used to calculate the change in the valence state of the Sn

More recently Sachdev and Schwank (9) carried out a similar study using both TPR and temperature programmed desorption (TPD) of H₂. In this study catalysts containing 0.7 wt% Pt and varying amounts of Sn (0 - 5wt%) were prepared. Precise quantitative data could not be determined from the TPR results as the profiles were complicated by the formation of HCl from the reduction of chloro-ligands on the Al₂O₃ support. However the TPD results indicated that two forms of Pt were present on the support surface, as there were two peaks in the TPD traces for Pt-Sn/Al₂O₃, 573K and 873K. The peak at ca. 873K was attributed to desorption from Pt sites. A number of theories were put forward for the origin of the second peak including the formation of a solid solution or alloy species between Pt and Sn, but it was pointed out that the TPD results could have indicated that the Pt sites enhanced the adsorption-desorption characteristics of Sn, or spillover of H₂ from Pt sites to Sn (9).

Balakrishnan and Schwank (10) examined Pt-Sn/Al₂O₃ catalysts containing 1wt% Pt and varying amounts of Sn, prepared by coimpregnation with acetone solutions of H₂PtCl₆ and SnCl₂, calcination at 773K in air for 2h and reduction at 673K for 5h. H₂, O₂ and CO chemisorption measurements were carried out on the samples in a static glass volumetric system at room temperature, after reduction in H₂ for 13h at 673K and evacuation at 693K. For H₂ adsorption they found that small amounts of Sn (less than or equal to 0.5wt%) increased H₂ uptake compared with monometallic Pt/Al₂O₃, but further increases in Sn content led to a decrease in the amount of adsorbed H₂, with a 5.0wt% Sn addition causing a fall in H₂ uptake of one third the value exhibited for a 1.0wt% Pt/Al₂O₃ sample. Balakrishnan and Schwank (10) concluded that for low Sn loadings the increased H₂ uptake indicated a higher Pt dispersion in comparison to the monometallic catalyst, a theory put forward by Burch (7) for increased H₂ uptake caused by Sn addition. Balakrishnan and Schwank (10) proposed a number of reasons for the observed decrease in H₂ uptake with increasing Sn content. Sn enrichment of the catalyst surface and coverage of the Pt surface with Sn was one reason proposed, since Sn has a lower surface energy than Pt. Another theory proposed was that the number of adjacent Pt atoms (required for H₂ chemisorption) would drop as the Pt was dispersed among Sn atoms stabilised by the Al₂O₃, leading to a drop in H₂ uptake. Other explanations put forward were Pt-Sn alloy formation at high Sn loadings or coverage of Pt atoms by a Sn-Al₂O₃ matrix, thus becoming inaccessible to chemisorbing gases.

Lieske and Volter (8) in their study also determined that with increasing Sn content there was a strong decrease in H₂ chemisorption. They proposed that this was due to alloy formation as Verbeek and Sachtler (11) found that D₂ uptake on Pt-Sn alloys was much lower than for monometallic Pt samples. In contradiction to both Balakrishnan and Schwank (10) and Lieske and Volter (8), the addition of larger amounts of Sn was found to increase H₂ chemisorption in the case of the study carried out by Burch (7). In this case the results were obtained using the TPR apparatus at the end of the reduction period, after quenching the sample at 273K, and were explained in terms of increased Pt dispersion.

For O₂ adsorption on Pt-Sn/Al₂O₃ samples prereduced in H₂ for 13h at 673K Balakrishnan and Schwank (10) found that there was an increase in O₂ uptake with increasing Sn content. Although it was acknowledged that this might be due to the formation of metallic Sn during reduction in H₂ prior to analysis, it was proposed that it was more likely that the chemisorption stoichiometry for O₂ adsorption on Pt atoms could have been modified due to the addition of Sn or that the increased O₂ uptake was caused by O₂ spillover from Pt to Sn (10). Lieske and Volter (8) and Muller et al (4) obtained similar results for O₂ adsorption in their studies. Although Muller et al (4) also attributed their results to a change in O₂ chemisorption stoichiometry, Lieske and Volter (8) concluded that increased O₂ uptake was due to the oxidation of metallic Sn, formed during reduction prior to analysis.

X-ray photo-electron spectroscopy (XPS) is a technique which has been widely used to examine the state of Sn in Pt-Sn/Al₂O₃ samples. Balakrishnan and Schwank (10) used XPS to analyse their samples after reduction in H₂. The reduction treatment in H₂ at 673K for 5h was carried out in situ. The results indicated no evidence for the formation of metallic Sn in Pt-Sn/Al₂O₃ catalysts, with Sn loadings from 0.1wt% to 5.0wt%, upon reduction, although the formation of a small amount of Sn(0) below the detection limit of the technique was not discounted. It was concluded that the resistance to reduction shown by Sn was due to the strong interaction between the Al₂O₃ support material and the Sn(II) ions (10) in agreement with the work of Burch (7). Evidence that the lack of metallic Sn after reduction was due to an interaction with the Al₂O₃ support was obtained by Balakrishnan and Schwank (10) when they examined a reduced 1wt% Pt, 1wt% Sn/SiO₂ sample using XPS. Almost half the Sn in the sample was reduced to the metallic state. It was believed that for Sn supported on SiO₂ the Sn-support interaction was much smaller than that when Al₂O₃ was the support.

Sexton et al (12) used both TPR and XPS to determine the state of Sn in Pt-Sn/Al₂O₃ systems. The samples examined were prepared by successive impregnation, first with SnCl₄ and then, after calcination at 773K overnight, with H₂PtCl₆. Pt-Sn/Al₂O₃ prepared by coprecipitation were also investigated. The samples contained 0.5wt% Pt and between 0.2wt% to 6.3wt% Sn. Their TPR results were essentially in agreement with Burch (7), with the average oxidation state of Sn after reduction being determined to be +2. Sexton et al (12) analysed the samples using XPS, either unreduced or after reduction at 773K for 2 to 3h. No attempt was made to examine the state of Pt in these samples since the Pt4f region of the spectrum was obscured by the overlap of the Al2p substrate peak at 74.3eV. Using reference materials it was found that the binding energy for metallic Sn in the Sn3d region of the spectrum was 484.8 ± 0.1 eV while that for Sn(IV) and Sn(II) (which were indistinguishable) was in the region of 486.6 eV. It was observed both for monometallic Sn/Al₂O₃ and bimetallic Pt-Sn/Al₂O₃ samples that no reduction of Sn(IV) or Sn(II) to Sn(0) occurred. X-ray diffraction analysis (XRD) was also carried out on the reduced samples and no evidence for the presence of metallic Sn or Pt-Sn alloy was found.

Adkins and Davies (13) also found no evidence for the formation of metallic Sn, in their XPS study of a number of Pt-Sn catalysts, containing a Pt/Sn molar ratio of 1/4, after reduction in H₂ at 673K for 17h. From their XPS data and from the results for alcohol conversion studies which will be discussed later in this section, a model was proposed for the surface of a reduced Pt-Sn/Al₂O₃ catalyst, illustrated in Fig 4.3. In the model, the Al₂O₃ substrate was covered by a Sn-aluminate "eggshell" structure, upon which Pt atoms or crystals were present. This "eggshell" structure did not behave in a catalytically similar manner to SnO₂ or SnO but did influence the catalytic behaviour of the Pt.

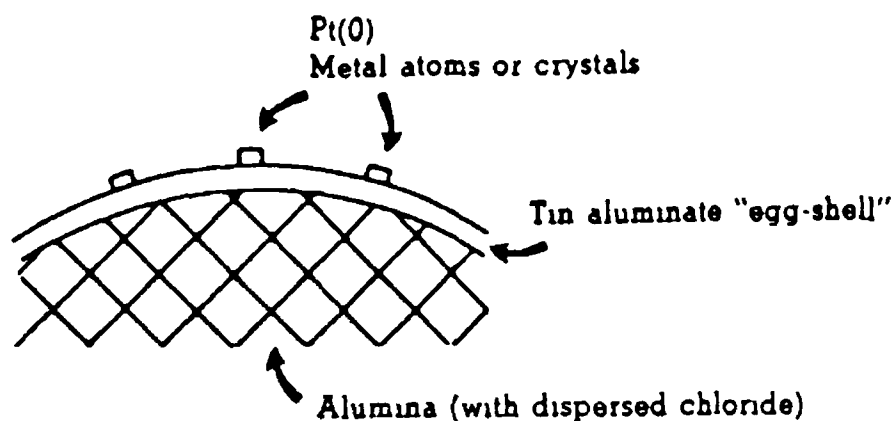


Fig 4 3 : Model for a reduced surface of Pt-Sn/Al₂O₃ (13).

A different approach to preparation of Pt/Sn catalysts was used by Hoflund et al (14) who characterised samples produced by the impregnation of γ -Al₂O₃ films, ca 300 Å thick, with acetone solutions of 2 mol% H₂PtCl₆ and 11 mol% SnCl₄. In the studies mentioned already (1, 3-13) all used bulk powdered Al₂O₃ as the support. Hoflund et al (14) used Auger electron spectroscopy (AES), XPS and TPD to characterise the samples, after reduction in H₂ at 775K for 1h. For the spectroscopic studies, the samples were not reduced in situ and after external reduction, prior to analysis, they were exposed to the atmosphere. For both reduced and unreduced samples no evidence for the presence of metallic Sn was obtained. Using the XPS technique the Pt4f region of the spectrum was examined, after a deconvolution process in which the Al2p overlapping peak was subtracted. In oxidised samples (calcined in air at 725K for 1.5h) the Pt was almost completely oxidised with contributions in the Pt4f region due to PtO, PtO₂ and Pt-O-Sn. Upon reduction the XPS results indicated that metallic Pt was the predominant Pt species on the surface, with both bulk and crystalline forms being present (an indication of sintering upon reduction). Some Pt-O-Sn was also present in the reduced samples. Hoflund et al (14) put forward models for the surfaces of reduced and oxidised samples, illustrated in Fig 4 4. For both models the interaction between the Pt and the Sn was through a Pt-O-Sn bond and Sn was present as Sn oxides and hydroxides. In calcined samples the Pt was primarily in the form of PtO and PtO₂, while

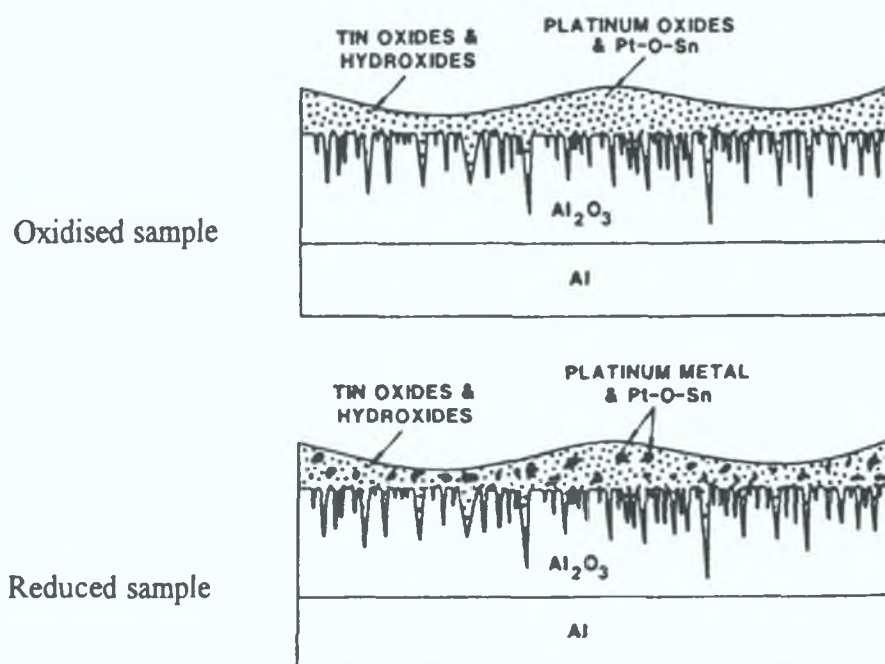


Fig.4.4 : Surface models for reduced and oxidised Pt-Sn/Al₂O₃ catalysts proposed by Hoflund et al. (14)

after reduction the surface consisted of bulk and crystalline metallic Pt, probably surrounded by and bound to the Pt-O-Sn species.

Meitzner et al. (15) also found that the average oxidation state of Sn in reduced Pt-Sn/Al₂O₃ catalysts was Sn(II), using extended x-ray absorption fine structure studies (EXAFS studies). The samples in question contained 1.1 wt% Pt and 1.2 wt% Sn and had been reduced in H₂ at between 775K and 795K, and passivated by controlled exposure to air prior to analysis. Pt dispersion, determined by EXAFS data, was found to be much greater in Pt-Sn/Al₂O₃ samples than Pt/Al₂O₃, with smaller metal clusters in the Pt-Sn/Al₂O₃ catalysts compared with the monometallic system. It was concluded that the system consisted essentially of Pt clusters dispersed on Al₂O₃ containing Sn²⁺ at the surface. The influence of Sn on Pt dispersion was attributed to the anchorage of Pt clusters to the Al₂O₃ support via the bonding of a few Pt atoms to Sn²⁺ ions at the surface of the Al₂O₃. A Pt-Sn/SiO₂ sample was also examined. The Pt in the Pt-Sn/Al₂O₃ bimetallic samples was more electron deficient compared to Pt in the Pt-Sn/SiO₂ sample. After reduction the Sn in the Pt-Sn/SiO₂ sample was found to be

reduced to the metallic state, in agreement with Balakrishnan and Schwank (10), and XRD data indicated that an ordered Pt-Sn alloy was formed on the SiO₂ support upon reduction at 775K.

In the studies so far mentioned there was little or no spectroscopic evidence for the formation of metallic Sn and/or Pt-Sn alloys during the reduction of Pt and Pt-Sn/Al₂O₃ catalysts. However Li and Hsia (16, 17) found evidence for the existence of metallic Sn in certain Pt-Sn/Al₂O₃ samples after reduction. In one study (16) Pt-Sn catalysts prepared by either coprecipitation on γ -Al₂O₃ or η -Al₂O₃ or coimpregnation or successive impregnation of η -Al₂O₃ with SnCl₂ and H₂PtCl₆. Catalysts were also prepared by the impregnation of η -Al₂O₃ support with a Pt-Sn complex. Mossbauer and XPS studies pointed to the formation of metallic Sn after reduction for samples prepared by coimpregnation of η -Al₂O₃ or by impregnation of η -Al₂O₃ with a Pt-Sn complex. In a subsequent study (17) the same authors examined the effects of supports and the methods of preparation on the reducibility of Sn in Pt-Sn samples containing 0.6 wt% Pt and 0.5wt% Sn. For η - and γ - Al₂O₃ supported catalysts the method of preparation was observed to have a profound effect on the reducibility of the Sn. Using Mossbauer spectroscopy, after reduction in H₂ at 773K for 2h, it was established that the order of reducibility of Sn for catalysts prepared with Al₂O₃ as the support was as shown below:

impregnation with a complex > coimpregnation > successive impregnation
> coprecipitation

In the case of the sample prepared by impregnation with a complex, the complex used was not identified. The resistance of Sn to reduction in the Al₂O₃ supported Pt-Sn catalysts prepared by coprecipitation was believed to be due to the strong interaction between Al₂O₃ lattice and Sn(II) ions (16). A similar trend was observed by Zhang and Li (18) who found that samples prepared by separate impregnation or coimpregnation of an Al₂O₃ support contained metallic Sn after reduction, while those prepared by coprecipitation did not contain metallic Sn after the same treatment.

Davis and co-workers (19) examined the effect of reduction on Sn present in a sample prepared by the impregnation of a Degussa Al₂O₃ with a Pt-Sn complex, [(C₂H₅)₄N]₂Pt₃Sn₈Cl₂₀. The samples were reduced in H₂ at temperatures in the range 648K-693K and were not exposed to the atmosphere prior to XPS analysis. On reduction Sn(0) was found to be produced and was in a 1:1 stoichiometric ratio with Pt, even after successive H₂-O₂ cycled treatments. The formation of a Pt-Sn alloy was suggested and results indicating Sn enrichment after O₂ treatment were cited as further evidence for the presence of a Pt-Sn alloy, as other workers (20, 21, 22, 23) found

similar behaviour was exhibited by Pt-Sn alloys. Bouwman et al (20) found that the surface of a Pt-Sn alloy could be drastically modified by a number of different treatments. Using AES they determined that H₂ exposure enriched the surface region with Pt while O₂ exposure enriched the surface region with Sn. Similar findings were reported by Hoflund et al (21) for a Pt₃Sn alloy. Asbury and Hoflund (22) examined the Sn enrichment of the surface of a Pt₃Sn alloy after annealing. They found that even at room temperature a Sn rich overlayer rapidly formed by a mechanism in which the rate of Sn diffusion to the surface was increased by a large concentration of surface defects, and that the thickness of this overlayer slowly increased over extended periods of annealing at 473K. A recent investigation (23) on the surface composition of an air exposed Pt₃Sn alloy, before and after reduction, determined that prior to reduction the surface was covered with a thick Sn oxide layer. Upon reduction it was found that O₂ loss occurred, particularly from a near surface region. This was accompanied by a migration of Pt to the surface from a Sn depleted Pt region below the Sn oxide layer.

Li et al (24) found that a major portion of Sn in Pt-Sn/Al₂O₃ samples, containing 1 wt% Pt and mole ratios of Pt Sn between 1/1 and 1/8, prepared by coprecipitation with SnCl₂ and H₂PtCl₆, could be reduced to the metallic state. The samples were reduced in situ at 648K for 2h prior to XPS analysis. As much as 68 % of the Sn in a sample containing a Pt Sn ratio of 1/5, was reduced to the metallic state according to their XPS results. Similar fractions of metallic Sn were found in reduced samples with varying Pt Sn ratios, indicating the presence of a variable alloy phase whose composition was dependent upon Sn content. For catalysts with Pt Sn mole ratios of 1/1, 1/2.7, 1/5 and 1/8 the atomic ratios of the Pt-Sn alloys found to be present after reduction, were determined to be PtSn_{0.66}, PtSn_{1.3}, PtSn_{3.4} and PtSn_{3.8} respectively. The study also demonstrated the air sensitivity of the alloys formed during reduction. A time period of only ten minutes exposure to air at room temperature was sufficient to entirely eliminate detectable amounts of metallic Sn formed during reduction. The air sensitivity exhibited by these alloys was proposed as one reason to explain the apparent disagreement between the XPS results of different studies, since minute amounts of O₂ could prevent alloy formation.

Although Unger et al (25) found no direct evidence for Pt-Sn alloy formation in Pt-Sn/Al₂O₃ (5 wt% Pt, 3 wt% Sn) they did obtain results which suggested the presence of alloy precursor species after calcination at 770K in air, from a FAB-MS study. It was proposed that there were patches of Pt-Sn alloy precursor species on the Al₂O₃ surface and that these species were transformed into alloys by subsequent reduction in H₂. It was suggested that the interaction between Pt and Sn species was established before or during calcination. It was also concluded that to facilitate alloy formation it was necessary to impregnate Al₂O₃ with solutions containing Pt-Sn complexes.

These types of complexes, composed of two Sn atoms per Pt atom, were found in H₂PtCl₆/SnCl₂ impregnating solutions by Baronetti et al (26). They investigated the

interaction between H_2PtCl_6 and SnCl_2 in a HCl solution with a Sn(II)/Pt(IV) molar ratio of 1.6. The interaction led to the formation of Sn(IV) and Pt(II) species and a complex of a $[\text{PtCl}_2(\text{SnCl}_3)_2]^{2-}$ structure in solution which was adsorbed on the Al_2O_3 support surface preserving its structure. Different deposition techniques affected whether this complex or the Pt and Sn in a different form were deposited on the support. Coimpregnation and step impregnation (first Pt, drying, then Sn) led to the deposition of this complex on the support, hence favouring a strong interaction between Pt and Sn. On the other hand, the use of step impregnation where first Sn and then Pt was added, resulted in the adsorption of Pt(IV) and Sn(IV) species in a separate manner on the support, causing a weak interaction between the two metals.

Baronetti and co-workers (27) carried out further studies on Pt-Sn systems prepared by different deposition techniques. Using TPR and XPS they found that for all the catalysts examined, zero valent Sn was produced after reduction in H_2 , due to the catalysing effect of Pt on Sn reduction. However it was observed that the extent of Sn reduction was found to be affected by the deposition technique used during impregnation. The XPS results indicated higher $\text{Sn(0)} / \text{Sn(II, IV)}$ ratios for catalyst samples with higher amounts of the $[\text{PtCl}_2(\text{SnCl}_3)_2]^{2-}$ complex, see Fig 4.5

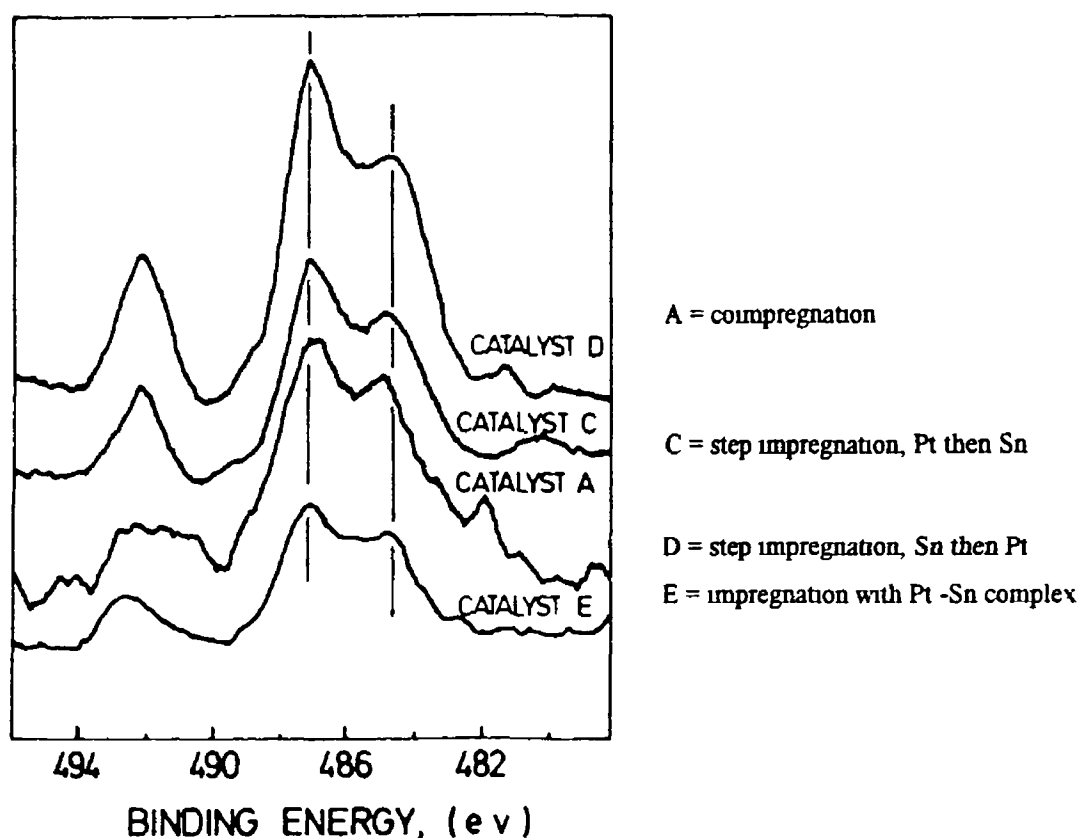


Fig 4.5 XPS results for reduced Pt-Sn catalysts produced by different deposition methods (27)

In a subsequent study Baronetti et al (28) examined the metallic phase of these catalysts after successive oxidation-reduction cycles. The catalysts were analysed after

calcination and after five oxidation/reduction cycles, each consisting of 5h at 773K in either O₂ or H₂ Pt-Sn/Al₂O₃ catalysts, obtained by both coimpregnation and successive impregnation, submitted to oxidation/reduction cycles, exhibited higher quantities of Pt-Sn alloys than the corresponding samples which were not subjected to the oxidation/reduction cycles. In addition catalysts where the [PtCl₂(SnCl₃)₂]²⁻ complex was deposited on the support underwent a modification of the surface composition of the alloy phase or a surface enrichment of Sn in the alloy particles, due to the oxidation/reduction cycles (28)

In another study (29) an electron microdiffraction technique was employed to identify crystal structure which developed in Pt-Sn/Al₂O₃. One sample was prepared by coimpregnation with H₂PtCl₆ and SnCl₄ onto Degussa Al₂O₃, while the other sample was prepared by the coprecipitation of Sn and Al oxides, followed by impregnation of the calcined material with H₂PtCl₆. XRD data indicated that although a Pt-Sn alloy was present in the sample prepared by coimpregnation after reduction, there was no evidence for alloy formation in the sample prepared by coprecipitation. EDX data for Pt and Sn metallic particles indicated that the dominant Pt Sn ratio was 1:1 for the co-impregnated sample. EDX analysis of metal particles large enough to be detected, for the coprecipitation sample indicated that only Pt was present, pointing to the majority of Pt being present in the metallic form and not alloyed to Sn. However a few particles were found to have a microdiffraction pattern consistent with a Pt Sn ratio of 1:2 for the coprecipitated sample. It was concluded that Pt was located on a few Sn rich or pure Sn oxide regions formed during coprecipitation. TEM results indicated that the coimpregnation and coprecipitation samples had different structures. For the coimpregnation sample both the Pt and Sn were located on the Al₂O₃ support surface after reduction. After calcination the Sn formed a Sn-aluminate egg-shell layer, while upon reduction Sn(IV) was converted to Sn(II) and Sn(0). The amount of Sn(0) depended on the Sn content while the amount of Pt-Sn alloy depended on the total amount of Sn relative to Pt. For the coprecipitated sample a significant amount of Sn was present in the bulk of the Al₂O₃ support and hence the Sn surface concentration was much lower, although isolated Sn (II) ions were present on the surface and were reduced to Sn(0). The small amount of Sn(0) which was found on the surface was believed to be formed from the reduction of pure Sn oxide particles produced during coprecipitation. Pt was present as isolated atoms and crystallites and it was concluded that Sn ions trapped Pt crystallites, retarding sintering.

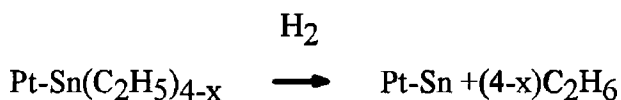
In contrast to the above studies (27, 28, 29), Stencel et al (30), using an XRD technique with in situ reduction, found that Sn was not reduced to the metallic state and that the extent of Sn reduction was independent of the mode of Sn introduction. However XRD analysis (again after in situ reduction) indicated that a Pt-Sn alloy was formed after reduction of catalysts prepared by impregnation of the Al₂O₃ support with a Pt-Sn complex, [Pt₃Sn₈Cl₂₀]²⁻. Similar XRD data was obtained by Srinivasan et al

(31) for catalysts prepared using the above complex. For high Pt metal loadings (ca. 5 wt%) evidence was obtained for both the presence of a Pt-Sn alloy and Pt phases. In another study Srinivasan et al. (32) investigated catalysts prepared using combined solutions of H_2PtCl_6 and SnCl_2 , with a constant Pt content (1 wt%) and Sn/Pt atomic ratios ranging from approximately 1 to 8. XRD results indicated that the only crystalline alloy phase present after reduction was Pt-Sn (1:1) and, as the intensity of the XRD lines for this species increased with increasing Sn/Pt ratios, it was concluded that unalloyed Pt was present in the samples containing low amounts of Sn. In all the studies involving XRD analysis (30, 31, 32) no lines for oxidised Sn were observed and it was concluded by Srinivasan et al. (31) that oxidised Sn was present in an x-ray amorphous form, probably as a surface layer of Sn-aluminate.

Different methods of preparation of Pt-Sn/ Al_2O_3 catalysts have been examined by Margitfalvi et al. (33). Controlled surface reactions for the preparation of catalysts with [A] direct Pt-Sn interactions, [B] Sn- Al_2O_3 interactions, and [C] Sn-Pt and Sn-support interactions, were developed. For catalysts with type [A] interactions preparation involved a surface reaction between different alkyl Sn compounds and H_2 chemisorbed on Pt supported on Al_2O_3 , i.e.



This was followed by a decomposition reaction in H_2 , i.e.

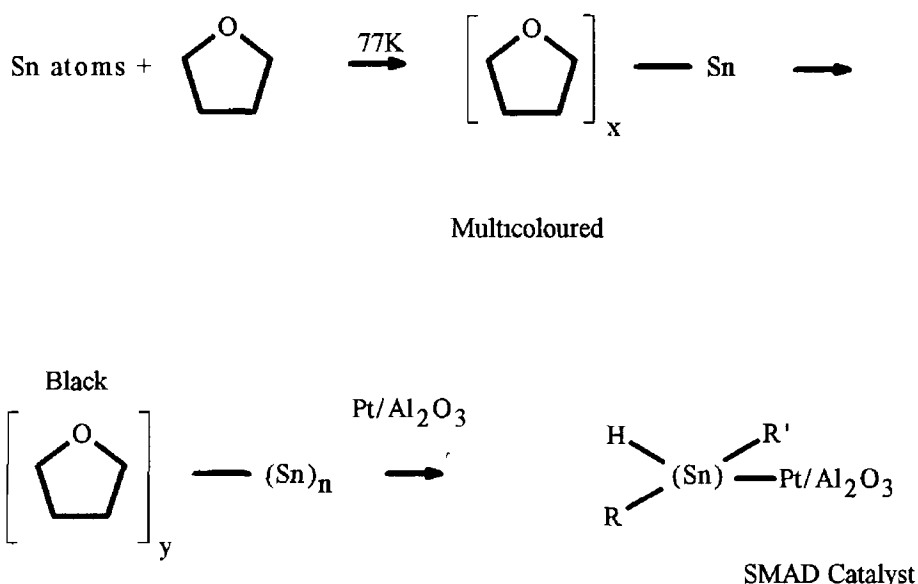


For catalysts with type [B] interactions preparation was achieved by the anchorage of SnCl_2 or SnCl_4 into a Li modified Al_2O_3 . The primary Sn containing complexes were then decomposed in a H_2 atmosphere at high temperatures, i.e.



Catalysts with type [C] interactions were prepared using a combination of methods for the preparation of catalysts containing type [A] and type [B] interactions as follows firstly samples were prepared so that a type [A] Sn-Pt interaction was produced and the resulting catalysts were then subjected to the procedures for the production of type [B] interactions. The catalysts thus produced were used in a reaction study, the results of which will be discussed later in this section.

A different preparation approach was examined by Li and Klabunde (34), who developed a method known as Solvated Metal Atom Dispersion (SMAD), which was used for the preparation of Pt-Sn/Al₂O₃ samples. The method involved the deposition of the metals in a reduced state, hence avoiding the necessity for a metal salt deposition step. The Al₂O₃ support already impregnated with a H₂PtCl₆ solution to give a 6 wt% Pt loading, was then treated with Sn as follows: a weighed amount of Sn metal was placed in a vaporization crucible in a reactor and evaporated under vacuum as solvent vapour (THF or toluene) was introduced into the reactor. The reactor walls were cooled using liquid N₂ so that the Sn atoms were co-deposited with the solvent as a frozen matrix. After 1 to 2 h the matrix was allowed to warm to room temperature. During warming the matrix melted and flowed down to the bottom of the reactor which contained the Pt/Al₂O₃ catalyst. The Sn-solvent-Pt/Al₂O₃ slurry was stirred for 0.5 h in vacuo and then 1 h under a N₂ atmosphere. Finally the solvent was removed by decanting and by evacuation. The preparation scheme for a THF system is shown below.



Some carbonaceous groups such as fragments of the solvent were incorporated into the catalyst (designated R, R'). The amount and the form of these carbonaceous groups was dependent on the metal and solvent. For example, heating dry Pt-Sn/Al₂O₃ under vacuum at 398K yielded the volatile products given in Table 4.

Table 4 . Hydrocarbon evolved during heating of SMAD Pt-Sn/Al₂O₃ catalyst (34)

SMAD Catalyst	Relative %					
	CH ₄	C ₂ H ₆	C ₃ H ₈	C ₃ H ₆	c-C ₃	C ₄
THF	0.3	7.4	29.8	42.6	5.1	14.8
Toluene	63.9	14.7	12.3	-----	-----	9.1

Studies on Pt-Sn/Al₂O₃ samples prepared using the SMAD method were carried out by Li et al (35, 36) Mossbauer, XRD and XPS data indicated that the SMAD procedure ensured that the Sn was added in the zero valent state and that greater than 95% of the Sn remained in that state. Although some surface Sn oxides were found, they were only present in small amounts. Regardless of the Sn loading or the support used, Sn was found to remain in the zero valence state, although there was no evidence for Pt-Sn alloy formation. It was suggested that a surface alloy may have been formed, even though there was no evidence from the characterisation techniques.

Activity studies have been carried out using Pt-Sn systems for reforming reactions due to their economic importance. Dautzenberg and co-workers (3) investigated the conversion of n-hexane over Pt-Sn supported (on Al₂O₃ and SiO₂) and unsupported catalysts. The addition of Sn to Pt decreased the deactivation of the dehydrocyclization reaction for benzene production and also changed the selectivity for methylcyclopentane formation. Formation of the latter compound was suppressed and the formation of coke deposits on the catalyst was decreased. Using Pt powder, temperature programmed n-hexane conversion experiments indicated that there were two distinct temperature regions where reaction took place, namely 548K - 725K and 755K - 823K. In the low temperature region benzene formation, isomerisation and cracking occurred while in the high temperature region benzene production and cracking, resulting in C₁ - C₅ products, occurred. However with 1 wt% Pt - 0.25 wt% Sn/Al₂O₃ the low temperature reactions (548K - 725K) typical for powdered Pt disappeared while in the high temperature region (755K - 823K) benzene production without extensive cracking proceeded at a high rate. The change in selectivity was interpreted in terms of an ensemble effect, where a change in the adsorption properties was due to the differences in the number of adjacent Pt atoms required for benzene or methylcyclopentane formation.

The conversion of cyclohexane and n-heptane over Pb-Pt/Al₂O₃ and Pt-Sn/Al₂O₃ catalysts has also been examined (37) The catalysts were prepared by coimpregnation They contained 0.5 wt% Pt and varying contents of Sn or Pb (0.15 wt% - 0.60 wt%) For the conversion of cyclohexane to benzene at 588K, increasing the amount of added Pb or Sn decreased the amount of dehydrogenation All the bimetallic catalysts were less active than the monometallic Pt catalyst However upon reaction at 773K, the monometallic catalyst rapidly poisoned, with the initial high selectivity for benzene decreasing with reaction time and increasing diene production In the case of both Pt-Sn and Pt-Pb bimetallic catalysts the activity remained constant and selectivity for benzene production remained at 100%, irrespective of reaction time Catalysts with Sn/Pt atomic ratios of 1/1 or 1/2 were found to have the best performance while others with a higher or lower content of Sn or Pb were less stable and less selective for benzene For the dehydrocyclization of n-heptane, reaction over bimetallic catalysts led to decreased deactivation compared with monometallic Pt catalysts, and over both types of bimetallic catalyst the production of toluene was increased while cracking was inhibited compared with Pt/Al₂O₃ With increasing Pb or Sn content the conversion and selectivity increased for toluene, but very large amounts of Sn and Pb (i.e. Sn or Pb/Pt >2) diminished the conversion and selectivity All of these results were obtained from reaction at a pressure of 0.1 mPa At higher pressure, 0.8 mPa, the bimetallic catalysts were less active than the monometallic Pt catalyst initially However again for the monometallic sample the activity decreased with time whereas over the bimetallic samples activity remained constant with time

It was also determined (37) that the amount of carbon deposition on the Pt-Sn samples was equal to or larger than that on the monometallic Pt sample, while on the Pt-Pb catalysts carbon deposition was slightly lower The addition of Sn or Pb to Pt catalysts was concluded to have a positive effect, by increasing activities and selectivities of aromatisation, and a negative effect, where activities and selectivities were decreased These effects were linked to reaction conditions, with a negative bimetal effect occurring under mild reaction conditions and a positive one occurring under severe conditions It was proposed that under severe conditions the Pt clusters were modified by both the second metal and carbon deposition The increase in selectivity towards aromatisation reactions and the decrease in hydrogenolysis activity of the bimetallic catalysts were explained by an ensemble effect The active Pt ensembles were believed to be blocked by inactive Pb or Sn so that hydrogenolysis was decreased Small amounts of Sn or Pb, < 0.6 wt%, were more effective in the blocking of ensembles

Pt-Sn/Al₂O₃ catalysts prepared using commercial Pt/Al₂O₃ catalysts were examined by Burch and Garla (38) in order to determine activity and selectivity for certain hydrocarbon reactions The reactions selected were the conversion of n-hexane, methylcyclopentane and cyclohexane at 750K and the hydrogenation of hex-1-ene at 373K As, under reforming conditions, reactions could occur either by metal-catalysed

processes or by a bifunctional mechanism involving both metal and acidic sites on the support, it was first determined whether changes in the acidity could cause variations in activity and selectivity. The conversion of methylcyclopentane to benzene was found to be bifunctional, while benzene and methylcyclopentane were produced from n-hexane on metal sites and did not require acidic sites. Again, compared to monometallic Pt catalysts, Pt-Sn/Al₂O₃ catalysts were much more resistant to deactivation. The bimetallic catalysts had much higher selectivities for aromatisation and isomerisation reactions producing much lower concentrations of cracked products. The Pt-Sn/Al₂O₃ samples increased the rate of dehydrogenation reactions and decreased the rate of hydrogenation reactions, compared with monometallic Pt catalysts, and produced more benzene from methylcyclopentane. The Sn modified the Pt, reduced self poisoning and modified the Al₂O₃ support by replacing the very acidic cracking site with selective olefin isomerisation sites. From a previous study on the same catalysts (7) the Sn had been found to be present as Sn(II) stabilised by the support and therefore it was concluded that the role of Sn was electronic rather than geometric in nature (38)

Sachdev and Schwank (9) also determined that Pt-Sn bimetallic catalysts were more resistant to deactivation than Pt/Al₂O₃ samples for the conversion of n-hexane between 423-623K, although less active initially. Calculated at 543K, the turnover frequency (normalised with respect to molecules of hexane converted per Pt atom per second after 200 sec of reaction at 1 atm pressure) dropped from approximately $6 \times 10^{-1} \text{ lsec}^{-1}$ for monometallic Pt/Al₂O₃ to approximately $1 \times 10^{-3} \text{ lsec}^{-1}$ over a Pt-Sn/Al₂O₃ sample containing 0.5 wt% Sn. For Pt-Sn samples, selectivities towards cyclical products were consistently higher than for isomerisation or cracking. It was proposed that the activity differences exhibited by monometallic Pt and bimetallic Pt-Sn catalysts were due to a spillover effect in which the bimetals improved the H₂ mobility from Pt sites to Sn sites, thus contributing to the enhanced activity of the catalysts with higher Sn loadings. The decline in activity with increasing Sn loading was believed to be due to the diluting effect of active Pt ensembles required for hydrogenolysis.

As has already been pointed out Sexton et al (12) carried out XPS measurements on various Pt-Sn/Al₂O₃ catalysts. As part of the same study the activities of these samples for reactions of methylcyclopentane and cyclohexane were determined. In agreement with the previous studies (3, 9, 37, 38) the addition of Sn was found to have an effect on both selectivities and activities (12). Also the method of Sn introduction during catalyst preparation influenced the activities and selectivities for methylcyclopentane and cyclohexane conversion. For catalysts prepared by coimpregnation small additions of Sn (< 2 wt% Sn) had a negligible effect on dehydrogenation rates for cyclohexane, but further Sn additions decreased the rate. For catalysts prepared by coprecipitation of Sn with Al₂O₃, followed by Pt deposition, the cyclohexane conversion rate was much lower than the rate exhibited by the catalysts prepared by coimpregnation with corresponding Sn loadings. A catalyst prepared using

a Pt-Sn complex, $[\text{Pt}(\text{SnCl}_3)_2\text{Cl}_2][\text{Et}_4\text{N}]_2$, was found to have a very low conversion for cyclohexane and produced up to 25 mol% cyclohexenes (12). For methylcyclopentane conversion a coprecipitated catalyst containing 0.5 wt% Sn demonstrated reaction behaviour which was characteristic of a coimpregnated catalyst with a Sn loading of >2.0 wt%. Catalysts formed using the Pt-Sn complex had a high selectivity toward the formation of methylcyclopentenenes. It was concluded that coprecipitation was the most efficient way of distributing Sn in Pt-Sn catalysts. The mechanism of modification of Pt reactivity by Sn(II) on $\gamma\text{-Al}_2\text{O}_3$ was considered to be due to Sn acting as an electronic modifier on the Al_2O_3 surface or being present on the Pt particles.

Another investigation was carried out by Kuznetsev et al. (39) on the catalytic properties of samples prepared by the impregnation of Al_2O_3 with Pt-Sn complexes. The composition of the complexes used were $\text{H}_4[\text{Pt}_3\text{Sn}_8\text{Cl}_{20}]$, $[(\text{C}_2\text{H}_3)_4\text{N}]_3[\text{Pt}(\text{SnCl}_3)_3]$ and $[(\text{C}_2\text{H}_3)_4\text{N}]_2[\text{Pt}(\text{SnCl}_3)_2\text{Cl}_2]$. Pt/ Al_2O_3 catalysts were more active for the dehydrogenation of cyclohexane at low temperature than Pt-Sn/ Al_2O_3 catalysts. Also reaction over the Pt-Sn/ Al_2O_3 catalysts obtained by Pt-Sn complex decomposition caused the formation of significant amounts of cyclohexene and traces of cyclohexadiene in addition to benzene. For the conversion of methylcyclopentane, the major pathway over the Pt-Sn/ Al_2O_3 samples was via dehydrogenation to methylcyclopentenenes and methylcyclopentadienes whereas for monometallic Pt catalysts dehydrogenation, hydrogenolysis and dehydroisomerisation of methylcyclopentane proceeded to an approximately equal extent. For n-hexane conversion, dehydrocyclisation was the predominant mechanism on Pt-Sn/ Al_2O_3 catalysts, while hydrogenolysis and aromatisation were pathways for Pt/ Al_2O_3 catalysts. Reaction data indicated that a significant change in both selectivity and activity for Pt-Sn/ Al_2O_3 occurred by varying the Pt-Sn complex used during preparation. The catalytic activity was found to decrease with increasing Sn content in the starting Pt-Sn complex for all the reactions studied. Catalysts produced by the deposition of $[\text{Pt}(\text{SnCl}_3)_3]^{3-}$ complex gave maximum yields of cyclohexenes and cyclohexadienes during the dehydrogenation of cyclohexane. The dehydrogenation of n-hexane occurred optimally over the catalyst prepared using the $[\text{Pt}_3\text{Sn}_8\text{Cl}_{20}]\text{H}_4$ complex, while the same sample also produced maximum yields of methylcyclopentenenes and methylcyclopentadienes compared with the other catalysts examined during the conversion of methylcyclopentane. It was suggested that in addition to the alteration of the electronic state of Pt by the interaction with surface Sn, the composition of the species formed could depend on the nature of the Pt-Sn complexes used for deposition and that both factors could be responsible to an equal extent for the observed changes in the catalytic properties of the metal. For example the addition of Sn might have affected the Pt electronically so that the strength of adsorption of hydrocarbons on Pt decreased leading to an increase in the rate of desorption of dehydrogenated intermediates. The factor causing low activity of the Pt-Sn bimetallics at up to 673K was thought to be the

Pt active surface by strongly adsorbed H_2 which hindered the adsorption of hydrocarbon molecules

Baronetti et al (27) observed that for dehydrogenation of cyclohexane and the hydrogenolysis of cyclopentane over Pt-Sn/ Al_2O_3 catalysts, the initial reaction rates indicated that the addition of Sn produced a decrease in dehydrogenation and dehydrogenolysis activities. The preparation technique used was found to influence the activity of the catalysts, believed to be due to the existence of distinct degrees of interaction between the Sn and the Pt. For both test reactions, monometallic Pt/ Al_2O_3 was most active, followed by the catalyst prepared by coimpregnation with H_2PtCl_6 and $SnCl_2$, with 0.28 wt% Pt and 0.14 wt% Sn. The sample prepared by successive impregnation with first Pt (0.29 wt%) and then Sn (0.28 wt%) had lower activity than the coimpregnated sample, and lower than the sample prepared by successive impregnation where the Sn (0.25 wt%) was added first, followed by Pt (0.28 wt%). A catalyst prepared using a Pt-Sn complex, $[(PtCl_2(SnCl_3))_2((CH_3)_4N_2)]$ exhibited the lowest activity. In a further study (28) the same authors examined the effect of a series of oxidative/reductive cycles on the catalysts mentioned above, with regard in particular to hydrocarbon reactions. Five oxidation/reduction cycles were carried out, the oxidation step by heating at 773K for 5h in an air stream and the reduction step by heating in H_2 at the same temperature for 5h. Compared with Pt/ Al_2O_3 samples, which maintained high activity even after the oxidative/reductive treatments, the bimetallics exhibited lower activity after oxidation/reduction cycles compared with the corresponding fresh bimetallic samples which did not undergo this treatment. It was also determined that the activation energy for cyclohexane dehydrogenation over bimetallic catalysts increased after the oxidation/reduction cycles. This was believed to be due to higher quantities of Sn being alloyed to the Pt after the treatment.

The conversion of n-hexane over Pt-Sn/ Al_2O_3 samples prepared by controlled surface reactions was investigated by Margitfalvi et al (33). The preparation details have been discussed previously in this section. Sn introduction decreased the initial rate of conversion of n-hexane in all the catalysts, while it was claimed that blocking of the Al_2O_3 acidic sites by Sn suppressed the formation of isohexanes, toluene and methylcyclopentane. Catalysts prepared with a direct Pt-Sn interaction resembled Pt/ Al_2O_3 monometallic samples (with regard to activity), except for slightly increased cracking selectivity over samples with Pt-Sn interactions. Samples with a Sn- Al_2O_3 interaction had a higher selectivity toward benzene, lower selectivity for 1-hexene formation and suppressed the formation of isohexanes and methylcyclopentane, compared with the activity exhibited by Pt/ Al_2O_3 samples and samples prepared specifically to have a Pt-Sn interaction. Finally catalysts prepared in order to contain both Pt-Sn and Sn- Al_2O_3 interactions exhibited decreased selectivity for the formation of benzene in conjunction with increased selectivity for 1-hexene and other unsaturated

hydrocarbons The formation of isohexanes and methylcyclopentanes was again suppressed

Margitfalvi and co-workers (40) also studied the reactions of methylcyclopentane over similar catalysts The introduction of Sn in different forms led to a considerable drop in the rates of methylcyclopentane conversion and changes in product selectivity In catalysts with Sn-Pt and Sn-Al₂O₃ interactions the yield of benzene was lower over these samples than over Pt/Al₂O₃ On Pt/Al₂O₃ and catalysts with Sn-Pt interactions, acidic sites on the Al₂O₃ were involved in benzene formation, while for samples containing Sn-Al₂O₃ interactions the metallic function was involved in the ring enlargement reaction For samples prepared to contain both Pt-Sn and Sn-Al₂O₃ interactions both metal and acid catalysed ring enlargement reactions were strongly hindered, with only two reaction products, methylcyclopentenenes and methylcyclopentadienes, being formed The suppression of benzene formation was caused by the simultaneous blocking of both types of active site

L1 and Klabunde (34) investigated the performance of Pt-Sn/Al₂O₃, produced by the SMAD technique, for the dehydrogenation, dehydroisomerisation, dehydrocyclisation and hydrogenolysis of various hydrocarbons From the activity data it appeared that Sn loadings between 1 and 1.5 wt% produced higher conversions of n-heptane and methylcyclopentane to toluene and benzene respectively compared with other Sn loadings Higher yields of benzene were obtained over all the Pt-Sn/Al₂O₃ catalysts compared with the monometallic Pt catalysts, during the dehydrogenation of cyclohexane For this reaction the SMAD catalysts exhibited activity higher than Pt/Al₂O₃ but lower than conventionally prepared Pt-Sn/Al₂O₃ samples On the other hand for the dehydrocyclisation of n-heptane, at low temperatures (633 - 758K) the SMAD samples had higher activity than conventional Pt-Sn/Al₂O₃ and Pt/Al₂O₃ catalysts Although lower than the activity exhibited by Pt/Al₂O₃, the SMAD samples possessed higher activity for ring opening reactions during the hydrogenolysis of cyclopentane, than conventional Pt-Sn/Al₂O₃ The differences in activity between the SMAD catalysts and the other samples was believed to be due to an ensemble effect, in which the Pt metal atoms were partially covered by Sn atoms leading to changes in selectivity

4.1.1 Pt/SnO₂ System

Stannic oxide, SnO₂, is found in nature as cassiterite mixed in granites, sands and clays (41, 42) It can be prepared artificially as a heavy white powder by burning metallic Sn in air, or by igniting metastannic acid (42) In a number of studies, SnO₂ was prepared by the action of HNO₃ on metallic Sn (43, 44) SnO₂ can also be prepared by the precipitation of chloride salts For example in one study (45) SnO₂ was prepared either by the addition of aqueous KOH to an acidic solution of SnCl₂ · 5H₂O or by the addition of NH₄OH to anhydrous SnCl₄ SnO₂ films have also

been used as catalyst supports, for example (46, 47) Watanabe et al (46) prepared SnO_2 films by spraying aqueous solutions of SnCl_4 in intermittent bursts onto a Pyrex surface heated at 723K. A similar method was used by Cox et al (47) to prepare SnO_2 films on Ti foil.

During the oxidation of metallic Sn both of the two stable oxides, SnO_2 and stannous oxide, SnO , are present during the oxidation process (48). It is very difficult to distinguish between SnO_2 and SnO using ESCA or AES since most of their spectral features are essentially identical (48), but the oxides can be distinguished using valence band ESCA (49) and ELS (50, 51). The conditions of oxidation influence the relative content of SnO_2 and SnO present, but for heavily oxidised samples an SnO_2 layer lies below an oxygen depleted layer or SnO like layer (48).

SnO_2 is important as an electrode material (52, 53, 54), in solar cell applications (55, 56), as a transparent conductor in electronic displays and as a sensor material (58, 59). This is due to the properties of SnO_2 , which is an n-type wide gap semi-conducting material and is transparent to visible light (48). Its geometric structure and chemical composition is very complex. SnO is always present to some extent. SnO_2 can exist in a number of structural forms. Usually large amounts of contaminants such as C, Ca, K, Na, S and Cl (60) and H_2 is always present in varying amounts on the SnO_2 surface (61). Also the treatment of SnO_2 in any way almost always alters the surface in some manner (48).

The chemical activity of SnO_2 and particularly its redox properties make it an important catalytic material, together with its modified forms. SnO_2 (44) and $\text{SnO}_2\text{-Cr}_2\text{O}_3$ catalysts (63) are active for NO reduction. In a review on the relevant literature, Viswanathan and Chokkalingam (63) have reported that Sb-doped SnO_2 has been found to be active for the oxidation of propylene (64), isobutylene (65), butene (66, 67), o-xylene (68) and naphthalene (69). An $\text{SnO}_2\text{-Bi}_2\text{O}_3$ catalyst has been observed to be active for the oxidative dehydroisomerisation and aromatisation of propylene (70) and the partial oxidation of methane (71).

According to Hoflund et al (72) there are five main preparation methods for the production of Pt/ SnO_2 . They are

- (a) chemisorption of Pt from a H_2PtCl_6 solution,
- (b) spray hydrolysis deposition in which the Pt salt is incorporated into the spray solution,
- (c) an electrochemical decomposition from a H_2PtCl_6 solution,
- (d) decomposition of an adsorbed metallo-organic compound,
- (e) deposition from a molten salt containing Pt,

Watanabe et al (46) studied the preparation of samples by method (a), the chemisorption technique. They found that SnO_2 alkaline pre-treatment with 10M NaOH at 363K increased the uptake of Pt, in agreement with an earlier study (73), and this

was believed to be due to an increase in the number of hydroxyl groups present on the surface Hoflund (74) and co-workers (75) using an electron stimulated desorption technique (ESD) found that the surface of an SnO₂ sample after the above mentioned caustic treatment, contained a considerably greater concentration of hydroxyl groups than the surface of an SnO₂ sample exposed to atmospheric humidity, which was also hydroxylated It was also observed that there were two adsorbed states of hydrogen present on the surface of the caustic pre-treated SnO₂ surface as opposed to one type of hydrogen on the untreated SnO₂ surface

Cox et al (47) examined Pt/SnO₂ samples, prepared by method (a), using XPS Again the SnO₂ was pre-treated in 10M NaOH prior to Pt addition XPS spectra of the samples were obtained after preparation, after high temperature oxidation at 873K for 0.5h, after reduction at 773K for 0.5h and after high temperature annealing in vacuo at 1073K After preparation the XPS spectrum contained evidence for the presence of small amounts of Pt metal and Pt(OH)₂, while most of the Pt was present as a Pt-O-Sn substrate bonded species After calcination at 873K for 0.5h in O₂, Pt was found to be present as PtO, PtO₂ and the Pt-O-Sn species Reduction did not result in the formation of metallic Sn, although PtO and PtO₂ species underwent complete reduction to metallic Pt The high temperature oxidation-reduction cycle resulted in a sintering of the supported species evident from the large fraction of Pt metal (indicated by the size of the peak for metallic Pt in the Pt4f XPS spectrum for the sample after reduction compared with the corresponding spectrum for the sample which did not undergo oxidation and reduction) and the remaining presence of some substrate-bonded species suggested that a fraction of these species acted as nucleation sites for crystallite growth The inability to completely reduce Pt indicated a strong chemical interaction between the Pt and the SnO₂

Pt chemisorption was believed to occur by replacement of the proton on the surface hydroxyl group with the loss of a coordinated ligand from the Pt solution species The chloroplatinate underwent hydrolysis causing a replacement of two chlorines by hydroxyl groups at the pH used for chemisorption from a H₂PtCl₆ solution Chemisorption could be described by the reaction



This was followed by dehydroxylation and loss of chlorine from the surface complex On the other hand for alkaline impregnating solutions such as Na₂Pt(OH)₆, the chemisorption process was proposed to occur initially by ionisation of the surface hydroxyl group through the loss of an acidic proton Then Pt addition would occur according to



Dehydration of the surface complex would then produce the substrate bonded Pt-O-Sn species (47)

Hughes and McNicol (45) prepared Pt/SnO₂ by impregnation and ion exchange. Addition of Pt was achieved with a solution of H₂PtCl₆ · 6H₂O or [Pt(NH₃)₄(OH)₂], added in sufficient amount to just wet the support and contain the required amount of Pt. For samples prepared by ion exchange, the SnO₂ support was mixed with a solution of the Pt salt for 1h and then washed. TPR studies were carried out on the as-prepared samples and after calcination in air at 573K or 773K. In addition XRD and SEM examinations were carried out. XRD results indicated that after impregnation (with up to 20wt% Pt), calcination and electrochemical reduction, no crystalline Pt was detectable. Only after reduction in H₂, at temperatures greater than 773K, were Pt crystallites detected. SEM studies of the morphological properties of the support were unable to provide images of any Pt particles on the surface of the SnO₂ support. TPR studies on the samples indicated that calcination in air led to the formation of a compound between Pt and SnO₂ which was difficult to reduce. TPR profiles for Pt/SnO₂ samples dried at 393K contained features below 573K characteristic of the reduction of Pt species. In the profiles for the samples calcined at 573K these Pt features decreased in intensity while those for the reduction of SnO₂ above 573K increased in intensity. Finally the profiles for the samples calcined at 773K were devoid of any Pt features and it was concluded that Pt reduction was occurring under the SnO₂ peak whose maximum was at ca 873K. It is probable that the Pt-SnO₂ compound, formed during calcination, was the Pt-O-Sn substrate bonded species proposed by Cox et al (47)

Katayama (76, 77) has discussed both the preparation and characterisation of samples prepared by method (b), spray hydrolysis. In this case Pt/SnO₂ samples were prepared by a method used to produce SnO₂ conducting glass, in which a small amount of Sb was present to increase conductivity (77). Katayama (77) prepared samples by spraying an ethanol solution of a mixture of SnCl₄, SbCl₃ and H₂PtCl₆ · 6H₂O onto a substrate of Pyrex glass at 823-873K in air. Apart from this no further heat treatments were carried out prior to spectroscopic analysis. XPS analysis of the samples thus prepared gave indications of four different types of Pt species being present on the surface, assigned as PtO₂, PtO, Pt(OH)₂ and metallic Pt.

There are two different ways of depositing Pt on SnO₂ electrochemically (48). The first involves using cathodic plating conditions from a Pt salt-containing electrolyte, a preparation technique utilised by Hoflund et al (73). This method was also used by Cox et al (47) in their XPS study of Pt/SnO₂ samples. In the latter study Pt was plated from a 5 × 10⁻⁵M H₂PtCl₆ solution buffered at pH 6.8, at a potential of -0.5V vs SCE for varying amounts of time. XPS investigation indicated that samples prepared for 10min contained primarily a Pt species with a higher binding energy than metallic Pt, with a small amount of metallic Pt also present. After plating for 40min, however the

XPS results indicated that the predominant Pt species was metallic Pt supported clusters. It was proposed that the observed differences in the Pt4f spectra, with plating time, pointed to the Pt deposition process proceeding via the formation of the higher binding energy Pt species which acted as nucleation sites for metallic Pt crystallite growth at longer plating periods. This higher binding energy Pt species was assigned as a substrate bonded Pt or Pt-O-Sn species, similar to that found in the Pt/SnO₂ samples prepared by chemisorption, mentioned previously.

The second method of electrochemical deposition involves the selection of an appropriate chemisorption reaction and influencing this using anodic potentials (48). This technique was used by Laitinen et al. (78). The reaction chosen was the electrochemisorption of hexahydroxy platinate onto SnO₂. They examined the amount of Pt deposited from a solution containing 0.01M KOH, 2.56×10^{-3} M Na₂Pt(OH)₆ and 1.0M NaClO₄, as a function of potential. A potential range of 0.0 to 1.0V vs SCE was used. Pt deposition on SnO₂ was found not to vary linearly with potential. Instead deposition increased with increasing potential up to ca. 0.4V vs SCE, where Pt deposition reached a maximum, and then decreased as potential was further increased. However above 0.5V vs the SCE, the amount of Pt deposited gradually increased again with increasing potential, but near to the same extent as the amount which was deposited at 0.4V.

The surfaces of Pt/SnO₂ after annealing under vacuum were examined by Gardener et al. (2). A chemisorption method was used to prepare the Pt/SnO₂ film samples. An ISS, AES and ESCA study was carried out on these samples after drying, calcining for 1h at 773K in air and reduction by annealing under vacuum at 523-723K. After annealing, an ISS spectrum for the Pt/SnO₂ sample closely resembled an ISS spectrum taken for a Pt-Sn alloy surface. The surface of the catalyst was estimated to consist of 60 atm% Pt from AES and ISS measurements. ESCA analysis of the annealed Pt/SnO₂ sample indicated that the SnO₂ support was reduced to either metallic Sn or alloyed Sn. The AES results indicated that there was an increased interaction between Pt and Sn in the near surface region after annealing at 723K. From the spectral results it was concluded that a Pt-Sn alloy was formed during the reduction of the Pt/SnO₂ surface. Further evidence was provided by examination of the surface of the sample after O₂ exposure at room temperature. The results indicated that the treatment induced changes similar to those exhibited by Pt₃Sn alloy surfaces after similar treatments. In the ISS spectrum it appeared that the O₂ exposure increased the height of the Sn peak with respect to the Pt peak indicating a surface enrichment of Sn.

Pt/SnO₂ catalysts are known to be effective for a number of reactions. Pt supported on Sb-doped SnO₂ has been studied as an electro-reduction catalyst (79) and has been found to be superior to Pt supported on carbon due to increased resistance to sintering under anodic operating conditions. The high activity was considered to result from the synergistic effect of O₂ spillover (79). This type of catalyst, Pt/Sb-SnO₂, has

also been reported to be 100 times more active per surface Pt atom than metallic Pt for the electrochemical oxidation of methanol (76, 77, 80, 81) The enhanced activity of Pt/SnO₂ samples has been claimed to be due to the fact that the deactivation on Pt/SnO₂ after anodic activation was considerably smaller than that for metallic Pt The deactivation was due to a decrease in the amount of active sites by the accumulation of adsorbed species from methanol (77) On the other hand Hughes and McNicol (45) found that Pt/Sb-SnO₂ samples after calcination in air had lower activity for methanol electro-oxidation than the activity of a commercial unsupported Pt catalyst This was attributed to resistance to reduction of Pt in Pt/SnO₂ samples calcined in air, mentioned previously in this section High temperature reduction of dried, but uncalcined samples, led to catalysts with high catalytic activity (45) Pt-Sn catalysts have also been reported to be active for the electrochemical oxidation of formic acid, formaldehyde and CO (82, 83, 84)

The Pt/SnO₂ system has also been shown to be a good catalyst for the efficient low temperature oxidation of CO, a fact which makes it important in CO₂ laser technology (2, 23) Stark and Harris (85) found that both Pd/SnO₂ and Pt/SnO₂ catalysts were effective as CO oxidation catalysts A first order rate law for the conversion of CO and O₂ was obtained

Miller et al (86) also examined the kinetics of CO oxidation over a 1 wt% Pt/SnO₂ catalyst bed, using a stoichiometric mixture of CO and O₂ in flowing He A first order rate law was observed for CO oxidation of the form

$$-\ln(P/P_0) = k\tau$$

where k is the rate constant (s⁻¹) and τ represents the contact time (s) of the gas in the catalyst bed The study was carried out at temperatures between 298K and 348K Using the Arrhenius equation of the form

$$-\ln k = -\ln B + E/RT$$

where B is the pre-exponential term (s⁻¹), E is the activation energy (kJ), R represents the universal gas constant and T is the absolute temperature (K), it was determined that the activation energy for the reaction was 24 kJmol⁻¹

Stark and Harris (85) also used the Arrhenius equation to determine the activation energy of the same reaction over Pd/SnO₂ and Pt/SnO₂ samples From their experimental results they determined that for CO oxidation over Pd/SnO₂ and Pt/SnO₂ samples the values for the energy of E were 40 kJmol⁻¹ and 41 kJmol⁻¹ respectively These results were obtained over a temperature range of 294-350K, using a gas mixture of 31% CO₂, 16% N₂, 43% He, 7% CO and 3% O₂

Batten et al (87) found that the production of CO_2 increased linearly with increasing catalyst sample mass, during an investigation of the conversion of CO over a 1wt% Pt/ SnO_2 sample at 373K. In another set of experiments the reaction rate constants for various temperatures in the range 338K to 394K were determined and the data indicated a first order reaction in agreement with the findings of Stark and Harris (87) and Miller et al (86). Batten et al (87) calculated the activation energy, E, to be 55kJmol^{-1} for CO oxidation over their sample. The difference between the results of Batten et al (87) and the previous study by Miller et al (86), who both used similar catalyst samples, was claimed by Batten et al (87) to be due, in part at least, to the more rigorous pre-treatment of the catalyst prior to reaction. Batten et al (87) pre-treated their catalyst at 498K for 20h in flowing He, while Miller et al (86) pre-treated the sample at the same temperature for only 1h.

Pre-treatment has been found to have a profound effect on the catalytic activity of Pt/ SnO_2 samples for CO oxidation. Schryer et al (88) studied the catalytic activity of a 2 wt% Pt supported on SnO_2 sample, obtained from Engelhard Industries, for CO oxidation. It was observed that the activity of the sample was dependent on the pre-treatment of the sample. Unpre-treated samples exhibited the lowest long term activity while pre-treatment at 373K in CO for 1h greatly improved long term activity. A further enhancement was brought about by a similar pre-treatment at 398K, but using higher temperature pre-treatments up to 498K did not bring about any change in activity compared with the sample pre-treated at 398K (88).

In a more recent study on similar commercial catalysts Drawdy et al (89) carried out characterisation using ISS, AES and ESCA before and after reduction in 40 torr CO for 1h at temperatures in the range 348K - 448K. The purpose of the study was to determine the surface composition and the chemical states of the surface species which were present, in order to gain a greater understanding of how the Pt/ SnO_2 converted CO to O_2 and CO_2 at low temperatures.

The non-reduced sample contained SnO_2 , SnO and SnOH_x , with small amounts of Pt present as Pt-O-Sn, Pt(OH)_2 , PtO and PtO_2 . Reduction in CO caused a loss both in O and OH from Sn, resulting in the formation of metallic Sn. The extent of reduction increased with increasing reduction temperature. Similarly the chemical state of Pt was found to undergo changes with reduction temperature. Up to 373K Pt was predominantly present as Pt-O-Sn and Pt(OH)_2 . As reduction temperature increased the amount of Pt(OH)_2 was also found to increase. It was therefore suggested that Pt(OH)_2 species played a crucial role in the oxidation of CO at low temperatures (89).

Brown et al (90) examined 1 wt% and 2 wt% Pt on SnO_2 prepared commercially, using CO and O_2 chemisorption analysis in order to determine the number of CO molecules capable of being adsorbed by the catalysts. The catalysts were examined as received from the manufacturers, with no pre-treatments prior to analysis. The area of chemisorbed CO at 313K was determined for the 2 wt% and the 1 wt% Pt

samples to be $0.170 \text{ m}^2\text{g}^{-1}$ and $0.062 \text{ m}^2\text{g}^{-1}$ respectively. The turnover frequency (TOF) of each sample for the reaction between CO and O₂ at 313K was also calculated. The TOF was defined as the ratio of the number of moles of product per second to the number of active sites available for reactant adsorption. It was observed that the TOF for the 1 wt% Pt sample was $1.2 \times 10^2 \text{ molecules site}^{-1} \text{ s}^{-1}$, while for the 2 wt% Pt sample the TOF was determined to be $2.7 \times 10^2 \text{ molecules site}^{-1} \text{ s}^{-1}$. The ratio of TOFs was approximately the same as the ratio of Pt loadings (90).

Gardener et al (91) compared the performance of Pt/SnO_x and Au/MnO_x for long term, low temperature CO oxidation. The experiments were carried out at 308K or 328K. The samples were investigated either unpre-treated or pre-treated for 2h in either a 5vol% CO/He mixture at 323K or 398K, or a 5vol% O₂/He mixture at 323K. The Au/MnO_x catalyst was found to perform better than the Pt/SnO_x samples with regard to both activity and long term stability. For both types of sample CO pre-treatment enhanced catalytic activity and increasing the CO pre-treatment temperature from 323K to 398K further enhanced the long term activity of the catalysts. In addition O₂ pre-treatment decreased the CO oxidative activity of all sample relative to unpre-treated samples.

In this section it has been attempted to give a summary of the literature on Pt-Sn/Al₂O₃ and Pt/SnO₂ systems. It is clear that the majority of the research on Pt-Sn/Al₂O₃ has been devoted to subjects related to reforming due to its industrial importance. There is obviously controversy in the literature as to the state of Sn after reduction at elevated temperatures in the Pt-Sn/Al₂O₃ system. Factors such as the method of preparation appear to effect the reducibility of Sn and there appears to be a growing body of evidence that at least in some cases the Sn can be reduced to the metallic state and that a Pt-Sn alloy might sometimes be formed. The addition of Sn has been found to increase Pt dispersion, increase the selectivity for certain reactions and increase long term stability of Pt/Al₂O₃ catalysts, by suppressing reactions which would poison the catalyst. The Pt/SnO₂ system has been found to be effective for the catalysis of a number of reactions, most importantly the low temperature oxidation of CO. The Pt in Pt/SnO₂ systems has been found to be difficult to reduce, probably due to the formation of a substrate bonded Pt species, and various pre-treatments have been found affect catalytic activity. In the next sections the study on Pt-Sn/Al₂O₃ and Pt/SnO₂ samples and their activity for butane oxidation will be outlined.

4.2 Experimental

4.2.1 Preparation of Catalyst Samples

The preparation details and alpha numeric sample codes corresponding to each catalyst are summarised in Table 4.1. The letter "P" of the code indicates the presence of Pt, "S" indicates "Sn", "A" indicates that Al_2O_3 is the support, "SO" indicates that SnO_2 is the support and the letters in brackets indicate the pre-treatment the support has undergone as follows: "u" indicates that the support is untreated, "N1" indicates pre-treatment with 0.1M HNO_3 , "N2" implies treatment with 1.0M HNO_3 and "h" implies that support was pre-treated with 10M NaOH. In the case of "P1aSO", this indicates an acetone solution was used for Pt impregnation.

Pt/ SnO_2 catalysts were prepared containing nominally 5wt% Pt (PSO) or 1wt% Pt (P1SO and P1aSO). The dry pre-weighed SnO_2 (BDH, GPR grade) was placed in a round bottomed flask. A solution of $\text{H}_2\text{PtCl}_6 \cdot 6\text{H}_2\text{O}$ (Johnson Matthey) dissolved in either acetone or water, containing the required amount of Pt, was added to the SnO_2 . After mixing for 0.5h at room temperature, the solvent was removed using a rotary evaporator. When acetone was the solvent this involved heating at 318K for 0.5h, while for water, heating at 343K for 2h was used. After solvent removal samples were dried at 323K for 16h in an oven and calcined for 2h at 773K in a muffle furnace in a static air atmosphere. One Pt/ SnO_2 sample (PSO(h)) was prepared using pre-treated SnO_2 . The pre-treatment involved soaking the SnO_2 in 10 M NaOH for 0.5h at 363K. The SnO_2 was then washed with portions of milli Q water to remove excess NaOH and dried at 333K for 16 h in an oven prior to impregnation.

A series of Pt-Sn/ Al_2O_3 catalysts were prepared, with nominally 5wt% Pt and varying Sn contents (0 - 3wt%) by coimpregnation with aqueous solutions of $\text{H}_2\text{PtCl}_6 \cdot 6\text{H}_2\text{O}$ (Johnston Matthey) and stannic chloride, $\text{SnCl}_4 \cdot 5\text{H}_2\text{O}$ (M & B Ltd, >95% purity). The Al_2O_3 fibre "Saffil" was used as supplied by I.C.I. (Runcorn) in mat form. The specifications for the material have been given previously in Sec. 2.1. Impregnation was achieved by spraying the Al_2O_3 mat with a very fine spray of the required Pt - Sn solution. The volume of solvent used was 25cm^3 per gram Al_2O_3 mat. The sample was dried in an oven at 313K for 16h prior to calcination. Calcination was carried out in static air at 773K for 2h in a muffle furnace. Again a number of samples were prepared with Al_2O_3 supports pre-treated with HNO_3 (Riedel de Haen, GPR Grade). The pre-treatment involved spraying the mats with either 0.1 M or 1.0M HNO_3 , $25\text{cm}^3 \text{ g}^{-1} \text{ Al}_2\text{O}_3$, and then washing with warm milli Q water until the washings were ca. pH7. The mats were then dried in an oven at 343K for 16h prior to impregnation.

Table 4 1: Preparation Details for Pt/Al₂O₃, Pt-Sn/Al₂O₃ and Pt/SnO₂ Catalysts

Code	Pt wt%	Sn wt%	Support	Support Pre-treatment	Impregnation Method	Calcination
PA(u)	5	0	Al ₂ O ₃	None	spray impregnated with H ₂ PtCl ₆ (aq)	0 25h @ 903K in air
PS0 3A(u)	5	0 3	Al ₂ O ₃	None	spray coimpregnated with H ₂ PtCl ₆ (aq) & SnCl ₄	2h @ 773K in air
PS1A(u)	5	1 0	Al ₂ O ₃	None	As PS0 3A(u)	As PS0 3A(u)
PS3A(u)	5	3 0	Al ₂ O ₃	None	As PS0 3A(u)	As PS0 3A(u)
PS0 3A(N1)	5	0 3	Al ₂ O ₃	Washed with 0 1M HNO ₃ , washed with warm milli Q H ₂ O, dried at 343K for 16h	As PS0 3A(u)	As PS0 3A(u)
PS1A(N1)	5	1 0	Al ₂ O ₃	As PS0 3A(N1)	As PS0 3A(N1)	As PS0 3A(N1)
PS1A(N2)	5	1 0	Al ₂ O ₃	As PS0 3A(N1) except 1 0M HNO ₃ Used	As PS0 3A(N1)	As PS0 3A(N1)
S3A(u)	0	3 0	Al ₂ O ₃	None	Spray impregnated with SnCl ₄	As PS0 3A(u)
PSO	5	----	SnO ₂	None	H ₂ PtCl ₆ (aq) added to the dry SnO ₂ Solvent removed using rotary evaporator	As PS0 3A(u)

Table 4 1. (contd)

Code	Pt wt%	Sn wt%	Support	Support Pre-treatment	Impregnation Method	Calcination
PSO(h)	5	----	SnO ₂	Soaked in 10M NaOH at 363K for 0 5h rinsed with milliQ H ₂ O	As PSO	As PSO
PISO	1 0	----	SnO ₂	None	H ₂ PtCl ₆ (aq) added to the dry SnO ₂ Solvent removed using rotary evaporator	2h @ 773K
P1aSO	1	----	SnO ₂	none	H ₂ PtCl ₆ with acetone as solvent added to the dry SnO ₂ Solvent removed using a rotary evaporator	2h @ 773K
A(N1)	----	----	Al ₂ O ₃	Washed with 0 1M HNO ₃ , washed with warm milli Q H ₂ O, dried at 343K for 16h	None	None

4 2 2 Aging Studies

Aging studies were carried out on a number of samples Powdered samples were placed in porcelain crucibles and then placed in a preheated muffle furnace at 1073K for 8h in a static air atmosphere

4 2 3 X-ray diffraction Measurements

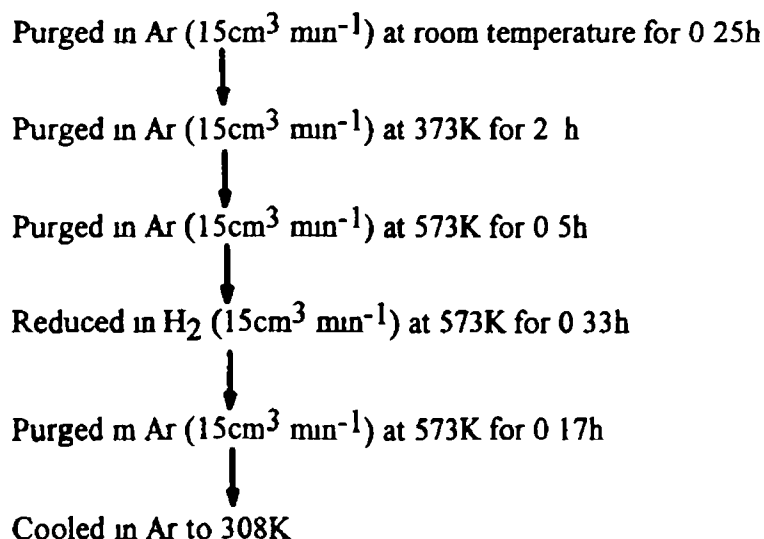
A Philips 1400 series X-ray diffractometer was used to obtain the XRD spectra The X-ray source was a copper source, $K\alpha$, $\lambda = 1.5405\text{\AA}$ Powdered samples were loaded into the sample holder which was then placed into the instrument for analysis

4.2.4 X-ray Photoelectron Spectroscopy

XPS measurements were carried out in the University of Ulster, Coleraine, using a Kratos XSAM 800 instrument. The excitation source used was an Al anode operating at 120 watts (10 mA and 12 kV). Catalyst samples were presented as powders dusted onto double-sided adhesive tape mounted on stainless steel sample studs. Due to the insulating nature of the samples, the resulting surface charging had to be partially compensated by using low energy UVs flood source. Further corrections for charging were made by using the position in the spectra of the C1s line and subtracting the difference between this value and the accepted value for the adventitious hydrocarbon C1s line at 285 eV from the other peak positions. For each sample examined, a survey scan from 1100 eV to 0 eV and expanded energy range scans of the most intense elemental peaks were obtained.

4.2.5 Hydrogen Chemisorption Measurements

The instrumental details used for chemisorption measurements have already been given in Sec. 3.1.3, together with the accuracy and consistency of the measurements. However for the Pt-Sn/Al₂O₃ and Pt/SnO₂ samples a different pre-treatment scheme was developed compared to the scheme used for the monometallic Pt samples in Ch. 3. In order to develop a pre-treatment scheme which gave the maximum H₂ uptake for Pt-Sn/Al₂O₃ samples, sample PS3A(u) was analysed after various pre-treatment procedures. The results for H₂ uptake together with the pre-treatment schemes used are summarised in Table 4.2. The pre-treatment scheme which gave the greatest H₂ uptake, 28 $\mu\text{mol g}^{-1}$ of sample, was used for the pre-treatment prior to H₂ chemisorption measurement for the other Pt-Sn samples. The details of the optimum pre-treatment scheme are given over below.



4.2.6 BET Surface Area Analysis

The experimental details for BET surface area analysis were identical to those used in Ch 2

4.2.7 DSC Activity Measurements

The instrumental details for this technique have already been given in Sec 3.1.6. An air (reagent grade, I I G Ltd) / 1-butane (CP grade, Air Products Ltd) was passed over 1 mg of powdered sample and 1 mg of α -Al₂O₃ reference material in the DSC furnace at a rate of 19.8 cm³min⁻¹. The mixture was passed over the sample for ca 0.18h prior to heating in order to achieve a homogeneous gas mixture. The furnace was then heated at 10K min⁻¹ to 573K and held at that temperature for 0.5h prior to cooling to room temperature. The light off temperature was measured three times for each sample, with the first value for the light off temperature being approximately 20K higher than for runs 2 and 3 which agreed within \pm 2K. The average value for runs 2 and 3 was used to determine the light off temperature. Duplicate samples of each catalyst were examined and values for light off temperature differed by less than \pm 10K.

Table 4.2: Summary of Preparation Methods Prior to Chemisorption and the Resulting H₂ Uptake for Sample PS3A(u)

Initial Purging Treatment in Ar (cm ³ min ⁻¹)	Reduction in H ₂ (15 cm ³ min ⁻¹)	Final Purging Treatment in Ar (cm ³ min ⁻¹)	H ₂ Uptake (μ mol g ⁻¹)
0.25h @ rt*, followed by 2h @ 373K and then 0.5h @ 523K	0.33h @ 373K	0.17h @ 473K	18.0
As above	0.33h @ 473K	As above	23.4
As above	0.33h @ 573K	0.17h @ 573K	28.1
As above	0.33h @ 673K	0.17h @ 673K	20.9
0.25h @ rt*, followed by 0.25h @ 323K, then 1h @ 373K and 1h @ 523K	1h @ 523K, then 2h @ 573K	0.25h @ 573K	20.1
As above	1h @ 523K, then 2h @ 673K	0.25h @ 673K	17.4

* rt = room temperature

4 2 8 Atomic Absorption Spectroscopy

Atomic absorption spectroscopy (AAS) was used to determine Pt and Sn contents of Pt-Sn/Al₂O₃ and Pt/SnO₂ samples. Analysis was carried out using a Varian Spectrophotometer. Sn analysis was carried out using a N₂O-acetylene flame, while for Pt an air-acetylene flame was used. The instrumental conditions used for Pt and Sn analysis are given in Table 4 3. Samples underwent digestion prior to analysis so that free Pt and Sn could be analysed. The digestion process involved the addition of 1cm³ of hydrofluoric acid, HF, (Merck, GPR grade) to a preweighed catalyst sample in a plastic beaker. The weight of sample was adjusted to give Pt and Sn contents of the order of 20 ppm after digestion. After HF had broken up the Al₂O₃ fibre, 5cm³ of aqua regia was added to the sample which was then boiled to near dryness. After cooling to room temperature the sample was then redissolved in 1cm³ conc HCl (Riedel de Haen, GPR Grade). The digested sample was made up to 100cm³ in milli Q water in a volumetric flask. For Pt analysis HCl and lanthanum chloride, LaCl₃ (Spectrosol) were added to prevent interference problems, with all solutions prepared to contain concentrations of 0.1M HCl and 200 ppm La³⁺ (including standards). Standard curves were prepared with solutions containing Pt and Sn concentrations within the linear working range of 0 to 150ppm Pt and 0 to 40ppm Sn. PtCl₂ (Spectrosol) and SnCl₂ (Spectrosol) were used to prepare these standards. In order to estimate the loss of Pt or Sn during the digestion procedure a 100ppm Sn solution and 100ppm Pt solution were analysed by AAS after the normal digestion procedure. In addition, a sample containing 100ppm Pt and 30ppm Sn was examined after digestion in order to determine whether either element interfered with the analysis of the other element. The effect of interference was found to be negligible. For Sn the error in the digestion process was $\pm 10\%$. The error in Pt digestion was lower, $\pm 8\%$. All samples and standards were analysed in triplicate and in random order.

Table 4 3 · Experimental conditions for atomic absorption analysis of Pt-Sn catalysts

Element	Light Source	Wavelength (nm)	Slit Width (nm)	Flame Description
Pt	Pt/hollow cathode	265.9	0.5	Air-acetylene, oxidising, fuel lean, blue
Sn	Sn/hollow cathode	284.6	0.2	N ₂ O-acetylene, reducing, fuel rich, red

4.3 Results and Discussion

AA analysis

AA analysis results are given in Table 4.4. The majority of the determined values for Pt and Sn contents were in agreement with the corresponding nominal values. However, sample PS1.0A (N2) had a very low Pt content, although the determined Sn value for this sample was in good agreement with the nominal value. It would appear that the pre-treatment of the Al_2O_3 support with 1.0M HNO_3 decreased the uptake of Pt, but not Sn, during impregnation. The concentration of HNO_3 would also seem to be important as pre-treatment of the Al_2O_3 support with lower concentrations of HNO_3 did not affect the Pt uptake. It is possible that the NO_3^- species occupied adsorption sites normally occupied by PtCl_6^{2-} anions and at higher NO_3^- concentrations progressively less of these adsorption sites would be available to the PtCl_6^{2-} anions and eventually a drop in Pt uptake might occur. Since the determined value for Sn was in agreement with the nominal value, the above theory could only be correct if the Sn was preferentially adsorbed on the Al_2O_3 surface compared with Pt and there was no interaction between the Pt and Sn in the impregnating solution prior to impregnation. Sexton et al (12) found that there was a strong interaction between Al_2O_3 and Sn and Burch (7) found that contacting a commercial Pt/ Al_2O_3 catalyst with a SnCl_4 solution led to displacement of much of the Pt compound present on the Al_2O_3 surface by Sn. Therefore it is feasible that Sn could be preferentially adsorbed on the Al_2O_3 surface. As to an interaction between Pt and Sn in the impregnating solution, a number of studies have been reported in the literature on this subject. According to Alt et al (92), who studied the interactions of H_2PtCl_6 and SnCl_2 in acetone solutions, and Shitova et al (93) who carried out a similar study in isopropanol solutions, H_2PtCl_6 was rapidly reduced by SnCl_2 and PtSn complexes were formed. Baronetti et al (26) found that $\text{H}_2\text{PtCl}_6/\text{SnCl}_2$ co-impregnating solutions change colour from yellow to dark red due to formation of Pt, Sn complexes. In all the above mentioned studies HCl in varying concentrations was also present. In this study, no HCl was present in the impregnating solution, SnCl_4 was used rather than SnCl_2 , there was no change in the colour of the impregnating solution (which remained yellow) and the impregnating solution was used shortly after preparation, i.e. ca 1 min. Therefore an interaction between the Pt and Sn solution, prior to impregnation may not have occurred.

For the Pt/ SnO_2 samples, pre-treatment of the SnO_2 support at 363K in 10M NaOH had little effect on the uptake of Pt during impregnation with similar values for Pt content being exhibited by PSO and PSO(h). This was in contradiction to work carried out by a number of workers (46, 47) who found that this pre-treatment resulted in enhanced uptake of Pt, compared with unpre-treated SnO_2 .

Table 4 4· AAS Results for Pt-Sn/Al₂O₃ and Pt/SnO₂ Samples.

Sample Code	Pt Content Theoretical (wt%)	Pt Content Determined (wt%)	Sn Content Theoretical (wt%)	Sn Content Determined (wt%)
PA(u)	5 0	4 5	0 0	0 0
PS0 3A(u)	5 0	4 8	0 3	0 3
PS1A(u)	5 0	4 9	1 0	0 9
PS3A(u)	5 0	4 9	3 0	2 8
PS0 3A(N1)	5 0	4 8	0 3	0 3
PS1A(N1)	5 0	4 8	1 0	1 0
PS1A(N2)	5 0	4 3	1 0	0 8
PSO	5 0	5 0	-----	-----
PSO(h)	5 0	4 9	-----	-----
P1SO	1	0 9	-----	-----

XPS Analysis

XPS analysis was carried out on aged (at 1073K for 8h in static air) and unaged samples of PS0 3A(u), PSO and PA(u). The spectra obtained are illustrated in Fig 4 6 to 4 8. Difficulty was encountered in analysing the data for the Al₂O₃ supported samples due to the overlap of the Pt4f and Al2p peaks in the region between 70 0eV and 80 0eV binding energy.

Fig 4 6(a) and Fig 4 6(b) illustrates the XPS spectra for unaged and aged PA(u) samples. The main features of the spectra were the O Auger peak at ca 975 0eV, the O1s peak at ca 525 0eV, the C1s peak at ca 290 0eV and the Al2p and Pt4f peaks in the region of 70 0eV to 80 0eV. Fig 4 6(c) shows an expanded energy range scan in the Pt4f region for both aged and unaged PA(u) samples. For the unaged sample the overlap of the Pt4f and Al2p peaks is clearly visible, the small shoulder at the low binding energy side of the envelope representing the Pt4f species, with the main contribution from the Al2p peak from the substrate material. The fact that the shoulder is in the region of 72 0eV, indicates that the Pt is not present as Pt (0) on the surface as according to the literature (14) the binding energies for bulk crystalline metallic peaks are 70 9eV and 71 3eV respectively. The spectrum in this region for the aged sample shows a slight increase in the intensity of the Pt4f shoulder and a shift in the Al2p peak to a slightly higher binding energy. There is little or no difference in the intensity or the area of the O1s peaks exhibited by the aged and unaged samples. Therefore it would appear that aging at 1073K caused a slight change in the composition of the Pt surface, but did not bring about an increase in the oxygen content of the surface.

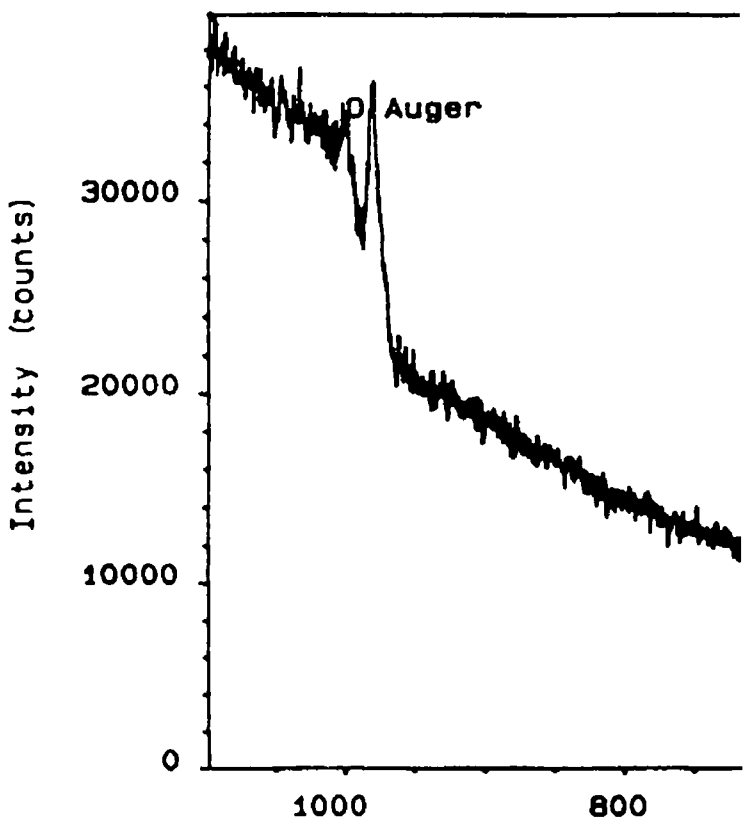
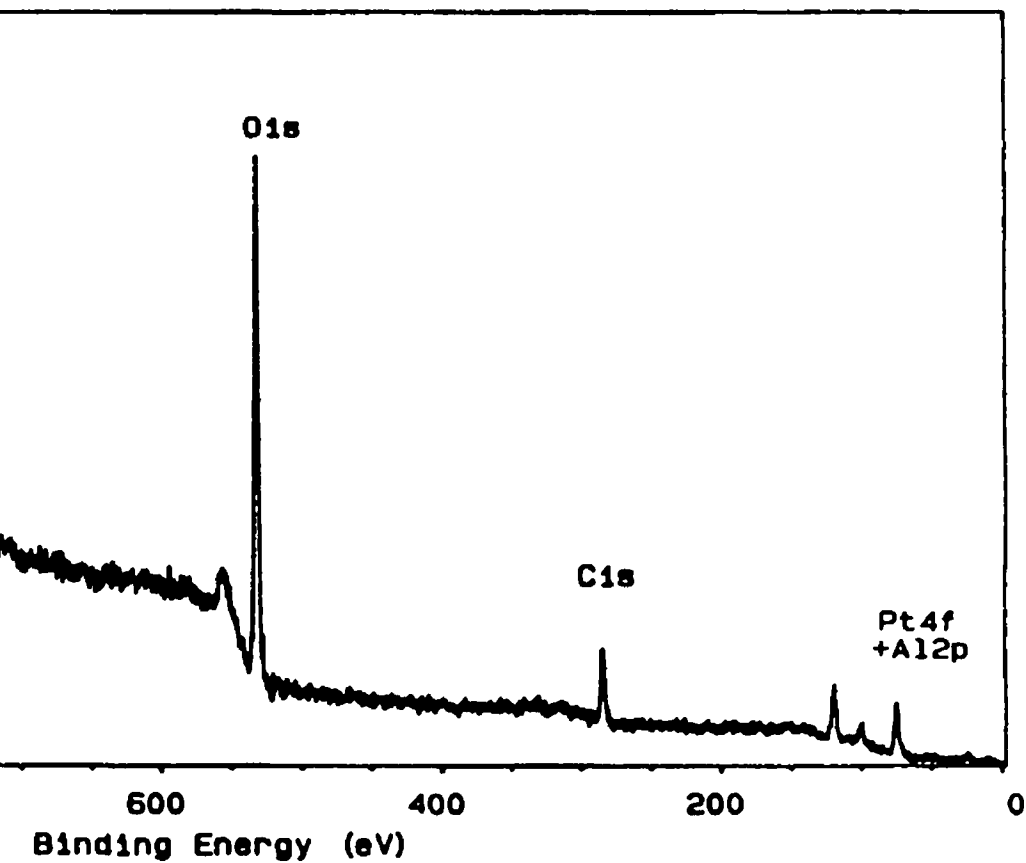


Fig 4 6 (a) XPS spectrum of PA(u) unaged.



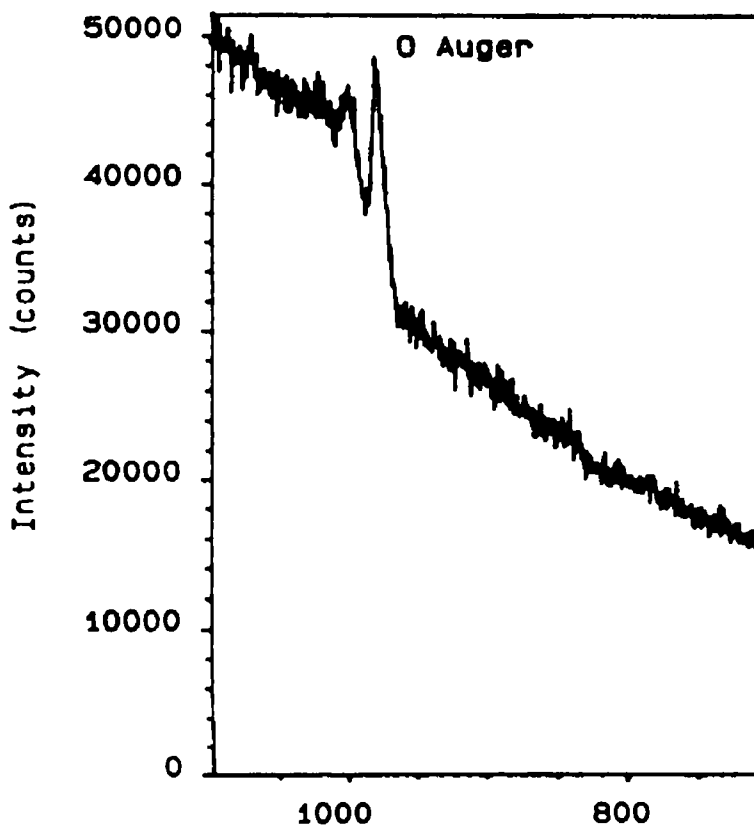
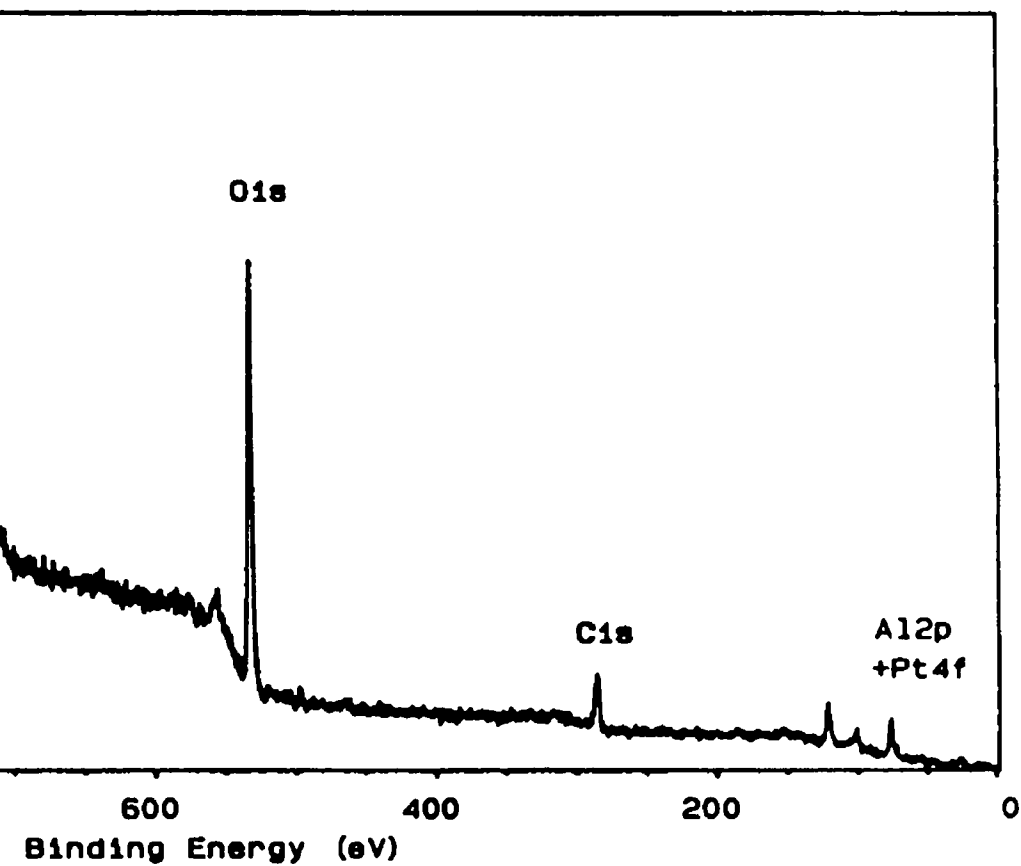


Fig 4.6 (b) XPS spectrum of PA(u) aged at 1073K for 8h



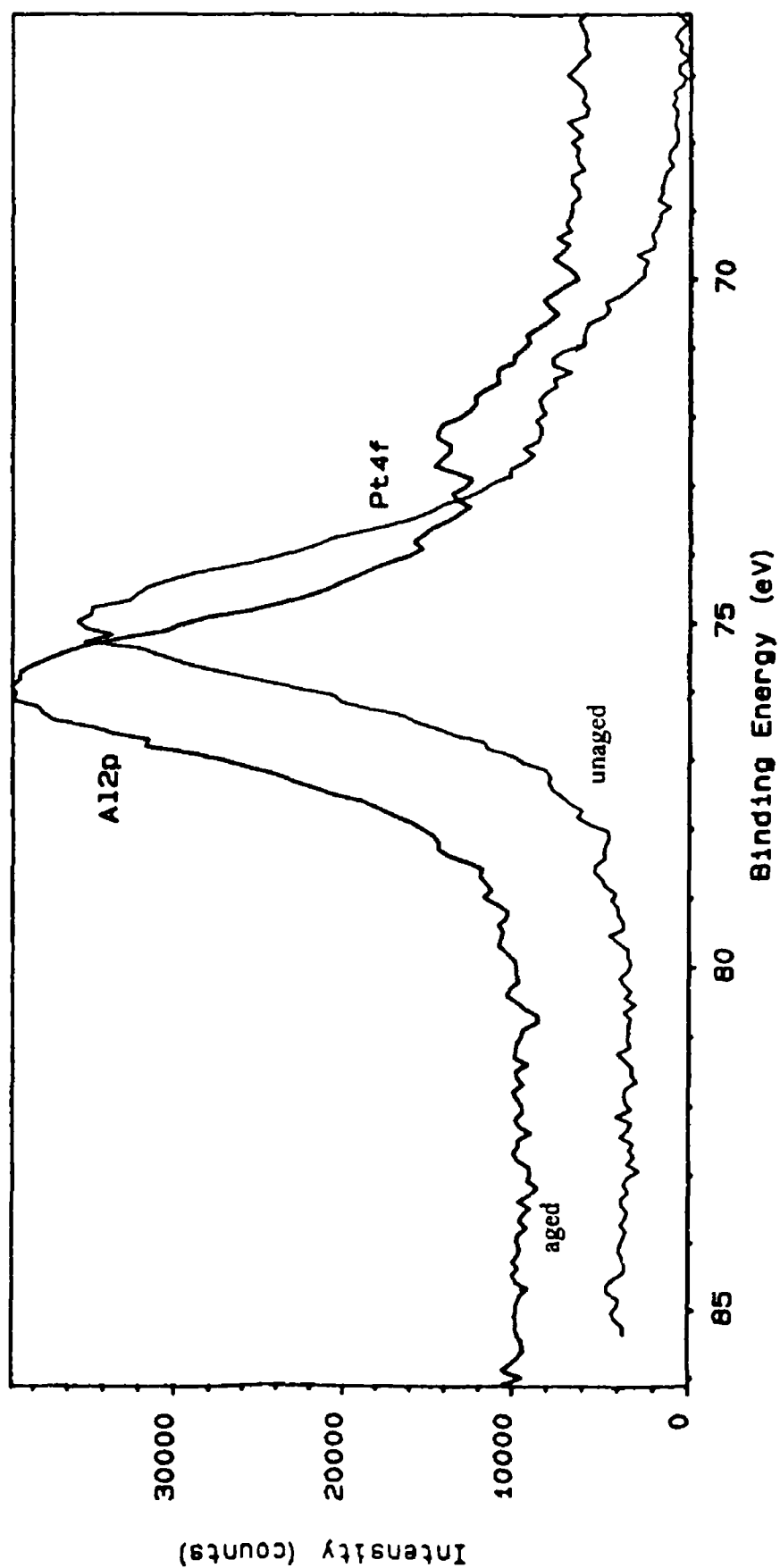


Fig.4.6 (c) XPS spectrum showing an expanded energy range scan in the Pt4f region for both aged and unaged PA(u) samples.

The XPS spectra for an unaged and aged sample of PS0 3A(u) are illustrated in Figs 4 7(a) to 4 7(d). Again the main spectral features in Figures 4 7(a) and 4 7(b) are the O Auger peak, the O1s peak, the C1s peak and the Pt4f and Al2p peaks. In addition, a doublet is present in the region between 500 0eV and 483 0eV due to Sn3d bands, Fig 4 7(c). The peak maxima are at 475 0eV and 487 5eV, corresponding to Sn3d_{3/2} and Sn3d_{5/2} respectively. There is no indication of a peak in the region of 484eV, the position reported in the literature for metallic Sn (12, 16, 18, 19). This is hardly surprising since the sample did not undergo any reduction treatment. The peak in the region of 487 5eV probably represents the presence of Sn (II) and/or Sn (IV) species. This peak is broad and the maximum at 487 5eV is at a slightly higher binding energy than that reported in the literature (12, 19, 24) for Sn oxides. It has been tentatively proposed by other workers (24) that this peak at a higher binding energy was due to the presence of a Sn-aluminate species. The spectrum in the Pt4f region is obscured by the overlap of the Al2p signal, with a single peak at 75 0eV being present, see Fig 4 7(d). The spectrum obtained for the aged PS0 3A(u) sample, differed only slightly from that exhibited by unaged samples. There is a slight decrease in intensity of the Sn3d peaks compared with the corresponding peaks exhibited by the unaged samples. It thus appears that there was little alteration in the Sn surface during aging at 1073K. In the Pt4f region, Fig 4 7(d) there is a difference between the spectra for the unaged and aged PS0 3A(u) samples. For the aged sample a distinct shoulder between 73 0eV and 70 0eV appeared in addition to the main Al2p peak at 75 0eV. In the literature the peak positions for metallic Pt crystallites and Pt-O-Sn species have been reported at 71 3eV and 72 3eV respectively (14) and it might be concluded that the shoulder represents the presence of some of the above species on the surface. However a similar peak was present in the aged PA(u) sample spectrum, Fig 4 6(c) which did not contain Sn so that assignment of the shoulder in the spectrum of the aged PS0 3A(u) as being due to the presence of a Pt-O-Sn species may not be correct. In fact for both PS0 3A(u) and PA(u) spectra the overlap of the Al2p peak makes the elucidation of the state of Pt in the samples very difficult and all that can be concluded is that there is a change in the Pt surface upon aging.

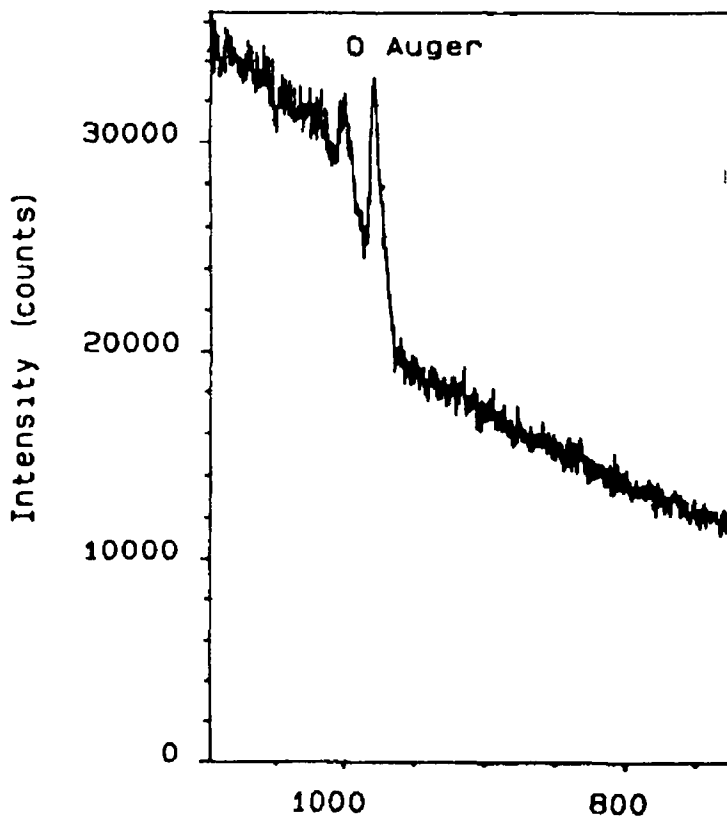
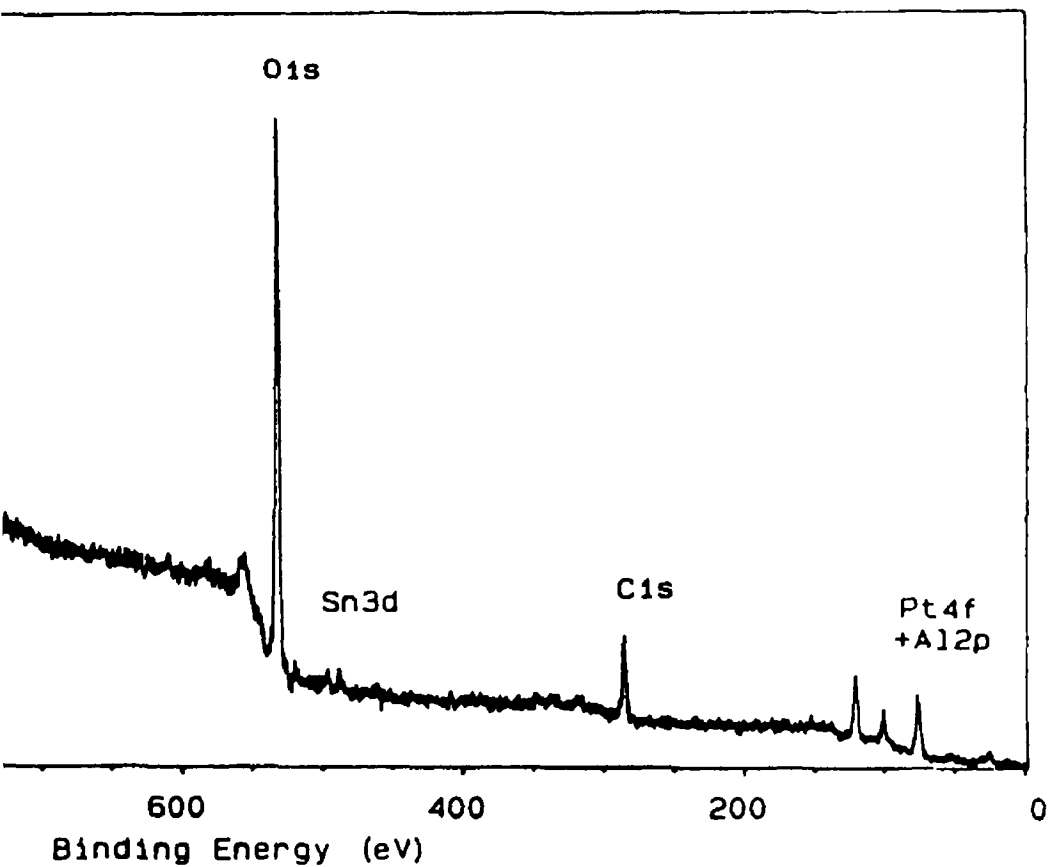


Fig 4.7 (a) XPS spectrum for PS0.3A(u) unaged.



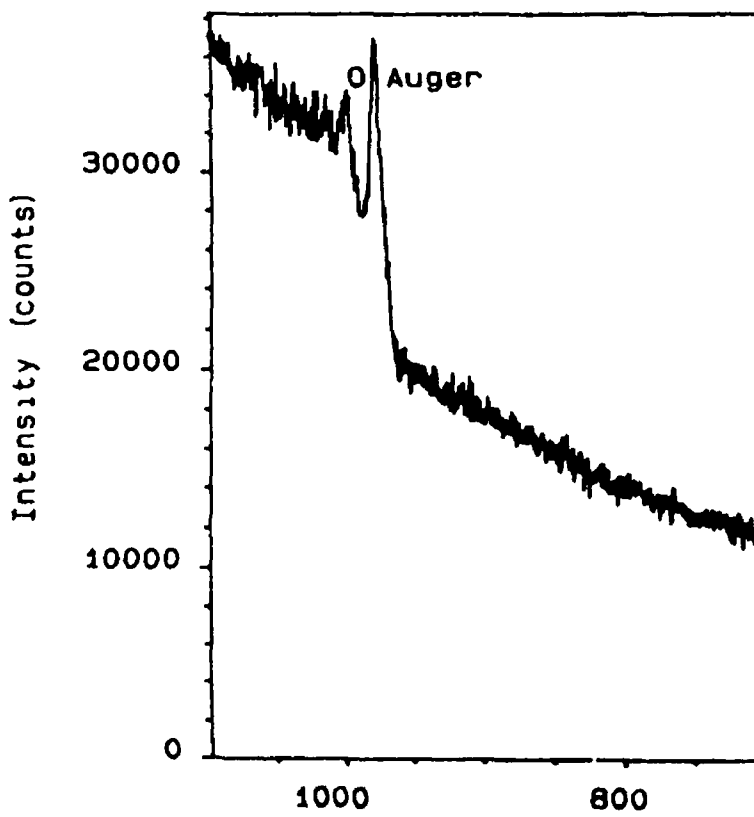
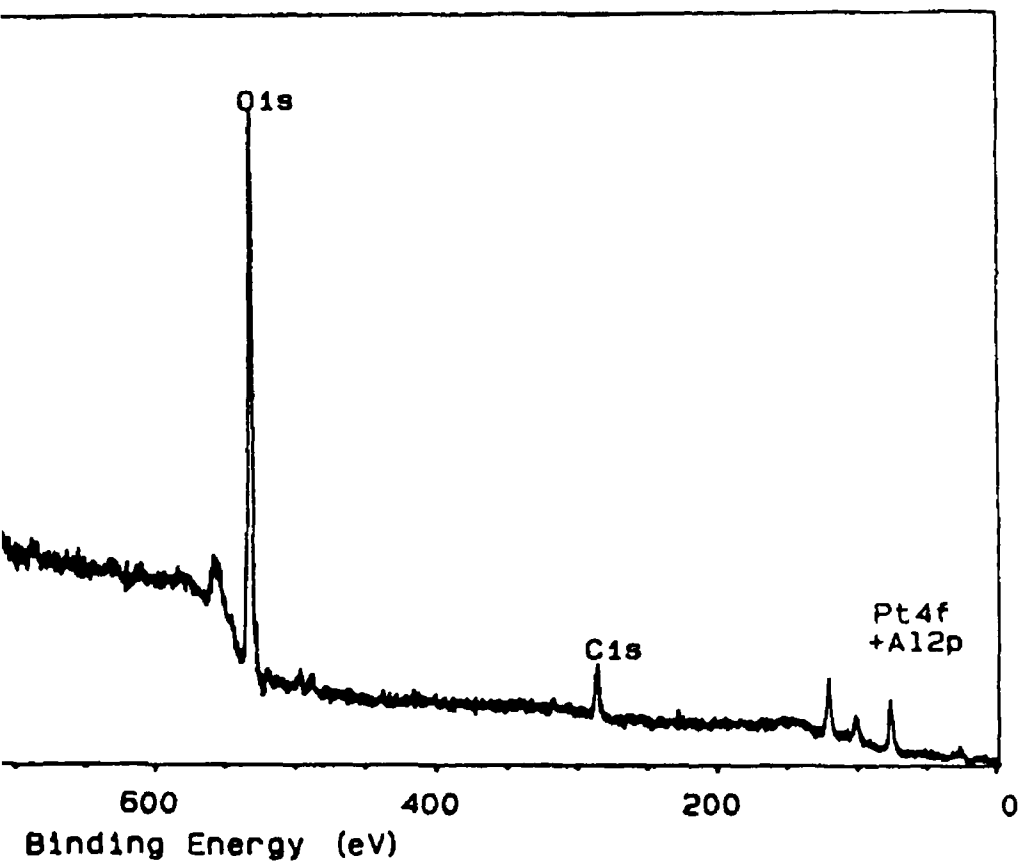


Fig 4.7 (b) · XPS spectrum of PS0 3A(u) aged at 1073K for 8h



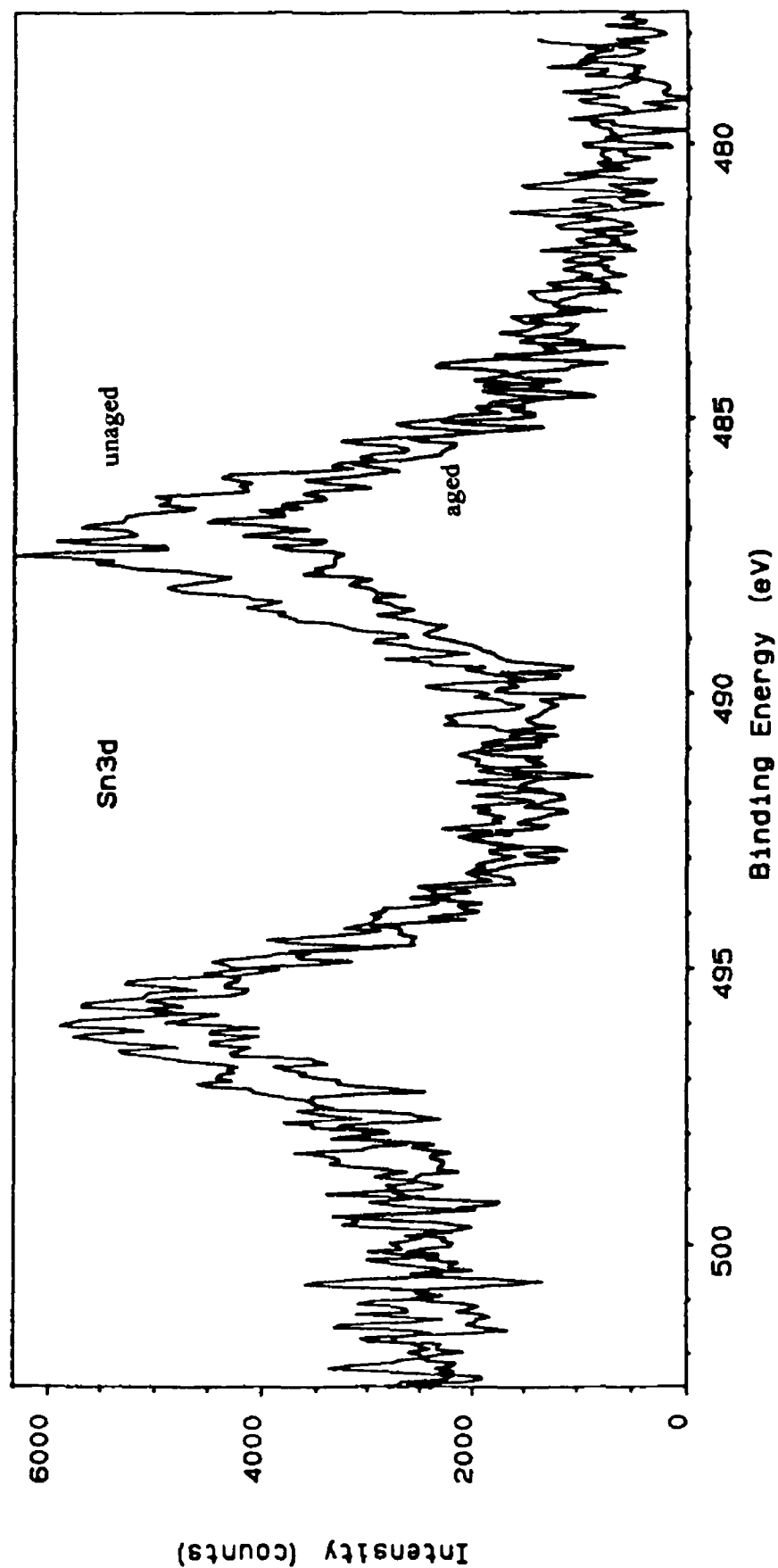


Fig 4 7 (c) : XPS spectrum showing an expanded energy range scan in the Sn3d region for both aged and unaged PS0 3A(u) samples

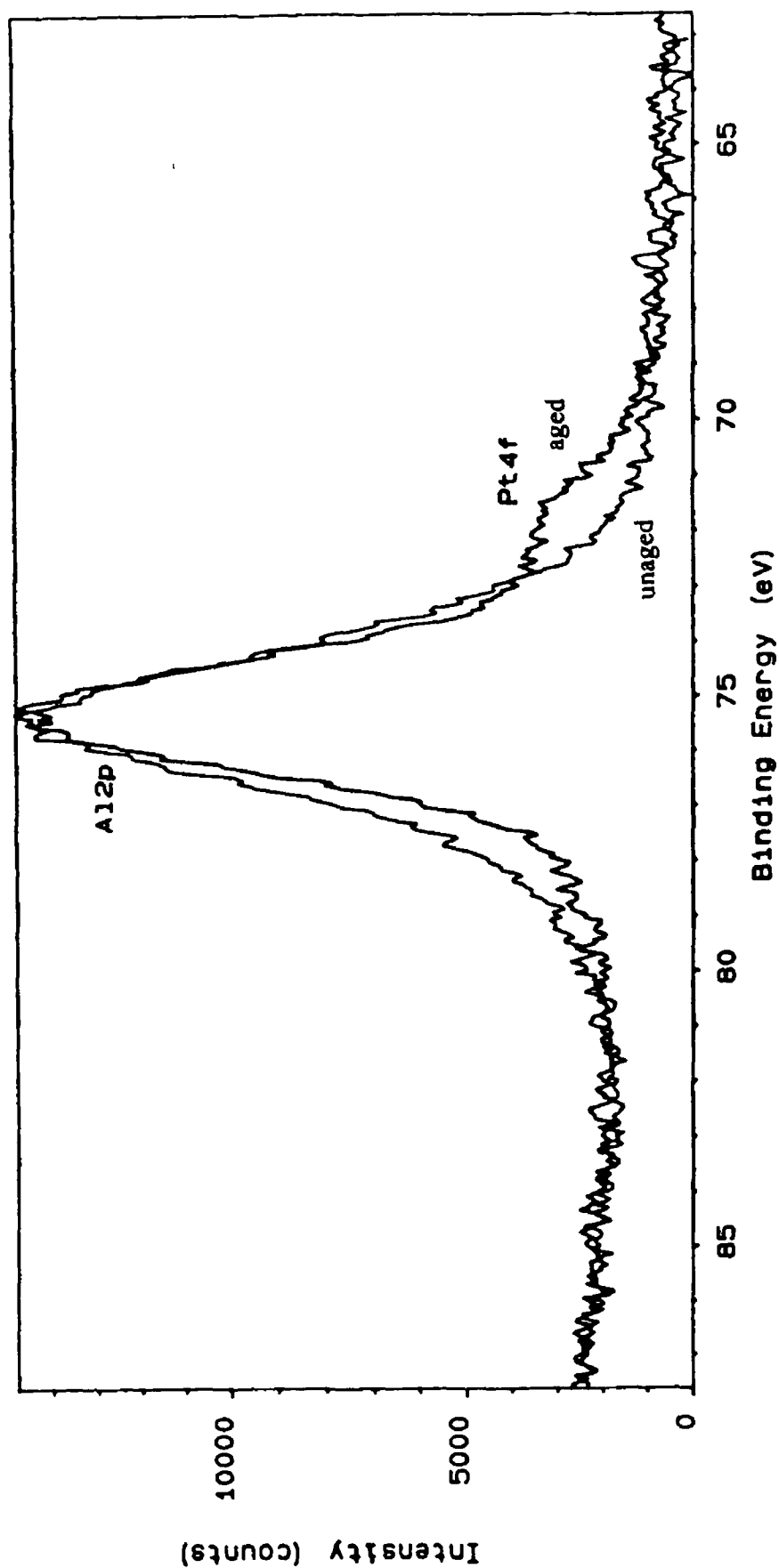


Fig 4.7 (d) XPS spectrum showing an expanded energy range scan in the Pt4F region for both aged and unaged PS0.3A(u) samples.

The spectra for aged and unaged samples of PSO are illustrated in Figs 4 8(a) to 4 8(d). The main differences between the spectra for these samples and those for the aged and unaged samples of PA(u) and PS0 3A(u) are the presence of an Sn Auger peak at 1100 0eV, the much greater intensity of the Sn3d peaks at about 480 0eV, see Fig 4 8(c) and the absence of a Al2p peak, Fig 4 8(d) in the spectra for samples of PSO. For an unaged PSO sample, the Sn3d peaks at 486 6eV and 495 5eV are sharp and intense. There is no evidence for the presence of metallic Sn, indicated by a peak at 484 0eV (18). It is clear from the intense peak at 486 7eV that the vast majority of the Sn was in the form of Sn(II) and/or Sn (IV). The Pt4f region of the spectrum from 80 0eV to 70 0eV contains three peaks overlapping, see Fig 4 8(d). The main peak is at 75 0eV, with two shoulders of lower intensity at ca 78 0eV and ca 72 0eV. The complexity of the Pt4f envelope indicates contributions from Pt in at least two oxidation states. A very similar spectrum for the Pt4f region was obtained by Hoflund et al (14) for Pt-Sn-O films supported on Al₂O₃. In their study a deconvolution procedure was used to subtract the contribution of the Al2p peak, based on the height of the Al2p peak at 120 0eV. They found three prominent features at binding energies of 72 3eV, 75 0eV and 78 0eV. The peak at 72 3eV was assigned to a Pt-O-Sn species, while that at 78 0eV was believed to be caused by the presence of PtO and PtO₂. Finally the peak at 75 0eV was assigned to the presence of PtO, PtO₂ and Pt-O-Sn (14). Similar results have been reported by Cox et al (47) for Pt/SnO₂. It would therefore appear that a similar assignment could be made for the unaged PSO sample. Certainly the absence of substantial peaks at 70 9eV or 71 3eV (the peak positions reported in the literature (14) for bulk and crystallite metallic Pt respectively) would indicate that if metallic Pt was present, it was in small amounts. The existence of Pt(OH)₂ can be discounted as it is known to decompose at 423K (94) and therefore should have been destroyed during calcination at 773K.

Quantification of the data from the XPS spectrum for unaged PSO was carried out using peak areas after subtraction of a suitable background and the appropriate sensitivity factors (due to the overlap of the Pt4f and Al2p peaks for the Al₂O₃ supported samples, this was only carried out for the SnO₂ supported sample). The relevant results are given in Table 4 5. The surface was found to contain 4 3 wt%Sn, 28 wt%Pt and 20%O with the remainder being composed of adventitious C.

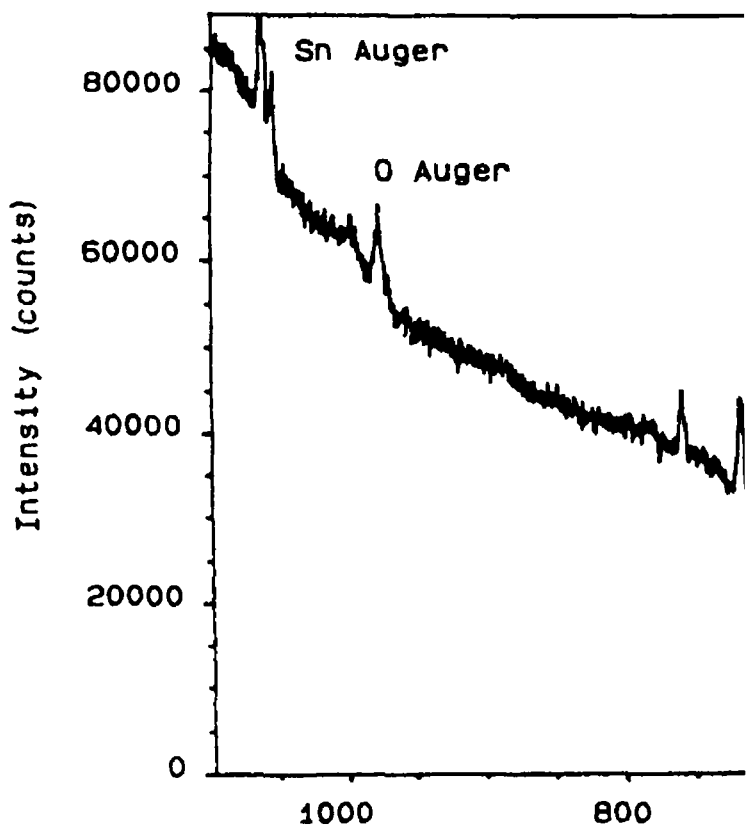
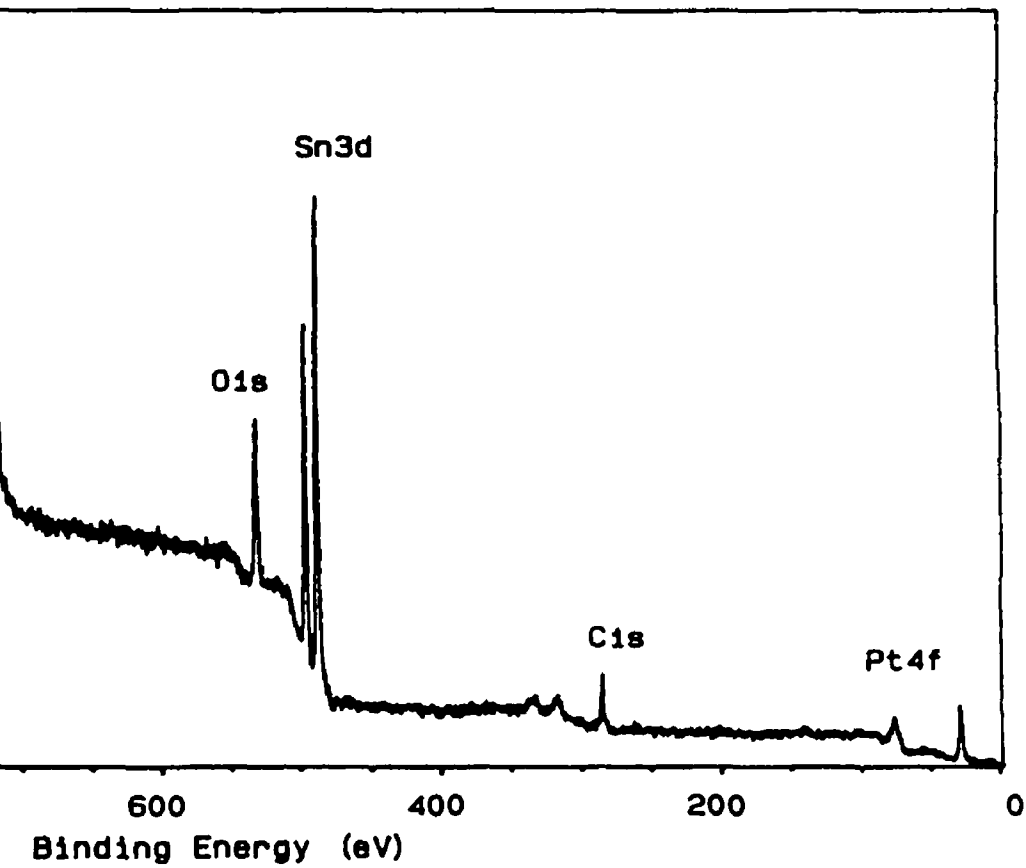


Fig 4 8 (a) - XPS spectrum of PSO unaged



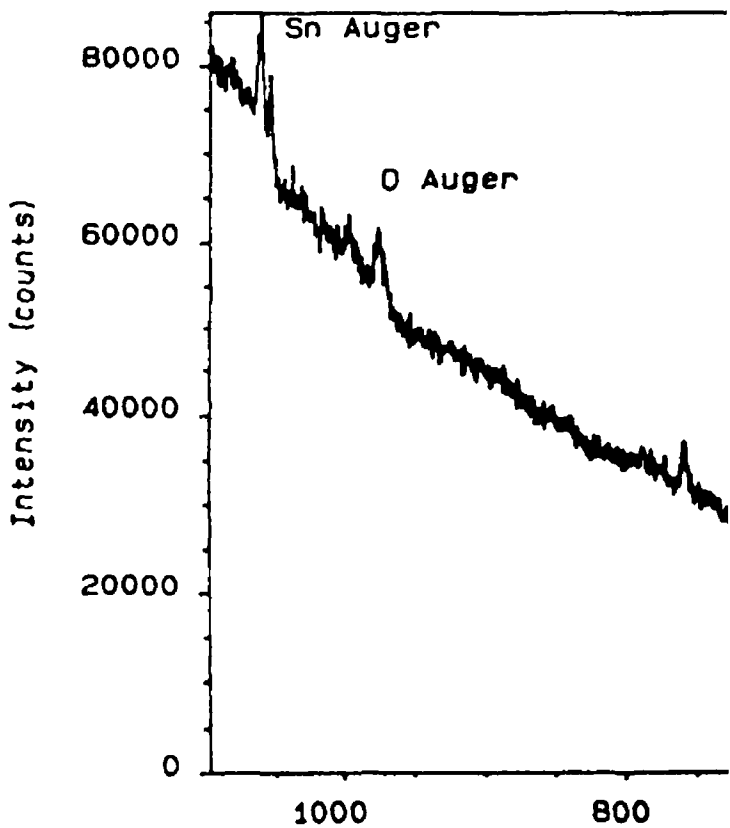
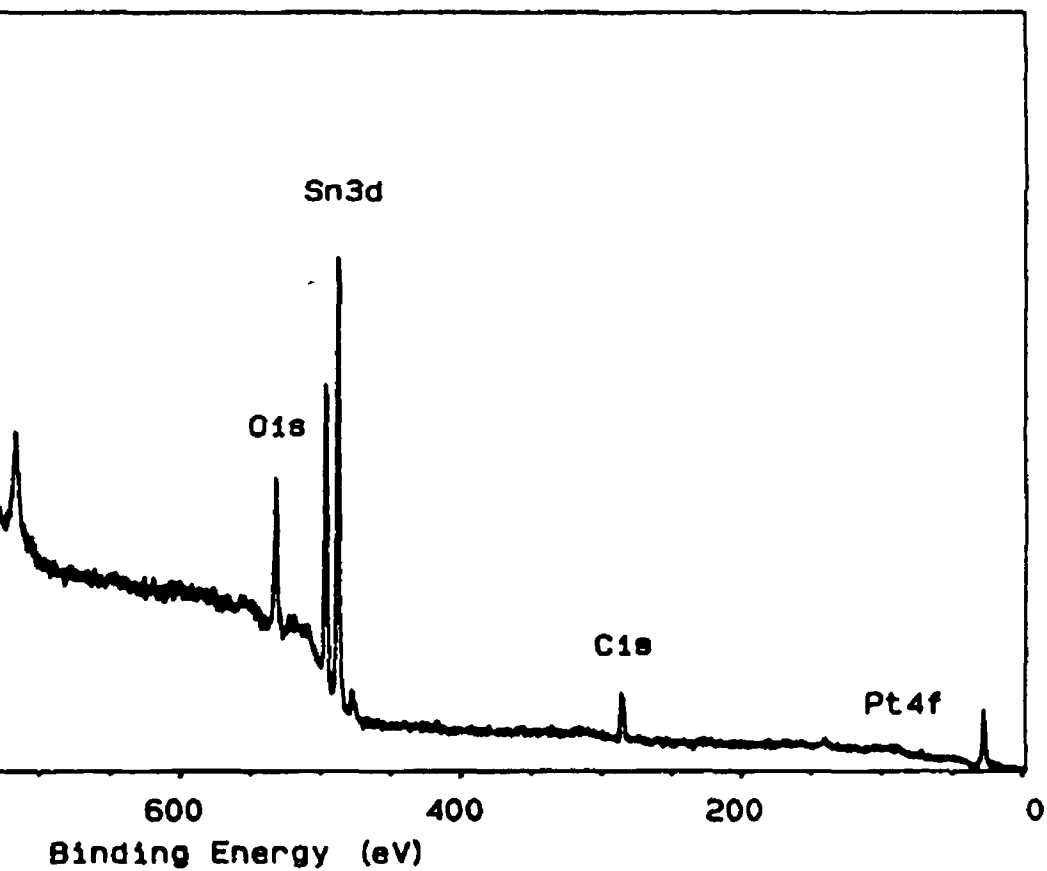


Fig.4.8 (b) XPS spectrum of PSO aged for 8h at 1073K.



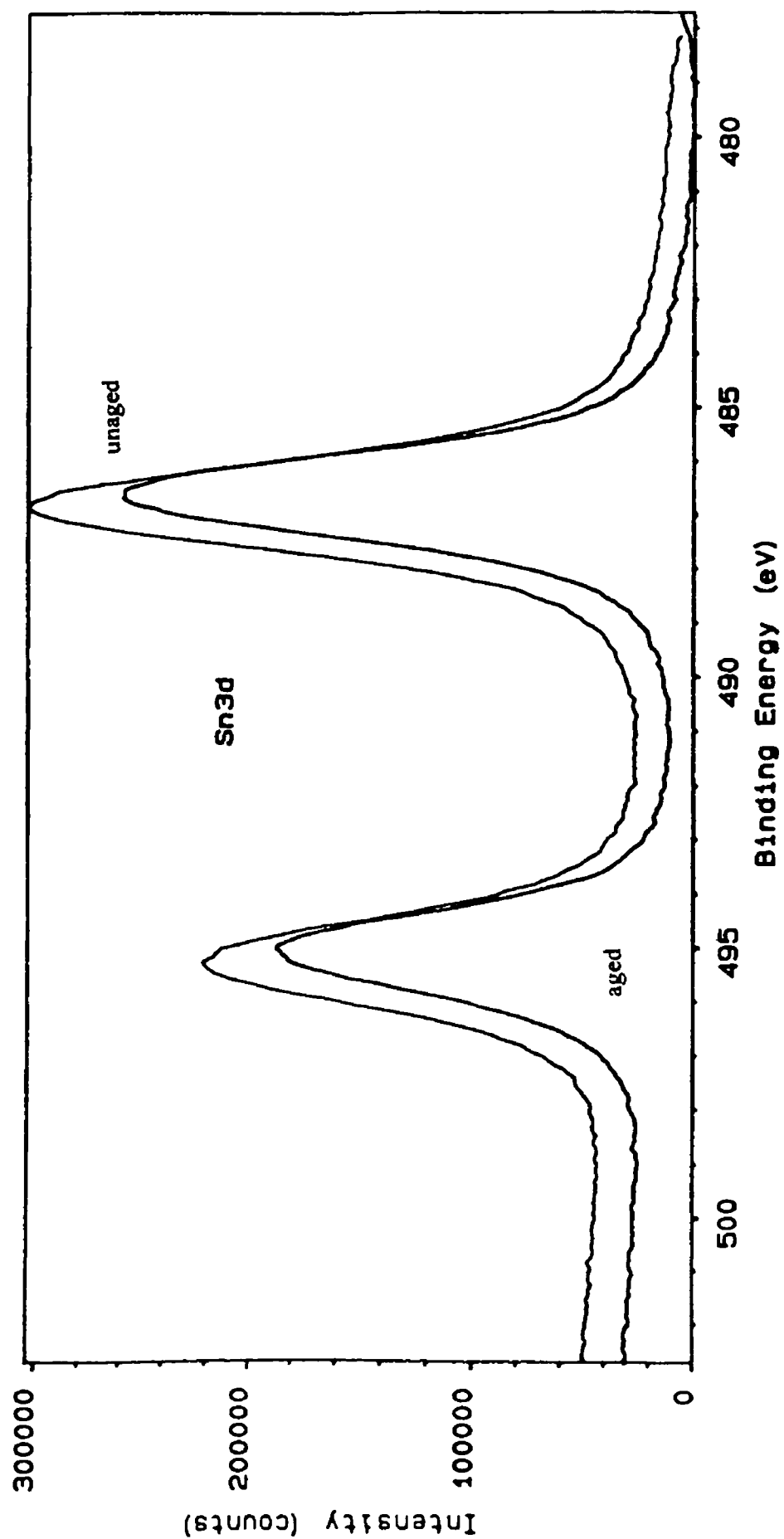


Fig.4 8 (c) XPS spectrum showing an expanded energy range scan in the Sn3d region for both aged and unaged PSO samples.

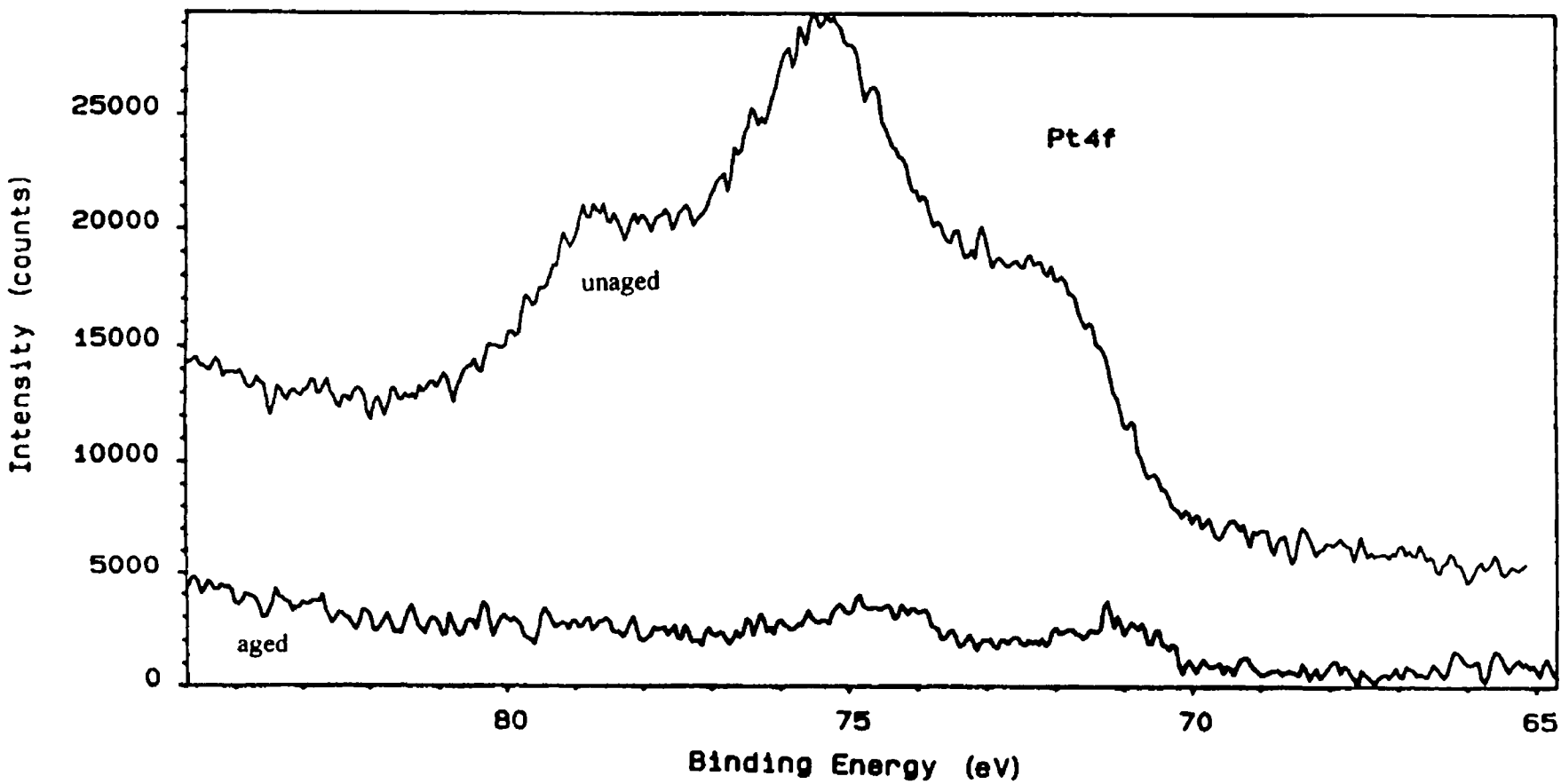


Fig.4.8 (d) : XPS spectrum showing an expanded energy range scan in the Pt4f region for both aged and unaged PSO samples

Table 4 5 · Quantitative XPS Data for Unaged PSO Sample

Element	Position (eV)	Width (eV)	Area	Quant Factor	Atomic Conc (%)	Mass Conc (%)
C1s	285.06	1.94	11625	0.24	30.52	9.29
O1s	530.86	2.22	48074	0.61	49.66	20.13
Sn3d	486.91	1.91	129244	5.75	14.16	42.61
Pt4f	75.36	5.35	17321	1.93	5.66	27.97

Aging of the PSO sample brought about major changes in the catalyst surface, as illustrated by the XPS spectra given in Fig 4 8(d). There is little change in the O1s peak, although the Sn3d are decreased slightly in intensity. However, there appears to be a major loss of Pt from the surface upon aging, with peaks of much lower intensity in the Pt4f region. Because of the low intensity the peaks are difficult to interpret, but it appears there are two peaks, at 75eV and 71eV. Quantification of the XPS data for the aged PSO sample was carried out, see Table 4 6. The Pt surface content dropped to 2wt% upon aging, with the Sn and O contents increasing to 56wt% and 27wt% respectively.

Table 4 6 Quantitative XPS Data for an aged PSO Sample

Element	Position (eV)	Width (eV)	Area	Quant Factor	Atomic Conc (%)	Mass Conc (%)
C1s	285.05	2.24	11929	0.24	35.70	14.61
O1s	530.90	2.16	42591	0.61	50.15	27.32
Sn3d	486.70	1.83	110521	5.75	13.81	55.82
Pt4f	71.30	0.32	914	1.93	0.34	2.26

To summarise, the XPS results would appear to suggest that aging had little effect on either the PA(u) sample or the PSO 3A(u) sample. Unfortunately, the state of Pt in both these samples could not be determined due to the overlap of the Pt4f and Al2p peaks. Sn appears to be in the form of Sn(II) and/or Sn(IV) in both aged and unaged samples of PSO 3A(u) with the possibility of a Sn aluminate species also being present. There is no evidence for the presence of metallic Sn. The XPS data for unaged PSO indicates that the surface of this sample is composed of SnO, SnO₂, Pt oxides and Pt-O-

Sn species The interaction between Pt and Sn is probably due to this Pt-O-Sn bond, as suggest by Hoflund and co-workers (14) for the surface of Pt-Sn-O films on Al_2O_3 Upon aging there is a dramatic loss of Pt from the surface and an increase in surface Sn content, possibly suggesting thermal degradation of the support during aging at 1073K leading to encapsulation of the surface Pt by Sn oxides In both aged and unaged samples of PSO there was no evidence for the presence of metallic Sn

XRD analysis

XRD measurements were carried out on a number of samples, the diffraction patterns illustrated in Figs 4 9 to 4 11 The diffraction pattern for the Al_2O_3 support material is shown in Fig 4 9 (a) As previously mentioned in Sec 2 2, the relative intensity of the diffraction peaks at $2\theta = 67.05^\circ$, 45.85° and 37.5° indicate that the major phase present is $\eta\text{-Al}_2\text{O}_3$, although a certain amount of $\gamma\text{-Al}_2\text{O}_3$ may also be present since many of the peaks in diffraction patterns of both phases coincide and differ only in relative intensity

Fig 4 9(b) illustrates the diffraction pattern for sample S3A(u), 3 0wt% Sn supported by Al_2O_3 It is similar to the pattern for the Al_2O_3 support material and contains no peaks due to Sn, SnO_2 or SnO or other Sn species The Sn particles may be very small, $<2\text{nm}$, and cannot be detected Another possibility is that some or all of the Sn is in some amorphous form on the support, perhaps Sn aluminate species

The diffraction pattern for the monometallic sample, PA(u), is shown in Fig 4 9(c) The pattern contains peaks due to Pt at $2\theta = 39.8^\circ$, 46.2° , 47.5° , 81.3° and 85.7° together with peaks for the Al_2O_3 support However, the (311) - Pt peak at $2\theta = 81.3^\circ$ is the only Pt diffraction line clearly distinguishable from the support material peaks Aging had little effect according to the XRD evidence, the only difference in the diffraction pattern for PA(u) aged at 1073K for 8h (Fig 4 9 (d)) being an increase in intensity of the Pt peaks compared with the corresponding peaks in the diffraction pattern for the unaged samples

The diffraction pattern for an unaged sample of PS3A(u) was identical to that exhibited by unaged PS0 3A(u) and no peaks indicative of the presence of any Pt or Sn species, including oxides or alloys, see Fig 4 10(a), can be distinguished from the background of the Al_2O_3 support There is no evidence for the presence of SnO_2 or SnO despite the fact that the XPS results for PS0 3A(u) indicated that Sn was present on the surface as Sn(II) or Sn(IV)

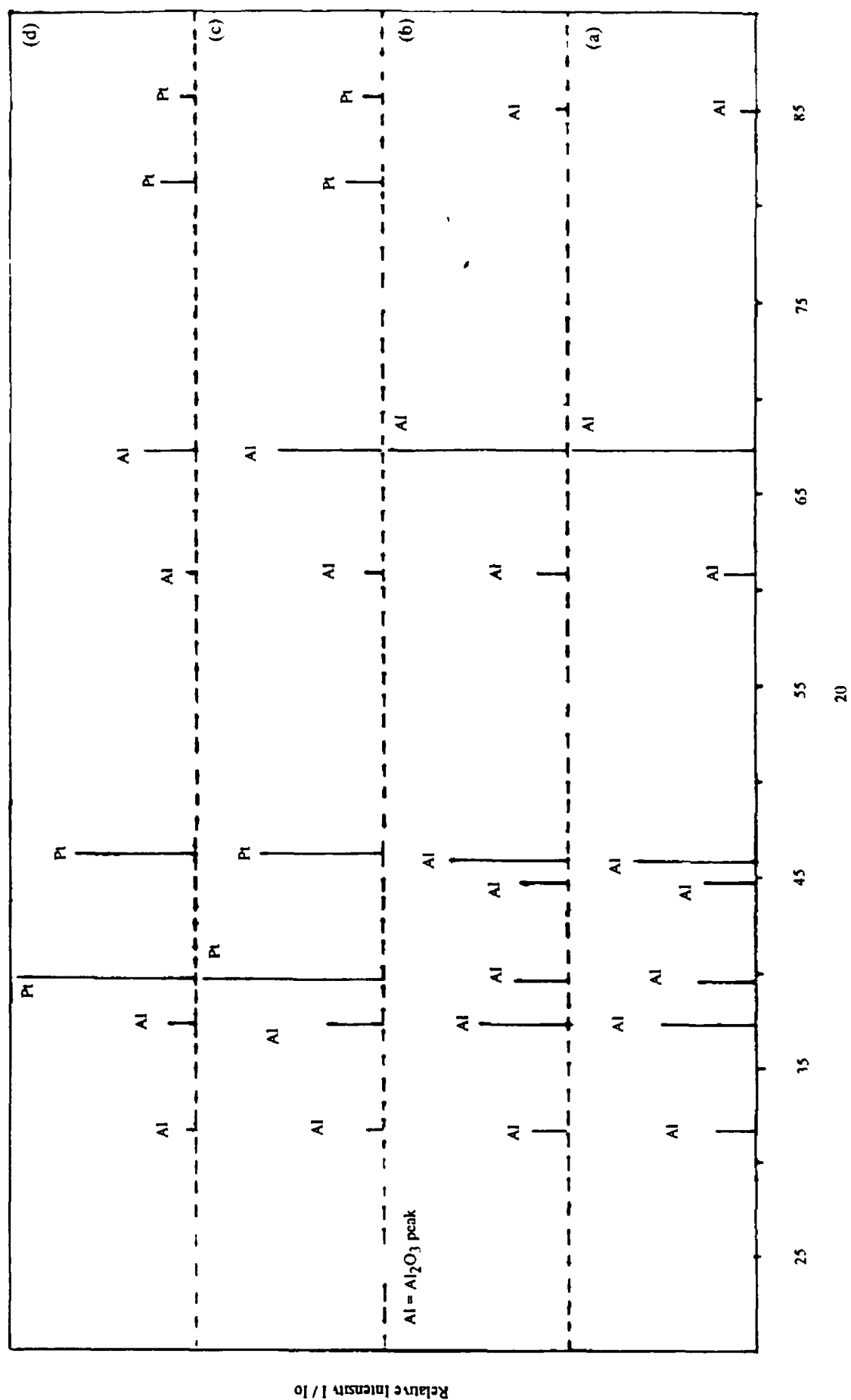


Fig 4 9. XRD pattern for (a) Al_2O_3 support, (b) S3A(u), (c) PA(u) and (d) PA(u) aged at 1073K for 8h Al represents $\eta\text{-Al}_2\text{O}_3$ peak.

It is possible that Pt or Sn is in some physical form undetectable by XRD. However the most likely cause is that the Pt and Sn particles are of a very small size, less than 2 nm (31), and thus cannot be detected by XRD. The XRD pattern for an aged PS3A(u) sample appears to confirm this theory, see Fig.4.10(b), in the case of Pt at least. The presence of Pt diffraction peaks of quite high intensity would suggest that aging caused an increase in Pt particle size due to sintering and hence was detectable by XRD. The apparent decrease in the intensity of the peaks for the Al₂O₃ support material in Fig.4.10(b) is due to an increase in the intensity of the Pt peaks rather than a drop in Al₂O₃ peak intensities.

In order to examine the effect of reduction in H₂, samples PA(u), PS0.3A(u) and PS3A(u) were examined by XRD after treatment in H₂ at different temperatures. All the patterns were obtained when the samples had been exposed to the atmosphere for at least 1h, i.e., no in situ reduction treatments were carried out. The diffraction patterns for PS3A(u) and PS0.3A(u) after reduction in H₂ for 0.33h at 573K, are illustrated in Figs.4.10(c) and 4.10(d) respectively, contain no evidence for the presence of Pt-Sn alloys, including PtSn₄, PtSn₂, Pt₃Sn, PtSn₃, or other Sn species. In the case of PS3A(u), Fig.4.10(c), the pattern is similar to that for the Al₂O₃ support. However, the diffraction pattern for PS0.3A(u) reduced at 573K, Fig.4.10(d) contained a peak at $2\theta = 39.8^\circ$ which is sharper than the broad peak in that region due to the Al₂O₃ support and this may be due to the presence of (100)-Pt peak superimposed on the diffraction peak for the support material. The diffraction patterns for PS0.3A(u) and PS3A(u) after reduction at 773K for 1h were again identical (see Fig.4.11(a) for PS3A(u)). The sharp peak at 39.8° was also present in the diffraction patterns for PS0.3A(u) and PS3A(u) reduced in H₂ at 773K for 1h, again probably indicating the presence of a certain amount of metallic Pt. No peaks for either Pt or Sn species can be distinguished in these XRD patterns. XRD studies in the literature on reduced Pt-Sn/Al₂O₃ samples have reported no evidence for the presence of Sn species, other than Pt-Sn alloys, and the remainder of the Sn in one study up to 65% (31) was postulated to be in an X-ray amorphous form, as a shell layer with a structure similar to Sn aluminate (30, 31, 32). This could be the case here, although another possibility is that the Sn particles are too small to be detected by XRD. There is no evidence for Pt-Sn alloys in reduced PS0.3A(u) and PS3A(u) samples. It must be remembered however that the XRD studies in the literature which reported evidence for alloy formation during reduction of Pt-Sn/Al₂O₃ samples all utilised either an in situ reduction step or passivation step in helium after reduction, prior to analysis (30, 31, 32). The air sensitivity of Pt-Sn alloys has been reported by Li et al. (24). They studied the state of Pt and Sn in Pt-Sn/Al₂O₃ after in situ reduction in H₂ by XPS. They were examining whether or not metallic Sn was formed during reduction which they claimed was a prerequisite for alloy formation. Although they found that metallic Sn was formed after in situ reduction at 648K in H₂, subsequent exposure of the sample to atmosphere for only 10 minutes at room temperature was adequate to

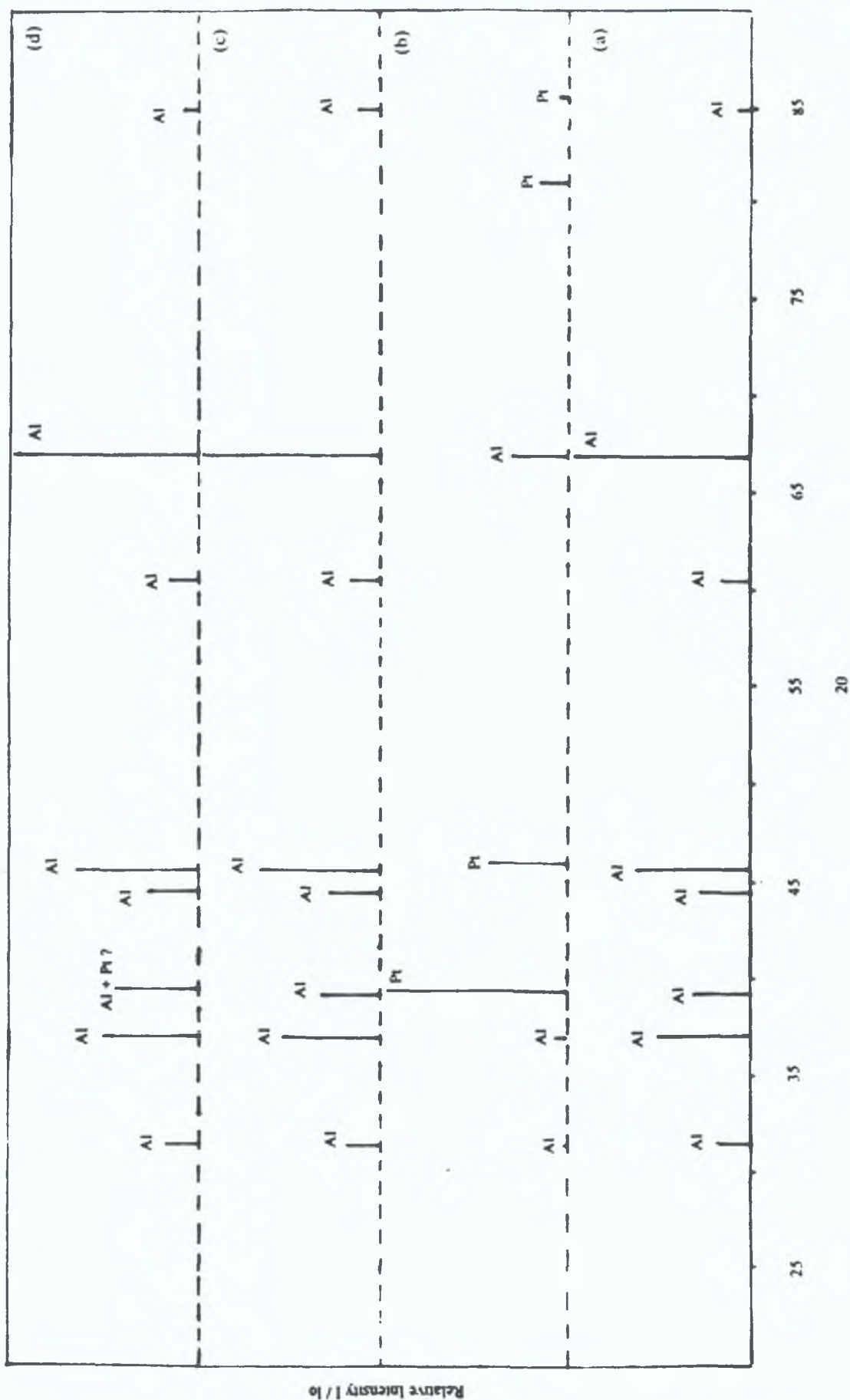


Fig.4.10 : XRD patter for (a) PS3A(u), (b) PS3A(u) aged at 1073K for 8h, (c) PS3A(u) reduced in H_2 at 573K for 0.33h and (d) PS0.3A(u) reduced in H_2 at 573K for 0.33h. Note Al represents η - Al_2O_3 peak.

eliminate XPS detectable metallic Sn. The absence of diffraction peaks for Pt-Sn alloys in the patterns for reduced Pt-Sn/Al₂O₃ samples, in this case might thus be explained by the fact that these samples were exposed to an air atmosphere for at least 1h prior to analysis.

In the diffraction pattern for PS3A(u) and PS0.3A(u) reduced at 773K, three peaks $2\theta = 38.5^\circ$, 41.7° and 65.1° were present which could not be assigned, Fig 4.11(a). However these peaks were also present in the diffraction pattern for PA(u) treated in the same way (see Fig 4.11(b)) and may be related to the reduction of some component of the support material. Fig 4.11(c) represents the XRD pattern for the SnO₂ support material after calcination at 773K for 2h (the sample was calcined for comparison with PSO which was also calcined during preparation). The pattern indicates that support material is predominantly SnO₂ with no evidence for the presence of significant concentrations of SnO. The diffraction pattern for sample PSO is very similar except that the peaks at $2\theta = 39.8^\circ$, 46.4° and 67.6° can also be distinguished, due the presence of Pt, see Fig 4.11(d).

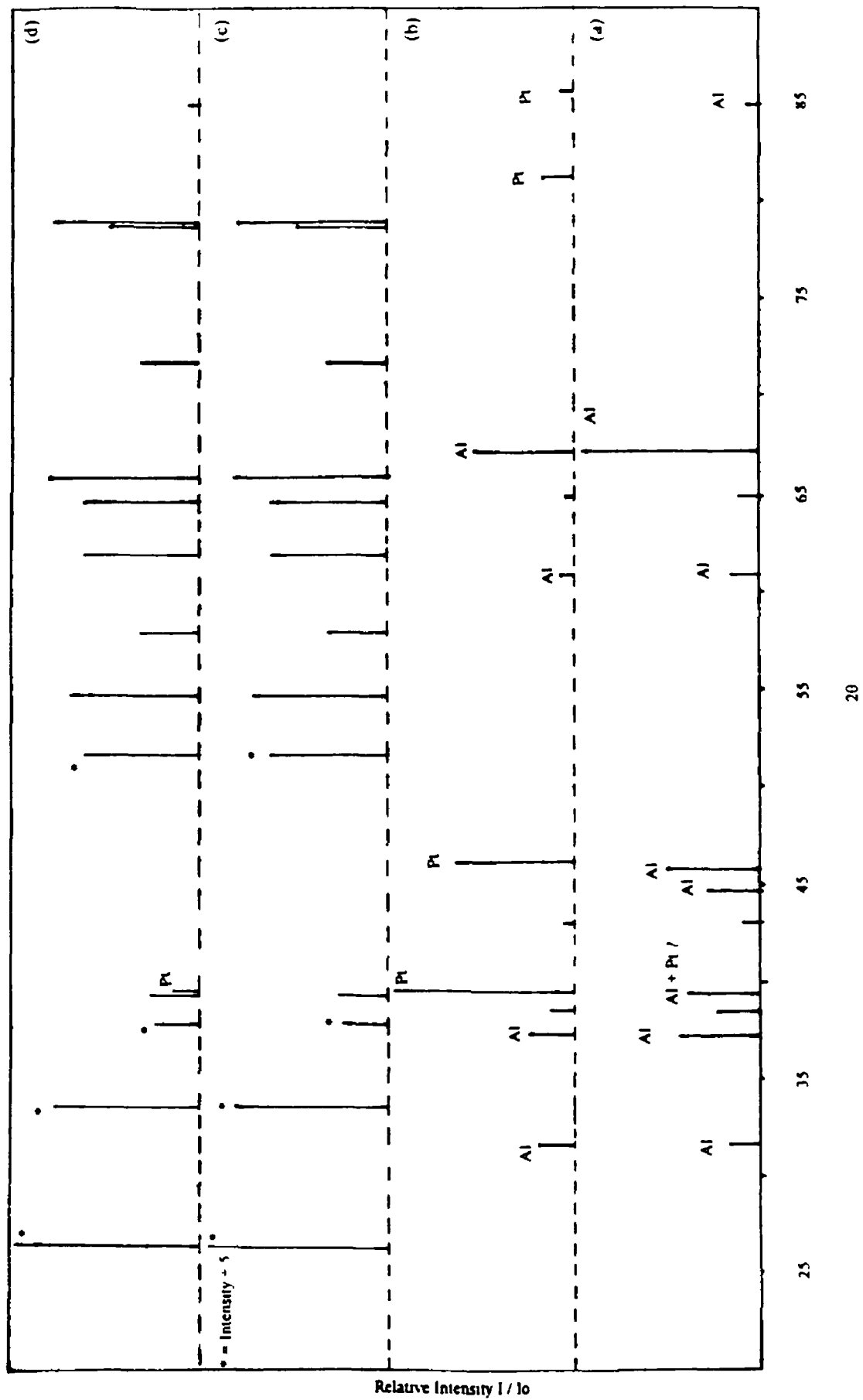


Fig 4 11 XRD pattern for (a) PS3A(u) reduced in H_2 for 1h at 773K, (b) PA(u) reduced in H_2 for 1h at 773K, (c) SnO_2 support material and (d) PSO . Al represents η - Al_2O_3 peak.

H₂ Chemisorption Analysis

The H₂ chemisorption results for Pt/Al₂O₃, Pt-Sn/Al₂O₃ and Pt/SnO₂ samples are given in Table 4.7, for both unaged samples and samples aged at 1073K for 8h. No attempt has been made to calculate Pt dispersions, Pt surface areas or Pt particle sites as for the Pt-Sn/Al₂O₃ samples the H : Pt chemisorption stoichiometry can not be assumed to be the same for all the samples examined. The presence of varying Sn contents will modify the Pt surface either changing the H₂ chemisorption stoichiometry or due to Pt - Sn alloy formation during reduction. Balakrishnan and Schwank (10) claimed that chemisorption measurements could not be used to calculate the average particle sizes of bimetallic particles especially where there was uncertainty as to the interaction between the two metals, since the two metals could form bimetallic clusters where the second metal could have a significant effect on the chemisorption of the primary metallic component.

It should first be pointed out that the reduction treatment regime prior to analysis had an effect on the results for H₂ uptake. It was mentioned in the experimental section of this chapter that the pre-treatment scheme prior to analysis was optimised using a PS3A(u) sample and the H₂ uptakes obtained using various reduction pre-treatments were given in Table 4.2. If this is re-examined, it is clear that reduction in H₂ at 573K for 0.33h gave the maximum H₂ uptake, while reduction at higher or lower temperatures or for longer time periods at 573K or 673K, led to a decrease in H₂ chemisorption. The low H₂ uptake exhibited by the samples reduced at temperatures below 573K may be explained by incomplete reduction of the Pt in the samples. From TPR studies monometallic Pt/Al₂O₃, Pt reduction has been reported to occur at various temperatures including 513K (28), 540K (7), 558K (9) and 568K (8) depending on the study. TPR profiles for Pt-Sn/Al₂O₃ samples have been found by Burch (7) to contain two main peaks and the first, assigned to Pt and some Sn reduction, occurred at temperatures between 560K (7), see Fig.4.1. Therefore, it is highly probable that reduction at temperatures less than or equal to 473K was insufficient to completely reduce all the Pt in the sample and led to lower uptakes of H₂ during analysis.

However incomplete Pt reduction would not explain the decrease in H₂ uptake for samples reduced for longer time periods at 573K or at higher temperatures. One possibility is that the decrease in H₂ uptake was caused by Sn enrichment of the surface, as Sn, with a lower surface energy than Pt (10) might migrate to the surface, covering the Pt. However spectroscopic studies on various Pt-Sn alloys (20, 21, 22, 23) have found that reduction in H₂, for example at 573K for 1h (23), led to a loss of oxygen from the surface and migration of Pt to the surface, while oxidation at elevated temperatures (for example 475K (22)) led to the migration of Sn to the surface. In the case of Pt-Sn/Al₂O₃ samples, it has been reported that there is a very strong interaction between Sn and the Al₂O₃ support (7, 12). Therefore it appears improbable that Sn migration to the surface caused the drop in chemisorption. Another possibility is that the

formation of a Pt-Sn alloy under the more rigorous reduction condition led to a decrease in the H₂ uptake. Li et al. (19) reported alloy formation after reduction at 648K for 24h, while Davis et al. (20) reported alloy formation after reduction of a Pt-Sn/Al₂O₃ in H₂ at 648K for 1h. Srinivasan et al. (32) has also reported the presence of Pt-Sn alloys in Pt-Sn/Al₂O₃ samples after reduction at 773K for 16h. Hence it is possible with more stringent reduction conditions Pt-Sn alloy formation could occur prior to chemisorption analysis. A study by Verbeek and Sachtler (11) which examined the chemisorption of Pt-Sn alloys found that D₂ uptake was decreased on the alloys compared with monometallic Pt. Thus alloy formation may be a reason for the drop in H₂ uptake exhibited by PS3A(u) after reduction at 573K for 24h and at higher temperatures. Although there was no XRD or XPS evidence to support this theory this could be due to the fact that an in situ reduction technique was not used. It has already been pointed out that reduced Pt-Sn/Al₂O₃ samples are air sensitive (24) and exposure to air prior to spectral analysis could have affected the results.

Table 4.7 : H₂ Chemisorption Results

Sample Code	H ₂ Uptake Unaged ($\mu\text{moles g}^{-1}$)	H ₂ Uptake Aged@1073K for 8h ($\mu\text{moles g}^{-1}$)
PA(u)	42	2
PS0.3A(u)	71	10
PS1A(u)	60	2
PS3A(u)	24	10
PS0.3A(N1)	98	3
PS1A(N1)	94	11
PS1A(N2)	48	9
PSO	0	0
PSO(h)	0	0
PISO	0	0
PlaSO	0	0
A(u)	0	0
S3A(u)	0	0
A(N1)	0	0
PS3A(u) (reduced @ 773K for 8h)	5	12

The first point to note from Table 4 7 is that neither the Al_2O_3 support, the SnO_2 support or sample S3A(u) (containing solely Sn supported by Al_2O_3) absorbed detectable amounts of H_2 . Thus the chemisorption of H_2 by the other samples must be due to the presence of Pt.

No Pt/ SnO_2 sample was found to chemisorb detectable quantities of H_2 , irrespective of Pt loading, support pre-treatment, method of preparation or whether the sample was unaged or aged at 1073K. This could be due to Pt-Sn alloy formation during reduction prior to analysis. Gardener et al (2) found evidence for Pt-Sn alloy formation with Pt/ SnO_2 systems upon reduction by annealing under vacuum at temperatures ranging from 523K to 673K. In this study the samples were pre-reduced in H_2 at 573K, within the above temperature range. Verbeek and Sachtler (11) reported that intermetallic Pt-Sn alloys adsorb lower amounts of H_2 compared with monometallic Pt or in some cases adsorb no H_2 whatsoever. However it is more likely that the lack of H_2 chemisorption was due to incomplete reduction of the Pt in the Pt/ SnO_2 samples during reduction prior to analysis. Hughes and McNicol (45) studied Pt/ SnO_2 containing up to 10wt% Pt by TPR. They found that after calcination in air at 773K, the TPR profiles of Pt/ SnO_2 samples were devoid of any Pt features and concluded that Pt reduction could be occurring at the same temperature as SnO_2 , in the region of 680K, and that the calcination step led to the formation of a compound between Pt and SnO_2 , which was difficult to reduce. The pre-treatment reduction temperature prior to chemisorption analysis used in this study was over 100K lower than the temperature mentioned by Hughes and McNicol (45) for Pt reduction in Pt/ SnO_2 systems and therefore it appears that incomplete Pt reduction resulted in no detectable H_2 chemisorption in these samples.

For the Pt-Sn/ Al_2O_3 samples prepared using untreated Al_2O_3 , the addition of small amounts of Sn, less than or equal to 1wt%, increased the uptake of H_2 dramatically compared with PA(u) and the lower the Sn content the greater the uptake of H_2 . For unaged Pt-Sn/ Al_2O_3 samples prepared using untreated Al_2O_3 , the trend in order of increasing uptake of H_2 was

$$\text{PS0.3A(u)} > \text{PS1.0A(u)} > \text{PA(u)} > \text{PS3A(u)}$$

An increase in Sn loading up to 3wt% caused a drop in H_2 uptake compared with the uptake for the monometallic sample PA(u). Sample PS3A(u) had a H_2 uptake which was only 57% of the value for H_2 adsorption by sample PA(u). After reduction the Pt and Sn in the samples may have been in the form of bimetallic clusters or the Sn may have been in an ionic form stabilised by the Al_2O_3 support, in the vicinity of Pt atoms. For lower Sn loadings the Sn may have increased the dispersion of Pt atoms, hence increasing H_2 uptake, as has been suggested by a number of other workers, i.e. (7, 10). With the addition of greater than 1wt% Sn, excess Sn may have migrated to the surface.

of the Pt-Sn ensembles, decreasing the surface area of exposed Pt and thus causing a drop in H₂ chemisorption. Another possibility is that with higher Sn loading (i.e. 3wt%), a Pt-Sn alloy was formed upon reduction which adsorbed less H₂ than sample PA(u). It may also be the case that with higher Sn loadings encapsulation of Pt by the Sn-Al₂O₃ matrix might cause the drop in chemisorption. Burch (7) found that with increasing Sn content the H₂ chemisorption uptake increased for Pt-Sn/Al₂O₃ samples, contradicting the results in this study, with lower Sn loadings giving greater H₂ uptakes. Burch (7) used catalysts contained 0.3wt% Pt and up to 5.0wt% Sn. However Balakrishnan and Schwank (10) reported a trend similar to the one found in this study, with lower Sn loadings (1.0wt% Pt, < 0.5wt% Sn) giving greater H₂ uptakes than samples containing more Sn (> 0.5wt%). One theory proposed by the latter workers was that the excess Sn was increasing the distance between adjacent Pt atoms on the surface, thus decreasing the number of adjacent vacant sites required for the dissociative chemisorption of H₂ (10).

Aging in air at 1073K for 8h brought about a dramatic drop in H₂ uptake for all the catalyst samples examined. The monometallic sample, PA(u) exhibited a drop in H₂ uptake upon aging of 95%, from 42 $\mu\text{mol H}_2 \text{ g}^{-1}$ for an unaged sample to 2 $\mu\text{mol H}_2 \text{ g}^{-1}$ for an aged sample. The Pt-Sn/Al₂O₃ samples also had markedly lower H₂ uptakes after aging, but there was no pattern with regard to Sn content and the magnitude of the drop in H₂ chemisorption upon aging. After aging, the H₂ uptake for samples PS0.3A(u), PS1A(u) and PS3A(u) dropped by 86%, 97% and 58% respectively. The drop in H₂ chemisorption would suggest a large drop in Pt surface area upon aging. In the case of the monometallic Pt/Al₂O₃ sample this loss of Pt surface area could be due to sintering or caused by support surface area loss due to thermal transformations. Previously in this study (Sec 2.2) it has been shown that the surface area of the untreated Al₂O₃ support material was unaffected by heating up to 1173K for 24h. However a number of workers (95, 96) have mentioned metal catalysed phase transformations of Al₂O₃ so that the presence of Pt might have caused a drop in the surface area of the support upon aging. In order to check whether this was the case the BET surface area of sample PA(u) was determined by N₂ physisorption before and after aging at 1073K. There was no change in surface area after aging, remaining at 120 m²g⁻¹. Therefore it appears that for sample PA(u) the primary cause of loss of surface area of the active phase was due to Pt sintering. The X-ray diffraction results appear to confirm this theory, since for an aged PA(u) sample the (100)-Pt diffraction peak was broader and of a greater intensity than the same peak for an unaged PA(u) sample, indicating an increase in Pt particle size upon aging.

For the Pt-Sn/Al₂O₃ samples, the drop in H₂ chemisorption could be due to Pt sintering or mobile Sn covering the Pt, upon aging. For Pt₃Sn alloy it has been shown that exposure to O₂ at temperatures greater than 473K leads to Sn enrichment of the surface (22), while reduction in H₂ leads to a migrating of Pt to the surface (23).

However in Pt-Sn/Al₂O₃ it is questionable whether Sn, which is known to strongly interact with Al₂O₃ i.e. (7, 12) would be mobile and would cover some of the Pt. In fact Sn has been suggested to stabilise Pt, with Sn strongly anchored to Al₂O₃ preventing Pt sintering (7). The XRD evidence would indicate that the drop in H₂ chemisorption is due to Pt sintering during aging. While an unaged sample of PS3 0A(u) had a diffraction pattern with no peaks due Pt, (see Fig 4 11) the diffraction pattern exhibited by the aged sample had Pt peaks which were quite broad and intense. As already mentioned, this could indicate an increase in Pt particle size upon aging at 1073K for 8h. de Miguel et al. (28) examined Pt-Sn/Al₂O₃ after they had undergone five oxidation/reduction cycles at 773K for 5h and found that Pt sintering occurred. Therefore it appears credible that at 1037K for 8h in air Pt sintering occurred causing a drop in H₂ uptake.

As with the monometallic Pt/Al₂O₃ sample (see Sec 3 3), the pre-treatment of the Al₂O₃ support with 0.1M HNO₃ led to a marked increase in H₂ uptake of unaged Pt-Sn/Al₂O₃ samples compared with the amount of H₂ adsorbed by samples with the same Pt and Sn contents, prepared with untreated supports (see Table 4 7). The H₂ uptakes for PS0 3A(N1) and PS1A(N1) were 38% and 57% respectively higher than the H₂ uptakes for samples PS0 3A(u) and PS1A(u). However treatment of the Al₂O₃ support with 1.0M HNO₃ prior to impregnation resulted in a catalyst which exhibited lower H₂ uptakes than the corresponding sample prepared with untreated Al₂O₃ support material. It would appear that the effect of the nitrate treatment is to alter the Pt dispersion rather than to directly increase or decrease H₂ chemisorption as sample A(N1), the Al₂O₃ support pre-treated with 0.1M HNO₃, did not adsorb detectable amounts of H₂. Increased Pt uptakes due to an alteration in the adsorption characteristics of the Al₂O₃ support by the nitrate treatment, can be discounted as a reason for the increase in H₂ chemisorption as no indication from the AAS results of increased Pt uptake by nitrate pre-treated Al₂O₃ supports was obtained.

On the contrary, the nitrate species adsorbed on the Al₂O₃ support may have occupied adsorption sites normally occupied by PtCl_xY⁻ anions and hence gave rise to a more dispersed Pt phase, at lower concentrations of HNO₃ pre-treatment. However, at higher nitrate concentrations progressively less of these adsorption sites might be available to the PtCl_xY⁻ anions and eventually would lead to a decrease in Pt uptake during impregnation, hence a lower Pt content and correspondingly the H₂ uptake would be decreased. The AAS results (see Table 4 4) indicated that there was a drop in Pt uptake for the sample whose support was pre-treated with 1.0M HNO₃ which would appear to support this theory.

Upon aging the Pt-Sn/Al₂O₃ samples prepared with pre-treated supports exhibited a similar drop in H₂ uptake as the corresponding samples prepared using untreated Al₂O₃, see Table 4 7. Again as discussed previously this drop in H₂ uptake can be attributed to a loss in Pt surface area due to sintering.

In order to examine the effect of reduction in H_2 at a higher temperature on the Pt-Sn/ Al_2O_3 samples, sample PS3A(u) was reduced in H_2 at 773K for 8h in situ prior to the normal pre-treatment and chemisorption analysis. After reduction the H_2 uptake was very low, $5 \mu\text{mol}^{-1} H_2 \text{ g}^{-1}$, (see Table 4.7) which was 79% lower than the value for H_2 chemisorption of PS3A(u) which was not reduced at 773K for 8h. This drop in H_2 uptake may have been caused by Pt sintering as this has been reported in the literature for Pt-Sn/ Al_2O_3 samples after reduction in H_2 at high temperatures (14, 28). Another possibility is that some of the H_2 adsorbed during reduction at 773K was not removed during the pre-treatment prior to analysis, blocking some of the Pt sites and hence leading to a decrease in H_2 uptake. Another explanation which cannot be ruled out is a strong metal support interaction (SMSI), as evidence for such an interaction in Pt/ Al_2O_3 systems has been reported in literature, i.e. (97, 98, 99, 100), and normally produces a suppression of H_2 chemisorption after reduction at high temperatures (greater than or equal to 773K), (101, 102). A final possibility is that upon reduction a Pt-Sn alloy was formed. It has already been pointed out that various studies have found Pt-Sn alloys in Pt-Sn/ Al_2O_3 samples after high temperature in situ reduction, (103) and that Pt-Sn alloys adsorb low amounts of H_2 (11). Alloy formation might thus explain the drop in H_2 uptake.

A sample of PS3A(u) reduced at 773K, was aged in air at 1073K for 8h and H_2 uptake for this sample is also given in Table 4.7. At $12 \mu\text{mol } H_2 \text{ g}^{-1}$, not only was H_2 uptake similar to the value for an aged, unreduced sample, but this value is also more than twice as high as the value for the H_2 uptake for the unaged PS3A(u) sample reduced at 773K. As Pt-Sn alloys have been reported to be air sensitive (24) it could be concluded that the high temperature oxidation treatment destroyed Pt-Sn alloys on the surface, resulting in an increase in H_2 uptake despite Pt sintering. However another explanation for the observed increase in H_2 uptake could be that the high temperature oxidation treatment reversed a strong metal support interaction which was brought about by reduction at 773K. It is known that suppression of H_2 chemisorption due to SMSI can be reversed by high temperature treatments in an oxidising atmosphere (104).

DSC Analysis

The DSC results for the light off temperatures (LOT) exhibited by Al_2O_3 , Pt/ Al_2O_3 , Sn/ Al_2O_3 , Pt/ SnO_2 , Pt-Sn/ Al_2O_3 and SnO_2 samples for the oxidation of i-butane are given in Table 4.8. Both the Al_2O_3 and the SnO_2 support material did not exhibit any detectable amounts of activity towards the oxidation of i-butane.

Table 4 8 . Light off temperatures for i-butane oxidation over Pt/Al₂O₃, Pt-Sn/Al₂O₃ and Pt/SnO₂ catalysts

Sample Code	Light Off Temperature Unaged	Light Off Temperature Aged
PA(u)	433K	478K
PS0 3A(u)	483K	488K
PS1A(u)	488K	475K
PS3A(u)	468K	468K
PS0 3A(N1)	478K	478K
PS1A(N1)	478K	482K
PS1(N2)	473K	469K
PSO	428K	499K
PSO(h)	443K	498K
P1SO	483K	513K
P1aSO	488K	515K
A(u)	nd	nd
S3A(u)	583K	585K
A(N1)	nd	nd
SO	nd	nd

* nd = not determined

The Sn/Al₂O₃ sample, S3A(u) showed some activity for i-butane oxidation with a very high LOT at 583K for an unaged sample. Of the other unaged samples, PSO and PA(u) had the lowest LOT. The Pt/SnO₂ sample prepared with NaOH pre-treated SnO₂, PSO(h) had the next highest LOT. All the Pt-Sn/Al₂O₃ samples had higher LOTs, ranging from 468K for PS3A(u) to 488K for PS1A(u). For Pt-Sn systems on HNO₃ pre-treated Al₂O₃, the LOTs were reduced by approximately 10K compared with the LOTs of the corresponding samples prepared with untreated Al₂O₃. With significant changes in Pt content, increases in LOTs did occur. The samples prepared containing 1wt% Pt supported on SnO₂ had LOTs similar to those for Pt-Sn/Al₂O₃ samples, much higher than those exhibited by samples containing 5wt% Pt supported on SnO₂. The order of increasing LOTs for unaged samples was as follows -

PSO < PA(u) < PS3 0A(u) < PS1 0A(N2) < PS1 0A(u) < PS1 0A(N2) < PS1 0A(N1) = PS0 3A(N1) < PS0 3A(u) = P1SO < PS1 0A(u) < P1aSO <<< S3 0A(u)

Aging at 1073K for 8h resulted in a significant increase in the LOTs for Pt/Al₂O₃ and Pt/SnO₂ samples. In the case of PA(u) and PSO and PSO(h) the LOT increased upon aging by 45K, 71K and 57K respectively. Similarly the LOT of P1SO and P1aSO increased to 513K and 515K respectively upon aging at 1073K. For the Pt-Sn/Al₂O₃ samples aging appeared to have little effect on the LOT values. With the exception of Pt/SnO₂ samples, the LOT of all the aged samples was in the range 483K ± 15K.

The large increase in the LOTs for the Pt/SnO₂ samples upon aging at 1073K may be explained by XPS and BET surface area measurements carried out on PSO before and after aging. The BET surface area measurements indicated that upon aging the surface area of the sample dropped dramatically from 9.5 m²g⁻¹ for an unaged sample to 5.9 m²g⁻¹ upon aging. Comparison of XPS spectra in the Pt4f region for aged and unaged PSO(u) samples (Fig 4.8(d)) show a very large drop in surface Pt for the aged samples. It can therefore be concluded that the increased LOTs, for the SnO₂ supported catalysts which were aged, were caused by thermal degradation of the support at 1073K, leading to encapsulation of the Pt by support and hence a decrease in the amount of exposed active phase present.

The magnitude of the DSC exotherms produced by reaction over the catalyst samples is given in Table 4.9. The exotherm size gives an indication of the extent of reaction over these samples and, as explained in Sec 3.2.1, can be used to calculate theoretical values for % butane conversion. These are also given in Table 4.9. The basis of the method of calculation is given in Appendix II. As can be observed from Table 4.9, for unaged samples, the largest exotherm occurred from the reaction over the monometallic Pt sample, PA(u). This represented a conversion of 37% of the butane passing through the DSC. Reaction over samples containing less than or equal to 1wt% Sn with either unpre-treated supports or supports pre-treated with 0.1M HNO₃ produced exotherms which were very similar in magnitude, on average 409mW, slightly lower than the exotherm determined from reaction over PA(u). There was no correlation between LOT and the magnitude of the DSC exotherms with samples which had low LOTs did not necessarily having exotherms greater in magnitude than samples with higher LOTs. The samples containing less Pt exhibited smaller exotherms than those containing higher quantities of Pt, but this was not proportional to the amount of Pt present in each sample.

Table 4.9. DSC exotherms and theoretical % conversions for i-butane oxidation over Pt/Al₂O₃, Pt-Sn/Al₂O₃ and Pt/SnO₂ catalysts

Sample	Unaged Exotherm Size (mW)	Unaged Theoretical i-Butane Conversion (%)*	Aged Exotherm Size (mW)	Aged Theoretical i-Butane Conversion (%)*
PA(u)	420	37	348	31
PS0 3A(u)	413	36	374	33
PS1A(u)	410	36	374	33
PS3A(u)	388	35	374	33
PS0 3A(N1)	411	36	383	33
PS1A(N1)	402	36	323	28
PS1A(N2)	337	30	332	30
PSO	364	32	292	26
PSO(h)	395	35	319	28
P1SO	282	25	237	20
P1aSO	220	16	201	17
A(u)	nd	nd	nd	nd
A(N1)	nd	nd	nd	nd
SO	nd	nd	nd	nd

* Note The extent of reaction was calculated from the magnitude of the exotherm assumming outlet flow rate of 0.38 cm³ i-butane nd = not determined

In all cases the effect of aging at 1073K for 8h was to cause a drop in the magnitude of the exotherm for each sample compared with the exotherms for the corresponding unaged samples. Depending on the sample concerned this corresponded to a drop in the extent of reaction of between 1% and 20%. The samples which exhibited the greatest drop in exotherm size were the monometallic Pt sample (PA(u)), the Pt-Sn/Al₂O₃ sample (PS1A(N1)), and the 5 wt% Pt/SnO₂ samples (PSO and PSO(h)). The Pt-Sn samples prepared with unpre-treated supports exhibited the same sized exotherm from reaction after aging, approximately 374mW. From the results in Table 4.9 it is unclear whether support pre-treatment with HNO₃ during the preparation of Pt-Sn/Al₂O₃ samples caused an increase or decrease in activity after aging. Reaction

after aging over the 1wt% Pt/SnO₂ prepared using an acetone impregnating solution produced the smallest exotherm but this sample was determined to be quite inactive prior to aging anyway

On first inspection the H₂ chemisorption results do not correlate with the 1-butane oxidation activity measurements and LOTs and therefore the reduced catalyst surfaces examined by H₂ chemisorption did not resemble the calcined surfaces involved in the oxidation reactions. For example, sample PSO which exhibited the lowest LOT did not adsorb detectable amounts of H₂ during chemisorption analysis. However, the lack of H₂ uptake by the Pt/SnO₂ samples can be explained by incomplete reduction of the Pt prior to analysis as already mentioned in the chemisorption section. Definitely there was no correlation between H₂ uptake and the extent of butane conversion over the corresponding catalysts. However on closer inspection of the chemisorption results, apart from those for the Pt/SnO₂ samples, it would appear that samples which exhibited lower H₂ uptakes had lower LOTs for 1-butane oxidation than samples which adsorbed higher quantities of H₂. Since samples with high H₂ uptakes normally have low Pt particle sizes it could be concluded that samples with large Pt particles are more effective for 1-butane oxidation at lower temperatures. It has been reported that for the total oxidation of propane large Pt particles are more effective than highly dispersed Pt (105). The XRD results in this study indicated that even in the unreduced samples the Pt particles in the Pt/Al₂O₃ and Pt/SnO₂ samples may have been larger than in the Pt-Sn/Al₂O₃ samples. But if the variations in activity were solely due to variations in the Pt particle size of the sample, with increased Pt particle sizes giving higher activities, then samples which underwent aging at 1073K might be expected to be more active. It is known that aging increased Pt particle size due to sintering (106). The XRD results indicated that in Pt-Sn/Al₂O₃ and Pt/Al₂O₃ samples aging brought about an increase in Pt particle size. Despite this increase in particle size the LOT for PA(u) increased markedly, while those for the Pt-Sn/Al₂O₃ samples were relatively unchanged upon aging. Therefore it would appear that the theory that there is a simple linear relationship between increases in Pt particle size and increases in activity is incorrect.

Another possibility is that there might be critical Pt particle size which is most efficient for butane oxidation and that above or below this particle size the activity for the oxidation reaction is lower at low temperatures. However PS3A(u) had the same LOT for both unaged and aged samples, 468K, even though the XRD evidence indicated a large increase in Pt particle size upon aging. Although it is possible that in the case of the unaged sample the Pt particle size was too small, while aging increased the particle size past the point where it was most efficient for butane oxidation, it would be very fortuitous that samples with different Pt particle sizes would have the same LOT, if Pt particle size was the only factor responsible for differences in activity between the samples. Therefore, the reasons for the differences in 1-butane activity, exhibited by the

Pt/Al₂O₃, Pt/SnO₂ and Pt-Sn/Al₂O₃ samples, would appear to be more complex than a simple dependence on Pt particle size.

The XRD results did not give an indication of what Pt or Sn oxides were on the surface as only peaks due to metallic Pt and the support material could be distinguished for aged samples. Differences in the state of the surface of the catalyst samples could also affect have resulted in activity differences. These differences in surface state are discussed below.

Temperature Programmed Reduction (TPR) studies reported in the literature may provide evidence to support this theory. Hughes and McNicholl (45) carried out a TPR study on Pt/SnO₂ systems and found that after calcination at 773K, the TPR profiles were devoid of any Pt features. It was concluded that the calcination step led to the formation of a compound between Pt and SnO₂, which was difficult to reduce, with Pt reduction occurring at the same temperature as SnO₂, in the region of 680K. TPR studies on Pt-Sn/Al₂O₃ systems calcined in air at 773K (7, 9) determined that Pt reduction occurred at temperatures in the vicinity of 573K and above. Pt in Pt/Al₂O₃ samples has been found to be reduced at temperatures between approximately 515K and 570K (7, 8, 9, 28). Therefore it is possible that Pt in the Pt/SnO₂ samples is in a different form to the Pt in either the Pt/Al₂O₃ or Pt-Sn/Al₂O₃ catalysts. Cox et. al. (47) both PtO and PtO₂ species were present at the surface of Pt/SnO₂ samples calcined at 773K. However the majority of the Pt was found to be bound to the SnO₂ support through surface lattice oxygen, with the presence of Sn-O-Pt surface species and the strong interaction between the Pt and the SnO₂ making these species difficult to reduce. In the case of Pt-Sn/Al₂O₃ systems, although one study reported the presence of some Pt-O-Sn in Pt and SnO films supported by Al₂O₃ (14), other studies on Pt-Sn/Al₂O₃ samples prepared by coimpregnation and calcination at 773K (13), found that most of the Sn was present in a surface egg-shell layer that chemically resembled a Sn aluminate species, SnAlO_x, and that Pt was associated with this SnAlO_x portion of the surface. Another model has been proposed for the surface of calcined Pt-Sn/Al₂O₃ samples where the Pt and Sn are in complete contact and the surface is covered by 2-dimensional patches of Sn(IV) and Pt(IV) (8). In addition, Pt in Pt-Sn/Al₂O₃ samples has been found to be more electron deficient than in Pt/SiO₂ samples (15), due to the electron withdrawal by Sn(II) ions on the Al₂O₃ surface. Hence the possibility exists that the differences in activity of the different samples may be due to an electronic effect, with the Pt being less electron deficient in the Pt/Al₂O₃ catalysts than in Pt/SnO₂ and Pt-Sn/Al₂O₃ samples.

Another possibility is that a geometric effect is responsible for the LOT differences exhibited by the samples. In Pt-Sn/Al₂O₃ systems changes in selectivity for certain reactions compared to monometallic Pt/Al₂O₃ has been ascribed to a geometric effect brought about by Sn addition. For example it has been reported that the addition of Sn to Pt/Al₂O₃ for the conversion of n-hexane altered the selectivity of the catalysts

and decreased the rates of deactivating reactions (3) The change in selectivity has been interpreted in terms of a change in adsorption properties due to differences in the number of adjacent Pt atoms necessary for different reaction pathways (3) A geometric effect has been proposed as a cause for the inhibition of hydrogenolysis reactions during the dehydrocyclization of n-heptane over Pt-Sn/Al₂O₃ samples, where dilution of the active metal by Sn was claimed to block the large Pt ensembles required for hydrogenolysis (37)

The high LOTs of the Pt-Sn/Al₂O₃ samples in this study may also have been caused by a geometric effect In the Pt-Sn/Al₂O₃ samples the surface Pt sites may be less accessible to the reactants The Pt atom may be surrounded by Sn or even partially covered by Sn decreasing the number of active sites for 1-butane oxidation For the Pt/SnO₂ and Pt/Al₂O₃ samples, the Pt may be more accessible to reactant The Pt may protrude above the surface of the Al₂O₃ or SnO₂ allowing more adsorption of reactants, with greater availability of the required active sites leading to a drop in LOT

The unaged Pt/SnO₂ samples exhibited differences in LOT depending on whether the SnO₂ support underwent pre-treatment and on the Pt loading The increased LOTs of the samples prepared with 1wt% Pt can be rationalised in terms of a decrease in the number of active sites on the catalyst surface Surprisingly, pre-treatment of the SnO₂ support with NaOH led to an increase in the LOT The sole purpose of the support pre-treatment was to increase the number of hydroxyl sites on the SnO₂ support, in order to increase the uptake of Pt during impregnation (46) Although in this study the pre-treatment had little effect on Pt uptake, it did cause a increase in LOT The pre-treatment poisoned the support surface and despite the fact that the material was then thoroughly washed with warm milli Q water it appears that residual amounts of contaminants brought about deactivation of the active sites for oxidation at low temperatures

The resistance to aging of the Pt-Sn/Al₂O₃ must have been due to the presence of Sn, as the Pt/Al₂O₃ sample exhibited a marked increase in LOT upon aging and also the exotherm for the aged PA(u) sample was approximately 30mW lower than the magnitude for the exotherms exhibited by the majority of the aged Pt-Sn samples The exceptions to this were samples PS1 0A(N1) and PS1 0(N2) which exhibited smaller exotherms when aged than an aged PA(u) sample In the case of PS1 0A(N2) the unaged sample also exhibited a lower activity than the corresponding monometallic Pt sample, probably due to the low Pt loading It is unclear why an aged sample of PS1 0A(N1) should be of lower activity than the other Al₂O₃ supported samples However in Ch 2 it was pointed out that the treatment of the Al₂O₃ support with acid increased phase transformation of the material to α -Al₂O₃ upon exposure at 1373K It is possible that aging at 1073K caused loss of support surface area due to similar phase transformations and may have resulted in loss of active sites for 1-butane oxidation

The resistance of the Pt-Sn/Al₂O₃ samples to thermal aging can't be attributed to a decrease in the amount of Pt sintering due to the presence of Sn. The XRD evidence indicated that Pt sintering also occurred in the Pt-Sn/Al₂O₃ samples upon aging at 1073K. Therefore again the differences in catalytic activity after aging must be due to differences in the active sites possessed by the Pt-Sn/Al₂O₃ and Pt/Al₂O₃ catalysts, discussed previously in this section, with the sites on the Pt-Sn/Al₂O₃ being more resistant to aging at elevated temperatures.

4.4 Conclusions

The study indicated that there was significant differences between the samples examined. The XRD results indicated that the Pt in the Pt-Sn/Al₂O₃ samples was of a smaller particle size than in the Pt/Al₂O₃ or Pt/SnO₂ samples. Although alloy formation could not be ruled out, no XRD evidence for Pt-Sn alloy formation in Pt-Sn/Al₂O₃ samples, after reduction at elevated temperatures, was found. The XPS results indicated that, for unreduced Pt-Sn/Al₂O₃ samples, the Sn was present on the surface as Sn(II) and/ or Sn(IV), with evidence for the presence of a Sn aluminate surface species. The H₂ uptake of Pt-Sn/Al₂O₃ samples was found to be dependent on Sn content, with low Sn loadings (<1wt%) giving higher uptakes in H₂. Pre-treatment of the Al₂O₃ support with HNO₃ affected H₂ uptake, but this was dependent on the concentration of the HNO₃ used.

The Pt/SnO₂ samples did not adsorb detectable amounts of H₂ and the XPS results indicated that Pt was present on the surface as a Pt-O-Sn substrate bonded species and Pt oxides.

The catalysts also varied in the LOT for i-butane oxidation. The Pt/Al₂O₃ and Pt/SnO₂ samples had lower LOTs than the Pt-Sn/Al₂O₃ samples, possibly due to Pt in different forms in different samples or due to a geometric effect. For the Pt/SnO₂ samples LOTs were influenced by both support pre-treatment and Pt content. The extent of reaction was greatest over unaged Pt/Al₂O₃ samples whilst the extent of reaction over the Pt-Sn/Al₂O₃ samples was lower. The extent of butane oxidation over Pt/SnO₂ samples was even lower than over the other monometallic Pt or the bimetallic catalysts.

Aging for 8 h at 1073K, in general, brought about a large decrease in H₂ uptake for samples which exhibited H₂ chemisorption when unaged. XRD evidence indicated that aging brought about a sintering of Pt in Pt/Al₂O₃ and Pt-Sn/Al₂O₃ samples. XPS evidence pointed to a major loss of Pt from the surface of Pt/SnO₂ samples upon aging. Aging brought about a significant increase in the LOTs for i-butane oxidation for Pt/Al₂O₃ and Pt/SnO₂ samples. The LOTs for the Pt-Sn/Al₂O₃ samples were virtually unchanged upon aging and although the activity dropped, in the majority of cases this drop was lower than for the aged Pt/Al₂O₃. This resistance to aging was not due to the stabilisation of Pt by Sn, through a geometric effect, as XRD evidence indicated Pt sintering in Pt-Sn/Al₂O₃ samples during aging. It must have been due to other differences in the nature of active sites on the Pt-Sn/Al₂O₃ and Pt/Al₂O₃ catalysts an electronic effect may have been responsible for the differences in activity between monometallic and bimetallic samples after thermal aging.

4.5 References

- (1) J. Biswas, G.M.Bickle, P.G.Gray, D.D.Do and J.Barbier, Catal.Rev. -Sci.Eng., 30, 161 (1988)
- (2) S.D.Gardener, G.B.Hoflund, M.R.Davidson and D.R.Schryer, J.Catal., 115, 132 (1989)
- (3) F.M.Dautzenberg, J.N.Helle, P.Biloen, and W.M.H.Sachtler, J.Catal., 63, 119 (1980)
- (4) A.C.Muller, P.A.Engelhard and J.E.Weisang, J.Catal., 56, 65 (1979)
- (5) R.Bacaud, P.Brusserie, F.Figueras and J.P.Mathieu, in, B.Delmon, P.A.Jacobs and G.Poncelet (Eds.), Preparation of Catalysts I, Studies in Surf. Sci. Catal., 1, p.509, Elsevier, Amsterdam, (1976)
- (6) R. Bacaud, P.Brusserie and F.Figueras, J.Catal., 69, 399 (1981)
- (7) R.Burch, J.Catal., 71, 348 (1981)
- (8) H.Lieske and J.Volter, J.Catal., 90, 96 (1984)
- (9) A.Sachdev and J.Schwank, Proceedings of the 9th International Congress on Catalysis, Chem.Inst. Canada, Ottawa, Ontario, 1275 (1988)
- (10) K.Balakrishnan and J.Schwank, J.Catal., 127, 287 (1991)
- (11) H.Verbeek and W.M.H.Sachtler, J.Catal., 42, 257 (1976)
- (12) B.A.Sexton, A.E.Hughes and K.Forger, J.Catal., 88, 466 (1984)
- (13) S.R.Adkins and B.H.Davis, J.Catal., 89, 371 (1984)
- (14) G.B.Hoflund, D.A.Asbury and R.E.Gilbert, Thin Solid Films, 129, 139 (1985)
- (15) G.Meitzner, G.Via, F.W.Lytle, S.C.Fung and J.Sinfelt, J.Phys.Chem., 92, 2925 (1988)
- (16) Y.Li and Y.Hsia, Hyperfine Interactions, 28, 875 (1986)
- (17) Y.Li and Y.Hsia, Hyperfine Interactions, 28, 879 (1986)
- (18) Y.Zhang and Y.Li, Kexue Tongbao, 32, 1626 (1987)
- (19) B.Davis, J.Stencel and J.Goodman, Proceedings of the 9th International Congress on Catalysis, Chem.Inst. Canada, Ottawa, Ontario, 1291 (1988)
- (20) R.Bouwman, L.H.Toneman and A.A.Holscher, Surf.Sci., 35, 8 (1973)
- (21) G.B.Hoflund, D.A.Asbury, P.Kirszensztejn and H.A.Laitinen, Surf.Sci.Lett., 161, L583 (1985)
- (22) D.Asbury and G.B.Hoflund, Surf. Sci., 199, 552 (1988)
- (23) D.S.Gardener, G.B.Hoflund and D.Schryer, J.Catal., 119, 179 (1989)
- (24) Y.Li, J.M.Stencel and B.H.Davis, React.Kinet.Catal.Lett., 37, 273 (1988)
- (25) W.Unger, G.Lietz, H.Lieske and J.Volter, Appl.Surf.Sci., 45, 29 (1990)
- (26) G.T.Baronetti, S.R.de Miguel, O.A.Scelza, M.A.Fritzler and A.A.Castro, Appl.Catal., 19, 77 (1985)
- (27) G.T.Baronetti, S.R.de Miguel, and O.A.Scelza, Appl.Catal., 24, 109 (1986)

- (28) S.R.de Miguel, G.T.Baronetti, A.A.Castro and O.A.Scelza, Appl.Catal., 45, 61 (1988)
- (29) R. Srinivasan, L.A. Rice and G.H. Davis, J. Catal., 129, 257 (1991)
- (30) J.M.Stencel, B.D.Adkins and B.H.Davis, Symposium on Advances in Naptha Reforming presented before the division of Petroleum Chem. Inc., Am.Chem.Soc., p.87, New Orleans Meeting, August 30 (1987)
- (31) R.Srinivasan, R.J. de Angelis and B.H.Davis, J.Catal., 106, 449 (1987)
- (32) R.Srinivasan, R.J.de Angelis and B.H.Davis, Catal.Lett., 4, 303 (1990)
- (33) J.Margitfalvi E.Talas, M.Hegedus and S.Gobolos, Heter.Catal., 6, 345 (1987)
- (34) Y.Li and K.J.Klabunde, Langmuir, 3, 558 (1987)
- (35) Y.Li , Y.Zhang and K.J.Klabunde, Langmuir, 4, 385 (1988)
- (36) Y.Li, Y.Zhang and K.J.Klabunde, Hyperfine Interactions, 41, 649 (1988)
- (37) J.Volter, G.Lietz, M.Uhlemann and M. Hermann, J.Catal., 68, 42 (1981)
- (38) R.Burch and L.C.Garla, J.Catal., 71, 360 (1981)
- (39) B.N.Kuznetsov, V.K.Duplyakin, V.I.Koval'Chuk, Y.A.Ryndin and A.S.Belyi, J.Kinet.Catal., 22, 1183 (1981)
- (40) J.L.Margitfalvi, M.Hegedus and E.Talas, J.Mol.Catal., 5, 279 (1989)
- (41) F.A.Cotton and G.Wilkinson, Basic Inorganic Chemistry, p.269, Wiley (1976)
- (42) P.J.Durrant, General and Inorganic Chemistry, p.419, Longmans, Green and Co. (1956)
- (43) T.Morimoto, M.Kiriki, S.Kittaka, T.Kadota and M.Nagao, J.Phys.Chem., 83, 2768 (1979)
- (44) F.Solymosi and J.Kiss, J.Catal., 41, 202 (1976)
- (45) V.B.Hughes and B.D.McNicol, J.Chem.Soc., Faraday Trans.I, 75, 2165 (1979)
- (46) M.Watanabe, S.Venkatesan and H.Laitinen, J.Electrochem.Soc., 130, 59 (1983)
- (47) D.F.Cox, G.B.Hoflund and H.A.Laitinen, Langmuir , 1, 269 (1985)
- (48) G.B.Hoflund, Closed Cycle Frequency-Stable CO₂ Laser Technology, NASA Conference Publication 2456, 179 (1987)
- (49) C.L.Lau and G.K.Werthelm, J.Vac.Sci.Technol., 15, 622 (1978)
- (50) R.A.Powell, Appl.Surf.Sci., 2, 397 (1979)
- (51) M.E.Woods and B.J.Hopkins, J.Phys., C 18, 3255 (1985)
- (52) D.Elliot, D.L.Zellmer and H.A.Laitinen, J.Electrochem.Soc., 117, 1343 (1970)
- (53) H.Kim and H.A.Laitinen, J.Am.Cer.Soc., 58, 23 (1975)
- (54) H.A.Laitinen, C.A.Vincent and T.M.Bednarskii, J.Electrochem. Soc., 115, 1024 (1968)
- (55) A.Franz, G.Kent and R.L.Anderson, J.Electron. Mater., 6, 107 (1977)
- (56) G.K.Bhagavat and K.B.Sundaram, Thin Solid Films, 63, 197 (1979)
- (57) R.N.Choshtagore, J.Electrochem.Soc., 125, 110 (1978)
- (58) H.Pink, L.Treitinger and L.Vite, J.Appl.Phys.. Jpn, 19, 513 (1980)

- (59) H.Oganva, A.Abe, M.Nishikawa and S.Hayakawa, J.Electrochem.Soc., 128, 2020 (1981).
- (60) G.B.Hoflund, D.F.Cox, G.L.Woodson and H.A.Laitinen, Thin Solid Films, 78, 357 (1981)
- (61) E.W.Giesekke, H.A.Gutowksy, P. Kirkov and H.A. Laitinen, Inorg.Chem., 6, 1294(1967)
- (62) F. Solymosi and J.Kiss, J.Chem.Soc., Chem.Comm., 509 (1974)
- (63) B.Viswanathan and S.Chokkalingam, Surf.Technol., 23, 231 (1984)
- (64) J.R.,Christie, D.Taylor and C.C.McCain, J.Chem. Soc., Faraday Trans.1, 72, 334 (1976)
- (65) Y.G.Rostevanov, I.B.Annenkova, R.A.Lemberanskii and T.G. Alkhazov, React.Kinet.Catal.Lett., 10, 201 (1979)
- (66) N.N.Sazonova, S.A.Venjaminov and G.K.Boreskov, J.Kinet.Catal., 15, 364 (1974).
- (67) H.H.Herniman, D.R.Pyke and R.Reid, J.Catal., 58, 68 (1979)
- (68) M.Figueras, M.Gasior, B.Grzybowska and J.L.Pontefaix, React.Kinet.Catal.Lett., 20, 367 (1982)
- (69) J.Haber, B.Grzybowska and M.Gasior, React.Kinet.Catal.Lett., 15, 395 (1980)
- (70) F.Solymosi and F.Bozso, in, G.C. Bond, P.B. Wells and F.C. Tomkins(Eds.), Proc.Int.Congr.Catal., 1976 , Chem.Soc., 365 (1977)
- (71) F.Solymosi, I.Tombacz and G.Kutsan, J.Chem.Soc., Chem.Comm., 1455 (1985)
- (72) G.B.Hoflund, in,G.Poncelet, P.Grange andP.A.Jacobs(Eds.), Preparation of Catalysts III, Studies in Surf. Sci. Catal., 16, 91, Elsevier, Amsterdam (1983)
- (73) G.B.Hoflund, D.F.Cox and H.A.Laitinen, Thin Solid Films, 83, 261 (1981)
- (74) G.B.Hoflund, S.E.M. Journal IV, 1391 (1985)
- (75) G.B.Hoflund, D.F.Cox, T.Ohuchi, P.H.Holloway and H.A.Laitinen, Appl.Surf.Sci., 14, 281 (1982)
- (76) A.Katayama, Chem.Lett., 1263 (1978)
- (77) A.Katayama, J.Phys.Chem., 84, 376 (1980)
- (78) H.A.Laitinen, J.R.Waggoner, C.Y.Chan, P.Kirszensztejn, D.A.Asbury and G.B.Hoflund, J.Electrochem.Soc., 133, 1568 (1986)
- (79) A.C.C.Tsueng and S.C.Dhara, Electrochim.Acta, 19, 845 (1974)
- (80) M.M.Janssen and J.Moolhuysen, J.Catal., 46, 289 (1977).
- (81) M.M.Janssen and J.Moolhuysen, Electrochim.Acta, 21, 861 (1976)
- (82) S.Motoo and M.Watanabe, J.Electroanal.Chem.Interfacial Electrochem., 69, 429 (1976)
- (83) S.Motoo, M.Watanabe and N.Furuya, Meeting of I.S.E. - Zurich, Switzerland, Extended Abs., 234 (1976)

- (84) S.Motoo, M.Shibata and M. Watanabe, J.Electrochem.Interfacial Electrochem., 110, 103 (1980)
- (85) D.S.Stark and M.R.Harris, J.Phys.E., 16, 492 (1983)
- (86) I.M.Miller, D.R.Schryer, R.V.Hess, G.M.Wood, B.T.Upchurch and K.G.Brown, Am.Chem.Soc., National Meeting, Chicago, Illinois, September 9 - 13 (1985)
- (87) C.E.Batten, I.M.Miller, P.A.Paulin and J.Schryer, Closed Cycle Frequency-Stable CO₂ Laser Technology, NASA Conf. Pub., 2456, 199 (1987)
- (88) D.R.Schryer, B.T.Upchurch, J.D.Van Norman, K.G.Brown and J.Schryer, J.Catal., 122, 193 (1990)
- (89) J.E.Drawdy, G.B.Hoflund, S.D.Gardener, E.Yngvadottir and D.R.Schryer, Surf.Interface Analysis, 16, 369 (1993)
- (90) K.G.Brown, J.Schryer, D.R.Schryer, B.T.Upchurch, G.M.Wood, I.M.Miller, B.D.Sydney, C.E.Batten and P.A.Paulin, Closed Cycle Frequency-Stable CO₂ Laser Technology, NASA Conf.Pub., 2456, 219 (1987)
- (91) S.D.Gardener, G.B.Hoflund, B.T.Upchurch, D.R.Schryer, E.J.Kielin and J.Schryer, J.Catal., 129, 114 (1991)
- (92) L.Y.Alt, A.S.Belyi, V.K.Duplyakin, V.I.Perevalova and N.P.Shitova, React.Kinet.Catal.Lett., 23, 13 (1983)
- (93) N.B.Shitova, L.Y.Alt, V.I.Perevalova, A.S.Belyi and V.K.Duplyakin, React.Kinet.Catal.Lett., 23, 17 (1983)
- (94) F.A.Cotton and G.Wilkinson, Advanced Inorganic Chemistry, 4th, p.906, Wiley, New York (1980)
- (95) N.S.Kozlov, M.Lazarev, L.Mostovaya and I.P.Stremok, J.Kinet.Catal., 14, 1130 (1973)
- (96) D.J.Young, P.Udaja and D.L.Trim, in, B.Delmon and G.F.Forment(Eds.) Catalyst Deactivation, Studies in Surf. Sci. Catal., 34, p.331, Elsevier, Amsterdam (1980)
- (97) G.Den Otter and F.M.Dautzenberg, J.Catal., 53, 116 (1978)
- (98) K.Kunimori, Y.Ikeda, M.Soma and T.Uchijima, J.Catal., 79, 185 (1983)
- (99) T.Huizinga, J.Van Grondelle and R.Prins, Appl.Catal., 10, 199 (1984)
- (100) T.Ren-Yuan, W.Rong-An and L.Li.Wu, Appl.Catal., 10, 163 (1984)
- (101) S.J.Tauster and S.C.Fung, J.Catal., 55, 29 (1978)
- (102) S.J.Tauster, S.C.Fung and R.Garten, J.Am.Chem.Soc., 100, 170 (1978)
- (103) R.S.Srinivasan and B.H.Davis, Platinum Metals Rev., 36, 151 (1992)
- (104) S.A.Stevenson, G.B.Raupp, J.A.Dumesic, S.J.Tauster and R.T.K.Baker, in, S.A.Stevenson, J.A.Dumesic, R.T.K.Baker and E.Ruckenstein (Eds.), Metal-Support Interactions in Catalysis, Sintering and Redispersion, Ch.2, Van Nostrand Reinhold Co., New York (1987)

- (105) K Otto, J M Andino and C L Parks, J Catal, 131, 243 (1991)
- (106) J Bournville and G Martino, in, B Delmon and G F Forment (Eds),
Catalyst Deactivation, Studies in Surf Sci Catal, 34, p 159,
Elsevier, Amsterdam (1980)

5 Conclusions

The aim of this work was to examine Pt/Al₂O₃, Pt/SnO₂ and Pt-Sn/Al₂O₃ catalysts for the oxidation of 1-butane. The main conclusion which can be drawn from this study is that although less active initially compared with the Pt/SnO₂ and Pt/Al₂O₃ samples, the Pt-Sn/Al₂O₃ catalysts were more resistant to thermal aging, maintaining a higher catalytic activity than the former catalysts after aging at 1073K.

Prior to aging the Pt/SnO₂ catalysts lit-off at a lower temperature than the Pt/Al₂O₃ samples (containing the same amount of Pt). However the former catalysts exhibited a major drop in catalytic activity upon thermal aging at 1073K, much higher in magnitude than the decrease observed in the Pt/Al₂O₃ or the Pt-Sn/Al₂O₃ catalysts. In the case of the Pt/SnO₂ catalysts, loss of catalytic activity upon aging was due to thermal degradation of the support material. Heating to 1073K caused a drop in the specific surface area of the SnO₂ and, according to the XPS results, resulted in a major loss of Pt from the surface.

The loss of catalytic activity upon aging for the Pt/Al₂O₃ was not due to the loss of surface area of the Al₂O₃ support material as the fibre was thermally stable at 1073K. The Al₂O₃ support consisted primarily of the η -phase. Aging at 1373K caused a decrease in both the support surface area and pore volume and also a certain amount of phase transformation to α -Al₂O₃ occurred. Addition of the cations La³⁺, Ce³⁺ and Si⁴⁺ prevented the formation of the α -phase but did not prevent surface area loss. Acid pre-treatment of the support material (a process used to increase the acidity of the support to facilitate the uptake of Pt during impregnation) resulted in acceleration of the phase transformation at 1373K. The decrease in catalytic activity upon aging for the Pt-Sn/Al₂O₃ samples prepared with HNO₃ pre-treated support material may thus have been due to loss of support surface area.

Apart from affecting the thermal stability of the Al₂O₃ support material pre-washing with acid also affected the uptake of Pt during impregnation and the dispersion of the Pt on the support. The type of acid and the concentration of the acid used were significant controlling factors. Treatment of the Al₂O₃ support with 0.1M HNO₃ prior to Pt impregnation led to a substantial amount of NO₃⁻ being retained on the Al₂O₃ (despite washing with water) and resulted in improved Pt uptake and increased dispersion compared with catalysts prepared with untreated Al₂O₃ supports. In this case the effect of the NO₃⁻ was probably to increase the acidity of the support, hence facilitating the adsorption of PtCl₆²⁻ anions, and also by taking up some of the Pt adsorption sites producing a more dispersed Pt phase in a similar manner to a competitive adsorbate. Increasing the HNO₃ concentration (1MHNO₃) for acid pre-washing of the Al₂O₃ produced a decrease in the uptake of Pt during impregnation and decreased H₂ chemisorption uptakes compared with samples prepared with supports

pre-treated with the lower concentration of HNO_3 . With the higher HNO_3 concentration the support surface may have become saturated with NO_3^- and hence caused a major drop in the number of Pt adsorption sites on the support surface.

Use of HCl to pre-treat the Al_2O_3 support resulted in lower Pt uptakes during impregnation and lower dispersions compared with catalysts with untreated or HNO_3 pre-treated supports. It is unclear why this occurred. It may be that the surface was saturated with strongly bound chloride and thus prevented the adsorption of Pt during impregnation.

Two methods of Pt impregnation were examined, namely spray impregnation of the Al_2O_3 mat and wet impregnation of the support material in powder form. Spray impregnation produced catalysts with higher Pt dispersions and better catalytic activity for i-butane oxidation than samples prepared by wet impregnation.

However it should be noted that there was no direct relationship between Pt particle size and catalytic oxidation activity. In some cases catalysts with well dispersed Pt were more active compared with other samples, i.e. Pt supported on untreated Al_2O_3 , while in other cases they were less active, i.e. Pt-Sn/ Al_2O_3 samples. Increasing the Pt particle size, i.e. through thermal aging, did not lead to an increase in catalytic activity (in the case of monometallic Pt/ Al_2O_3 the opposite was found to be the case). Most of the Pt/ Al_2O_3 catalysts exhibited an increase in oxidation activity at a distinct temperature compared with initial activity. This could possibly have indicated two types of active site, one which operated at low temperature and another operated at a higher temperature. Over the majority of samples whose activity was monitored by GC no hydrocarbon oxidation products were detected but since this was not carried out for all catalysts the possibility of a secondary reaction occurring over some of the catalyst samples can not be ruled out. The differences in catalytic activity could not be solely ascribed to differences in Pt particle size and must be due to the presence of different forms of Pt or different amounts of a particular active site for butane oxidation possessed by the monometallic and bimetallic catalysts. There was no direct evidence that under oxidation conditions Pt was in different forms in the Pt/ SnO_2 , Pt/ Al_2O_3 and Pt-Sn/ Al_2O_3 catalysts. Although the XPS evidence indicated that Pt was present as PtO , PtO_2 and Pt-O-Sn in the Pt/ SnO_2 catalyst, no information on the state of Pt in the Al_2O_3 supported samples could be obtained because of the overlap of the $\text{Al}2p$ peak in the Pt4f region. Indirectly the H_2 chemisorption results indicated that the Pt in the Pt/ SnO_2 samples was different to that in the Pt/ Al_2O_3 and Pt-Sn/ Al_2O_3 catalysts. While the Al_2O_3 supported catalysts did chemisorb H_2 , the SnO_2 supported catalysts did not adsorb detectable amounts of H_2 . Any conclusions as to the difference in the nature of Pt in the three types of catalyst is speculative. The initially lower activity exhibited by the Pt-Sn/ Al_2O_3 catalysts may be due to a electronic effect where the Pt is more electron deficient than that in Pt/ Al_2O_3 due to an electron withdrawing effect of Sn(II) ions on

activity would be lowered. It may also be that if there was two types of active site i.e. high and low temperature and then the Pt-Sn/Al₂O₃ catalyst may have possessed less low temperature sites and hence have lower activity and be less active at lower temperatures. The activity differences prior to aging could also be due to a geometric effect. If the active sites for butane oxidation consisted of a number of atoms of Pt then the addition of Sn may have decreased the number of active sites by dilution of the Pt atoms on the support surface.

This resistance to aging for Pt-Sn/Al₂O₃ catalysts was not due prevention of Pt sintering by the Sn as both H₂ chemisorption measurements and XRD evidence indicated that upon aging the Pt particle size also increased in the Pt-Sn/Al₂O₃ catalysts in a similar manner to the Pt in the Pt/Al₂O₃ samples. Therefore it appears that the electronic nature of the active sites in the Pt-Sn/Al₂O₃ catalysts is such that they are more resistant to thermal aging than those on the Pt/Al₂O₃ catalysts. Again if there were two types of active site it may be that the lower temperature type site is less resistant to aging. If the Pt-Sn/Al₂O₃ catalysts possessed less of these lower temperature sites then the activity drop upon aging for these catalysts would be lower than for the Pt/Al₂O₃ samples if they possessed more of them initially. Finally it must be restated that there was no direct experimental evidence as to the nature of Pt in the Pt/Al₂O₃ or Pt-Sn/Al₂O₃ and that the above theories are all speculative.

Appendix I

Basis of surface area determination by N₂ physisorption

The physical adsorption of gas on a solid surface is described by the BET equation , one form of which is shown below

$$(p/p_0) / (V[1-p/p_0]) = 1/(V_m C) + [(C-1)/(V_m C)] p/p_0 \quad (I)$$

where V = volume of gas adsorbed @ STP

p = gas pressure

p₀ = saturated vapour pressure of liquefied gas at the adsorbing temperature

V_m = volume of gas @ (STP) required to form an adsorbed monomolecular layer

C = constant related to the energy of adsorption

The surface area (S) of a sample giving V_m can be calculated from

$$S = V_m A N / M \quad (II)$$

where A = Avogadro's number

M = molar volume of the gas

N = area of each adsorbed gas molecule
(for nitrogen N = 16.2 × 10⁻²⁰ m²/molecule)

By plotting values for (p/p₀) / V[1-(p/p₀)] on the ordinate against p/p₀ on the abscissa, the slope and intercept of the resulting straight line, gives values for (C-1) / (V_mC) and 1 / (V_mC) respectively The surface area (S) can be obtained using equation II -

$$S = 6.023 \times 10^{23} \times 16.2 \times 10^{-20} / (22414 \times (\text{slope} + \text{intercept}))$$

This is the basis of multipoint surface area determinations used in this study

The constant C in equation (I) is typically a relatively large number, i.e. $C \gg 1$, from which equation I reduces to -

$$(p/p_0)/V [1-(p/p_0)] = (1/V_m) [(1/C) + (p/p_0)]$$

When $p/p_0 \gg 1/C$, the above equation reduces to -

$$V_m = V[1-(p/p_0)]$$

By substituting for V_m in equation (II) -

$$S = VAN [1-(p/p_0)] / M$$

Taking into account STP, the surface area can be calculated i.e. -

$$S = \frac{V \times 273.3 \times \text{atm pressure} \times 6.023 \times 10^{23} \times 16.2 \times 10^{-20} \times [1-(\%N_2/100)] \times \text{atm Pressure}}{\text{Room Temp} \times 760 \times 22.414 \times 10^3 \times \text{saturated pressure}}$$

$$= V \times \text{constant}$$

This is the basis for the single point surface area determination

For calibration purposes, this means that for example a syringe injection of $V = 1.00 \text{ cm}^3$ of N_2 at 295K and 760mmHg results in a constant with a value of 2.84, assuming saturation pressure is 775mmHg. The value of the constant changes with changes in the ambient pressure and temperature and hence the instrument has to be calibrated to measure the surface area given by 1 cm^3 of N_2 prior to surface area analysis.

Appendix II

Calculation of theoretical % 1-C₄H₁₀ from DSC exotherm size

Theoretical 1-C₄H₁₀ conversions were calculated from the magnitude of the DSC exotherms (mW) taking into account an outlet flow rate of 1-C₄H₁₀ of 0.38 cm³ min⁻¹

Using the formula given below the volume occupied by 1 mole of 1-C₄H₁₀ at a pressure of 1.4 atm can be calculated

$$P_1 V_1 = P_2 V_2$$

when $P_1 = 1 \text{ atm}$, $V_1 = 22414 \text{ cm}^3$ and $P_2 = 1.4 \text{ atm}$, then $V_2 = 16010 \text{ cm}^3$ Therefore $0.38 \text{ cm}^3 \text{ min}^{-1} \text{ 1-C}_4\text{H}_{10} = 3.95 \times 10^{-7} \text{ mol s}^{-1}$ Since the combustion of 1 mol 1-C₄H₁₀ produces -2877 kJ then at a flow rate of 0.38 cm³ min⁻¹ the amount of energy produced assuming total combustion = 1.138 J s⁻¹ = 1.138 W This figure was thus assumed to represent 100% conversion and % conversions were calculated on this basis